Universitat Internacional de Catalunya
Departament de Ciències Bàsiques

Tesis doctoral

CPT1c in specific hypothalamic nuclei and its role in lípid sensing and metabolic adaptation

Anna Fosch Masllovet

UNIVERSITAT INTERNACIONAL DE CATALUNYA

MEDICINE AND HEALTH SCIENCE FACULTY

BASIC SCIENCE DEPARTMENT

CPT1C IN SPECIFIC HYPOTHALAMIC NUCLEI AND ITS ROLE IN LIPID SENSING AND METABOLIC ADAPTATION

Anna Fosch Masllovet

2022

CPT1C IN SPECIFIC HYPOTHALAMIC NUCLEI AND ITS ROLE IN LIPID SENSING AND METABOLIC ADAPTATION

Doctoral thesis manuscript presented by Anna Fosch Masllovet to opt for the degree of Doctor of Philosophy (PhD) awarded by the Universitat Internacional de Catalunya.

This thesis has been conducted in the Basic Science Department from the Medicine and Health Science Faculty of the Universitat Internacional de Catalunya, under the co-direction of Dr. Núria Casals Farré and Dr. Rosalía Rodríguez Rodríguez.

This thesis is part of the Doctoral program of Health Sciences, included in the Neuroscience Research line of Universitat Interancional de Catalunya

Sant Cugat del Vallès, 2022

Dr. Núria Casals Farré	**Dr. Rosalía Rodríguez Rodríguez**	**Anna Fosch Masllovet**
Director	Director	PhD student

“Sempre tindrem menys paraules que món. I és una sort.”

Més Món, Roc Casagran

A totes les companyes de cordada d’aquesta vi(d)a...

L'obesitat s'ha convertit en una pandèmia en els últims 40 anys. L'OMS estima que la població amb sobrepès gairebé s'ha triplicat des del 1975, i la tendència continua creixent. Aquestes dades tenen un gran impacte tant en la salut com en la despesa sanitària d'un país. L'obesitat és una malaltia crònica d'origen multifactorial que va lligada a altres condicions patològiques, com la Diabetis mellitus tipus 2. L'obesitat apareix degut a un desequilibri en el metabolisme energètic de l'organisme, el qual està estretament regulat per l'hipotàlem, encarregat d'integrar senyals de la perifèria i donar una resposta homeostàtica. En els últims anys, s'ha investigat sobre els mecanismes moleculars i els nuclis de l'hipotàlem implicats en la desregulació de la homeòstasis energètica per poder reconèixer possibles dianes terapèutiques.

Aquesta tesi està centrada en estudiar el paper de la proteïna carnitina palmitoil transferasa 1c (CPT1c), un sensor energètic neuronal, en la regulació de la homeòstasis energètica en l'hipotàlem com a resposta a diferents reptes metabòlics. Recentment, la seva expressió en el nucli ventral de l'hipotàlem (VMH) ha estat assenyalada com a necessària per a l'activació de la termogènesis del teixit adipós marró en resposta a una alimentació rica en greixos. La població neuronal més abundant del nucli VMH són les neurones SF1. Així doncs, hem generat un nou model genètic de ratolí que no expressa CPT1c en aquestes neurones (SF1-*CPT1c*-KO) per poder conèixer-ne la funció concreta en aquesta població neuronal. Paral·lelament, també hem estudiat el paper de la CPT1c en la resposta central als àcids grassos de cadena llarga (AGCL). Primerament, hem definit l'efecte diferencial dels AGCL saturats i insaturats en la ingesta, el control del pes i la termogènesis del teixit adipós marró, així com els nuclis hipotalàmics implicats i les possibles rutes de senyalització involucrades, en ratolins salvatge (WT) , i seguidament hem avaluat aquests efectes en ratolins deficients per aquesta proteïna (CPT1c-KO).

Els resultats de la tesi evidencien, per una banda, que la CPT1c en les neurones SF1 del VMH és necessària per una l'adaptació metabòlica, facilitant que els teixits perifèrics utilitzin preferentment els greixos com a substrat energètic en comptes de la glucosa, durant els primers dies d'exposició a la dieta grassa, en una situació de dejú o en l'exposició al fred. Per altra banda, hem confirmat que els àcids grassos administrats centralment activen de forma diferencial la sacietat i la termogènesis del teixit adipós marró depenent del grau de saturació/insaturació de la seva cadena alifàtica. També hem identificat els nuclis hipotalàmics arcuat, paraventricular i VMH com a mediadors d'aquesta senyal i l'activació diferent de l'eix AMPK-ACC i la proteïna FAS segons el nivell

de saturació dels àcids grassos de cadena llarga. Finalment, hem descrit que la proteïna CPT1c es troba implicada en aquest eix.

En el seu conjunt, els resultats obtinguts confirmen el paper important de la CPT1c davant de reptes metabòlics, i aporta nous coneixements dels processos centrals durant el desenvolupament de l'obesitat.

Abstract

Obesity has become a pandemic disease in the last 40 years. The WHO estimates that the population with overweight has nearly tripled since 1975, and the tendency is still growing. These data have an impact on health and on country's healthcare costs. Obesity is a chronic disease of multifactorial origin that is associated to other pathophysiological conditions such as Type 2 Diabetes mellitus. Obesity appears due to an imbalance in the energy metabolism, which is primarily regulated by the hypothalamus, the central structure responsible for integrating signals from the periphery and orchestrating a homeostatic response. In the last years, research has been focused on the molecular mechanisms and the hypothalamic nuclei involved in the dysregulation of energy homeostasis of obesity in order to identify potential therapeutic targets.

This thesis studies the role of the protein carnitine palmitoyltransferase 1c (CPT1c), a neuronal energy sensor, in the regulation of energy homeostasis within the hypothalamus in response to different metabolic challenges. Recently, its expression in the ventromedial nucleus of the hypothalamus (VMH) has been found as necessary for the activation of thermogenesis in brown adipose tissue (BAT) in response to a high-fat diet. The most abundant neuronal population of the VMH nucleus are SF1 neurons. Thus, we have generated a new genetic mouse model deficient in CPT1c in these neurons (SF1-*CPT1c*-KO) to explore the specific function of the protein in these neurons. At the same time, we have studied the role of CPT1c in the central response to long-chain fatty acids (LCFAs). First, we defined the differential effects that saturated and unsaturated LCFAs have on food intake, body weight and brown adipose tissue thermogenesis, as well as the hypothalamic nuclei involved and the possible signalling pathways involved, in wild-type mice (WT). Then we evaluated the same effects on mice deficient for CPT1c (CPT1c-KO).

Results of this thesis showed, on the one hand, that CPT1c in the SF1 neurons is necessary for the metabolic adaptation, facilitating that the peripheral tissues use fat but not glucose as the energy substrate, during the first days of high-fat diet administration and under fasting or cold exposure situation. On the other hand, we have defined that centrally administered LCFAs differently activate satiety and BAT thermogenesis depending on the level of saturation. We have also identified that the hypothalamic nuclei arcuate, paraventricular and VMH are mediators of unsaturated LCFA signals and that LCFAs differently activate the AMPK-ACC axis and FAS expression depending on the level of saturation. Finally, we have described that CPT1c is involved in this axis.

Abstract

Overall, our results confirm the important role of CPT1c under metabolic challenges and provide new knowledge of the central processes underlying obesity development.

TABLE OF CONTENT

Table of content

Table of content

INTRODUCTION

1 Obesity: Pathophysiological frame

Obesity is a chronic multisystemic disease in the modern public health program, but it is not a newly recognized term. In the Classical Greece, it was postulated by Hippocrates that "Corpulence is not only a disease itself but the harbinger of others". Already in that period, it was recognized that obesity is a disease and that it is associated with many comorbidities. The World Health Organization (WHO) reported that worldwide obesity has nearly tripled since 1975. In 2016, WHO declared that more than 1.9 billion adults were overweight, which represents 39% of the adult global population, of these over 650 million were obese (13%) (WHO). The predictive models suggest that the prevalence will continue to rise, since over 340 million children and teenagers between 5 and 19 are currently overweight or obese (**Fig. 1**). Although obesity used to be considered a high-income country problem, nowadays the rate of obesity is rising in low- and middle-income countries, which makes to classify obesity as a pandemic disease. In fact, obesity and overweight already cause more deaths than underweight (WHO). It is also important to highlight that obesity is not only a worldwide health problem with an important impact in patient's quality of life and dependence on polimedication, but also an economic burden because of the healthcare costs. In 2019, the Spanish economic impact was estimated in more than 25,000M€ (2.1% of Spanish GNP) and it is predicted it will rise a 211% up to 2060 ('Global Obesity Observatory').

WHO defined obesity as abnormal or excessive fat accumulation that may impair health and it is diagnosed through the body mass index (BMI). A BMI equal to or greater than 25 stands for overweight and if it is higher than 30, it indicates obesity (WHO). The definition includes the impairment of health because of all the comorbidities linked to obesity, such as type 2 diabetes, cardiovascular diseases and cancer. While increased BMI generally means an increased risk of various complications, this index *per se* is not always sufficient to identify all the individuals with high chances of developing comorbidities. In particular, BMI does not always reflect increased adiposity or fat distribution and it does not take into account additional components such as psycho-social, genetic, environmental, endocrine and microbial factors (Sarma *et al.* 2021). Regarding the psycho-social component, it is important to mention that the classical view of obesity as an imbalance between energy in and energy out has led to a stigmatization of obesity, with the misperception of the disease as a result of personal weakness, such as eating high-sugar

high-fat products and not practising exercise, rather than the result of a complex biological process (Brewis *et al.* 2018). In fact, individuals with obesity are vulnerable to social stigma and discrimination and this fact has a detrimental impact on the mental health of patients (Brewis *et al.* 2018). Because of these reasons, alternative definitions of obesity are being proposed and they should consider the central nervous system (CNS) impairments, among other factors.

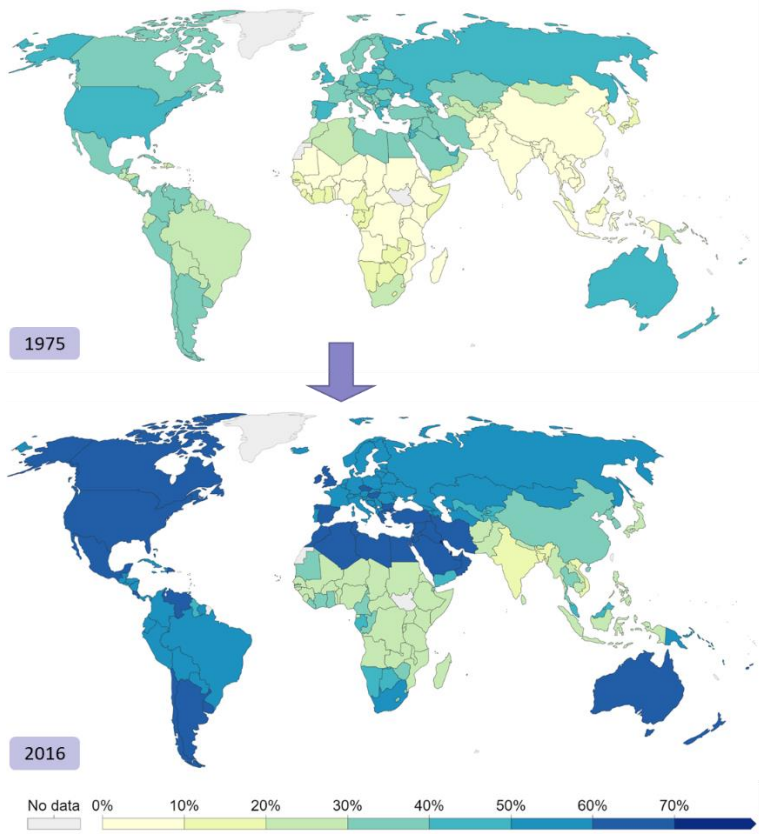

Fig. 1. Worldwide map of prevalence of overweight and obese adults aged ≥ 18 years in 1975 and in 2016. BMI equal or greater than 25 has been considered as overweight. The pattern at 1975 is closely aligned with the richer the country is, the higher obesity trend has. Over years, this pattern has been mostly maintained, but the rate of obesity has increased over the world. Modified from 'Obesity - Our world in data'.

One of the most important aspects of obesity is its association with increased risk of insulin resistance and impaired glucose tolerance, which are early steps for Type 2 Diabetes Mellitus. Obesity has been also correlated with chronic diseases such as hypertension, hypercholesterolemia and hypertriglyceridemia. All these abnormalities present in obesity are described as the metabolic syndrome, as they form a cluster of

simultaneous conditions that increased the prevalence of other disorders such as type 2 diabetes, cardiovascular diseases, musculoskeletal disorders, some cancers and other pathologies reviewed in **figure 2** (Wang *et al.* 2020). Recently, obesity has also been linked to a higher risk of developing COVID-19 infection (Sawadogo *et al.* 2022). These obesity comorbidities are due to a dysfunction of crucial metabolic organs during the progression of the disease. For instance, in the liver, triglycerides accumulation leads to abnormalities of glucose, fatty acid and lipoprotein metabolism, that may result into non-alcoholic fatty liver disease (NAFLD) (Fabbrini *et al.* 2010). Fat is also accumulating in pancreas, which disrupts the pancreatic β-cells and insulin secretion, thus accelerating the process of type 2 diabetes: insulin resistance with less production of insulin (Verma & Hussain 2017). Finally, under overnutrition conditions, adipose tissue expands and remodels, and adipocytes increase in size and number. If this situation is largely maintained over time, fat accumulation appears in ectopic tissues and in the visceral adipose depots causing local inflammation and insulin resistance too. This event is known as lipotoxicity and it is also a trait of obesity (Longo *et al.* 2019).

.

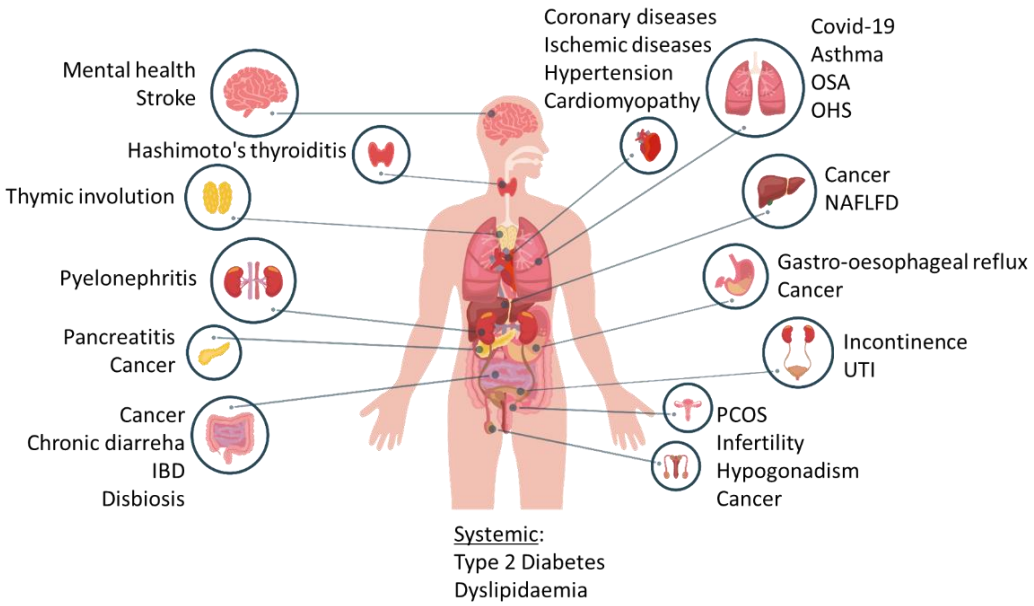

Fig. 2. **Obesity and its main comorbidities affecting systems, organs and tissues**. Obesity is accompanied by a cluster of pathological conditions that increases the prevalence of other disorders. IBD: inflammatory bowel diseases. NAFLD: Non-alcoholic fatty liver disease; OHS: Obesity hypoventilation syndrome; OSA: Obstructive sleep apnoea; PCOS: Polycystic ovary syndrome; UTI: Urinary tract infection.

The investigation of obesity has been largely performed through the use of different mouse models, resembling the metabolic alterations that are found in humans. The monogenic models are mainly focused on the study of the hormones insulin and leptin, but they are far from the reality of the current pandemic situation (Nilsson *et al.* 2012). For this reason, the most accepted model mimicking obesity in humans is the diet-induced obesity (DIO) (Nilsson *et al.* 2012).

Regarding the therapeutic strategies of obesity, people with increased adiposity usually require lifestyle changes with pharmacological treatment and/or bariatric surgery (Sarma *et al.* 2021), depending on the severity of the disease. All these clinical approaches to manage obesity are focussed on reducing food intake and increasing energy expenditure, but it has been demonstrated that this classical treatment is not enough to combat this pandemic situation. This management is usually insufficient as body weight regain is very common: one-third to two-thirds of lost weight is regained within the following year (Tchang *et al.* 2000). Moreover, a new higher body weight set point has usually been established, making it more difficult to lose the weight gained (Tchang *et al.* 2000). In addition, the clinical use of the current anti-obesity drugs is extremely limited due to their off-target actions and side effects (e.g. sympathomimetic actions leading to tachycardia and hypertension). The fact that the molecular mechanisms underlying obesity progression are not well-known hampers the development of more efficient long-term treatments against specific targets.

Against this backdrop, it is a matter of urgency to identify new therapeutic targets and to develop long-term therapeutic approaches against obesity and its comorbidities. These approaches need to be effective and safe. A promising strategy could be the modulation of central and peripheral mechanisms that increases energy expenditure, for example through enhancing thermogenesis activity (Zhang *et al.* 2015). In this thesis, we want to contribute to a better understanding of obesity development, focusing on the changes in the hypothalamus and their impact in the peripheral metabolism.

1.1 Role of the hypothalamus in obesity development

The regulation of energy balance is not only driven by peripheral responses of organs and tissues to nutrients and other signals but also by the control of the CNS, specially through the hypothalamus. The hypothalamus is a primary site of integration of hormone- and nutrient-related signals and central and peripheral neural inputs. All this information is

integrated by different nuclei to emit a response to compensate energy expenditure with calorie intake, with the final aim of maintaining energy homeostasis and stability of the fat depots of the organism (Lam *et al.* 2005a; Velloso & Schwartz 2011).

At the onset of obesity and once it is established, this hypothalamic complex system is impaired and peripheral signals are altered. Overload of fatty acids or a dysfunction in the sensing of these signals by neurons can impair the hypothalamic control of energy and glucose homeostasis and contribute to obesity progression and type 2 diabetes (Moullé *et al.* 2014). Increased circulating levels of leptin or insulin also led to hypothalamic resistance of these hormones, which is also translated into detrimental systemic effects (Thon *et al.* 2016). Moreover, food intake control from the hypothalamus converges to reward circuits that regulate hedonic behaviours. Therefore, alteration of this hypothalamic circuits often drives psychiatric components in individuals with obesity, which is also important to take into account when looking for new therapeutic targets (Dietrich & Horvath 2012).

This thesis is focused on the exploration of some of the hypothalamic mechanisms that sense nutrients and the peripheral signals impaired in obesity development and the study of the specific hypothalamic nuclei involved in these processes.

1.1.1 Hypothalamic nuclei

The hypothalamus is formed by several neural populations grouped into different nuclei, all of them interconnected for the regulation of energy homeostasis (**Fig. 3**).

The paraventricular nucleus of the hypothalamus (PaV) is found in the most anterior and rostral part of the third ventricle. It integrates orexigenic and anorexigenic inputs from other hypothalamic nuclei and, at the same time, it represents the primary hypothalamic output to other satiety regions of the brain. PaV is composed of different neuronal populations, all of them related to feeding behaviour (Sutton *et al.* 2016). Among them, the single-minded homolog 1 (SIM1) expressing neurons are the most abundant type of neurons and are also associated with the regulation of BAT thermogenesis activity. The magnocellular neuroendocrine populations (oxytocin, vasopressin and corticotropin expressing neurons) project to the pituitary. Another important characteristic of PaV neurons is that some of the neurons express the melanocortin 4 receptor (MC4R) that is linked to energy balance control, specifically SIM1 neurons that also expresses MC4R are

closely linked to feeding control (Sutton *et al.* 2016). This nucleus is also related to stress and anxiety responses (Sutton *et al.* 2016) **(Fig. 3)**.

The dorsomedial nucleus of the hypothalamus (DMH) is located from the dorsal to the ventral part of the third ventricle, in a posterior position of PaV. DMH has been largely related to energy expenditure control through the regulation of BAT thermogenesis and through the development of brown adipocytes in white adipose tissue (WAT), both actions associated with neuropeptide Y (NPY) expressing neurons and through the sympathetic nervous system (Bi *et al.* 2012). DMH also participates in the control of food intake (Bi *et al.* 2012) and in the control of body temperature (DiMicco & Zaretsky 2007) **(Fig. 3).**

Following the dorsal-ventral order, the ventromedial nucleus of the hypothalamus (VMH) is recognized for being a nutrient sensing region that controls energy and glucose homeostasis mainly through the regulation of the autonomic nervous system (Fosch *et al.* 2021). This nucleus also contains a high heterogeneity of neuronal populations, but with the particularity that one of these types is only expressed in this nucleus: the steroidogenic factor 1 (SF1) expressing neurons (Fosch *et al.* 2021). As a main core of this thesis, VMH and SF1 neurons will be extensively described in section 2 of the introduction **(Fig. 3)**.

The arcuate (ARC) nucleus, located below the VMH, contains two main neuronal populations, with opposing effects: the anorexigenic pro-opiomelanocortin (POMC) expressing neurons and the orexigenic neuropeptide Y (NPY) / agouti-related peptide (AgRP) expressing neurons (Jais & Brüning 2022). POMC neurons also participate in adipose tissue browning (Quarta *et al.* 2021). ARC is located close to the median eminence which is a privileged location for neurons to integrate hormonal signals and to sense circulating nutrients levels from the periphery with the final aim of regulating feeding behaviour (Jais & Brüning 2022). ARC nucleus has also been associated with glucose homeostasis, blood pressure and innate immune responses (Jais & Brüning 2022) **(Fig. 3).**

Finally, in a more lateral position, the lateral hypothalamic area (LHA) controls feeding behaviour and drinking. LHA is composed of several neuronal populations. Of all of them, the melanin-concentrating hormone expressing neurons are implicated in the regulation of feeding and the orexin producing neurons are also linked to BAT thermogenesis

responses (Oldfield *et al.* 2007). This nucleus is also involved in reward behaviour and sleep control (Stuber & Wise 2016) **(Fig. 3).**

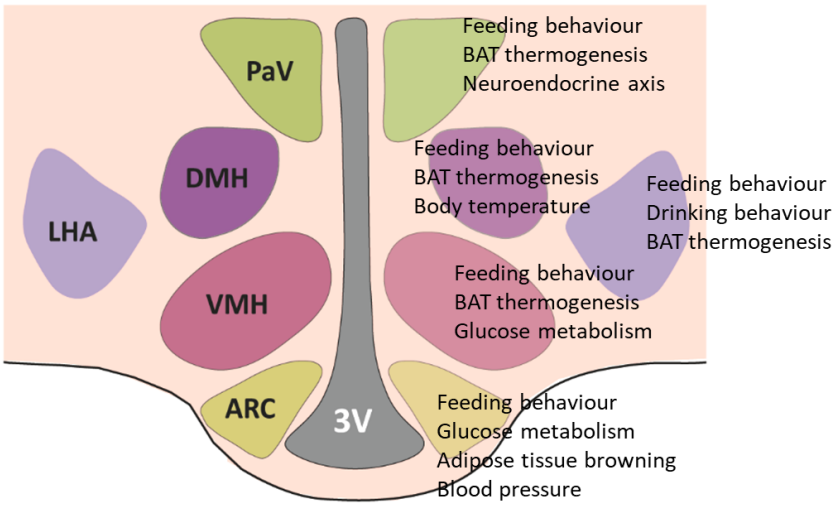

Fig. 3. Hypothalamic nuclei and their main functions. The hypothalamus consists of five different nuclei, all of them interconnected to regulate feeding and energy expenditure. The hypothalamus has the role to maintain energy homeostasis of the organism taking information from different inputs and orchestrating a response to it. ARC: arcuate nucleus; DMH: dorsomedial hypothalamus; LHA: lateral hypothalamic area; PaV: paraventricular hypothalamus; VMH: ventromedial hypothalamus.

1.1.2 Early changes in the hypothalamus during obesity development

Diet-induced obesity leads to the expression of pro-inflammatory cytokines in adipose tissue and other tissues, and it was hypothesized that these cytokines were the cause of systemic inflammation and whole-body insulin resistance (Fresno *et al.* 2011). However, later, it was described that hypothalamic inflammation precedes by many weeks the appearance of systemic inflammation and obesity. In fact, the hypothalamic inflammatory signalling is detected after 1 to 3 days of HFD feeding in rodents and after 1 week in humans (Velloso & Schwartz 2011; Thaler *et al.* 2012). Astrocytes and microglia become activated in the hypothalamus by short-term HFD feeding resulting in their proliferation and the release of pro-inflammatory cytokines (de Git & Adan 2015). These early changes in the hypothalamus act as signals of metabolic adaptation to the nutritional overload but, subsequent administration of HFD disrupts this adjustement followed by the progression of the disease. These observations suggest that some of the detrimental effects of HFD feeding and the systemic complications can be due to an impaired hypothalamic function during the first days of HFD feeding. This hypothesis has been supported by studying

hypothalamic leptin resistance linked to obesity, as it has been described to appear before the disease and it results into a vicious cycle as, once obesity is stablished, leptin resistance leads to overnutrition (de Git & Adan 2015). Impaired leptin receptor trafficking and deficient leptin signalling have been proposed as mechanisms mediating central leptin resistance and both processes have been linked to inflammatory signals and ER stress (de Git & Adan 2015). In addition, insulin signalling is also blunted in an overfeeding situation resulting into central insulin resistance before the peripheral tissues become resistant to this hormone (Scherer *et al.* 2021). In this case, the responsible mechanisms described are a reduction in the intracellular insulin signalling cascade and a reduction of insulin resistance or the BBB transport of this hormone. Hypothalamic inflammation and ER stress have been shown to reduce neuronal insulin signalling followed by systemic diabetes (Scherer *et al.* 2021).

Therefore, leptin and insulin resistance seem to be mediated, at least in part, by HFD-induced inflammation. Consistent with this idea, a reduction of hypothalamic inflammation by inhibition of pro-inflammatory pathways resulted in a reduction of hypothalamic leptin resistance and an improvement of insulin signal transduction and glucose production in the liver (Milanski *et al.* 2012). Central administration of certain fatty acids also resulted in hypothalamic inflammation, evidence which is described in section 4.3 of the introduction. Therefore, circulating dietary fats can contribute to the hypothalamic inflammation before or, at least, in parallel to the systemic inflammation.

1.2 BAT thermogenesis as a possible therapeutic target against obesity

One of the consequences of energy homeostasis impairment during the development of obesity is the impact on adipose tissue function. Two different types of adipose tissue have been described. On the one hand, white adipose tissue (WAT) is the main energy storage in the organism. It is composed of white adipocytes, cells containing uni-locular lipid droplets (LD) and a few mitochondria. On the other hand, BAT is characterized by its thermogenic capacity, producing heat using fat as fuel. BAT is composed of brown adipocytes that contain multi-locular LD and a high amount of mitochondria **(Fig. 4)**. Apart from these two types of adipose tissue, a third one has been described: the beige or brite ("brown in white") adipose tissue, which has intermediate characteristics between BAT and WAT. It is composed of white adipocytes that express thermogenic markers, which makes the cells resemble brown adipocytes, being this process called browning (Jeremic

et al. 2017). It has been described that during obesity development, WAT gets expanded to accumulate more fat, while the amount and functionality of BAT is decreased (Trayhurn 2017).

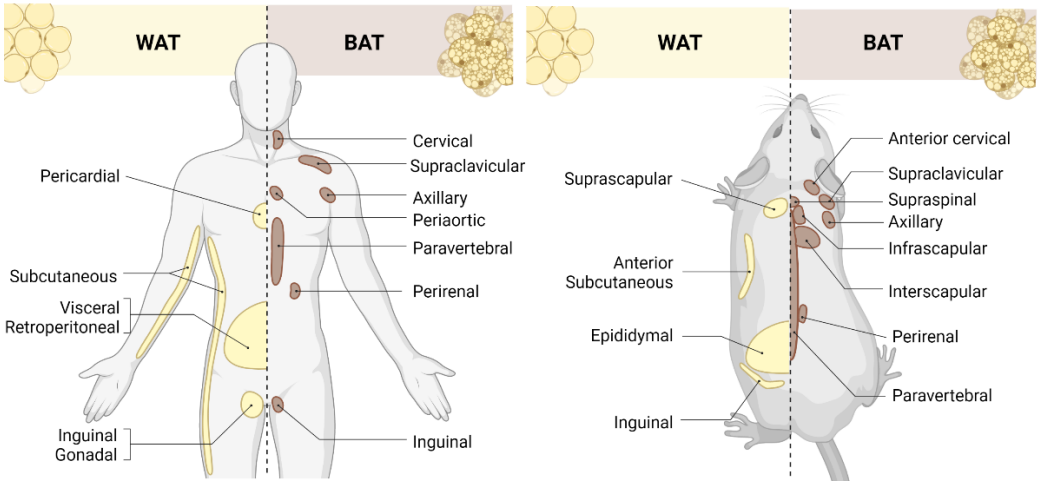

Fig. 4. Schematic representation of WAT and BAT in humans and mice. For a long time, BAT was thought to be found only in rodents and human neonates, but ten years ago, BAT depots were also found in adult humans. Mice and humans share a similar distribution of these fat depots. BAT: brown adipose tissue; WAT: white adipose tissue. Modified from Soler-Vázquez *et al.* 2018; Zhang *et al.* 2018.

BAT was thought to exist only in rodents and newborn humans until 2009, when a functional BAT was described in adult humans **(Fig. 4)**. BAT is present in newborns with the important role of maintaining the temperature of vital organs, then it declines over time, being its mass age- and gender-dependent. Remarkably, BAT can increase up to 20% the daily energy expenditure in humans (Cypess *et al.* 2009).

BAT thermogenesis and browning in WAT are regulated by several neuronal populations and signalling pathways of the hypothalamus. Thermogenesis can be activated by cold exposure or by peripheral signals related to energy status such as leptin or dietary fat. Thus, the hypothalamus integrates all this information and activates an autonomous response through the sympathetic nervous system to BAT or WAT (Contreras *et al.* 2017a). During the development of obesity, there is a substantial decrease in BAT thermogenesis, and this impairment has also been related to hypothalamic inflammation (Arruda *et al.* 2011a) and hypothalamic ER stress (Contreras *et al.* 2014).

These findings suggest BAT as a great target for treating obesity. Different therapeutic approaches are currently under study such as an induction of BAT thermogenesis activity,

browning of WAT or their regulators (Whittle *et al.* 2013). Another therapeutic approach under investigation is the transplantation of brown or beige cells to obese mice (Soler-Vázquez *et al.* 2018). Although thermogenesis has been widely studied, there are still some unresolved questions related to the hypothalamic control of BAT, particularly which factors are activating thermogenesis and how.

2 SF1 neurons in obesity and diabetes

2.1 Location of SF1 neurons within the VMH and gene expression pattern

Within the hypothalamus, the VMH was identified in the mid-1900s as the satiety centre, and when it was injured resulted in hyperphagia as well as body weight gain (Hetherington & Ranson 1942). Later, this nucleus was described to play an important role in the central control of glucose homeostasis: VMH-lesioned rats had the counterregulatory response (CRR) blunted to hypoglycemia (Borg *et al.* 1994). Lesions in VMH also resulted in decreased core body temperature (Monda *et al.* 1997a) and decreased post-prandial BAT thermogenesis (Monda *et al.* 1997b). Since then, a vast number of studies have been focusing on the role and the different type of neurons that integrates VMH **(Fig. 5)**. Nowadays, with all the new techniques and approaches developed, several investigations relating VMH to glucose and energy homeostasis have been published, specially targeting SF1 neurons, as these neurons are VMH-exclusive.

SF1 neurons can be found in the dorsomedial (VMHdm) and central regions (VMHc) of VMH **(Fig. 5)**. These neurons express the nuclear receptor steroidogenic factor 1 (SF1), whose gene is also officially designated as *NR5A1*. This factor is considered a key marker of VMH in the brain, although it can be found in other organs such as the pituitary gland, gonads, adrenal cortex and spleen (Parker *et al.* 2002). In all tissues where it can be found, it has an essential role during development. Focusing on the brain, SF1 is expressed at embryonic d9 (E9.5) in the embryonic ventral diencephalon, the area where VMH will develop (Ikeda *et al.* 2001). Initially, SF1 was classified as an orphan nuclear receptor but, after 2007, several studies demonstrated that phospholipids can be ligands of SF1, modulating its activity. This factor controls the expression of various downstream genes, including CB1, BDNF and Crhr2 (Hoivik *et al.* 2010). To explore the importance of SF1, different researchers studied transgenic mice lacking this nuclear receptor. Mice lacking SF1 died shortly after birth due to a failure in the development of adrenal glands and

gonads (Sadovsky *et al.* 1995). This outcome was solved by an adrenal transplant from wild-type (WT) mice and corticosteroid injections. These mice presented increased adiposity resulting in a robust body weight gain (Majdic *et al.* 2002). Interestingly, a similar phenotype could be observed in humans with the *SF1* gene mutated, showing mild to severe obesity (Correa *et al.* 2004; Hasegawa *et al.* 2004).

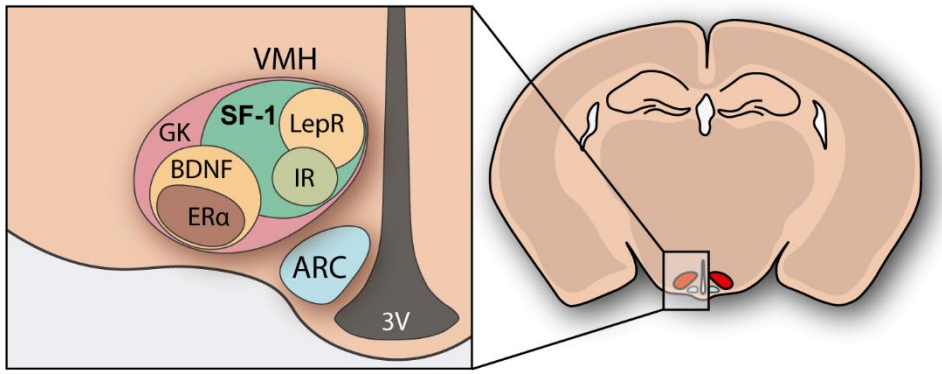

Fig. 5. Schematic illustration of the location of SF1 neurons and other genes highly expressed in the VMH. The majority of the VMH neurons expresses the SF1 nuclear receptor, especially those found in the dorsomedial and in the central region of the VMH. SF1: steroidogenic factor 1. Adapted from Fosch *et al.* 2021.

Some years later, CNS – specific pre- and post-natal SF1-KO mice were developed (Zhao *et al.* 2008; Kim *et al.* 2011). Pre-natal SF1 deletion resulted in decreased expression of leptin receptors and, when exposed to HFD, mutant mice were obesogenic (Kim *et al.* 2011). However, mice with this pre-natal deletion exhibit also structural abnormalities and altered distribution of cells in the VMH nucleus (Davis *et al.* 2004), therefore the phenotype could be due to the lack of the steroidogenic factor or to the impaired VMH architecture. Post-natal SF1 deletion maintained VMH structure, but mice still presented increased body weight when fed with HFD, accompanied by markedly increased adiposity, reduced BAT thermogenesis and high glucose, insulin and leptin levels (Kim *et al.* 2011). Later studies showed that SF1 expression was also needed for the beneficial effects of exercise in metabolism, such as increased energy expenditure and better glycaemia (Fujikawa *et al.* 2016). All these results suggested that SF1 is post-natally required in the VMH for a proper energy homeostasis, especially for the metabolic adaptation to a HFD. In the attempt to clarify SF1 neurons contribution to energy and glucose homeostasis, several transgenic mice models have been developed by deleting specifics genes in SF1 neurons in the last 16 years. Also, new neuronal-based approaches such as optogenetics

and chemogenetics have provided insights into the implication of SF1 neurons on energy balance and glucose metabolism.

2.2 SF1-CRE transgenic mice to study SF1 neurons

2.2.1 Cre-loxP system

The Cre-loxP recombination system has evolved as a powerful tool to manipulate DNA molecules with the aim of studying the specific role of a gene in a specific cell type, area or tissue, even at a specific time – point (McLellan *et al.* 2017). This strategy of recombination has a potential use for overcoming all the limitations such as lethality or secondary effects in other tissues that global knock-out mice were presenting. From then, the Cre-loxP is used for specific Knock-out mice generation **(Fig. 6)**.

Because of the interest in SF1 neurons, different groups generated a transgene that targets Cre expression in tissues that express SF1 (Bingham *et al.* 2006; Dhillon *et al.* 2006) **(Fig. 6)**. Thanks to the availability of this SF1-Cre mouse line, the specific role of SF1 neurons has been studied using the optogenetic and the chemogenetic approaches, but also the specific role of various proteins in this kind of neurons has been found through the generation of SF1 specific Knock – out mice, explained below and reviewed in **Table 1** and in Fosch et al. 2021.

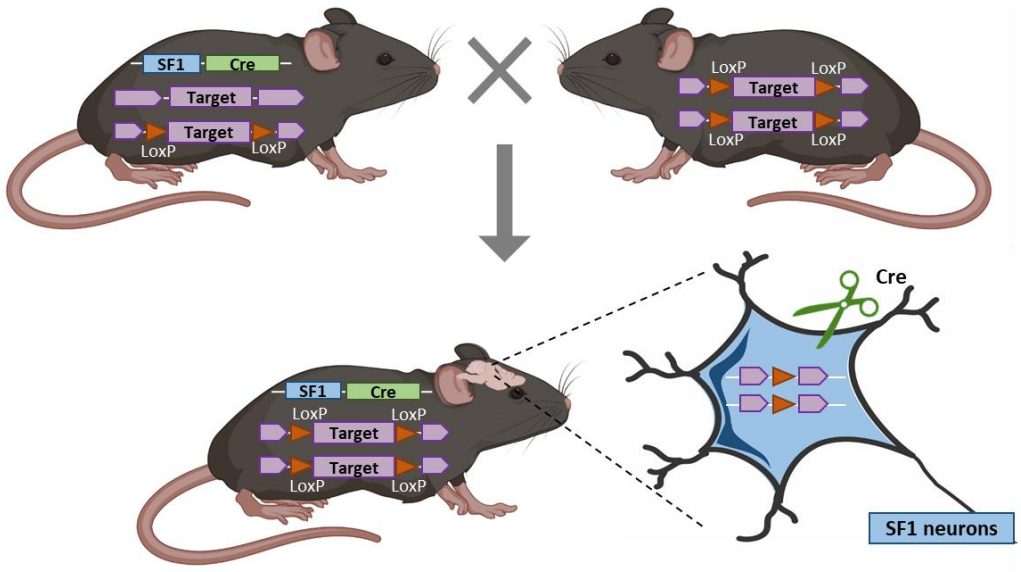

Fig. 6. Schematic representation of Cre-loxP technology on SF1 neurons. The target region of the gene is flanked by two LoxP sequences and, once recombined, it will be excised. Cre is only expressed under the SF1 promotor and it will recombine the LoxP sequences.

2.2.2 SF1 rodent models used for optogenetic and chemogenetic approaches

The incorporation of optogenetic and chemogenetic approaches allows researchers to manipulate a specific neuronal population in a physiological context and in a temporal and spatial resolution, which results in an improved understanding of the role of these neurons, but also the neuronal circuits where these neurons participate (Rein & Deussing 2012; Sternson & Roth 2014)

Focusing on the optogenetic approach, SF1-Cre mice were injected with adeno-associated virus (AAV) particles expressing channel-rhodopsin (ChRs) in a Cre dependent manner, which resulted in the expression of this type of channel only in SF1 neurons of the VMH (Viskaitis *et al.* 2017; Zhang *et al.* 2020). Activation of SF1 neurons resulted in a different effect depending on the frequency used. High frequency (>20 Hz) activation was linked to defensive behaviour, but low frequency (2Hz) activation did have an effect on food intake, which was suppressed after fasting (Viskaitis *et al.* 2017). Regarding the chemogenetic approach, SF1-CRE mice were injected with AAV expressing the hM3Dq and hM4Di designer receptors activated by designer drugs (DREADDs) in a Cre depending manner. The expression of these two kinds of receptors in SF1 neurons allow to excite or inhibit them respectively in response to clozapine (CNO) (Coutinho *et al.* 2017). In line of the optogenetic-based results, administration of CNO to mice expressing hM3Dq in SF1 neurons resulted in a reduction of food consumption and body fat mass, and the opposite results were observed when CNO was administrated to mice expressing hM4Di (Viskaitis *et al.* 2017). More recently, it was discovered that mice expressing hM3Dq in SF1 neurons had an increased energy expenditure and fat oxidation within 2-hour of CNO administration (Zhang *et al.* 2020), which would explain the decrease in body fat mass observed before. In mice expressing tetanus toxin in SF1 neurons, mimicking the inhibition of these neurons, energy expenditure was reduced (Flak *et al.* 2020).

If we focus on the hypothalamic regulation of glucose metabolism, SF1 neurons also have a role. Optogenetic stimulation of these neurons induced diabetic-hyperglycemia because of the activation of the CRR. On the other hand, optogenetic inactivation of SF1 neurons blocked recovery from insulin-induced hypoglycemia (Meek *et al.* 2016). By contrast, chemogenetic stimulation induced a non-significant increase in the basal blood glucose levels but it did increase whole-body glucose utilization, especially in red-type skeletal muscle, heart and BAT. This CNO activation by hM3Dq also resulted in increased insulin sensitivity (Coutinho *et al.* 2017).

Altogether, selective activation and inhibition of SF1 neurons have proved their involvement in the metabolic regulation of energy balance and blood glucose levels.

2.2.3 Rodent models lacking hormone receptors in SF1 neurons

The physiological effect of the anorectic hormone leptin in SF1 neurons has been deeply studied because of its key role in the central control of energy homeostasis. Abrogating leptin signalling in SF1 neurons through deletion of leptin receptor (LEPR) resulted in deficient adaptation to HFD or to an inability to activate energy expenditure (e.g., thermogenesis) (Dhillon *et al.* 2006) **(Fig. 7)**. To better understand the role of the leptin pathway in this neuronal population, mice with selective inactivation of negative mediators of the central leptin pSTAT3 signalling such as SOCS3, the subunit $G_s\alpha$ of G-protein coupled receptor or PTP1B were developed. In these models, and conversely to the deletion of LEPR, the weight-reducing effects of leptin were enhanced: mice presented a reduction in food intake and an improvement in energy expenditure in chow diet or HFD condition. Therefore, these mice presented resistance to DIO and hypersensitivity to leptin (Bence *et al.* 2006; Zhang *et al.* 2008; Berger *et al.* 2016) **(Fig. 7) (Table 1)**. Deletion of the PTP1B, a negative mediator of STAT3, showed an increase in adiposity only in female mice fed HFD, although leptin sensitivity was enhanced. These mice also presented increased insulin response, which could overcome the hypersensitivity to leptin with the final result of adiposity induction (Chiappini *et al.* 2014). These findings reinforce the importance of leptin signalling in energy balance through SF1 neurons.

Leptin also plays a role in glucose homeostasis improving insulin sensitivity, as intra-VMH injection of leptin resulted in increased glucose uptake in peripheral tissues (Minokoshi *et al.* 1999) and normalized hyperglycemia in mice lacking LEPR in SF1 neurons (Meek *et al.* 2013). Mice lacking the negative leptin-mediator SOCS3 in SF1 neurons had improved glucose homeostasis **(Fig. 7) (Table 1)**, being protected from the disturbances of hyperglycemia and hyperinsulinemia caused by HFD feeding (Zhang *et al.* 2008). However, the restoration of LEPR only in SF1 neurons in LEPR-KO mice did not protect against obesity (Senn *et al.* 2019) and it was insufficient to mediate the antidiabetic leptin's action (Gonçalves *et al.* 2014). Therefore, SF1 neurons work in conjunction with other types of neurons also expressing LEPRs, and this neuronal population by itself cannot compensate for the whole-brain receptor deficiency.

Another key hormone implicated in the balancing of energy metabolism is insulin. Blunted expression of insulin receptor (IR) in SF1 neurons protects mice from obesity and improves glucose homeostasis and leptin sensitivity when fed HFD (Klöckener *et al.* 2011) **(Fig. 7) (Table 1)**. In conformance with that, deletion of FOXO 1, a downstream transcription factor of insulin, in SF1 neurons concluded in lean mice with high energy expenditure an enhanced insulin sensitivity and glucose tolerance, the same phenotype as deleting IR (Kim *et al.* 2012).

Leptin depolarizes or hyperpolarizes SF1 neurons, while insulin only hyperpolarizes them, both actions in a downstream PI3K-dependent manner (Xu *et al.* 2005, 2010; Dhillon *et al.* 2006; Sohn *et al.* 2016) **(Fig. 7).** One of the subunits of PI3K is p110, specifically, the subunit p110β is necessary for depolarizing and hyperpolarizing SF1 neurons, while p110α is only needed in the hyperpolarization process (Sohn *et al.* 2016). Mice lacking any isoforms of the subunit p110 in SF1 neurons presented an obesogenic phenotype due to decreased energy expenditure (reduced thermogenesis) (Xu *et al.* 2010; Fujikawa *et al.* 2019) **(Table 1)**. Although leptin and insulin can depolarize SF1 neurons using the same molecular cascade, they are anatomically segregated within VMH (depolarizing neurons expressing LEPR are located in the VMHdm and hyperpolarizing LEPR neurons are scattered throughout the nucleus, whereas those expressing IR are in the VMHc close to the 3rd ventricle) (Sohn *et al.* 2016) **(Fig. 5)**.

The role of estrogens in SF1 neurons has also been studied because of the definition of VMH as a sex-dimorphic nucleus. Female mice lacking the estrogenic receptor α (ERα) presented increased adiposity and reduced BAT thermogenesis activity resulting in higher body weight when fed a HFD, whereas no differences were observed in male mice (Xu *et al.* 2011) **(Table 1).**

All the studies performed using specific KO mice indicate VMH as a key nucleus for regulating energy expenditure specially during the adaptation to a HFD feeding, as most of the mouse models only presented phenotypic alterations under this kind of diet **(Table 1)**.

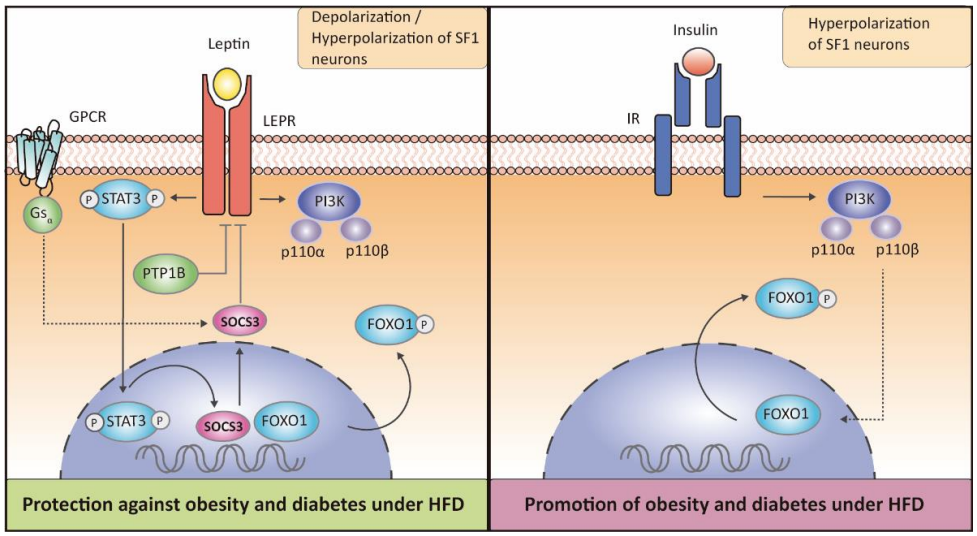

Fig. 7. Leptin and insulin signalling in SF1 neurons. Through the generation of different specific KO mice in SF1 neurons, the role of different targets associated to energy metabolism has been studied in this neuronal population. Overall, the action of leptin signalling triggers protection against obesity and diabetes while insulin signalling promotes obesity and disrupts the glucose metabolism under HFD feeding. Modified from Fosch *et al.* 2021.

2.2.4 Rodent models lacking the nutrient sensors AMPK and SIRT1 in SF1 neurons

In the homeostatic control of energy balance, AMPK and SIRT1 play a critical role as nutrient and energy sensors in response to metabolic challenges, particularly in SF1 neurons.

AMPK is a highly conserved regulator of metabolism, which under low energy conditions, increases energy production and reduces energy expenditure. Dr Miguel Lopez' lab has reported that the specific deletion of $AMPK_{\alpha1}$ isoform in SF1 neurons resulted in a lean phenotype feeding-independent (Seoane-Collazo *et al.* 2018) **(Table 1)**. Mice presented DIO resistance due to the increased energy expenditure via overactivation of BAT thermogenesis activity and WAT browning induction. These mice were also protected from the obesity-associated impairment of glucose metabolism, although no changes were observed in insulin sensitivity (Seoane-Collazo *et al.* 2018) **(Table 1)**. Another study reported the role of AMPK in glucose sensing in SF1 neurons, suppression of AMPK activity led to selective depletion of SF1 glucose-inhibited (GI) neurons, which activated CRR without affecting the presence of glucose-excited (GE) neurons. These findings support the idea of two different subsets of SF1 neurons: the one regulating hyperglycemia by enhancing insulin sensitivity and the second one regulating hypoglycemia by activating

CRR (Quenneville *et al.* 2020). Recently, extracellular vesicles directed to SF1 neurons of the VMH containing a plasmid encoding an $AMPK_{\alpha 1}$ dominant-negative mutant have been developed. Administration of these vesicles resulted in a remarkable weight reduction due to a significant increase of BAT thermogenesis activity. Interestingly, this therapeutic approach did not show rebound effects neither hepatic nor cardiovascular side effects, being a promising therapeutic platform to manage obesity (Milbank *et al.* 2021).

Apart from AMPK, the deacetylase SIRT1 is also highly expressed in the VMH where participates in the adaptive response to fasting (Ramadori *et al.* 2008). Deletion of SIRT1 expression in SF1 neurons resulted in hypersensitivity to DIO, with higher body weight and lower energy expenditure in a food-intake independent manner **(Table 1)**, whereas SIRT1 overexpression protects against dietary diabetes (Ramadori *et al.* 2011). This protein has also been involved in the synchronization of the circadian clock in SF1 neurons (Orozco-Solis *et al.* 2015).

Overall, SIRT1 and AMPK in SF1 neurons can be other possible targets for obesity treatment through their impact on energy expenditure and, in the final term, on body weight.

2.2.5 Importance of glutamatergic neurotransmission and synaptic receptors in SF1 neurons

SF1 neurons are mainly glutamatergic and the impact of impairing their transmission has been studied using a mouse lacking VGLUT2, the synaptic vesicular transporter needed to uptake glutamate into synaptic vesicles **(Fig. 8)**. These mice were not able to raise glucagon levels, resulting in an attenuated response to insulin-induced hypoglycemia and central 2-deoxyglucose (2-DG) administration (Tong *et al.* 2007) **(Table 1).** Disruption of the metabotropic glutamate receptor mGluR5 also showed the importance of the glutamatergic neurotransmission in SF1 neurons, as female, but not male mice, had the glucose balance impaired (Fagan *et al.* 2020) **(Table 1).**

A synaptic receptor regulating the excitability of SF1 neurons is the subunit α2δ-1 of the high-voltage calcium channel. The group led by Dr Maribel Rios has demonstrated that α2δ-1 is essential for excitability and firing activity of SF1 neurons, showing a non-canonical role of this receptor to control glucose and lipid homeostasis (Felsted *et al.* 2017, 2020) **(Fig. 8) (Table 1).** Male mice lacking α2δ-1 presented impaired lipolysis and insulin resistance (Felsted et al., 2017), but female mice presented the opposite effects:

enhanced glycaemic control and increased insulin sensitivity. When female mice were exposed to HFD, this better control of glucose metabolism was abolished (Felsted et al., 2020) **(Table 1).**

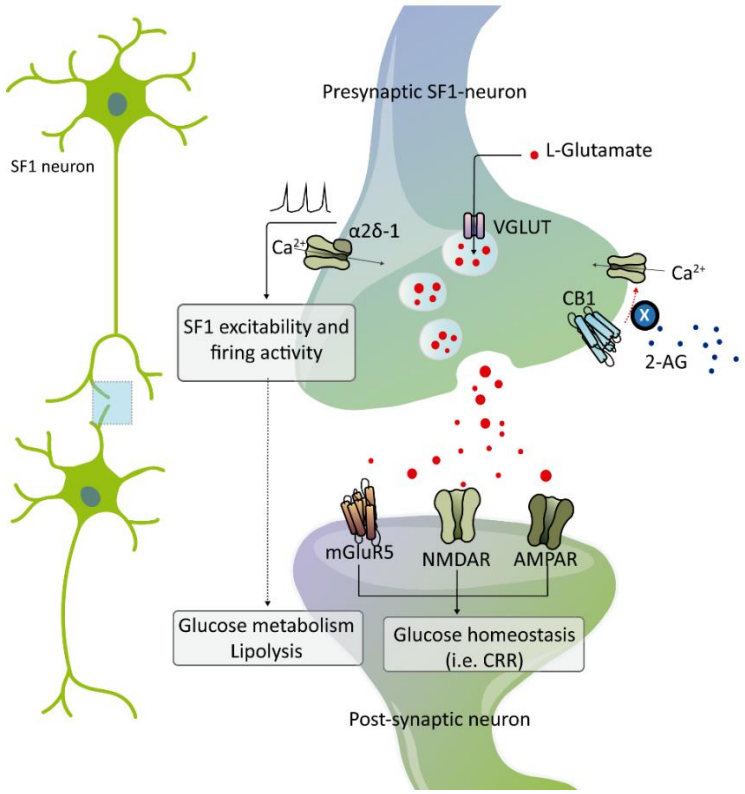

Fig. 8. Glutamatergic neurotransmission and synaptic receptors in SF1 neurons related to energy balance. Different transporters and receptors have been described to be important for a proper SF1 neuronal activity to control food intake and glucose metabolism as a result of the generation of different SF1-Cre transgenic mice. 2-AG: 2-Arachidonoylglycerol (endocannabinoid); AMPAR: glutamatergic AMPA receptor; mGluR1/5: metabotropic glutamate receptor 1/5; NMDAR: glutamatergic NMDA receptor; VGLUT2: vesicular glutamate transporter 2. Modified from Fosch *et al.* 2021.

The endocannabinoid system also has a role in SF1 neurons neurotransmission. CB1 receptor in this type of neurons is a key player in the metabolic switch when feeding HFD since its deletion resulted in decreased adiposity under chow diet and in an obesogenic phenotype under HFD (Cardinal *et al.* 2014) **(Table 1)**.

All the findings presented above support the idea of SF1 neurons as key players in the central regulation of energy homeostasis and glucose homeostasis, with particular importance in the metabolic adaptation to HFD feeding. Most of the mutant mice

presented no changes to mild metabolic alterations under chow diet, but they show important metabolic dysregulations under HFD exposure.

These studies also indicate the sexual dimorphism in the VMH neurons. The first evidence was that females had higher ER concentration than males within the VMH (Cao & Patisaul 2011). Estrogens could affect and change some intracellular signalling cascades leading to these differences between males and females. Other sex-specific effects observed in SF1 neurons were described in their synapses with POMC neurons. Estradiol attenuated the retrograde inhibitory endocannabinoid signalling from POMC to SF1 neurons, so the glutamatergic input was increased (Fabelo *et al.* 2018). Therefore, estrogens may also interact with other neurons acting on SF1 neurons. Most of the studies presented were performed only on male mice and those using mice of both sex resulted in different outcomes between them **(Table 1)**.

2.3 Circuitry of SF1 neurons in the control of body weight and glucose homeostasis

As the glutamatergic transmission of SF1 neurons is needed for a proper metabolic adaptation, it is important to also describe the neurocircuitry of SF1 neurons to other brain areas. To trace SF1 axonal projections, two models have been used: $SF1^{TauGFP}$ mice and $Z/EG^{Sf1:Cre}$ mice, both expressing a fluorescent protein only in SF1 neurons (Cheung *et al.* 2013).

SF1 neurons project to other nuclei in the hypothalamus, thalamus, the basal forebrain and the brainsteam. Regarding the hypothalamus, SF1 neurons signal to other areas of the hypothalamus related to body weight regulation, such as PaV (Cheung *et al.* 2013; Xu *et al.* 2017). Using optogenetics, a fibre optic was implanted into the PaV in SF1-ChR2 mice, so the light only stimulated SF1-PaV projections. This photostimulation caused a reduction in food intake (Zhang *et al.* 2020) **(Fig. 9)**.

Regarding the role of SF1 neurons in regulating glycaemia, the sitmulation by an optogenetic strategy revealed that SF1 neurons projected to the anterior bed nucleus of the stria terminalis (aBNST) to increase blood glucose level (Meek *et al.* 2016) **(Fig. 9).**

Summing up, SF1 neurons play a key role in the central control of blood glucose levels, insulin sensitivity in peripheral tissues, food intake and energy expenditure including thermogenesis activation. This neuronal population is also involved in the metabolic

switch needed to adapt to HFD feeding. Due to the outcomes in the studies evaluating glucose metabolism, it has been demonstrated that SF1 neurons are divided into distinct subpopulations. Another key point of SF1 neurons is that they have sex-specific effects. Finally, it is necessary to be mentioned that possible developmental compensatory mechanisms can occur when using pre-natal specific KO mice. This adaptation can mask the specific roles of SF1 neurons.

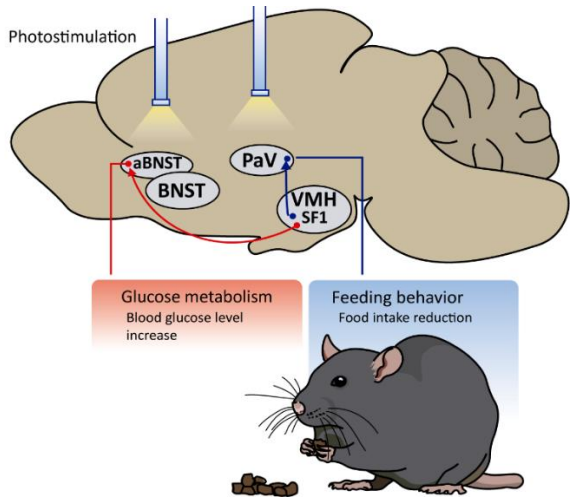

Fig. 9. Neurocircuitry of SF1 neurons to other brain areas to control energy and glucose metabolism. Using optogeneitc tools it has been described that SF1 neurons project to the PaV to regulate feeding behaviour and to the aBNST to regulate glucose homeostasis. aBNST: anterior bed nucleus of the stria terminalis; PaV: paraventricular nucleus; VMH: ventromedial hypothalamus. Modified from Fosch *et al.* 2021.

Table 1. Specific knock-out transgenic models developed to study SF1 neurons in energy balance and glucose homeostasis. Extracted and adapted from Fosch *et al.* 2021.

Type of target	Target	Sex	Challenge	BW	FI	EE	Adiposity	Glycaemia	Glucose tolerance	Insulin sensitivity	Leptin sensitivity	SNS activity	Ref.
Hormone receptors and related signaling pathways	LEPR	M	SD	↑	n.s.	n.s.	↑	n.s.	-	-	-	-	(Dhillon *et al.* 2006)
			HFD	↑	↑	↓	↑	n.s.	-	-	-	-	
	SOCS3	M	SD	n.s.	↓	↓	-	↓	↑	↑	↑	-	(Zhang *et al.* 2008)
			HF-HS	n.s.	↓	↓	-	↓	↑	↑	↑	-	
			Leptin[(a)]	↓	↓	-	-	-	-	-	↑	-	
	$G_s\alpha$	M[(b)]	SD	n.s.	n.s.	n.s.	-	n.s.	n.s.	n.s.	n.s.	-	(Berger *et al.* 2016)
			HFD	n.s.	n.s.	n.s.	-	↓	↑	↑	↑	-	
	PTP1B	F	HFD	↑	↓	↓	↑	-	-	↑	↑	↓	(Chiappini *et al.* 2014)
		M	HFD	n.s.	-	-	n.s.	-	-	-	-	-	
	IR		SD	n.s.	n.s.	n.s.	n.s.	-	-	-	-	-	(Klöckener *et al.* 2011)
			HFD	↓	↓	n.s.	↓	n.s.	↑	↑	↑	-	
	p110α	M	SD	n.s.	n.s.	n.s.	n.s.	n.s.	-	n.s.	↓	-	(Xu *et al.* 2010)
			HFD	↑	n.s.	↓	↑	-	-	-	-	-	
	p110β	M	SD	n.s.	n.s.	↓BAT th.[(C)]	n.s.	n.s.	↓	↓	-	-	(Fujikawa *et al.* 2019)
			HFD	↑	n.s.	↓	↑	↑	-	-	-	-	
	FOXO1	M	SD	↓	n.s.	↑	↓	-	-	-	-	-	(Kim *et al.* 2012)
		F	SD	↓	n.s.	↑	↓	-	-	-	-	-	
		M	HFD	↓	n.s.	↑	↓	↓	↑	↑	↑	-	
	ERα	F	SD	↑	n.s.	↓	↑	n.s.	↓	-	-	-	(Xu *et al.* 2011)
		F	HFD	↑	n.s.	↓	↑	-	-	-	-	↓	
Nutrient sensors	$AMPK_{\alpha1}$	M	SD	↓	n.s.	↑	↓	-	-	-	-	↑ [(d)]	(Seoane-Collazo *et al.* 2018)
		M	HFD	↓	n.s.	↑	↓	↓	↑	n.s.	-	-	
	SIRT1	M/F	SD	n.s.	n.s.	n.s.	n.s.	n.s.	-	-	-	-	(Ramadori *et al.* 2011)
			HFD	↑	n.s.	↓	↑	↑	↓	↓	↓	-	

Continuation of Table 1

Type of target	Target	Sex	Challenge	BW	FI	EE	Adiposity	Glycemia	Glucose tolerance	Insulin sensitivity	Leptin sensitivity	SNS activity	Ref.
Glutamatergic neurotransmission and synaptic receptors	VGLUT2	M/F	SD	n.s.	-	-	-	↓	-	-	-	-	(Tong *et al.* 2007)
		M/F	HFD	↑	↑	n.s.	↑	-	-	-	-	-	
	mGluR5	F	SD	n.s.	n.s.	n.s.	-	n.s.	↓	↓	-	↓	(Fagan *et al.* 2020)
		M	SD	n.s.	n.s.	n.s.	-	n.s.	n.s.	n.s.	n.s.	n.s.	
		M/F	HFD	n.s.	n.s.	n.s.	-	-	-	-	-	-	
	α2δ-1	M	SD	n.s.	n.s.	n.s.	n.s.	n.s.	↓	↓	-	↓	(Felsted *et al.* 2017, 2020)
		M	HFD	n.s.	n.s.	n.s.	n.s.	n.s.	n.s.	n.s.	-	-	
		F	SD	n.s.	n.s.	n.s.	n.s.		↓	↓	-	-	
		F	HFD	n.s.	n.s.	n.s.	n.s.	n.s.	↓	↓	-	↑	
	CB1	M	SD	n.s.	n.s.	↑BAT th.	↓	n.s.	↑	↑	↑	↑	(Cardinal *et al.* 2014)
		M	HFD	↑	↑	n.s.	↑	-	↓	n.s.	↓	↓	

n.s.: No significant changes appreciated; -: not studied/unknown; BAT th.: brown fat thermogenesis; BW: body weight; EE: energy expenditure; F: female; FI: food intake; HF-HS: high fat-high sucrose diet; HFD: high-fat diet; M: male; SD: standard diet; SNS: sympathetic nervous system; Ref.: rerefenreces.

[(a)] Subcutaneously implanted osmotic minipumps, infusing for 14 days at 0,5 g/h. [(b)] The study was performed on both males and females, but the metabolic alterations were only appreciated in male mice. [(c)] No changes in EE but a significant decrease in BAT thermogenesis. [(d)] Increased sympathetic activity in brown fat.

3 Carnitine Palmitoyltransferase 1C, a key target in hypothalamic obesity

Carnitine palmitoyltransferase 1 C (CPT1c) was the last member of the carnitine palmitoyltransferase (CPT) family to be discovered and it is the most puzzling of the isoforms. This family of proteins has been considered to facilitate the transport of long-chain fatty acids (LCFA) inside the mitochondria, so they can be oxidized through the process of β-oxidation (Casals *et al.* 2016).

Four different isoforms belong to the CPT family: the CPT2, which can be found in the mitochondrial inner-membrane and it is ubiquitously expressed in the organism (Demaugre *et al.* 1990), the CPT1a, which is found in the mitochondrial outer membrane and it is expressed in liver, lungs, intestine, ovary, pancreas and brain, the CPT1b, which is also found in the outer membrane of the mitochondria but it is expressed particularly in muscle, brown adipose tissue and testis (McGarry & Brown 1997) and, finally the CPT1c, which is found in the endoplasmic reticulum (ER) and it is only expressed in neurons. CPT1c will be described in detail in this section. The canonical isoforms CPT1a and b catalyse the transesterification of acyl-CoA esters and carnitine to form acylcarnitine esters, that can be transported through membranes by specific translocases. Apart from acylcarnitine esters, Coenzyme A is also produced in this reaction **(Fig. 10)**. CPT2 transforms acyl-carnitines to acyl-CoA to later be transported to the mitochondrial matrix, where it will be oxidised (Casals *et al.* 2016).

A common characteristic of the CPT1 isoforms is their physiological inhibitor malonyl-CoA (Casals *et al.* 2016), an intermediate precursor of the fatty acid (FA) synthesis **(Fig. 10)**. It is important to highlight that levels of malonyl-CoA fluctuate depending on the nutritional status of the organism, particularly in the hypothalamus, being a signal of the energy depots to the hypothalamus (Lane *et al.* 2008).

3.1 General features of CPT1c

CPT1c was discovered using *in silico* sequences 20 years ago when Price and colleagues were searching expressed sequence tag (EST) using the CPT1a sequence (Price *et al.* 2002). Results showed similarities in the sequences of mouse and human clones, but at the same time the senquences found were different from CPT1a and mainly expressed in

the brain. They named the new gene CPT1c because of the cDNA's high affinity to the two other isoforms CPT1a (81.6% of affinity) and CPT1b (85% of affinity). Regarding tissue distribution, CPT1c was primarily expressed in the mammalian brain and testis and the human clone was also found in tumour cells (Price *et al.* 2002). Some years later, another study was focused on exploring CPT1c expression in brain cells, they found CPT1c was enriched in areas of the hypothalamus related to food intake and energy expenditure (PaV, VMH and ARC) and also in the amygdala and in the hippocampus (Dai *et al.* 2007). It was also described that CPT1c was found predominantly in neuronal cell bodies and was not detectable in glial cells or endothelial cells (Dai *et al.* 2007; Sierra *et al.* 2008). CPT1c is also expressed in the peripheral nervous system (Rinaldi *et al.* 2015).

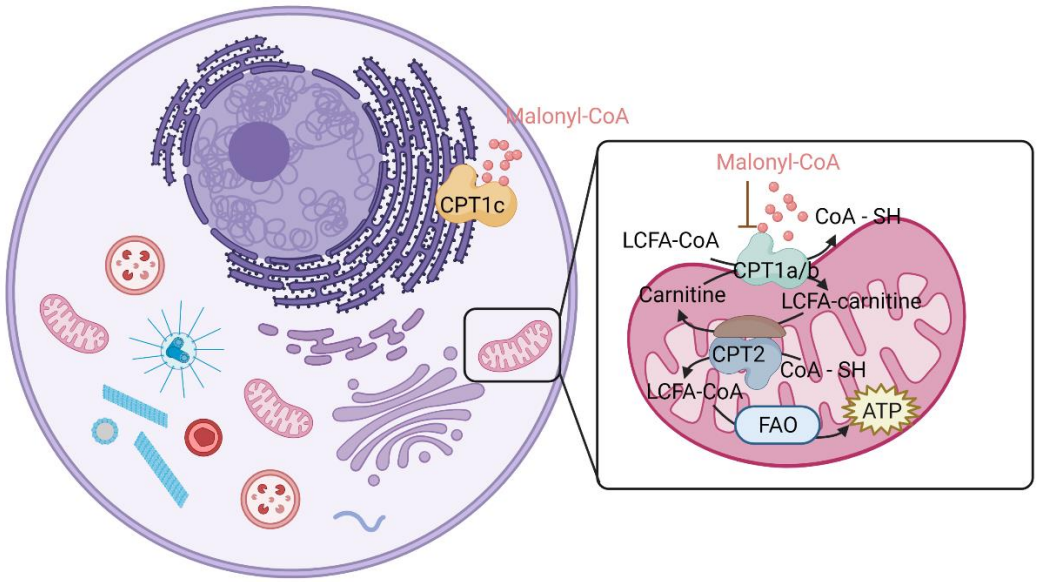

Fig. 10. Carnitine palmitoyltransferase (CPT) enzymes and their cellular location. Schematic representation of the whole cell and mitochondria with the canonical CPT isoforms and their activity. CPT1a and CPT1b are found in the outer membrane of the mitochondria, while CPT1c is found on the ER. The isoforms CPT1a and CPT1b are negatively regulated by malonyl-CoA levels, while this metabolite modulates the interaction of CPT1c with other proteins. CoA: Coenzyme A; ER: endoplasmic reticulum; FAO: fatty acid oxidation; LCFA: long-chain fatty acids. Adapted from Casals *et al.* 2016.

According to subcellular localization, CPT1c was first described to be localized at the outer mitochondrial membrane (Price *et al.* 2002; Dai *et al.* 2007), as the canonical isoforms CPT1a and b, and also in the microsomal fraction (Price *et al.* 2002), but later our group demonstrated that CPT1c colocalizes with ER markers and not with mitochondrial markers

(Sierra *et al.* 2008). Therefore, CPT1c is found in the ER, in contrast to the other two canonical isoforms.

Exploration of CPT1c activity revealed that CPT1c has all the motifs related to carnitine acyltransferase activity conserved as well as the malonyl-CoA binding site (Price *et al.* 2002). For this reason, several groups started testing its catalytic activity using different acyl-CoA esters and carnitine. Surprisingly, CPT1c presented no detectable catalytic activity (Price *et al.* 2002; Wolfgang *et al.* 2006) and years later our group found that CPT1c could present just a residual carnitine palmitoyltransferase activity, with a 20-fold lower efficiency compared to CPT1a activity (Sierra *et al.* 2008). In line with these results, it was demonstrated that CPT1c-KO mice had the same fatty acid oxidation (FAO) rate as WT mice (Wolfgang *et al.* 2006). Concerning this lack of activity, two theories have been studied. On the one hand, it has been proposed that CPT1c expression is repressed by an upstream open reading frame and this repression is relieved in response to specific stress stimuli (Lohse *et al.* 2011). On the other hand, it has also been suggested that the N-terminal of CPT1c could be the regulatory domain, having two conformational states depending on specific conditions. Then CPT1c could be permanently in the inactive state because of higher stability and the N-terminal domain could change to a non-inhibitory state if the interaction with other proteins stabilizes it (Samanta *et al.* 2014).

Another important and unique feature of CPT1c is the longer tail in the C-terminal region, since it has 39 additional residues compared to the C-terminal of the other two canonical CPT1s. Recently, it has been reported that this longer tail is necessary for the interaction of CPT1c with other ER-resident proteins such as ABHD6, Sac1 or protudin, with the final aim of regulating their activity (Palomo-Guerrero *et al.* 2019; Casas *et al.* 2020; Miralpeix *et al.* 2021a). Considering all the features of CPT1c and all the differences presented to the other two CPT1 isoforms, it seems that CPT1c would participate in more complex functions regarding lipid metabolism of the brain and, at the same time, in modulating the activity of other proteins.

3.2 CPT1c, a nutrient sensor

Although CPT1c has no catalytic activity, it maintains the capacity to bind malonyl-CoA with high affinity as the isoform CPT1a (Price *et al.* 2002). Malonyl-CoA is synthesized by acetyl-CoA carboxylase (ACC) using acetyl-CoA as substrate and, afterwards, it is used to generate LCFA by the fatty acid synthase (FAS) enzyme **(Fig. 11)**. Malonyl-CoA can also be

converted to acetyl-CoA by the malonyl-CoA decarboxylase (Fadó *et al.* 2021). The enzymes involved in its synthesis and degradation are highly regulated by the nutritional status of the organism. In particular, ACC can be inhibited by AMPK (Hardie 2015). AMPK is activated in an energy depletion state, which results in reducing malonyl-CoA levels and, therefore, LCFA will not be produced and the organism will save energy (Hardie 2015) **(Fig. 11)**. In fact, it has been described that malonyl-CoA levels in different brain regions, such as hypothalamus, are dynamically regulated decreasing during fasting and increasing after feeding (Tokutake *et al.* 2010) **(Fig. 11)**.

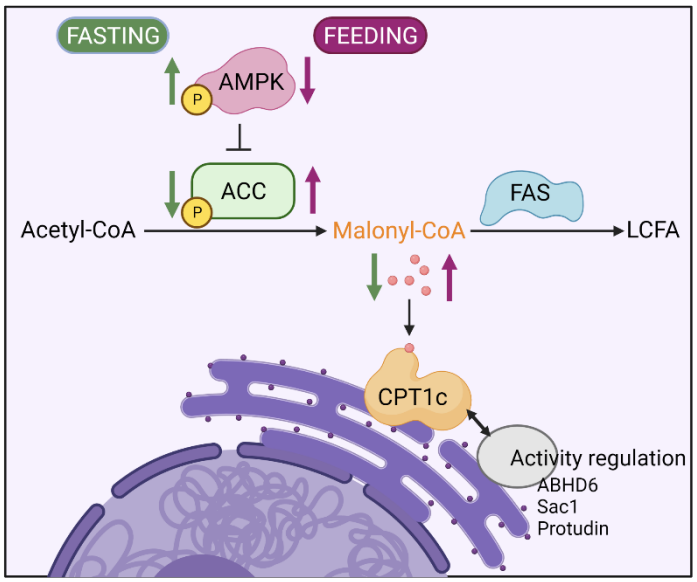

Fig. 11. Malonyl-CoA levels modulation through the axis AMPK-ACC and FAS expression. CPT1c regulate the activity of other proteins, such ABHD6, Sac1 or protudin, interacting with them in a malonyl-CoA dependent-manner. A fasting situation would increase phosphorylated AMPK levels, which would lead to low levels of malonyl-CoA. Under an overnutrition state, the opposite situation is found. ACC: acetyl-CoA carboxylase; AMPK: AMP-activated protein kinase; CPT1c: Carnitine palmitoyltransferase 1 C; FAS: fatty acid synthase.

Considering that malonyl-CoA levels have been defined to be an indicator of the energy status of the cell, as well as a regulator of energy homeostasis within the hypothalamus and considering that CPT1c is able to bind malonyl-CoA and regulate the function of other proteins (Wolfgang & Lane 2006; Palomo-Guerrero *et al.* 2019; Casas *et al.* 2020; Miralpeix *et al.* 2021a), we and other authors agree that CPT1c acts as a nutrient sensor in the hypothalamus (Fadó *et al.* 2021).

3.3 Role of CPT1c in energy homeostasis

To evaluate the physiological role of CPT1c in energy homeostasis, a mouse model deficient for this protein (CPT1c-KO) was developed in 2006 by Wolfgang and colleagues, targeting exons 1 and 2 of the gene *Cpt1c* (Wolfgang *et al.* 2006). Under basal conditions, CPT1c-KO mice presented slightly lower body weight and food intake. However, when fed with a HFD for six weeks, the transgenic mice resulted to be more susceptible to developing obesity than WT mice, in a feeding-independent manner (Wolfgang *et al.* 2006) **(Fig. 12)**.

Gao and colleagues developed another CPT1c-KO mouse model, deleting exon 3 of the gene *Cpt1c* (Gao *et al.* 2009). This last mouse model also presented an obesogenic phenotype and, moreover, severe insulin resistance after 8 weeks of HFD compared to WT mice, which was explained by an enhanced hepatic gluconeogenesis and an attenuated glucose uptake in skeletal muscle (Gao *et al.* 2009). In the same study, a decrease in liver and muscle FAO was described, which resulted in higher levels of triglycerides in these tissues. Our group also developed a CPT1c-KO mouse model, in our case, exons 12 to 15 of *Cpt1c* gene were excised (Carrasco *et al.* 2012). In line with the CPT1c-KO phenotypes described, recent studies of our group showed an attenuated BAT thermogenesis activity after seven days of HFD compared to WT mice and an impairment in hypothalamic leptin signalling (Rodríguez-Rodríguez *et al.* 2019), contributing to the obesogenic phenotype previously described **(Fig. 12)**.

Under fasting conditions, CPT1c-KO mice presented an attenuated decrease in adiposity and weight loss (Pozo *et al.* 2017), unable to increase FAO in contrast to WT mice (Wolfgang *et al.* 2006; Pozo *et al.* 2017). Fasted CPT1c-KO mice also presented enhanced liver gluconeogenesis and higher glycolysis in skeletal muscle (Pozo *et al.* 2017) **(Fig. 12).**

In agreement with these data, CPT1c overexpression in the hypothalamus of WT mice resulted in protection from DIO with no reduction in food intake (Dai *et al.* 2007). In addition, reversion of CPT1c expression in the mediobasal hypothalamus (VMH and ARC) of null mice for this protein restored the phenotype to a proper nutrient partitioning in liver and muscle, causing the normalization of the fasting-induced body weight loss (Pozo *et al.* 2017). Re-expression of CPT1c in the VMH in CPT1c-KO also restored BAT thermogenesis activity after seven days of HFD (Rodríguez-Rodríguez *et al.* 2019)

Regarding food intake control, CPT1c overexpression in the hypothalamic ARC nucleus increased food intake antagonizing leptin anorexigenic effects (Gao *et al.* 2011). In relation to the orexigenic hormone ghrelin, central administration of this hormone was unable to stimulate feeding in CPT1c-KO mice (Ramírez *et al.* 2013). In both studies, the blunted effects of these appetite-related hormones were related to a role of CPT1c in ceramide metabolism in the hypothalamus. Leptin reduced ceramide levels in the ARC and ghrelin increased them in WT mice, whereas these levels were dysregulated in CPT1c-KO mice (Gao *et al.* 2011; Ramírez *et al.* 2013).

Altogether indicates the role of hypothalamic CPT1c in the regulation of energy expenditure through a peripheral crosstalk to the liver, muscle and BAT under metabolic challenges such as HFD feeding or fasting, most of these actions in a feeding-independent manner. However, CPT1c also participates in the central response to orexigenic and anorexigenic hormones.

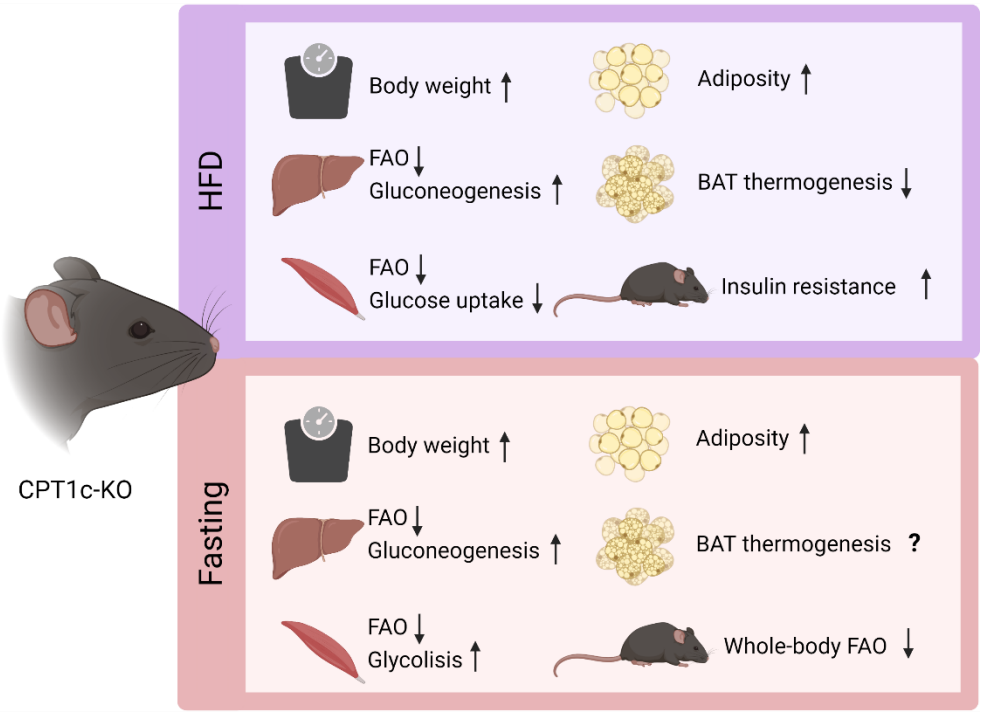

Fig. 12. Metabolic phenotype of CPT1c-KO mice under the metabolic challenge of HFD exposure and fasting. CPT1c-KO mice are not able to do the metabolic switch needed to properly adapt to the challenging situation that can be HFD feeding or fasting. All the parameters here described are described in comparison to WT mice. BAT thermogenesis under fasting has not been studied in these transgenic mice. BAT: brown adipose tissue; FAO: fatty acid oxidation; WAT: white adipose tissue.

3.4 Interaction of CPT1c with other neuronal proteins related to energy homeostasis

Although a direct interaction between CPT1c and the nutritional sensor AMPK has not been reported, several studies demonstrate that CPT1c is downstream the AMPK signalling. First, it was described that AMPK inhibition can release the uORF dependent repression of CPT1c expression (Lohse *et al.* 2011). In line with this, CPT1c mRNA levels were increased after AMPK activation in mouse embryonic fibroblasts (Zaugg *et al.* 2011). Afterwards, in ghrelin effect studies, it was observed that basal levels of pAMPK and, subsequently, of pACC were increased in CPT1c-KO mice (Ramírez *et al.* 2013). More recently, other publications have identified the AMPK – CPT1c axis in hypothalamic regulation of energy balance. In a study of food preference after fasting, CPT1c resulted to be a crucial downstream factor for AMPK-induced carbohydrate selection in CRH neurons of the PaV nucleus (Okamoto *et al.* 2018) **(Fig. 13A)**. One year later, our group also demonstrated that CPT1c was downstream of AMPK, as the inhibition of the kinase in VMH by an AMPK-dominant negative resulted in an increase of thermogenesis activity in WT mice but no changes in this activity were observed in CPT1C-KO mice (Rodríguez-Rodríguez *et al.* 2019) **(Fig. 13A)**. Considering the capacity of CPT1c for malonyl-CoA binding and the essential role of AMPK in regulating the levels of this metabolite (Fadó *et al.* 2021), the relationship between AMPK and CPT1c could be through the regulation of malonyl-CoA levels in the hypothalamus **(Fig. 13A)**.

CPT1c has also been described to interact with the enzyme ABHD6 (Brechet *et al.* 2017; Miralpeix *et al.* 2021a), which hydrolyses the endocannabinoid 2-arachidoniyglycerol (2-AG) and the endosomal lipid Bis(monoacylglycero)phosphate (BMP) (Cao *et al.* 2019). In the hypothalamus, CPT1c inhibited ABHD6 activity in a malonyl-CoA dependent manner (Miralpeix *et al.* 2021a) **(Fig. 13B)**. Particularly, under fasting conditions, where malonyl-CoA levels are low, the CPT1c inhibitory effect on ABHD6 was blunted (Miralpeix *et al.* 2021a) **(Fig. 13B)**. The importance of this interaction stands with ABHD6 in the VMH playing a role in cold-induced thermogenesis and delaying the onset of obesity (Fisette *et al.* 2016) **(Fig. 13B)**. Therefore, if CPT1c can inhibit ABHD6 activity, it could indirectly control all those functions in energy homeostasis that have been attributed to the hydrolase enzyme.

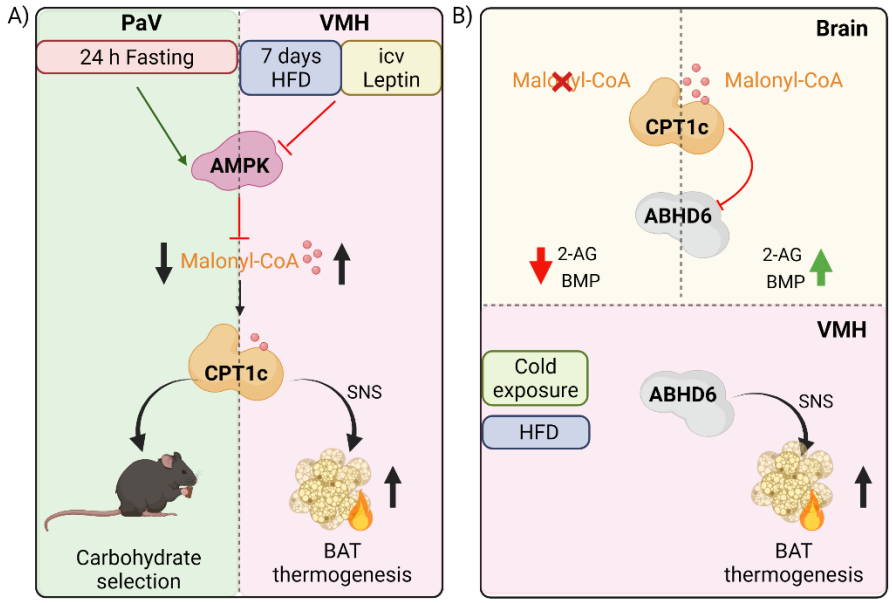

Fig. 13. CPT1c interaction with other proteins related to energy metabolism. A) CPT1s is found downstream of AMPK in the VMH for BAT thermogenesis regulation and in the PaV for nutrient selection after fasting. B) CPT1c has been defined to inhibit ABHD6 in a malonyl-CoA depedent manner in brain tissue homogenates, and ABHD6 has been defined to regulate BAT thermogenesis under cold exposure and HFD feeding in the VMH. The interaction of both proteins in the VMH have not been tested. Adapted from Fisette *et al.* 2016; Okamoto *et al.* 2018; Miralpeix *et al.* 2021a.

3.5 Role of CPT1c beyond energy homeostasis

CPT1c has been described to participate in other functions beyond energy homeostasis such as cognition and motor function, and it also plays a role in cancer (Casals *et al.* 2016) **(Fig. 14).**

Regarding its function in cognition, mice deficient in CPT1c had a worse performance in learning and memory tests than WT mice (Carrasco *et al.* 2012). This result was associated with an impairment in neuronal dendritic spines maturation. In the same study, they showed that overexpression of CPT1c or ceramide treatment reverted the phenotype in hippocampal neuronal cultures of CPT1c-KO mice (Carrasco *et al.* 2012). Some years later, it was reported that CPT1c in the ER regulated posttranscriptional GluA1 protein synthesis, the most abundant subunit of AMPAR, and it also regulated AMPAR trafficking to the cell surface (Fadó *et al.* 2015; Gratacòs-Batlle *et al.* 2015). Our group recently published that this traffic regulation is through the phosphatase Sac1 which is down-regulated by CPT1c in a malonyl-CoA dependent manner (Casas *et al.* 2020). In fact, CPT1c

and Sac1 had been identified in the AMPAR interactome through a proteomic study, together with ABHD6 (Brechet *et al.* 2017) **(Fig. 14)**.

CPT1c is also involved in motor function, since KO mice showed reduced motor activity and impaired coordination, associated with muscle weakness, altogether worsened with increased age (Carrasco *et al.* 2013). In accordance with these results, a form of hereditary spastic paraplegia (HSP), characterized by impaired function of corticospinal motor neurons, was related to a CPT1c mutation in patients. In this study, CPT1c was shown to interact with another protein in the ER: Atlastin-1 (ATL1) (Rinaldi *et al.* 2015). Regarding studies performed in CPT1c-KO mice, the damaged motor functions were related to an impairment in complex lipid metabolism (Carrasco *et al.* 2013) and, in the HSP studies, a decreased lipid droplets biogenesis was suggested (Rinaldi *et al.* 2015). CPT1c has recently been related to axonal growth, as it enhances the late endosomes/lysosomes (LE/Lys) anterograde transport in a malonyl-CoA dependent manner interacting with the ER protein protudin (Palomo-Guerrero *et al.* 2019). In a nutrient deprivation situation, CPT1c would slow down this kind of transport and this would stop axon growth (Palomo-Guerrero *et al.* 2019) **(Fig. 14)**. This is an important transport for motor neurons and could also explain the HSP cases observed in humans with mutations in CPT1c (Rinaldi *et al.* 2015).

Finally, CPT1c has also been linked to tumour cell survival. CPT1c expression in tumourous cells increased FAO and ATP production and resulted in higher resistance to glucose or oxygen deprivation (Zaugg *et al.* 2011). At the same time, these last two conditions were defined to increase CPT1c expression conferring a higher capacity of survival to the cell (Zaugg *et al.* 2011). CPT1c has also been identified as a target of the AMPK-p53 pathway in cancer cells and the depletion of CPT1c in murine tumour model delayed its development (Sanchez-Macedo *et al.* 2013). Some years later, our group studied CPT1c expression in human mesenchymal stem cells (hMSCs) and CPT1c was related to a promotion of autophagy under glucose deprivation and hypoxia although no increase in FAO was found (Roa-Mansergas *et al.* 2018). The autophagy enhancement was related to a higher number of lipid droplets and increased ATP levels, which provide a protective role for the cell (Roa-Mansergas *et al.* 2018) **(Fig. 14)**. All these data suggest CPT1c as a possible target for cancer therapy.

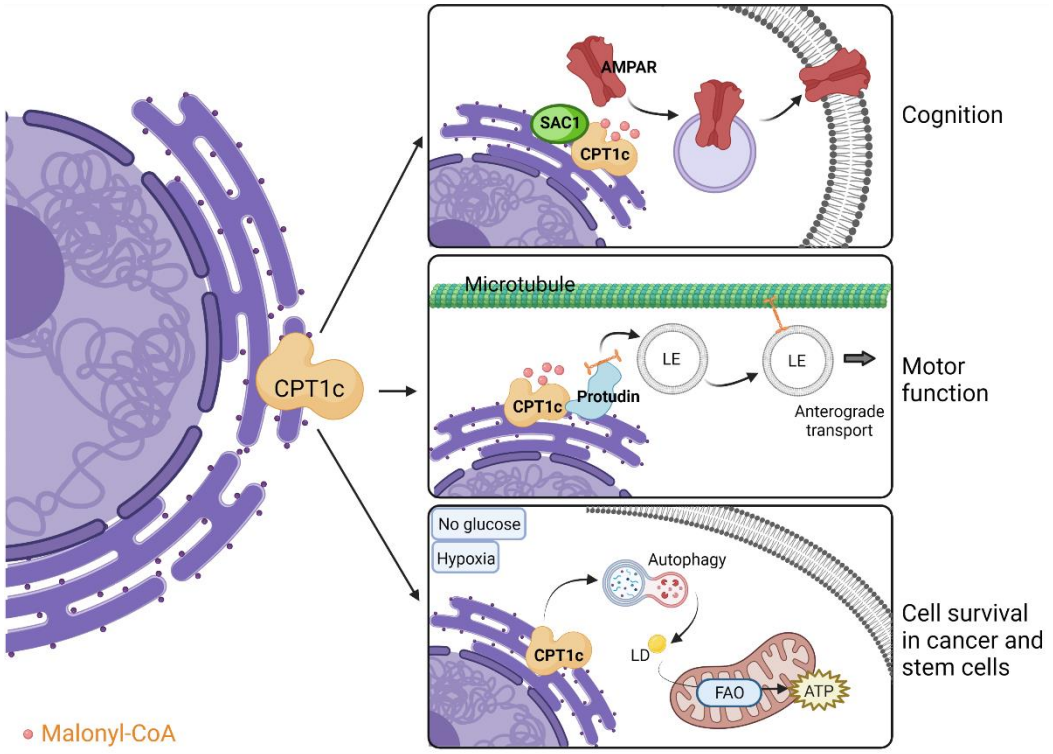

Fig. 14. Role of CPT1c beyond energy homeostasis of CPT1c. CPT1c not only participates in energy and glucose metabolism but also in cognition, motor function and in cell survival. FAO: Fatty acid oxidation; LD: lipid droplet; LE: late endosome.

4 Hypothalamic lipid sensing: role of LCFAs as central signalling molecules

It is well known that brain is the highest demanding organ of the organism: despite the brain only represents the 2% of the body mass, about 20% of oxygen and 25% of glucose consumed by the organism are dedicated to brain functions (Bélanger *et al.* 2011). Under prolonged fasting, ketogenic diets, or situations of carbohydrates deprivation, brain can change the energy substrate from glucose to ketone bodies (Romano *et al.* 2017). FA play a minimal role as energy substrates in neurons (Tracey *et al.* 2018), however they do play an important role as signalling molecules in the hypothalamus. A lot of studies have shown that hypothalamic lipid metabolism controls energy expenditure, calorie intake, glucose homeostasis and lipogenesis energy balance (Lam *et al.* 2005a). Intermediates of FA metabolism, or even participating enzymes, act as signalling molecules, and aberrations

in lipid metabolism can result in metabolic disorders such as obesity or type 2 diabetes mellitus (Bruce *et al.* 2017). It has been proposed that there are lipid-sensing mechanisms in the hypothalamus and that FAs act as signalling molecules to inform about the energy status of the organism (Dragano *et al.* 2020). Despite the importance of the hypothalamus in nutrient sensing, it cannot be understood as an individual entity, but as part of the central cross-talk with the peripheral organs.

4.1 Metabolism of LCFAs

FAs represent the building blocks of lipids, and their molecular structure consists of a carbon chain with a final carboxylic acid group. They can be classified depending on their length into short-chain FA (SCFA) (2-4 carbon atoms), medium-chain FA (MCFA) (6-12 carbon atoms), long-chain FA (LCFA) (14-18 carbon atoms) and very long-chain FA (VLCFA) (more than 18 carbon atoms). Apart from their length, FA can also be divided depending on the saturation of the carbon atoms into saturated (SFA) (no double bonds), monounsaturated (MUFA) (one double bond) and polyunsaturated (PUFA) (more than one double bond) (Agostoni & Bruzzese 1992) **(Fig. 15)**. The length and saturation of the FA determine the functions and the subcellular location.

Dietary FAs are transported from the circulatory system to the brain crossing the blood brain barrier (BBB), by passive diffusion or by transporters. Regarding transporters in the BBB, a group of proteins have been described such as CD36 and FATP (Le Foll *et al.* 2009; Mitchell *et al.* 2011). Independently of the strategy used by FAs to cross the BBB, the amount of FAs that enter into the CNS is proportional to their plasma concentration (Rapoport 1996).

Once FAs have entered into the cell, they are esterified to a fatty acyl-CoA by the acyl-CoA synthetase and, at this point, they can be used in synthetic pathways of complex lipids, but also for oxidation in the mitochondria. This last process is regulated by the availability of malonyl-CoA, a metabolite from the glycolysis derived products, which inhibits the first step of β-oxidation: the entry of FAs into the mitochondria through a CPT1 (Lam *et al.* 2005a; Tracey *et al.* 2018).

Regarding the synthetic pathway of LCFAs **(Fig. 15)**, it occurs in the cytosol in lipogenic tissues such as adipose tissue, liver, skeletal muscle, heart and brain (Kreuz *et al.* 2009). It starts with the acetyl-CoA being carboxylated to malonyl-CoA by ACC. After the first

carboxylation step, malonyl-CoA is transacylated and the final product of this reaction is the starting point of a four-reaction cycle catalysed by one enzyme, the FAS. This cycle takes place in seven repetitions to finally obtain a LCFA of 16 carbon atoms. Finally, a thioesterase enzyme terminates the carbon chain obtaining palmitic acid **(Fig. 15)**. From this point, palmitic acid can be elongated or desaturated **(Fig. 15)**. It is important to mention that the organism does not rely only on de novo synthesis but it takes the vast majority from the diet, especially some essential PUFAs (Tracey *et al.* 2018).

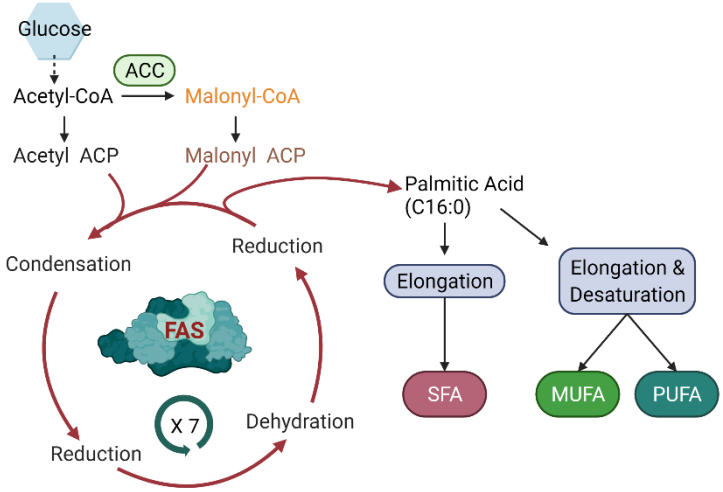

Fig. 15. Synthetic pathway of long-chain fatty acids. This anabolic pathway occurs in the cytosol where glucose is converted to acetyl-CoA**,** which at the same time can be carboxylated by the ACC enzyme to malonyl-CoA. After, both substrates enter to a cycle of four step, that will be repeated 7 times, and it is conducted by FAS. The final product is 16-carbon chain (palmitic acid) that can be elongated and/or desaturated. ACC: acetyl-CoA carboxylase; ACP: acyl-carrier protein; FAS: fatty acid synthase; MUFA: monounsaturated fatty acid; PUFA: polyunsaturated fatty acid; SFA saturated fatty acid. Adapted from (Tracey *et al.* 2018).

4.2 Role of LCFAs as signaling molecules in the regulation of food intake

One of the first evidence of lipid sensing in controlling food intake was studied in primates nearly 30 years ago. After peripheral injection of lipids, food intake was suppressed and it was an independent insulin effect, therefore circulating lipids were providing information to CNS about the energy status (Woods *et al.* 1984). Some years later, hypothalamic FA sensing was demonstrated by different research groups.

The first demonstration of central LCFA sensing was done by Obici and colleagues. They demonstrated that after central administration of oleic acid (OA) (a LCFA), but not octanoic acid (a MCFA), food intake and glucose production were reduced (Obici *et al.* 2002). These satiating effects of OA were blunted after 3 days of a highly palatable energy-dense diet (Morgan *et al.* 2004). In both studies, reduced levels of hypothalamic NPY but no differences in POMC levels were found in those mice treated with OA intracerebroventricular (icv) administration. Another investigation compared the central effects of OA, palmitic acid (PA) or docosahexaenoic acid (DHA) in energy balance in rats (Schwinkendorf *et al.* 2011). The icv administration of the saturated PA did not change body weight nor food intake while administrating the unsaturated OA or DHA resulted in a significant reduction of both parameters analysed. In addition, hypothalamic POMC expression was also increased in the unsaturated-treated groups but no changes were observed after PA administration (Schwinkendorf *et al.* 2011). In line with these results, another study also showed a food intake reduction after the central administration of OA and linoleic acid (LA), but not when injecting stearic acid (SA) (Cintra *et al.* 2012). The anorexigenic effects observed with the two unsaturated fatty acids, OA and LA, was accompanied by a reduction in adiposity too (Cintra *et al.* 2012). Regarding the effect of LCFAs on the excitability of neurons, OA was defined to excite POMC neurons (Jo *et al.* 2009). However, a more recent research tested the electrical excitability of POMC and NPY neurons after administration of OA and PA and it resulted in contrary outcomes: excitability of POMC neurons was inhibited by OA and PA while NPY were excited by both FAs (Michael & Watt 2020), being these results in contrast to the idea that OA represents an energy surfeit signal. However, those experiments were performed in brain slices from overnight-fasting animals, suggesting that FAs can have different effects depending on the nutritional status. This agrees with the emerging idea that POMC and AgRP/NPY neurons are heterogenous and respond to distinct combinations of interoceptive and nutrient signals to regulate body energy homeostasis (Quarta *et al.* 2021). Possibly, FAs are oxidized upon fasting conditions while they enter into anabolic pathways in the context of satiety, activating completely different signalling pathways in hypothalamic targeted neurons.

Dissociated VMH neurons were also studied in response to OA administration and compared to glucose administration. OA excited 43% of dissociated VMH neurons and inhibited up to 29%, but these percentages changed in the presence of glucose (Le Foll *et al.* 2009). Authors concluded that OA changed VMH neuronal activity by affecting multiple

pathways such as FAO, reactive oxygen species (ROS) formation and ATP-sensitive K^+ channels. All these hypothalamic neurons could be defined as metabolic sensing neurons as they respond differently depending on the presence of different types of nutrients.

The exploration of the possible intracellular mechanism that can be related to LCFA effects, evidenced that elevated LCFA circulating levels result in high LCFA-CoA hypothalamic levels, being the latter a signal of satiety (Lam *et al.* 2005a). This esterification, mediated by LCFA-CoA synthase (ACS), was essential for the OA effects on hypothalamus (Lam *et al.* 2005b). As high levels of hypothalamic LCFA-CoA could be a signal of energy surfeit, the oxidative pathway was analysed too. Since LCFA-CoA are translocated into the mitochondria to undergo β-oxidation through CPT1a, inhibition of this protein resulted in food intake suppression, with reduced expression of NPY and AgRP in ARC (Obici *et al.* 2003) **(Fig. 16)**.

Considering that the intracellular energy indicator malonyl-CoA inhibits CPT1 action, this metabolite and all the enzymes involved in their synthesis or degradation such as ACC, AMPK and FAS control LCFA levels. Regarding the uptake of FAs, the translocase CD36 has been described as essential for OA effects on food intake in VMH neurons (Le Foll *et al.* 2013). It has been proposed that CD36 can also act as a receptor apart from being a transporter (Moullé *et al.* 2014) **(Fig. 16)**.

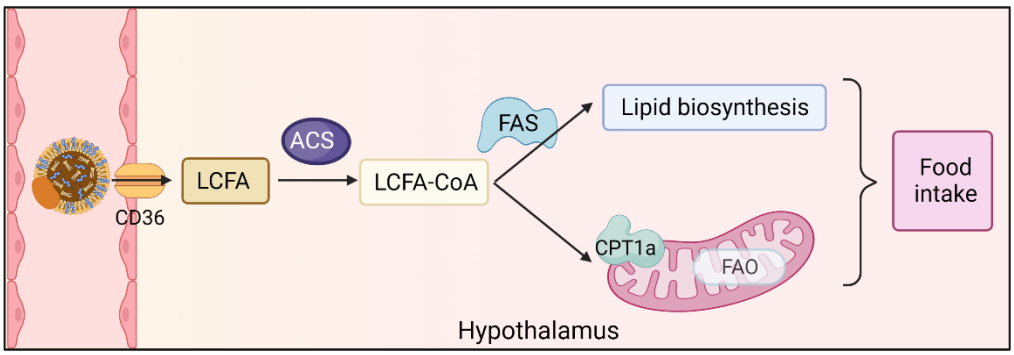

Fig. 16. Schematic representation of metabolism and function of LCFAs in the hypothalamus. LCFA can be derived from different forms such as chylomicrons or circulating lipoproteins. They can cross the BBB though a transporter such as CD36, that will also be a transporter of LCFA in the cell membrane. Upon entry to the cell, LCFA are esterified to LCFA-CoA which can modulate food intake. The pool of LCFA-CoA is determined by its formation and use (β-oxidation and lipid synthesis). Modified from Lam *et al.* 2005a.

In agreement with these findings, a study performed in patients concluded that under obesity conditions, there is an increase in the LCFA uptake in the brain, which results in higher LCFA and LCFA-CoA levels in the hypothalamus (Karmi *et al.* 2010). In the same investigation, when body weight is reduced, the accumulation of LCFAs is also restored, indicating that during a sustained situation of high levels of FAs, the hypothalamic lipid sensing system is impaired. Altogether, circulating LCFA and LCA-CoA levels are an essential component of lipid sensing in hypothalamic neurons, although it remained to be explored the specific role of the different hypothalamic nuclei and the neuronal populations involved.

Among the neuronal mechanisms involved in the action of LCFAs in the hypothalamus, the melanocortin system seems to play a critical role. This system consists of several components: melanocortin peptides, the melanocortin receptors coupled to a G-protein (MCRs), endogenous agonists and mediators. This complex system is involved in the control of feeding (Seeley *et al.* 2004). The initial transcript of the melanocortin peptides is the POMC gene that will suffer various post-transcriptional modifications to get the active peptides. One of these is the α-melanocyte-stimulating hormone (α-MSH), which can interact with the melanocortin receptors MC3R and MC4R expressed in the CNS. Agonism of both receptors has been related to the inhibition of food intake (Seeley *et al.* 2004). Within the hypothalamus, POMC neurons in the ARC release α-MSH to MC4R expressed in the PaV for an orexigenic effect (Sohn 2015). Due to the importance of this system and the observations that central OA administration elevates POMC neuropeptide levels, the melanocortin system has been studied in this response. In particular, the MC4R/MC3R antagonist SHU9119 abolished OA and DHA effects on body weight and food intake after icv administration (Schwinkendorf *et al.* 2011), showing the role of the melanocortin system in food intake regulation within the hypothalamic lipid sensing.

4.3 Role of LCFAs in hypothalamic inflammation

As explained before in section 1.1.2 of the introduction, hypothalamic inflammation is one of the first signs of obesity development. Some groups have studied the role of LCFA in this early hypothalamic inflammation.

Three days of central administration of OA or α-linolenic acid, both unsaturated LCFAs, were sufficient to increase the expression of anti-inflammatory interleukins IL-6 and IL-10 in the hypothalamus, while PA or SA increased the pro-inflammatory TNFα ant he

interleukin IL-1β (Milanski *et al.* 2009). This output was the same as injecting a low dose of TNFα into the hypothalamus (Arruda *et al.* 2011b). Another investigation reported the inhibitory action of icv administration of OA and LA in the expression of inflammatory markers in hypothalamus and an enhanced expression of anti-inflammatory markers after seven days of treatment in the same area (Cintra *et al.* 2012). These effects of LCFAs were not only found after central administration, but also by exposure to diets enriched with olive oil (at least 10% kcal of saturated FA substituted by OA) or flaxseed oil (at least 10% kcal of saturated FA substituted by LA) for 8 weeks in mice, leading to an attenuation in the hypothalamic inflammation previously induced by a HFD (37% of fat correspond to HFD) (Cintra *et al.* 2012). It has to be mentioned that there is a current discussion about the omega-6 PUFAs, such as LA, as this LCFA is the precursor of pro-inflammatory lipid mediators, but at the same time, LA presents anti-inflammatory effects by itself (Innes & Calder 2018).

The molecular mechanism underlying the pro-inflammatory effect of the saturated FAs seems to be mediated by the toll-like receptor 4 (TLR4), which is defined as responsible for inducing cytokine expression as well as ER stress (Milanski *et al.* 2009). Focusing on the anti-inflammatory effect of the unsaturated LCFAs, the receptor GPR40 has been described to be one of the responsible for OA and LA effects in neurons and to be implicated in the hypothalamic inflammation after HFD feeding (Dragano *et al.* 2017).

Considering that hypothalamic inflammation plays a key role in the pathophysiology of obesity and diabetes mellitus type 2, nutrients such as unsaturated FAs could be an alternative or complementary choice to pharmacological approaches to control hypothalamic inflammation in obesity.

4.4 Role of LCFAs in BAT thermogenesis activity

It has been described that hypothalamic regulation of BAT thermogenesis activity is dependent on hormone signalling (Contreras *et al.* 2017a), but hypothalamic nutrient sensing can also modulate this response (Blouet & Schwartz 2010). An investigation using different HFD enriched with specific LCFA described that the group fed with HFD enriched with shea butter (saturated FA, 45% Kcal from fat) presented the lowest thermogenesis level compared to those mice with other kind of HFD. Regarding those mice fed with olive oil enriched-HFD (unsaturated FA, 45% Kcal from fat), they were the ones with the lower body fat accumulation and the higher heat production (Shin & Ajuwon 2018). In

concordance, central administration of the unsaturated LCFA, OA and LA, resulted in an increased expression of UCP1 in BAT (Cintra *et al.* 2012), whereas icv injection of the saturated SA resulted in a reduced UCP1 expression in brown fat (Arruda *et al.* 2011b).

In all the studies presented, the protocol of administration of LCFA (timeline of the experiment and the dose of LCFA) varies and it is difficult to compare the central effect of the different LCFA. Some of these publications were using diets to define LCFA effects, but this approach is difficult to discern between central and peripheral effect of diets. In addition, the specific protein targets in the hypothalamus which mediate BAT-induced thermogenesis in response to LCFA were not described. In this thesis we want to describe the hypothalamic effect that different LCFA have on BAT thermogenesis activity elucidating which hypothalamic nuclei could be participating as well as the signalling pathways involved.

HYPOTHESIS

Hypothesis

We hypothesize that CPT1c in SF1 neurons of the ventromedial hypothalamus and in other specific nuclei of the hypothalamus senses different type of fatty acids and hormone signals to drive the metabolic adaptation to nutritional challenges and cold exposure.

OBJECTIVES

1 General objective

To investigate the physiological function of CPT1c in SF1 neurons of the ventromedial hypothalamic nucleus in the metabolic adaptation to high fat diet feeding, fasting and cold exposure and to explore the role of CPT1c in hypothalamic LCFA sensing and the control of BAT thermogenesis.

1.1 Specific objectives

1. To develop a transgenic mouse model deficient of the protein CPT1c specifically in SF1 neurons of the ventromedial hypothalamic nucleus.
2. To determine the role of CPT1c in SF1 neurons of the ventromedial hypothalamus in the onset and development of diet-induced obesity and in the metabolic adaptation to fasting, cold exposure and leptin administration.
3. To explore the central effects of LCFA sensing in food intake and BAT thermogenesis within different nuclei of the hypothalamus.
4. To identify the role of CPT1c in hypothalamic LCFA sensing for the control of food intake and BAT thermogenesis.

The specific objectives 1 and 2 will be covered in chapter I of results whereas the specific objectives 3 and 4 will be covered in chapter II of results.

METHODOLOGY

1 Animal procedures

C57BL/6J mice (Wild type, WT), global Knock-out of CPT1c (CPT1c-KO) mice and specific Knock-out of CPT1c in SF1 neurons of the VMH (SF1-*CPT1c*-KO) mice were used for experiments. Mice were housed on 12h/12h light/dark cycle (light on at 8 a.m., light off 8 p.m.) in a temperature- and humidity-controlled room. Animals were allowed free access to water and standard laboratory chow diet, otherwise indicated. At the end of the studies mice were sacrificed by cervical dislocation and tissues collected for molecular and biochemical analysis.

All animal procedures were performed in agreement with European guidelines (2010/63/EU) and approved by the University of Barcelona Local Ethical Committee (Procedure ref. CEEA-C-303/18 and CEEA-C-233/19, Generalitat de Catalunya).

1.1 Mice models

1.1.1 Global Knock-out of CPT1c

CPT1c-KO mice have exons 12 to 15 of *Cpt1c* gene deleted, which results into a truncated non-functional protein (Carrasco *et al.* 2012). They have the same genetic background as WT C57BL/6J mice.

1.1.2 Specific Knock-out of CPT1c in SF1 neurons of the VMH

Mice deficient of CPT1c in SF1 neurons of the VMH were generated on this thesis project trough different steps using the Flp-FRT and the Cre-loxP technologies **(Fig. 17)**. Sperm of the strain C57BL/6N-Cpt1c$^{tm1a(EUCOMM)Wtsi}$ was obtained from KOMP Repository from University of California, Davis. This sperm contained the *Cpt1c* gene modified, with exons 4 to 6 flanked with two sequences of LoxP. The *Cpt1c* gene of C57BL/6N-Cpt1c$^{tm1a(EUCOMM)Wtsi}$ included two more cassettes: one with the lacZ gene and the second one with the neo gene **(Fig. 17)**. This sperm was used for an in vitro fecundation (IVF) performed by Dr. Anna Pujol at CBATEG from Universitat Autònoma de Barcelona. Heterozygous mice with one WT copy of the *Cpt1c* gene and a second copy coming from the sperm from KOMP Repository were generated by IVF. These mice were called Knock-out First (KO First) **(Fig. 17 and 18)**.

The second step was deleting LacZ and Neo cassette using the technology of FLP-FRT recombination. Both cassettes are flanked by FRT sequences as illustrated in **figure 17**. These two FRT sequences can be recombined using the protein FlpO with the final outcome of the whole sequence between FRT sites being excised. Mice containing FlpO in heterozygosis (FlpO mice) were obtained from the Mouse Mutant Core Facility (MMCF) from IRB Barcelona and they were bred with the KO First mice obtaining different genotype possibilities. Our target mice were the ones that got one copy of the *Cpt1c* gene modified and FlpO gene. Those mice got the cassettes LacZ and Neo excised by the protein FlpO and they were called heterozygous floxed mice or heterozygous Conditional KO mice, since exons 4 to 6 of *Cpt1c* can be deleted in any tissue using the Cre/LoxP system. This last system is a site-specific recombinase technology used for gene editing, the Cre recombinase enzyme recombines two LoxP sequences **(Fig. 17)**.

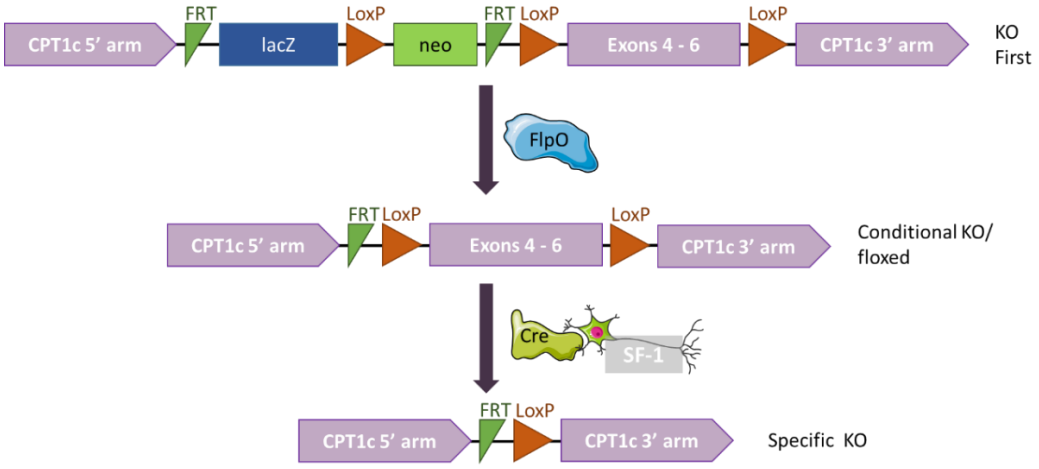

Fig. 17. Schematic representation of the modification of *Cpt1c* gene through Flp-FRT and Cre-loxP technologies. The first step was using the complete construct from KOMP repository for the IVF in order to get the KO First mice. Then, using the FRT-Flp technology, FRT sequences were recombined obtaining the Contidional KO or floxed mice. Finally, Cre-LoxP recombination was used to cut exons 4-6 of *Cpt1c* gene.

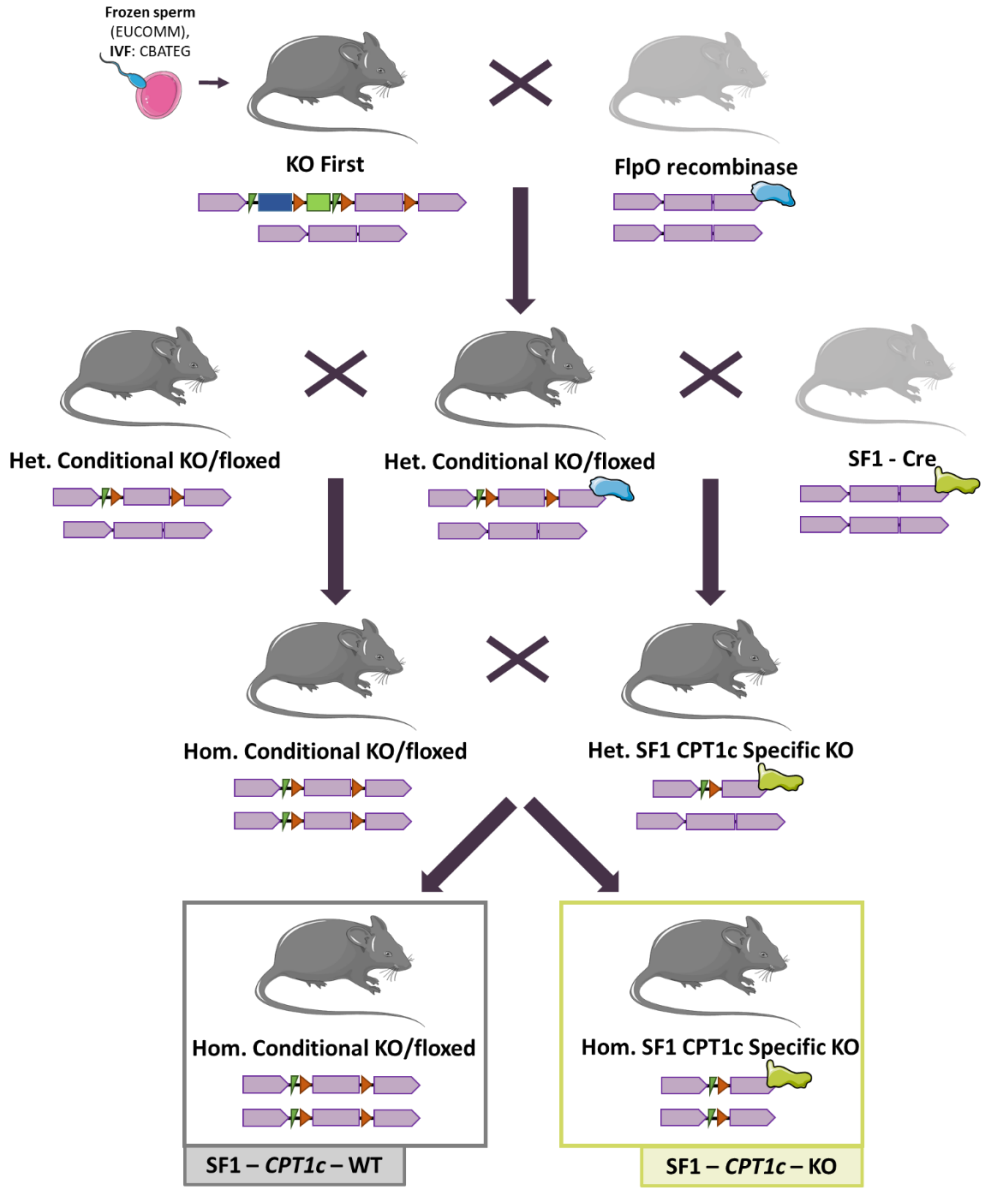

Fig. 18. Schematic representation of breeding strategy used to get mice deficient of CPT1c in SF1 neurons, only interested genotypes are represented. The first step was based on the IVF, and the resulting mice were bred with mice containing the FlpO recombinase gene and, as a result, 25% of the outcome were the heterozygous Conditional KO / floxed. After that, these last mice were bred with two different genotypes. First breeding was with the same genotype to obtain the homozygous floxed (25% of the offspring). The second breeding was with SF1–Cre mice which resulted in 25% heterozygous Specific KO. These last ones were bred with homozygous floxed to finally get homozygous Specific KO mice (25%) and homozygous floxed mice (25%). These mice are called SF1-*CPT1c*-KO and SF1-*CPT1c*-WT mice, respectively. Current breeding between them is going on to expand and maintain the colony. Het.: heterozygous, Hom.: homozygous.

0As we were interested in deleting functional CPT1c in SF1 neurons, these heterozygous floxed mice were bred with mice carrying Cre protein under the promotor of SF1 gene, also in heterozygosis (SF1-Cre) **(Fig. 18)**. These mice, referred as SF1-Cre mice, were kindly provided by Dr. Miguel López from CIMUS, Universidad Santiago de Compostela. The offspring of this breeding resulted in 4 different genotypes and we were just interested in those mice having C*pt1c* floxed gene in heterozygosis and CRE gene in heterozygosis (heterozygous Specific KO). Since our final aim was to get exons 4 – 6 of CPT1c excised in both copies of the gene, as a final step we bred the heterozygous Specific KO with a homozygous floxed mice, (obtained in parallel during this whole process). 25% of the progeny were homozygous for CPT1c floxed and heterozygous for CRE and, those ones, were the Specific KO mice, called SF1-*CPT1c*-KO mice in this thesis **(Fig. 18)**.

With the objective of amplifying the colony for experiments, the current breeding are SF1-*CPT1c*-KO mice with homozygous floxed mice, which results in 50% of each genotype. The floxed mice resulting from this breeding are called SF1-*CPT1c*-WT mice as they are the control littermates of the specific KO SF1-*CPT1c*-KO. Every mouse was genotyped previous each experiment following the procedure explained below (subsection 2.2).

1.2 Experimental designs

1.2.1 Administration of viral vectors within the VMH

For the stereotaxic surgery, mice were anesthetized with 75mg/kg of body weight of ketamine (Ketamidor® 100mg/mL Richter Pharma AG, Bagres Austria) and 10mg/kg of body weight of xylazine (Rompun® 20mg/mL Bayer, Leverkusen, Germany). Stereotaxic surgery had the aim to target VMH so injections were directed to 1.5mm posterior from Bregma, ± 0.5 mm lateral to midline and 5.8mm deep. Purified adeno-associated virus (AAVs) expressing mCherry under Cre activity **(Fig. 19)** were kindly provided by Dr Dolors Serra (Universitat of Barcelona). AAVs were injected bilaterally over 10 minutes trough a 33-gauge injector connected to a 5µL Hamilton® Syringe (65460-02, Hamilton Company, Reno, USA) and an infusion pump. 0,4nL with a viral titer of $1{,}23 \times 10^{12}$ pfu/mL were infused in each injection site. After surgery, an analgesic solution (Meloxidyl® 5mg/mL, Ceva Santé Animale, Libourne, France) was subcutaneously administered to a final dose of 1mg/Kg of body weight. During the first two days of recovery, the analgesic was administered through the drinking water with a final solution of 5mg/L. Mice underwent 3 weeks of recovery before virus were expressed.

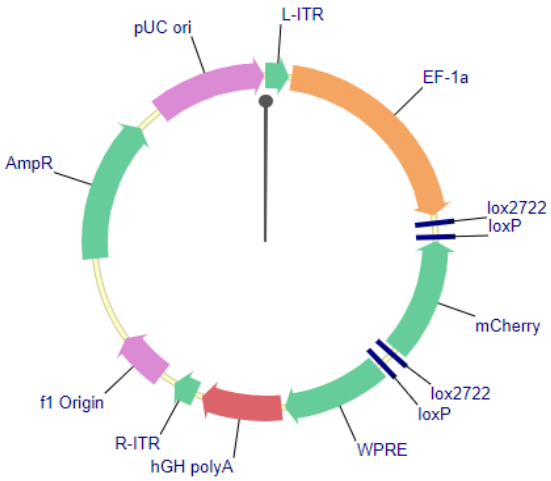

Fig. 19. Schematic representation of AAVs. mCherry gene is flanked by two LoxP sequences and its sequence is positioned in the opposite direction. When Cre protein is present, LoxP sequences recombined and mCherry gene is inverted, thus mCherry can be expressed.

1.2.2 Lateral ventricle cannulation

First of all, mice went under anaesthesia using the mix of ketamine and xylazine explained above. Chronic cannulae of 1.2 cm of length (Tubing 014x041 PE20, Plastics One, Roanoke, USA) were stereotaxically implanted into lateral cerebral ventricle, coordinates used were 0.58mm posterior from Bregma, 1 mm lateral to the midsagittal suture and 2.2mm dorsal depth. After surgery, an analgesic solution (Meloxidyl® 5mg/mL, Ceva Santé Animale, Libourne, France) was subcutaneously administered to a final dose of 1mg/Kg of body weight. Finally, mice were individually caged with no objects inside and they were allowed to recover for five days before the experiment. During the first two days of recovery, the analgesic was also administered through the drinking water with a final solution of 5mg/L.

1.2.3 Angiotensin test

Two days before the experiment, proper cannula placement was verified by the angiotensin test. Particularly, 2µL of Angiotensin II (1nmol/mL A9525, Sigma Aldrich) were icv administrated using a Hamilton® syringe (80358, Hamilton Company, Reno, USA). Mice were controlled for 10 minutes to observe a positive (drinking water) or negative response. Only positive-response ones were selected for experiments.

1.2.4 Intracerebroventricular administration of compounds

Five days after cannula placement, the specific icv administration of the compound under study was done using a Hamilton® syringe of 10µL. Two type of protocols were used depending on the aim of the experiment **(Fig. 20)**:

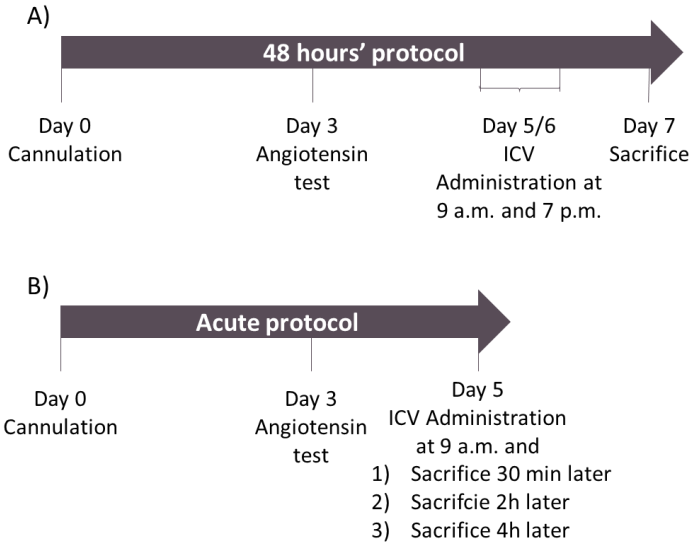

Fig. 20. Timeline representation of the intracerebroventricular administration protocols. A) Representation of 48 hour's protocol over time. B) Representation of acute protocol over time.

I. 48 hours' protocol

The 48 hours' protocol was used for FAs administration **(Table 2)** to evaluate the effect of the different LCFAs on body weight, food intake and BAT thermogenesis activity. Icv administration was performed for two days, at 9a.m. (1 h after dark cycle) and 7p.m. (1 h before the dark cycle) each day. Mice were sacrificed after 48 hours **(Fig. 20A)**.

II. Acute protocol

The acute protocol was used to evaluate the effect of the compounds under investigation **(Table 2)** on neuronal activation or metabolic parameters. For immunohistochemistry or biochemistry studies, icv administration was performed at 9a.m. and mice were sacrificed the same day **(Fig. 20B)**. This scheme was used following these protocols:

1) For biochemistry evaluation of 2-deoxy-D-glucose (2-DG) administration: mice were sacrificed 30 minutes after treatment. **(Fig. 20B-1) (Table 2)**.

2) For evaluating the effect of LCFAs and/or the MCR3/MC4R antagonist SHU 9119 through immunohistochemistry experiments: mice were sacrificed 2 hours after treatment. Mice had no access to food after drug treatment **(Fig. 20B-2) (Table 2)**.

3) For leptin-induced BAT thermogenesis activity evaluation: mice were fasted for 3 hours before injection and sacrificed 4 hours after treatment **(Fig. 20B-3) (Table 2)**.

Table 2. Icv-administrated compounds. Type of compounds, protocol, administration timing and dosage that was used for the icv administration.

TYPE	COMPOUND	PROTOCOL	VEHICLE	ADMIN. TIME	DOSE	REF.
FATTY ACID	Linoleic acid	48-hour	HPB	9am & 7pm (2 days)	36 nmols (9nmol/inj)	L8134, *Sigma-Aldrich, St Louis, USA*
FATTY ACID	Oleic acid	48-hour	HPB	9am & 7pm (2 days)	36 nmols (9nmol/inj)	O3880, *Sigma-Aldrich, St Louis, USA*
		Acute	HPB	9am	9 nmols	
FATTY ACID	Palmitic acid	48-hour	FFA BSA, NaOH	9am & 7pm (2 days)	36 nmols (9nmol/inj)	P5177, *Sigma-Aldrich, St Louis, USA*
		Acute	FFA BSA, NaOH	9am	9 nmols	
FATTY ACID	Stearic acid	48-hour	FFA BSA, NaOH	9am & 7pm (2 days)	36 nmols (9nmol/inj)	S3381, *Sigma-Aldrich, St Louis, USA*
GLUCOSE ANALOGOUS	2-DG	Acute	aCSF	9am	1mg	D8375 *Sigma-Aldrich, St Louis, USA*
HORMONE	Leptin	Acute	PBS	11am	0.2µg	450-31, Bionova-Peprotech, Madrid, Spain
MC4R/MC3R ANTAGONIST	SHU9119	Acute	aCSF	9am	0,5 nmols	M4603, *Sigma-Aldrich, St Louis, USA*

2-DG: 2 – deoxy-D-glucose; aCSF: artificial cerebrospinal fluid (p000151 M Dialysis AB, Stockholm, Sweden); ADMIN: administration; FFA BSA: free-fatty acid bovine serum albumin; HBP: 2-hydroxypropyl – β – cyclodextrin (H107, *Sigma-Aldrich, Snt Louis, USA*); MC4R/MC3R: melanocortin 4 receptor; REF.: reference.

1.2.5 Diet administration

For the experiments in which mice were fed with a special diet **(Table 3)**, different from the chow diet, mice were kept for at least 1 week in the specific standard diet (SD) before the administration of the specific high fat diets. In this thesis, we have applied three protocols of diet administration:

I. Short – term protocol: special diets were administrated for a period between 5 to 7 days.
II. Long – term protocol: special diets were administrated for a period between 6 to 8 weeks.
III. Fast-refeeding protocol: mice were fasted for three hours followed by a refeeding period of two hours using special diets.

Table 3. Diets used in the experiments.

DIET	ABB.	CHARACTERISTIC	FAT KCAL %	REFERENCE
Standard diet	SD	Low-fat	10%	D12450J, *Research Diets, New Brunswick, USA*
High-fat diet	HFD	High fat diet	60%	D12492, *Research Diets, New Brunswick, USA*
Monounsaturated fat diet	MUFA diet	High oleic sunflower oil	49%	D19121203, *Research Diets, New Brunswick, USA.* Personalized
Saturated fat diet	SFA diet	High coconut oil	49%	D19121204, *Research Diets, New Brunswick, USA.* Personalized

ABB.: abbreviation

SD, MUFA and SFA diets were designed for these experiments, and composition can be found on **table 4**, whereas HFD is a commercial diet.

Table 4. Composition of personalized diets and SD. Specification of nutrients and products in grams and Kcal for the personalized diets done by Research Diets (New Brunswick, USA).

PRODUCT	D12450J (SD)		D19121203 (MUFA)		D19121204 (SFA)	
	gm%	Kcal%	gm%	Kcal%	gm%	Kcal%
Protein	19	20	24	20	24	20
Carbohydrate	67	70	38	31	38	31
Fat	4	10	26	49	26	49
Total		100		100		100
Kcal/gm	**3.8**		**4.9**		4.9	
FAT INGREDIENT	**gm**	**Kcal**	**gm**	**Kcal**	**gm**	**Kcal**
Soybean oil	25	225	25	225	25	225
High oleic sunflower oil	0	0	176	1584	10	90
Flaxseed oil	0	0	0	0	14	126
Coconut oil, 101	0	0	10	90	122	1098
Butter, anhydrous	0	0	10	90	50	450
Lard	**20**	**180**	**0**	**0**	**0**	0
TOTAL FAT	**gm**	**Kcal%**	**gm**	**Kcal%**	**gm**	**Kcal%**
SFA	10.1	2.2	31.3	7.0	156.7	34.8
MUFA	12.8	2.8	155.9	34.6	32.1	7.1
PUFA	20.2	4.5	28.7	6.4	27.4	6.1

1.2.6 Fasting protocols

In this thesis, the effects of fasting were studied using a protocol of 24 hours with total restriction of food, starting at the beginning of light phase if the aim was collecting tissues, and at the beginning of dark phase if the objective was performing indirect calorimetry measurements.

Others experiments included short-periods of fasting as a part of the protocol, usually from 2 to 6 hours of food restriction. The shorter ones were for protocols of fast-refeeding or icv administration followed by an intracardiac perfusion to mice. The 6-hour fasting was used for glycaemia measurement in tests related to the glucose metabolism.

1.2.7 Thermoneutrality and cold exposure procedures

These experiments were aimed to study the effect of different temperatures on the metabolic phenotype of SF1-*CPT1c*-KO mice. On the one hand, for thermoneutrality studies, mice were placed at 33ºC for 48h in a temperature-controlled chamber (TSE

Systems GmbH, Moos, Germany). On the other hand, for cold exposure experiments, mice were kept at 4ºC using two different protocols:

I. Short – term cold exposure: mice were exposed to 4ºC for 6 hours, matching the end of the experiment with the beginning of dark phase.
II. Long – term cold exposure: mice were exposed to 4ºC for 24h, starting at the beginning of dark phase.

1.2.8 Body weight and food intake determination

Mice were weighted at the same time of the day during the same experiment. Body weight change was calculated as the difference between the final (or a specific time) and the initial body weight.

Food intake was measured using a precision balance. Measurements were done at the beginning of the experiment and at the same time as body weight control while the duration of the experiment.

1.2.9 Magnetic resonance image

During the stay at Dr. Cota's lab (Neurocentre Magendie, Université de Bordeaux), in vivo body composition analysis of SF1-*CPT1c*-WT and SF1-*CPT1c*-KO mice was performed by nuclear echo magnetic resonance imaging (EchoMRI 900; EchoMedical Systems, New York, USA) to evaluate the total amount of fat and lean mass of mice. Mice were weighted and placed into a movement restrainer before going inside the EchoMRI. The analysis was performed at the arrival to the housing facility, previously to HFD exposition and after the 5-day and the 6-week exposure to HFD. All measurements were taken in duplicates.

1.2.10 Indirect calorimetry

During the stay at Dr. Cota's lab (Neurocentre Magendie, Université de Bordeaux), indirect calorimetry, in-cage locomotor activity and gas exchange analysis were carried out in light, temperature and humidity controlled calorimetric chambers (TSE Systems GmbH, Moos, Germany) to analyse the metabolic phenotype of SF1-*CPT1c*-WT and SF1-*CPT1c*-KO mice. Light cycle was 12h/12h light/dark phase (lights on 3 a.m., lights off 3 p.m.). and temperature was fixed at 22ºC. Mice were acclimated in this kind of chambers for 5 days before recording. O_2 consumption and CO_2 production were measured in order to calculate the gas exchange, the respiratory exchange ratio and the energy expenditure. At the same time, locomotor activity was determined using an infrared light beam system.

Food intake and water intake was measured continuously thanks to the integration of scales inside the cages. All measurements were taken every 20 minutes. Body weight was measured daily during this time. For thermoneutrality recordings, temperature in the calorimetric chambers was increased up to 33ºC and when recording for cold exposure measurements temperature was decreased to 4ºC (subsection 1.2.7 of methodology).

1.2.11 Interscapular BAT temperature measurement

Interscapular skin temperature around BAT (iBAT temperature) was measured using infrared technology (camera FLIR E95 24º, Teledyne FLIR Systems, Wilsonville, USA) and analysed with its specific software, FLIR TOOLS Thermography Software. Videos were recorded first and last day of treatment at the beginning of light phase, each mouse was recorded for 1 minute. Skin surrounding interscapular BAT was shaved under isoflurane (IsoFlo®, Zoetis, London, UK) anaesthesia 2 days before recordings. The increment of iBAT temperature was calculated as the difference of temperature from last day to first day of treatment.

1.2.12 Glucose and insulin tolerance tests

All glucose measurements were performed using the glucometer Aviva from Accu-Chek® (Roche, Basel, Switzerland) and their glucose test strips (06453970, Roche, Basel, Switzerland). A little cut to the tale of mice was done, the first drop of blood discarded and the second drop was collected by the glucose test strips.

Glucose tolerance test (GTT) was done in mice fasted for 6 hours, fasting started at the beginning of light phase. A solution of 20% glucose (Glucose 20% B. Braun Medical, Melsungen, Germany) was injected intraperitoneally (ip) with a final dose of 2g/kg body weight.

Insulin tolerance test (ITT) was also done in mice fasted for 6 hours. A solution of 0.1 IU/mL of human insulin (Humulin 100IU/mL, Lilly Medical, Indianapolis, USA) was prepared and injected ip to the mice with a final dose of 0.5 IU/kg body weight.

For both tests, glycaemia was tested just before injection (time 0 – basal) and after 15, 30, 90, 60 and 120 minutes. Data were represented as glycaemia evolution over time and area under curve was analysed. For ITT, we also calculated the glucose disappearance rate (K_{ITT}) using glycaemia measurements of the first 30 minutes.

1.2.13 Leptin sensitivity test

For the leptin sensitivity test, mice were weighted and fasted 1 hour before injection. To test leptin sensitivity in mice, the dose of 2.5mg of leptin/Kg of body weight was used. Mice were ip injected with PBS (vehicle condition) or with a solution of 0.5mg/mL of leptin (498-OB-05M, Bio-Techne Sales Corp, Minneapolis, USA). 4 hours post injection, they were weighted again and had free access to meal.

Food intake was measured at 1h, 2h, 4h and 24h. At last point, mice were weighted again. All mice received one-day vehicle injection and the following day leptin injection.

1.2.14 Tissue dissection and sample collection

For tissue collection, mice were sacrificed by cervical dislocation. Different tissues were collected from each mouse, placed in dry ice and stored at -80ºC until processing.

For serum collection, mice were sacrificed by decapitation and blood collected in tubes with heparin (Fibrilin, 0318, Laboratorios Rovi, Madrid, Spain). Blood was kept in ice until the end of the sacrifice/test, after those tubes were centrifuged at 2000g for 10 minutes and supernatant collected in new tubes. Serum was stored at -80ºC until processing.

1.2.15 Intracardiac perfusion

Intracardiac perfusion was performed to fix brains for immunohistochemistry. Mice were anesthetized with the ketamine and xylazine mix explained before. When no reflex was observed in the animal, an incision in the ventral part of the mice was done and the heart was punctured into the bottom of left ventricle.

Then, the infusion bomb (Minipuls®3, Gilson, Madison, USA) was turned on before heart stopped beating and vena cava was cut next to the heart. The infusion bomb used was at a flow of 10 mL/min. PBS was first used to shift blood for 2 minutes, with a total volume of 20 mL per mice and, after that, neutral buffered formalin (HT501128, Sigma-Aldrich, Saint Louis, USA) was infused for 8 more minutes.

2. Molecular biology

2.1 Complexing fatty acids for central administration

Unsaturated and saturated FAs were complexed differently. Unsaturated FAs (oleic acid and linoleic acid in **Table 2**) were complexed using freshly 40% HPB (H107, Sigma-Aldrich, Saint Louis, USA) and prepared to 160mM. They were kept at room temperature into dark glass for 3 hours. Saturated FAs (stearic acid and palmitic acid in **Table 2**) were diluted with 0.1 M of NaOH at 80-100ºC and afterwards solution was mixed with a second solution of 188 mg/mL of free fatty acid BSA (126575, EMD Millipore, Burlington, USA) diluted with 0.9 % NaCl. Final concentration for complexed saturated fatty acids was 4.5 mM. All conjugated FAs were filtered before being administrated to mice.

2.2 Genotyping

Mice with four different genotypes were used: WT, CPT1c-KO, SF1-*CPT1c*-WT and SF1-*CPT1c*-KO. Since it was necessary to identify or verify its genotype, ear samples were collected from each mouse and analysed by polymerase chain reaction (PCR). For DNA preparation, 50 µL of NaOH 50 mM were added to the sample and placed at 98ºC for 30 minutes. After that, we mixed it with 50 µL of dH_2O and 5 µL of TRIS 1M pH 8. Finally, samples were centrifuged at 14000 rpm for 10 minutes. In order to perform PCR, the following reaction mix was prepared:

MIX REACTION	1 sample	Reference
H_2O DEPC	Up to 25 µL	
dNTP 2.5 mM	2.5 µL	GC-013-004 Genecraft, Lüdinghausen, Germany
Buffer Taq 10x	2.5 µL	GC-002-007 Genecraft, Lüdinghausen, Germany
$MgCl_2$ Buffer 50 mM	1.25 µL	
Forward enhancer 12.5 µM	Depends on PCR	Table 5
Reverse enhancer 12.5 µM	Depends on PCR	Table 5
DNA Polymerase Taq	0.35 µL	GC-002-050 Genrecraft, Lüdinghausen, Germany
DNA Sample	1.5 µL	

Thermocycler PCR protocol was run using the following details:

- **Hot Start:** 94ºC – 3 min
- **30 cycles:**
    - **Denaturalization:** 94ºC – 30 sec

- **Annealing:** depending on oligonucleotides enhancers
- **Elongation:** 72ºC – time depending on amplicon size

- **72ºC – 2 min**

Afterwards, samples were mixed with 10 % of volume of loading buffer (50% Glycerol, 50% dH_2O and Bromophenol Blue) and they were separated on agarose gel placed into TAE buffer (50mM EDTA pH 8.0, 5.7% acetic acid and 500mM Tris). Finally, the gel was revealed with UV-light. Oligonucleotide enhancers and their particularly conditions can be found on **table 5**.

2.2.1 Genotyping using VMH samples

VMH of SF1-*CPT1c*-WT and SF1-*CPT1c*-KO mice were used to verify the proper recombination between LoxP sites of CPT1c modified gene **(Fig. 21)**, and therefore to evaluate if exons 4-6 were excised in SF1-*CPT1c*-KO mice. VMH samples were collected using a brain matrix and a micropunch and stored at -80ºC until they were processed. DNA preparation for PCR and specific buffers used are detailed below:

1) To boil VMH samples at 95ºC for 10 minutes in 50 µL of digestive buffer with fresh β-mercaptoethanol (1/100).
2) To add 0.7 µL of Proteinase K (3115887001, Roche, Basel, Switzerland).
3) To incubate samples at 55ºC overnight, in constant agitation.
4) To boil samples at 95ºC for 10 minutes.
5) To add 50 µL of a mix of phenol and chloroform in a dilution 1:1.
6) To mix and centrifuge 5 minutes at maximum speed.
7) To separate superior phase into new tubes and to add 50µL of chloroform.
8) To mix and centrifuge 5 minutes at maximum speed.
9) To add 125 µL of EtOH 99 % and 12.5 µL of AcNa 3M pH 5.3.
10) To keep samples 2 h at -20ºC.
11) To centrifuge 25 minutes at maximum speed.
12) To add EtOH 75 %.
13) To centrifuge 10 minutes at maximum speed.
14) Let samples to dry and
15) To dilute the pellet with 35 µL of DEPC H_2O.

Digestive buffer (300 mL): 13.4 mL of Tris-Cl 1.5M pH 8.8, 5 mL of $(NH_4)_2SO_4$ 1M, 2 mL of $MgCl_2$ 1 M, 1.5 mL of triton X-100 100 %, dH_2O to 300 mL.

Table 5. Oligonucleotides enhancers. Oligonucleotides enhancers used for genotyping mice before experiments. Sequence and experimental details are also indicated. All oligonucleotides were bought at Integrated DNA Technologies (IDT™).

GENOTYPE	PRIMER	SEQUENCE	AMPLICON SIZE	VOLUME	AGAROSE GEL	ANNEALING
CPT1c – KO	F9	5'- GAGTCAGCCATGACCCGACTGTT -3'	200pb	0.9 µL	0.8%	65ºC – 30''
	R1	5'- CCGGTAGAATTGACCTGCAGGGGC -3'		0.6 µL		
	R9	5'- CGCTAAAGCCCAGACAGAACACAC -3'		1.6 µL		
KO FIRST 1	F – 5'arm	5'- ATGGACCCATAGTCTTGAAACCTGG-3'	625 pb and 432pb	2 µL	2%	63.5ºC – 30''
	F - Neo	5'- GGGATCTCATGCTGGAGTTCTTCG -3'				
	R - Targ	5'- GTGTTTGCCTAGCATGCGAACG -3'				
KO FIRST 2	F - Lox	5'- GAGATGGCGCAACGCAATTAATG -3'	292bp	2 µL	2%	63.5ºC – 30''
	R – 3'arm	5'- ATTCTTGATTCGTGTGACTCATTCCG -3'				
CONDITIONAL KO/FLOXED	F – 5'arm	5'- ATGGACCCATAGTCTTGAAACCTGG-3'	517pb	1.5 µL	2%	63.5ºC – 30''
	R - Targ	5'- GTGTTTGCCTAGCATGCGAACG -3'				
FLPO	F – FlpO	5'- CTATCGAATTCCACCATGGCTCCTAAGAAGAA -3'	1300pb	1 µL	0.8%	58ºC – 1'
	R - FlpO	5'- CAATGCGATGAATTCTCAGATCCGCCTCTTGATGTA -3'				
SF1-CRE	F – Cre	5'- CTGAGCTGCAGCGCAGGGACAT -3'	250pb	1 µL	2%	68ºC – 1'
	R – Cre	5'-TGCGAACCTCATCACTCGTTGCAT -3'				

F: forward, R: reverse.

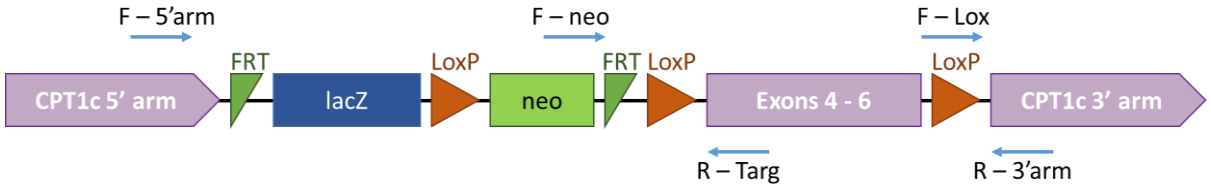

Fig. 21. Schematic representation of modified *Cpt1c* gene, and all oligonucleotide enhancers used for genotyping**.**

Once DNA samples were diluted in water, PCR was run using the same PCR mix and thermocycler conditions as in ear samples for genotyping. Oligonucleotides enhancers used were F-5'arm and R-3'arm **(Table 5)**. Micropunch of hippocampus and cortex were processed in the same way as the VMH, and they were used as a control of non-recombination in SF1-*CPT1c*-KO mice.

2.3 RNA analyses

2.3.1 RNA extraction

Total RNA was extracted using TRIzol® Reagent (15596018, Invitrogen, Waltham, USA), which is a monophasic reactive that facilitates RNA isolation. This reactive has the ability to inhibit RNAase activity while dissolving all other cellular components.

To homogenate the sample, 25-30 mg of tissue with 500 µL of TRIzol® were placed in screw tubes filled with ceramic beads (13113-325, Qiagen, Hilden, Germany), and tubes were introduced to the homogenater Fast-Prep®-24 (MP Biomedicals, Irvine, USA) to run 3 cycles at 6.5M/sec for 35 seconds plus 2 cycles at 6M/sec for 30 seconds. Samples were kept 5 minutes in ice between cycles. Then, chloroform (at -20ºC, 200µL/mL TRIzol®) was added to the homogenate to separate RNA in a superior aqueous phase while all the other components (proteins and DNA) were retained in the inferior organic phase trough a 15-minute centrifugation at 13400 rpm. This aqueous phase was placed into new tubes and RNA precipitated using isopropanol (at -20ºC, 500 µl isopropanol/mL TRIzol®) and a second centrifugation of 13400 rpm for 20 min. RNA pellet had to be cleaned with 75% ethanol and finally RNA pellet was diluted with autoclaved DEPC H_2O at 60ºC in agitation. RNA quantification was done by micro-plate Synergy™ HT (Biotek, Winooski, USA).

2.3.2 cDNA synthesis

In order to analyse gene expression from RNA, it was necessary to synthesize cDNA through a reverse transcription from RNA. M-MLV was the inverse retrotranscriptase used in our laboratory. In this reaction, it was necessary to add random primers, oligonucleotides which bind to RNA template in random regions and allow the transcription of the whole RNA present in the sample. RNAase inhibitor, dNTPs and buffer enzyme were also needed. Reaction was performed at 37ºC for 1 h.

For the reverse transcription, 1 µg of RNA and the following reaction mix was used in a total volume of 20 µL:

MIX REACTION	1 sample	Reference
Random Hexamers	0.5 µL	79236 Qiagen, Hilden, Germany
Buffer 10x	2 µL	F88903-1 Lucigen, Middleton, USA
dNTP 10 mM	4 µL	GC-013-004 Genecraft, Lüdinghausen, Germany
M-MLV	2 µL	30222-1 Lucigen, Middleton, USA
RNAase inh	0.5 µL	30281-1 Lucigen, Middleton, USA
1 µg RNA sample	Depends on concentration	
DEPC H_2O	Up to 20 µL	

2.3.3 Quantitative real – time polymerase chain reaction (qRT-PCR)

qRT-PCR technique is a conventional PCR with the possibility to quantify amplifications while the reaction is ongoing. To achieve this purpose, a fluorescent dye was added to the reaction mix and the thermocycler was complemented with spectrophotometry technology. We used two kind of fluorescent reporters for this type of reaction:

- Double-stranded DNA intercalating agents, which are non-specific. They bind to any new synthesized double-strand DNA and, once the reporter is bound, it can emit fluorescence. SYBR®Green was the one used in this thesis.
- Amplicon-specific labelled hybridization or fluorescent probes, which are highly specific and allow the detection of different gene expression in the same reaction (multiplex). In this work, TaqMan™ assay was used. It consists of primers with a quencher and a reporter fluorophore that, when new DNA is being synthesised, quencher is released and the reporter emits fluorescence.

Depending on the kind of the reporters used in qRT-PCR, two different super mix reactions were used: SsoAdvanced™ SYBR®Green Supermix (172-5261, BioRad, Hercules, USA) for double – stranded DNA intercalating agents and SsoFast™ Probes Supermix (172-5231, BioRad, Hercules, USA) for TaqMan assay. The whole mix reaction was prepared using the following formulas (for 1 sample):

SYBER®Green	TaqMan™
10 µL super mix	10 µL Super mix
0.5 µM oligonucleotide F	1X Probe gene of interest
0.5 µM oligonucleotide R	1X Probe housekeeping gene
20 ng DNA template	20 ng DNA template
up to 20 µl of dH_2O	Up to 20 µL of dH_2O

Table 6 and **table 7** include all the oligonucleotide sequences used in this investigation (all provided from Integrated DNA Technologies, Coralville, USA).

Table 6. Oligonucleotide enhancers and their sequence used in SYBR®Green assay.

GENE	SEQUENCE
AgRP F	5'-TTTGTCCTCTGAAGCTGTATGC- 3'
AgRP R	5'- GCATGAGGTGCCTCCCTA - 3'
Cpt1a F	5'-GACTCCGCTCGCTCATTC - 3'
Cpt1a R	5'-AAGGCCACAGCTTGGTGA - 3'
G6P F	5'-TCAACCTCGTCTTCAAGTGGATT- 3'
G6P R	5'-CTGCTTTATTATAGGCACGGAGCT - 3'
Gapdh F	5' – TCCACTTTGCCACTGCA - 3'
Gapdh R	5' - GAGACGGCCGCATCTTCTT - 3'
Npy F	5'-TCCGCTCTGCGACACTACAT- 3'
Npy R	5'-TGCTTTCCTTCATTAAGAGGT- 3'
Pdk4 F	5'-CGCTTAGTGAACACTCCTTCG - 3'
Pdk4 R	5'-CTTCTGGGCTCTTCTCATGG - 3'
Pepck F	5'-CCACAGGCACTAGGGAAGGC - 3'
PepcK R	5'-GGCGGAGCATATGCTGATCC- 3'
Pgc1α F	5' - GAAAGGGCCAAACAGAGAGA - 3'
Pgc1α R	5' - GTAAATCACACGGCGCTCTT - 3'
Prdm16 F	5'- CCTAAGGTGTGCCCAGCA - 3'
Prdm16 R	5'- CACCTTCCGCTTTTCTACCC - 3'
Pomc F	5'-TGAACATCTTTGTCCCCAGAG - 3'
Pomc R	5'-TGCAGAGGCAAACAAGATTGG - 3'
S18 F	5'-CGGACAGGATTGACAGATTG - 3'
S18 R	5'-CAAATCGCTCCACCAACTAA - 3'

Table 7. Oligonucleotide enhancers used in Taqman assay.

Gene	Reference	Dye
UCP1	Mm.PT.58.7088262	Hex
GAPDH	Mm.PT.39a.1	Fam

qRT-PCR was performed in the thermocycler C1000 Thermal Cycler CFX96™ (BioRad, Hercules, USA), following a different protocol depending on the assay type **(Table 8)**. The efficiency of the amplification and the annealing temperature of forward and reverse oligonucleotides enhancers were tested performing standard curves with serial dilutions.

Housekeeping genes as GAPDH or S18, depending of the sample, were used to normalize the relative gene expression.

Table 8. Detailed protocol of SYBR®Green and Taqman qPCR assay.

SYBR®Green assay	TaqMan™ assay
1. 95 ºC for 30 seconds	1. 95 ºC for 30 seconds
2. 95 ºc for 5 seconds	2. Plate read
3. 60 ºC for 20 seconds	3. 95ºC for 5 seconds
4. Plate read	4. 60ºC for 30 seconds
5. Go to step 2, 39 more times	5. Plate read
6. 95 ºc for 10 seconds	6. Go to step 2, 39 more times
7. Melting curve 65 ºC to 95 ºC: increment 0.5 ºC for 5 seconds	
8. Plate read	

2.4 Protein analyses

2.4.1 Protein tissue extraction

Total protein was obtained from frozen tissues. All the protein extraction process was performed at 4ºC. Tissues were homogenated in screw tubes with ceramic beads and lysis buffer in the homegenator Fast-Prep®-24 (MP Biomedicals, Irvine, USA). Lysis buffer consists in RIPA buffer (R0268 Sigma-Aldrich, Saint Louis, USA) complemented with protease inhibitors (A32955, Fisher Scientific, Hampton, USA) and phosphatase inhibitors (32957, Fisher Scientific, Hampton, USA), in a ratio of 1/40 to RIPA buffer. 3 cycles at 6.5M/sec in the Fast-Prep®-24 were done and samples were kept 5 minutes in ice between cycles. Homegenates obtained were transferred into new tubes.

In order to break all cell components that remained entire, samples were sonicated. Afterwards, samples were placed in a wheel for 20 minutes at 4ºC and frozen at -20ºC for at least 3 hours. Once unfrozen, samples were centrifuged at 13.000 *g* for 10 minutes at 4ºC and supernatant collected into new tubes.

2.4.2 Western Blot

Western Blot technique allows to detect one concrete protein from the total protein of a sample, this detection can be done through specific antibodies against the specific protein. The whole technique can be divided into 7 steps:

1.1.1.1 Sample preparation

Protein samples extracted as explained above were quantified by Pierce™ BCA Protein Assay Kit (23225, Thermo Fisher Scientific, Waltham, USA) and a plate reader, following kit instructions. After quantification, samples were usually prepared to a final concentration of 0.5 µg/µL adding water and loading buffer.

Loading buffer 5X: 125 mM Tris pH 6.8, 25 % glycerol, 50 % SDS-20 %, 10 % β-mercapto-ethanol, 2.5 % dH_2O and Bromophenol blue.

1.1.1.2 Electrophoresis

Protein extracts were boiled at 95ºC for 5 minutes in order to denaturalize proteins. This step is important to allow them to migrate proportionally to their molecular weight among a polyacrylamide gel (SDS-PAGE). Two types of gel with different percentage of acrylamide were used: hand-made **(Table 9)** or prefabricated (Midi-PROTEAN® gels, BioRad, Hercules, USA). Electrophoresis was run to a fixed voltage of 130V or at 180-200V, respectively, submerged in electrophoresis buffer.

Electrophoresis buffer: 25 mM Tris-HCl pH 8.3, 192 mM glycine and 0.05 % SDS-20 %.

Table 9. Hand-made polyacrylamide gels.

STACKING GEL			RUNNING GEL		
%	**Solution components**	**10 ml**	**%**	**Solution components**	**20 ml**
5%	H_2O	5,55 mL	**10%**	H_2O	4 mL
	30% Acrylamide mix (37,5:1)	1,7 mL		30% Acrylamide mix (37,5:1)	3,3 mL
	Tris 0.5 M pH=6.8	2,5 mL		Tris 1.5 M pH=8.8	2,5 mL
	SDS 10%	100 µL		SDS 10%	100 µL
	APS 10%	100 µL		APS 10%	100 µL
	TEMED	10 µL		TEMED	4 µL

1.1.1.3 Electrotransfer

Protein was transferred from SD-PAGE gel to a PVDF membrane (Immobilion-P PVDF IPVH 00010, Merck Millipore, Burlington, USA). The protocol for the transfer was to create a "sandwich" including the gel with molecular weight separated-proteins and the PVDF membrane. This "sandwich" consists in: a sponge, Whatman paper (11330744, Fisher Scientific, Hampton, USA), SDS-PAGE gel, PVDF membrane, Whatman paper and a sponge.

All these elements had to be introduced in a tray filled with transfer buffer. Electrotransfer were run at a fixed amplitude of 400 mA at 4ºC for 90 minutes.

Transfer buffer: 25 mM Tris pH 8.3, 192 mM glycine and 20 % methanol.

1.1.1.4 Membrane blocking

PVDF membrane can have unspecific unions sites and protein transferred can be some of them for some primary antibody, therefore this union sites had to be blocked with other proteins that would join them. After the electrotransfer, membranes were rinsed with TBS-T and incubated for 1 h at room temperature with blocking solution, prepared with 5 % fat-free powdered-milk diluted in TBS-T.

TBS-T: 0.1 % Tween 20 (P9416, Sigma-Aldrich, Saint Louis, USA) in TBS 1X.

TBS: 20 mM Tris, 137 mM NaCl and 3.9 mM HCl

1.1.1.5 Primary antibody incubation

Primary antibody incubations were performed at 4ºC overnight in plastic-sealed bags and in constant agitation. Each antibody was diluted according to data sheet instructions **(Table 10)**.

Table 10. Primary antibodies and their dilution factor used for protein detection.

Antibody	Reference	Dilution	Host
Anti ACC	3676, Cell Signaling, Danvers, USA	1:1000	Rabbit
Anti AMPKα	23A3, Cell Signaling, Danvers, USA	1:1000	Rabbit
Anti FAS	sc-48357, Santa Cruz, Dallas, USA	1:1000	Rabbit
Anti GAPDH	AM4300, Ambion, Austin, USA	1:50000	Mouse
Anti phospho – ACC (Ser 79)	3661, Cell Signaling, Danvers, USA	1:2000	Rabbit
Anti phospho – AMPKα (Thr172)	2535S, Cell Signaling, Danvers, USA	1:1000	Rabbit

1.1.1.6 Secondary antibody incubation

To detect the complex antigen-primary antibody, a secondary antibody was needed. It allowed to visualize the complex through an indirect enzymatic immunoassay. The secondary antibody was a horseradish peroxidase-conjugated immunoglobulin against primary antibody host and it depends on primary antibody specie. Two different types have been used:

Antibody	Reference	Dilution
Anti-rabbit – HRP	111-035-144, Jackson, West Grove, USA	1/10000
Anti-mouse – HRP	515-035-003. Jackson, West Grove, USA	1/20000

Previously at and after the secondary incubation, membranes were cleaned three times in TBS-T for 10 minutes in agitation. Afterwards, incubation was performed in plastic-sealed bags for 1 hour at room temperature in constant agitation, secondary antibodies were diluted in TBST.

1.1.1.7 Developing and quantification

Secondary antibody was detected using a chemoluminescence substrate named Luminata Forte Western HRP substrate (WBLUF0500, Merck Millipore, Burlington, USA). The horseradish peroxidase conjugated to secondary antibody react to Luminata and emit light, which can be detected by a camera. Images were collected by Syngene G:Box (Syngene, Cambridge, UK) and quantified by densiometry using ImageJ Software (NIH, Wisconsin, USA). The housekeeping gene GAPDH was used as control to normalize protein expression levels. In figures, all bands of each experiment (proteins of interest and housekeeping proteins) come from the same gels, although images were cut to show a representative band for each type of samples.

3. Biochemistry

3.1 Glucose determination

Glucose levels from serum samples were determined using the Spinreact glucose determination kit (41012, Glucose - LQ, Spinreact, Girona, Spain) following commercial instructions. Basically, this kit is a colorimetric enzymatic assay **(Fig. 22)** which consists in the oxidation of glucose to gluconic acid by the glucose oxidase enzyme (GOD). From this reaction, hydrogen peroxide is formed (H_2O_2) and it is detected by a chromogenic oxygen acceptor. In presence of the enzyme peroxidase (POD), phenol and 4-aminophenazone (4-AP) are condensed by the hydrogen peroxide forming a quinone. The intensity of the colour formed is directly proportional to glucose concentration of the sample and it is measured by the plate reader Synergy™ HT.

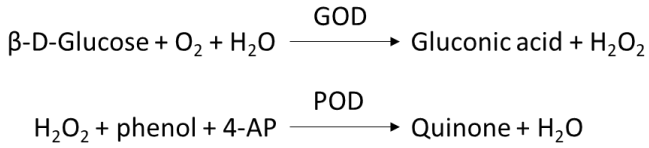

Fig. 22. Colorimetric assay to detect glucose levels in serum. 4-AP: 4-aminophenazone GOD: glucose oxidase enzyme; POD: peroxidase.

3.2 Glycerol and Triglycerides determination

To determine triglycerides (TG) from tissues, first step was to separate fat from the rest of the tissue. Afterwards, a commercial kit was used to determine the amount of TG in samples.

To extract fat from frozen tissue, in this case liver tissue, 40 mg of tissue were prepared in Eppendorf tubes containing ceramic bead (13113-325, Qiagen, Hilden, Germany) and 800 µL of cold acetone 100 % (32201-1L-M, Sigma-Aldrich, Saint Louis, USA). In order to disrupt the tissue, these tubes were homogenated using the homogenater Fast-Prep®-24 at a speed setting of 6.5 M/sec for 3 cycles of 30 second with 5-minute ice incubations in between. After that, samples were incubated in rotatory homogenization overnight at room temperature. Next day, tubes were placed in static position during 15 minutes and the upper layer was used for glycerol and TG measurement.

The measurement was done using the Serum Triglyceride Determination kit (TR0100, Sigma Aldrich, Saint Louis, USA), following manufacturer instructions. This kit is based on a 4-step colorimetric enzymatic assay **(Fig. 23)**. Basically, first step consists in the TG hydrolysis into glycerol and free fatty acids trough a lipoprotein lipase. Glycerol is then phosphorylated forming glycerol – 1 – phosphate (G-1-P) in a reaction catalysed by the glycerol kinase (GK). This product is oxidized to dihydroxyacetone phosphate (DAP) and hydrogen peroxide (H_2O_2) by the glycerol phosphate oxidase (GPO) enzyme. In the last reaction, peroxidase (POD) couples H_2O_2 with two substrates (4-AAP and ESPA) to finally produce a quinoneimine dye, a product that has an absorbance at 540nm. This absorbance is directly proportional to TG concentration of the sample. Free glycerol of samples is measured after the first reaction.

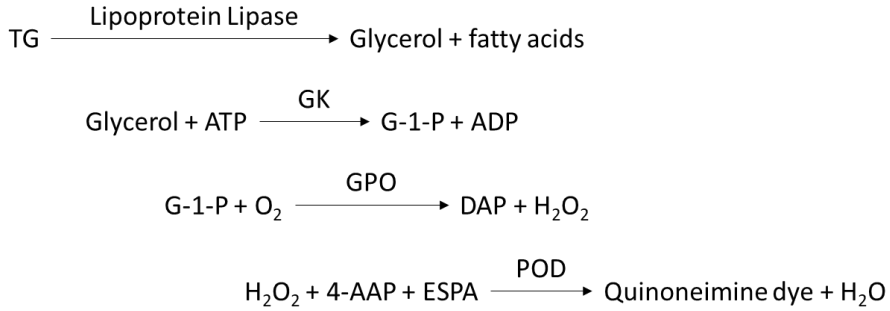

Fig. 23. Colorimetric assay to detect TG and glycerol levels in tissue samples and serum. 4-AAP: 4-aminoantipyrine; DAP: dihydroxyacetone phosphate; ESPA: sodium N-ethyl-N-(3-sulfopropyl) m-anisidine; G-1-P: glycerol – 1 – phosphate; GK: glycerol kinase; GPO: glycerol phosphate oxidase; POD: peroxidase; TG: triglycerides.

3.3 Hepatic glycogen determination

As in the triglycerides determination, for hepatic glycogen determination two steps were needed. First step consisted in extracting glycogen from liver and the second step was to quantify the amount of it using the glucose determination kit.

To extract glycogen from frozen liver, 100 mg of tissue was used and homogenated with 0.25 mL of 30 % KOH using the homogenater Fast-Prep®-24. Then samples were boiled for 15 minutes at 95ºC. Afterwards, to precipitate glycogen the following steps were done:

i. To add 120 µL of homogenate sample or 30 % KOH (blank) to 2x2 cm of Whatman paper (11330744 Fisher Scientific, Hampton, USA).
ii. To wash Whatman paper with 66 % EtOH, being fully covered by it. Glycogen precipitates and it is retained to Whatman paper. Repeat this step 3 times at room temperature.
iii. To dry Whatman paper at 70ºC.
iv. To transfer Whatman paper to new tubes containing 1 mL of 0.5 mg/mL of amiloglucosidase (A7420, Sigma-Aldrich, Saint Louis, USA) prepared in 400 mM of sodium acetate pH 4.8.
v. To incubate the samples at 37ºC for 90 minutes.

The digested samples contained an amount of glucose directly proportional to the amount of glycogen. Therefore, the Spinreact glucose determination kit was used for this samples as explained in the subsection 3.1. of glucose determination.

4. Immunofluorescence assays

For immunofluoresnce assays, mice were perfused and tissue was kept in neutral formalin buffered (HT501128, Sigma-Aldrich, Saint Louis, USA) for 24 h. After that, tissues were washed twice using PBS and cryopreserved using a 30 % sucrose solution. Finally, samples were frozen in isopentane (2-methylbutane) and kept at -80ºC until proceed.

4.1 Multiplex nucleic acid FISH

The fluorescent *in situ* hybridization (FISH) assay to detect multiple RNAs in brain slices was done using the technology of RNA Scope® (ACD Bio, Newark, USA). Fixed brain slices of 15 µm thick containing ventromedial hypothalamus were cut using a Leica cryostat and they were placed into Superfrost Plus Slides (J1800AMNZ, Thermo Fisher Scientific, Waltham, USA). RNA Scope® fluorescent multiplex assay was performed following commercial instructions. This technology consists in several steps. First, slices were fixed using neutral formalin buffered and dehydrated with increasing ethanol concentrations. This first step was followed by an antigen retrieval and a protease III - digestion, both solutions were part of the pre-treatment kit of RNA Scope® (322340, ACD Bio, Newark, USA). Then, the hybridization step with probes designed especially for detecting RNA of SF1 and CPT1c. Last steps consisted in amplifying and detecting the signal of the probes used. Hybridization and signal amplification was done using the RNA Scope® Fluorescent Multiplex assay (320851, ACD Bio, Newark, USA). Finally, DAPI was used to counterstain slides, whose were mounted using antifade Fluoromount-G® (0100-01, Southern Biotech, Birmingham, USA) and coverslips (DIO2460, Deltalab, Barcelona, Spain). The confocal microscope of LEICA DMi8 was used to take pictures of probes signal.

4.2 Immunohistochemistry

To determine presence and distribution of a specific antigen in brain tissue, floating immunohistochemistry technique was used. Fixed frozen brain were 30 µm sliced and washed using PBS in 24-well plates. Then tissue antigens were blocked using a blocking buffer for 1 hour at room temperature and afterwards brain slices were incubated with the primary antibody **(Table 11)** diluted in blocking buffered. Slices were kept 1 hour at room temperature and overnight at 4ºC in soft agitation. Next day, slices were washed using KPBS and they were 2-hour incubated with the secondary antibody anti-Rabbit

Alexa 647 (A21244, Invitrogen, Waltham, USA) at a dilution of 1:1000 in blocking buffer. Three washes after, slices were counterstained with Hoescht (1mg/mL, 14530, Sigma-Aldrich, Saint Louis, USA) 1:1000 and mounted into Superfrost Plus Slides (J1800AMNZ, Thermo Fisher Scientific, Waltham, USA) using antifade Fluoromount-G® (0100-01, Southern Biotech, Birmingham, USA) and coverslips (DIO2460, Deltalab, Barcelona, Spain). The Confocal microscope of LEICA DMi8 was used to take pictures of secondary antibody signal.

Table 11. Primary antibodies and their dilution factor used for antigen detection.

Antibody	Reference	Dilution	Host
Anti c-Fos	2250, Cell Signaling, Danvers, USA	1:20	Rabbit
Anti Iba-1	019-19741, FUJIFILM Wako, Richmond, USA	1:500	Rabbit

Blocking buffer: 2% goat serum (g-9023 Sigma-Aldrich, Saint Louis, USA), 3% BSA (10735078001, Roche, Basel, Switzerland), 0.1% triton x-1000 (T8787, Sigma-Aldrich, Saint Louis, USA) and KBPS.

KPBS: 155mM NaCl, 40mM K_2HPO_4, 10mM KH_2PO_4, dH_2O.

5. Data processing and statistical analyses

Prism 9.0 (Graphpad Software, San Diego, USA) was used to process data and to perform the statistical analyses. Data were expressed as mean ± SEM. Comparative analyses were performed using two tests depending on the number of groups aimed to compare. For only two groups, a t-student test was used, whilst if the objective was to compare more than two groups between them the 2-way ANOVA test was used. A p value less than 0.05 ($p<0.05$) expressing differences between groups was considered statistically significant. For each group of experiments, number of mice and statistical test used is specified.

RESULTS

Chapter I

Metabolic phenotype of mice deficient of CPT1c in SF1 neurons in response to high-fat diet and other metabolic challenges

Our group has been studying the role of CPT1c in energy homeostasis. As stated in the introduction section, CPT1c-KO mice present an obesogenic phenotype with higher susceptibility of body weight gain under HFD administration compared to WT mice. These transgenic mice also show lower levels of FAO in muscle and liver than WT mice with no difference in food intake. In a short-term exposure to a HFD (7 days) or central leptin administration, CPT1c-KO mice also present impaired BAT thermogenesis activation contributing to the obesogenic phenotype. Moreover, reversion of CPT1c expression in the VMH of CPT1c-KO recovered thermogenesis activity. In response to other metabolic challenges such as fasting, these mice show an inappropriate selection of energy substrate.

Because of the importance of SF1 neurons within the VMH in the control of energy and glucose homeostasis, most of them feeding-independent effects, we aimed to generate a mouse model with specific deletion of CPT1c in SF1 neurons of the VMH (SF1-*CPT1c*-KO) using the FRT-Flp and Cre-lox recombination technologies as described in the methodology section 1.1.2. In this chapter, we present the genotype validation and the metabolic phenotype characterisation of the SF1-*CPT1c*-KO mice under different metabolic challenges.

1 Genotype validation

For the genotype validation of SF1-*CPT1c*-KO mice, we used three different techniques. These techniques allowed us to determine, on the one hand, that Cre protein showed recombinase activity in the specific region and, on the other hand, that LoxP sites were recombined resulting in the deletion of exons 4 to 6 of *Cpt1c*. After these validations, we confirmed that these mice had lost CPT1c expression in SF1 neurons of VMH by RNAScope® FISH.

1.1 Validation of Cre activity

For this purpose, we used the AAVs indicated in methodology section 1.2.1. These AAVs contained the mCherry sequence reversed and flanked by LoxP sites. If SF1 neurons of SF1-*CPT1c*-KO mice were Cre positive and the protein had recombinase activity, LoxP sites would recombine and mCherry would flip, leading to its expression (red signal). We performed a stereotaxic surgery to bilaterally inject the AAVs into the VMH **(Fig. 24A)**.

After three weeks of recovery, we observed mCherry signal on VMH of SF1-*CPT1c*-KO mice, but this signal was not detected on VMH of SF1-*CPT1c*-WT mice **(Fig. 24B)**. These results indicate that the Cre protein was active on SF1 neurons of the specific KO mice.

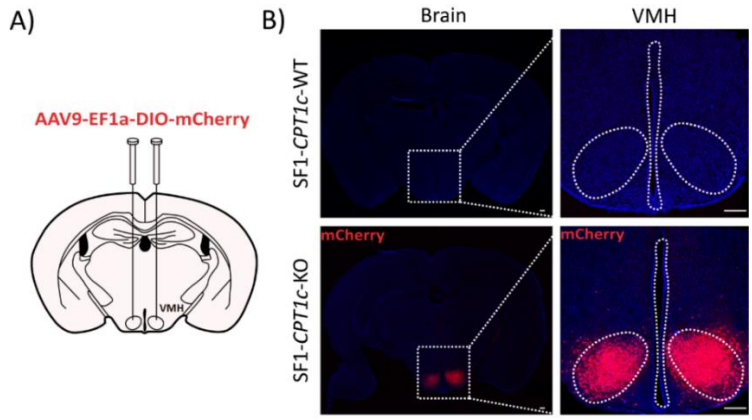

Fig. 24. Validation of Cre activity in SF1-*CPT1c*-KO mice. A) Schematic representation of stereotactic injection of AAVs. B) Brain sections and VMH area of SF1-*CPT1c*-WT and SF1-*CPT1c*-KO mice, 3 weeks after stereotaxic surgery. Scale bar: 250 µm.

1.2 Validation of excision of exons 4 to 6 of CPT1c in VMH

The second technique for the validation of the mouse model was to check if *Cpt1c* genomic amplification from the VMH of the specific KO resulted in a shorter band than the one from control mice, because of the loss of exons 4 to 6 of the *Cpt1c* gen in the transgenic mice. VMH, hippocampus and cortex were collected from SF1-*CPT1c*-KO and SF1-*CPT1c*-WT mice and DNA was extracted. Afterwards, a PCR using enhancers from the sequence before and after the exons 4-6 was performed (**Fig. 21**, methodology section 2.2.1, enhancers F - 5'arm and R - 3'arm). Results showed that only the SF1-*CPT1c*-KO mice had a lower weight band product from the PCR at the VMH and this band could not be observed in control mice or in any other part of the brain of the null mice **(Fig. 25)**. In some VMH obtained from SF1-*CPT1c*-KO mice, a second less intense band could be observed **(Fig. 25)**. This second band showed the same weight than the one that appeared in the VMH of control mice. We attributed this band to other neurons of the VMH that are not SF1 neurons and also to a lack of precision when using the micropunch dissection. Despite of this additional band, it was clear that the shorter band was only present in VMH samples coming from SF1-*CPT1c*-KO mice and this band had the weight expected for the deletions of exons 4 to 6 of CPT1c gene.

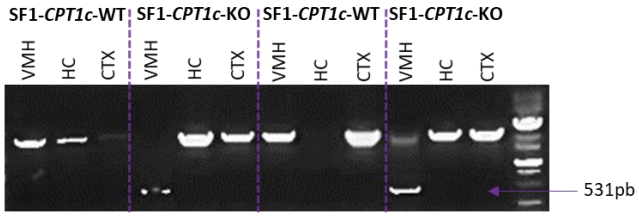

Fig. 25. PCR results for the excision validation of the exons 4 to 6 of the gene *Cpt1c* in SF1-*CPT1c*-KO mice. Picture of agarose gel after PCR product was run. Samples derived from three different parts of the brain from SF1-*CPT1c*-WT and -KO mice were used. CTX: cortex; HC: hippocampus; VMH: ventromedial hypothalamus.

1.3 Validation of CPT1c expression in SF1 neurons

At this point, we believed that exons 4-6 of *Cpt1c* gene had been excised in SF1 neurons, but to be truly sure that CPT1c was not expressed, we decided to run the RNAScope® kit using probes against SF1 and CPT1c mRNAs, as no specific antibodies for immunohistochemistry were available. Results of this kit showed that most VMH neurons of SF1-*CPT1c*-WT showed signal of SF1 and CPT1C probes in the soma while only few neurons in SF1-*CPT1c*-KO sections, indicating that SF1-*CPT1c*-KO mice do not express mRNA of CPT1c in SF1 neuron **(Fig. 26)**.

After ensuring the genotype of SF1-*CPT1c*-KO mice through the three techniques, we proceeded with the analysis of the metabolic phenotype.

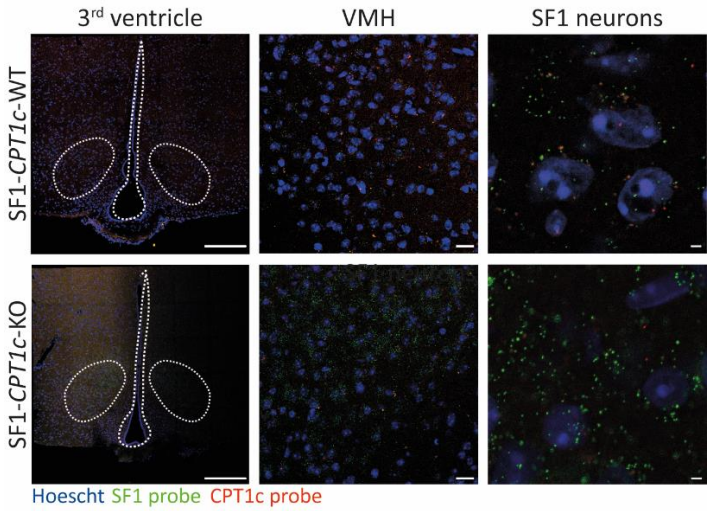

Fig. 26. mRNA expression of SF1 and CPT1c using RNAScope® FISH technique. Probes against SF1 mRNA and CPT1c mRNA were designed and used in brain sections obtained from SF1-*CPT1c*-WT and -KO mice. From left to right: 3rd ventricle, VMH and zoom of VMH area (SF1 neurons). Scale bar 3rd ventricle: 250 µm; VMH: 25 µm; SF1 neurons: 5 µm.

2 Metabolic phenotype of SF1-*CPT1c*-KO mice under chow diet

2.1 Body weight, food intake and mass distribution

We monitored the evolution of body weight of male and female mice over 8 weeks of SD feeding. Male mice did not show any significant difference in body weight **(Fig. 27A)** or food intake **(Fig. 27B)**. Regarding female mice, body weight **(Fig. 27C)** and food intake **(Fig. 27D)** were also similar between the genotypes.

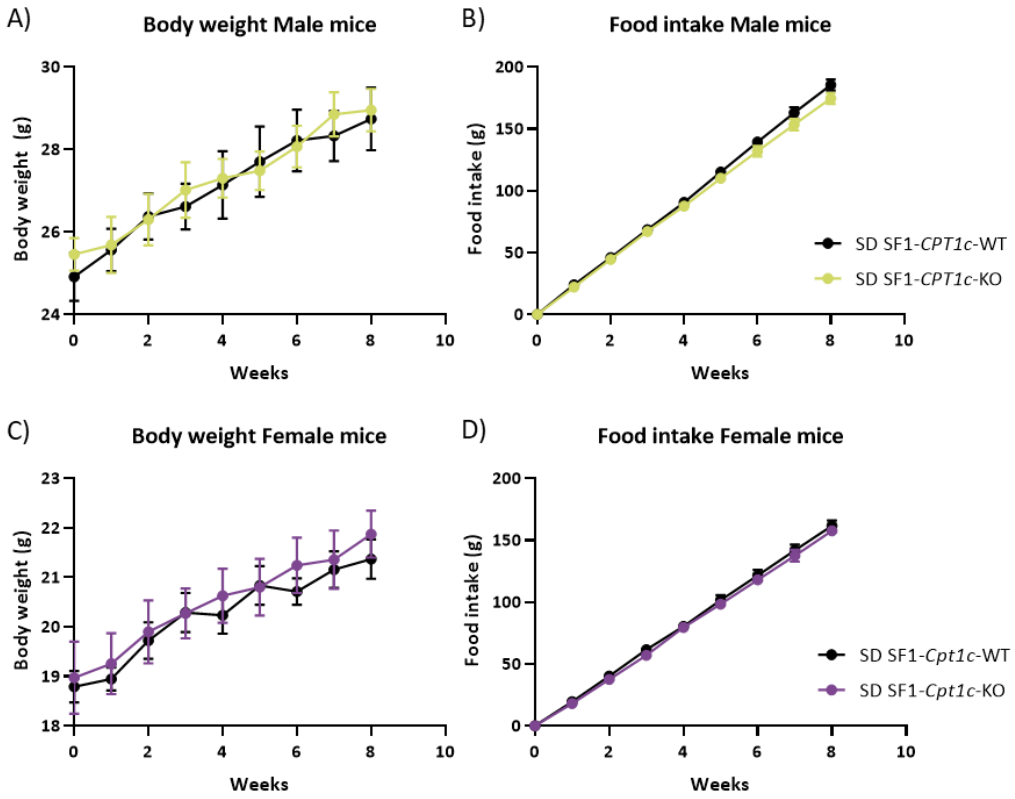

Fig. 27. Body weight and food intake of male and female mice over 8 weeks fed SD. A) Male mice body weight. B) Male mice food intake. C) Female mice body weight. D) Female mice food intake. Data were represented as mean ± SEM, male and female mice, 8-week-old, n= 7-9/ group. Statistical significance was determined by ANOVA test with post-hoc Bonferroni. Olive green: male mice, purple: female mice.

When mice were sacrificed after 8 weeks of SD feeding, BAT, subcutaneous WAT (sWAT) and epididymal WAT (eWAT) were collected and weighed. No significant differences were observed between genotypes, although there was a tendency of SF1-*CPT1c*-KO male mice of having more fat mass than SF1-*CPT1c*-WT male mice **(Fig. 28A-C)**. The tendency was not observed studying female mice **(Fig. 28D-F)**.

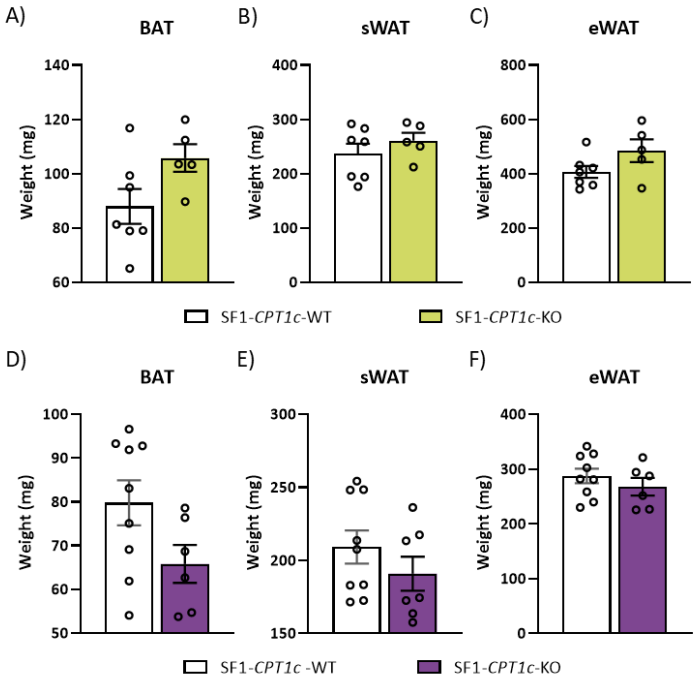

Fig. 28. Weight of BAT, sWAT and eWAT collected from male and female mice. A) Weight of BAT from male mice. B) Weight of sWAT from male mice. C) Weight of eWAT from male mice. D) Weight of BAT from female mice. E) Weight of sWAT from female mice. F) Weight of eWAT from female mice. Data were represented as mean ± SEM, male and female mice, 16-week-old, n= 7-9/ group. Statistical significance was determined by a t-student test. BAT: brown adipose tissue; eWAT: epididymal white adipose tissue; sWAT: subcutaneous white adipose tissue. Olive green: male mice, purple: female mice.

Mass distribution was also evaluated using magnetic resonance imaging (MRI) with a different batch of mice during my stay at Dr Cota's lab in Neurocentre Magendie (Bordeaux, France). We only analysed male mice during the stay because of a limitation of time and space in the mouse animal facility. Results of MRI showed that both groups of male mice had the same amount of lean mass **(Fig. 29A)**. Regarding fat mass, although no significant differences were appreciated **(Fig. 29B)**, SF1-*CPT1c*-KO mice showed the same tendency observed in fat depot weighted after sacrifice **(Fig. 28A-C)**.

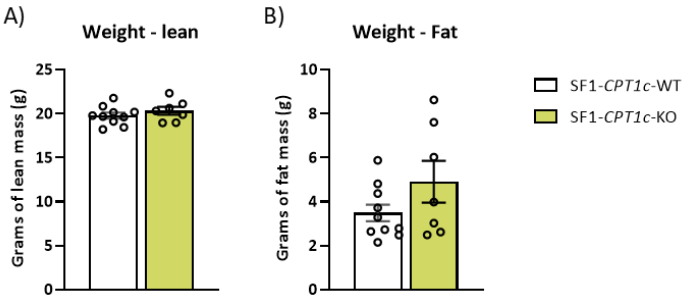

Fig. 29. MRI analysis of lean and fat mass of male mice. A) Amount of lean mass. B) Amount of fat mass. Data were represented as mean ± SEM, male mice, 12-week-old, n= 7-10/ group. Statistical significance was determined by a t-student test.

2.2 Energy expenditure and respiratory exchange ratio parameters

For assessing energy expenditure, we explored BAT thermogenesis in male and female mice using an infrared camera. Moreover, total energy expenditure and basal locomotor activity was measured in male mice using the calorimetric chambers, during the stay in Dr Cota's lab. As observed in **figure 30** and **figure 31**, no differences in BAT thermogenesis **(Fig. 30)**, energy expenditure nor basal locomotor activity **(Fig. 31)** were observed between both genotypes.

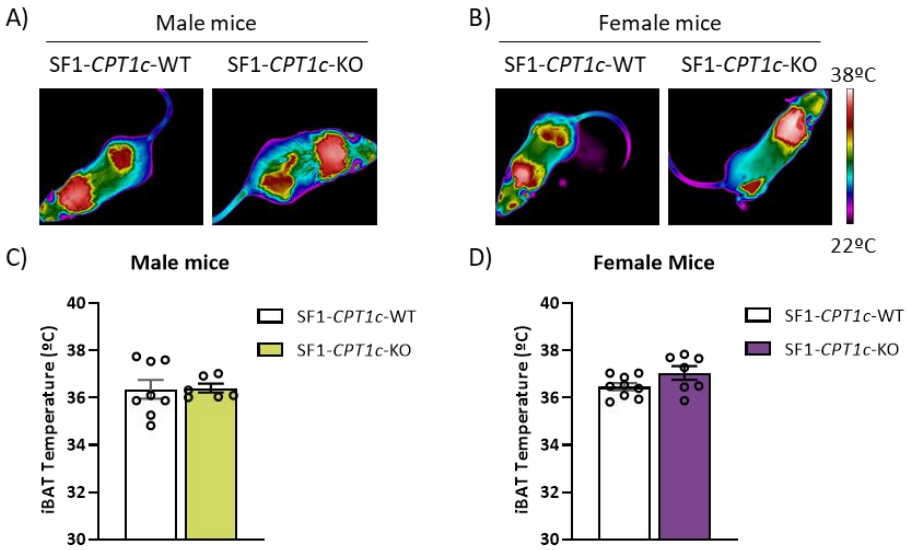

Fig. 30. iBAT temperature of male and female mice. A-B) Representative IR pictures used for iBAT temperature measurement for male (A) and female (B) mice. C-D) iBAT temperature normalized to the temperature of back's male (C) and female (D) mice. Data were represented as mean ± SEM, male and female mice, 16-week-old, n= 7-9/ group. Statistical significance was determined by a t-student test. Olive green: male mice, purple: female mice.

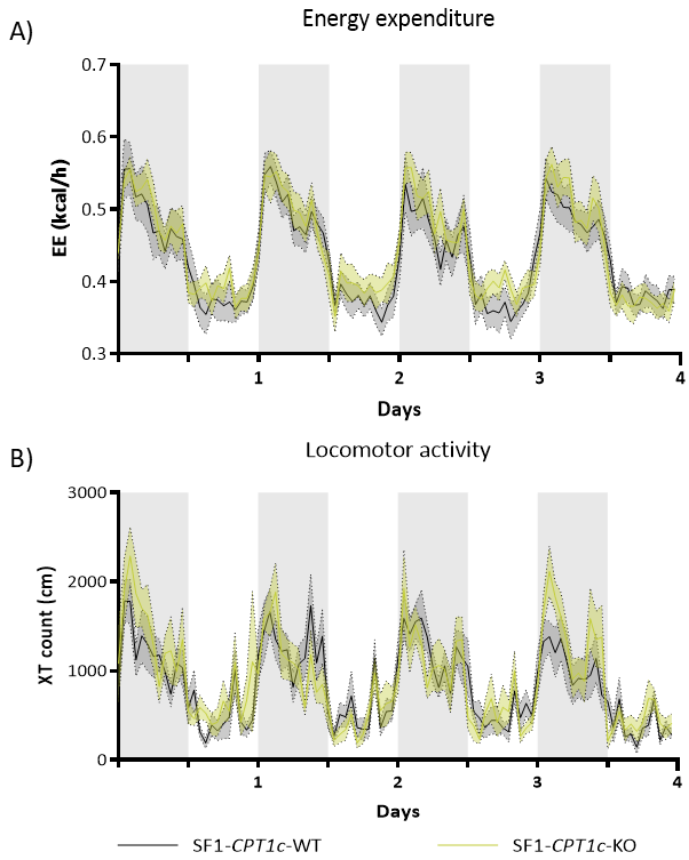

Fig. 31. Energy expenditure (EE) and locomotor activity of male mice monitored for 4 days. A) EE. B) Locomotor activity on the horizontal axis of the cage (XT). Data were represented as mean ± SEM, male mice, 12-week-old, n= 7-10/ group. Statistical significance was determined by ANOVA test with post-hoc Bonferroni.

We also evaluated the respiratory exchange ratio (RER) using the calorimetric chambers. RER is the ratio between the volume of CO_2 being produced by the organism and the amount of O_2 being consumed. This parameter indicates the nutrient substrate used for energy production: a RER near 0.7 indicates that fat is the main fuel source, while if carbohydrates are predominant, RER is 1.0. This analysis revealed no differences between genotypes after 4 days of measurement **(Fig. 32)**.

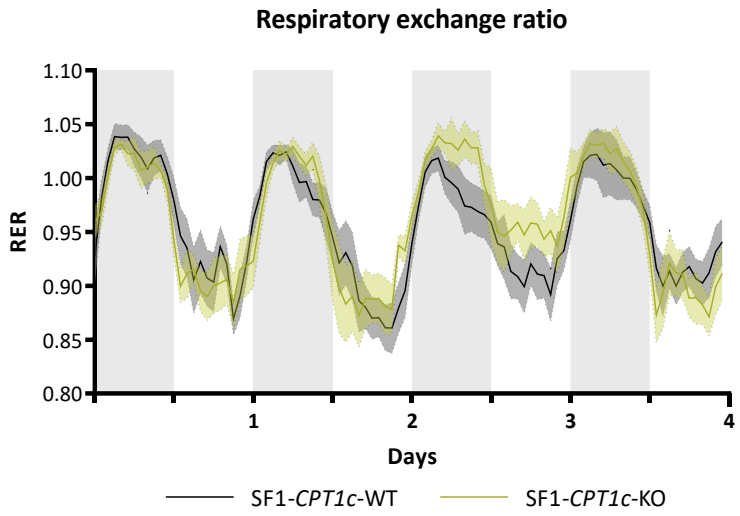

Fig. 32. Respiratory exchange ratio (RER) of male mice monitored for 4 days. Data were represented as mean ± SEM, male mice, 12-week-old, n= 7-10/ group. Statistical significance was determined by ANOVA test with post-hoc Bonferroni.

2.3 Leptin sensitivity

Due to some SF1 transgenic mice reported changes in leptin sensitivity, we performed a leptin-sensitivity test, during the stay in Dr Cota's lab, fasting mice 1 hour before leptin administration and giving food back 4 hours post-injection. As illustrated in **figure 33**, both floxed and transgenic mice showed the similar positive response in body weight change **(Fig. 33A)** and food intake **(Fig. 33B)** after ip administration of leptin. Results suggest that lacking CPT1C in SF1 neurons do not have an impact in leptin sensitivity under chow diet conditions.

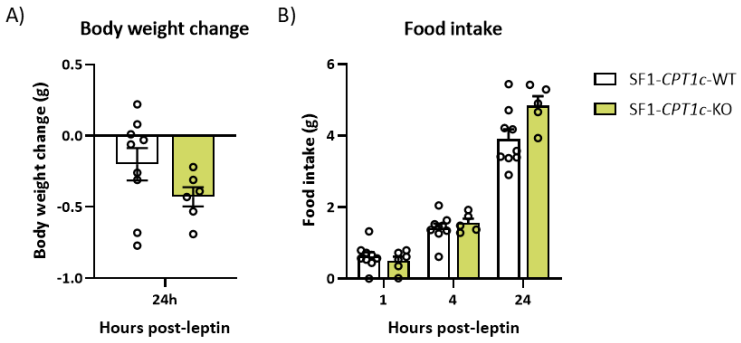

Fig. 33. Leptin sensitivity test. A) Body weight change 24h-after leptin ip injection. B) Food intake post-leptin ip injection. Data were represented as mean ± SEM, 15-week-old male mice, n= 7-10/ group. Statistical significance was determined by ANOVA test with post-hoc Bonferroni.

2.4 Glucose metabolism

GTT and an ITT were performed on male and female mice at the end of 8-weeks fed with SD. Both tests were performed with one week of delay between them to give mice time to recover from the stress produced. Regarding male mice, no differences were observed in GTT or ITT tests, and basal glucose levels were the same between the groups **(Fig. 34A-F)**, although SF1-*CPT1c*-KO mice showed higher glucose clearance observed through the K_{ITT} value calculated using the first 30-minute response to insulin **(Fig. 34G)**. Regarding female mice, no differences in GTT or ITT were observed **(Fig. 35A-G)**.

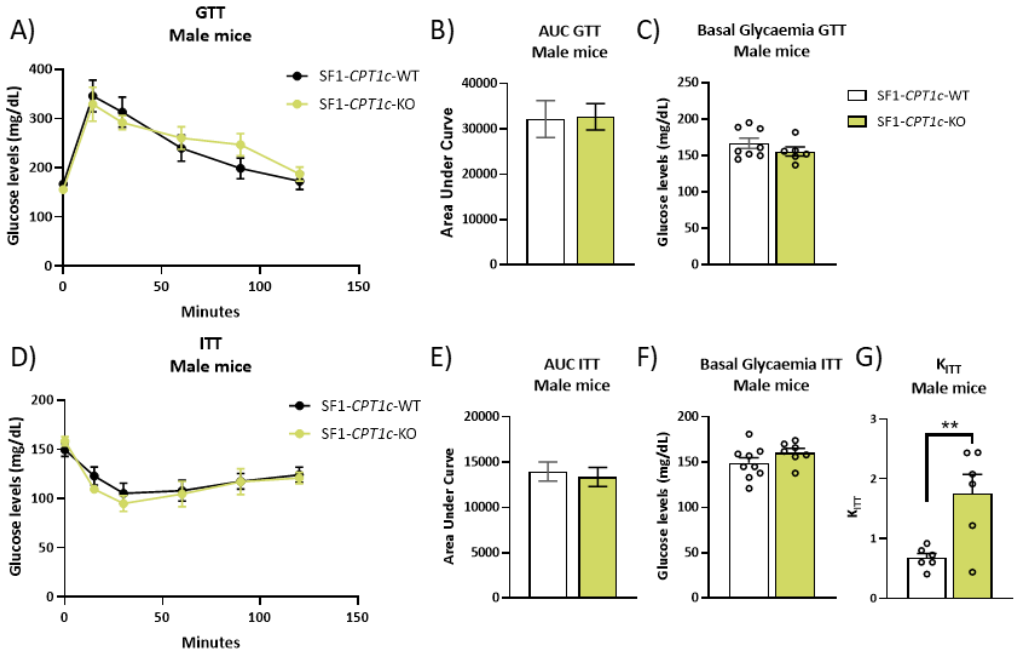

Fig. 34. Glucose and insulin tolerance tests in male mice. A) GTT. B) Area under curve of GTT. C) Basal glycaemia of GTT. D) ITT. E) Area under curve of ITT. F) Basal glycaemia of ITT. G) K_{ITT} calculated on the first 30 min of ITT. Data were represented as mean ± SEM, male mice, 8-week-old, n= 7-9/ group. **p<0.01 vs SF1-*CPT1c*-WT mice. Statistical significance was determined by ANOVA test with post-hoc Bonferroni (A and D) and by t-student test (B-C and E-G). GTT: glucose tolerance test. ITT: insulin tolerance test

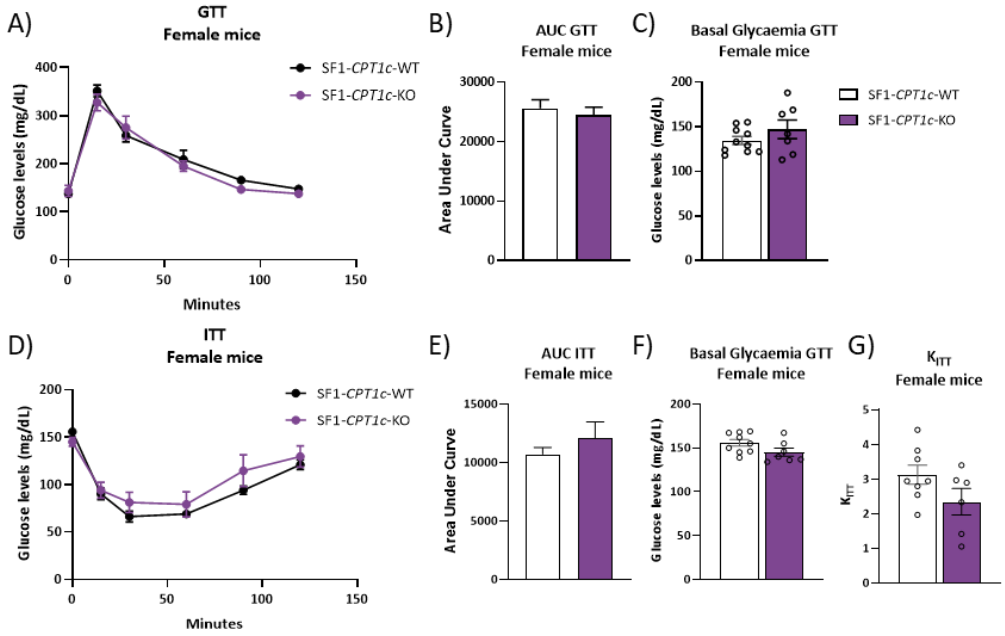

Fig. 35. Glucose and insulin tolerance tests in female mice. A) GTT. B) Area under curve of GTT. C) Basal glycaemia of GTT. D) ITT. E) Area under curve of ITT. F) Basal glycaemia of ITT. G) K_{ITT} calculated on the first 30 min of ITT. Data were represented as mean ± SEM, female mice, 8-week-old, n= 8-10/ group. Statistical significance was determined by ANOVA test with post-hoc Bonferroni (A and D) and by t-student test (B-C and E-G). GTT: glucose tolerance test. ITT: insulin tolerance test

As expected from CPT1c-KO studies, taking into account all the results presented, it could be said that SF1-*CPT1c*-KO mice do not differ in energy metabolism from SF1-*CPT1c*-WT mice under basal conditions (fed SD). However, the specific KO male mice have a tendency of accumulating more fat mass and higher rate of glucose disappearance.

3 Metabolic phenotype of SF1-*CPT1c*-KO mice under high-fat diet exposure

Next, we aimed to explore the metabolic phenotype in response to metabolic challenges, specifically under HFD exposure. We were interested in two stages of obesity: during the initial stages of obesity development and once the disease is established. Therefore, studies were conducted at the beginning of the dietary change (short-term exposure) and after 6 or 8 weeks of HFD exposure (long-term exposure).

3.1 Short-term exposure to HFD

To study the metabolic switch of SF1-*CPT1c*-KO mice under HFD exposure, metabolic parameters were monitored during the first five days of HFD administration. These studies were performed in male mice, 16-week-old, at Dr Cota's lab.

3.1.1 Body weight, food intake and mass distribution

Body weight evolution was significantly different between genotypes, showing KO mice higher body weight than WT animals over time, initial body weight did not show a significant difference **(Fig. 36A)**. Body weight change over time between both genotypes showed a trend, but no significant differences were observed **(Fig. 36B)**.

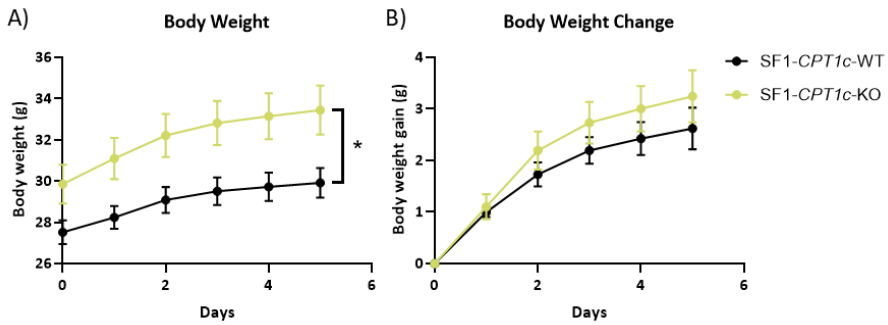

Fig. 36. Body weight evolution of male mice fed HFD for five days. A) Body weight. b) Body weight change. Data were represented as mean ± SEM, male mice, 16-week-old, n= 7-10/ group. *p<0.05 vs SF1-*CPT1c*-WT mice. Statistical significance was determined by ANOVA test with post-hoc Bonferroni.

Food intake was also measured every 20 minutes during these five days, using the integrated scales of calorimetric chambers. Results showed that SF1-*CPT1c*-KO mice ate more amount of food compared to SF1-*CPT1c*-WT mice. This difference was significant from the third day of HFD feeding when analysing the cumulative food intake **(Fig. 37B)**. The pattern of the cumulative food intake of the five days before and after HFD administration **(Fig. 37A** and **B**, respectively) was also different between KO and WT mice.

Food intake was also analysed day by day **(Fig. 37C-D)**. The first day of HFD, SF1-*CPT1c*-WT group adapted to the new higher caloric diet eating less food, but the SF1-*CPT1c*-KO continued eating the same amount of food **(Fig. 37C)**. It was not until day 5 of HFD exposure that the specific KO mice seemed to start adjusting the amount of eaten food, although there was still a significant difference compared to the control littermates **(Fig. 37C)**. Food intake was also monitored by dark/light phase day by day, and we found that

all the differences in food intake were appreciated during the dark phase **(Fig. 37D)**, when mice usually eat the highest amount of food. Regarding calorie intake, WT mice ate less amount of food to adapt the calorie intake, while the higher food intake observed in SF1-*CPT1c*-KO mice is reflected in the higher calorie intake **(Fig. 37E)**.

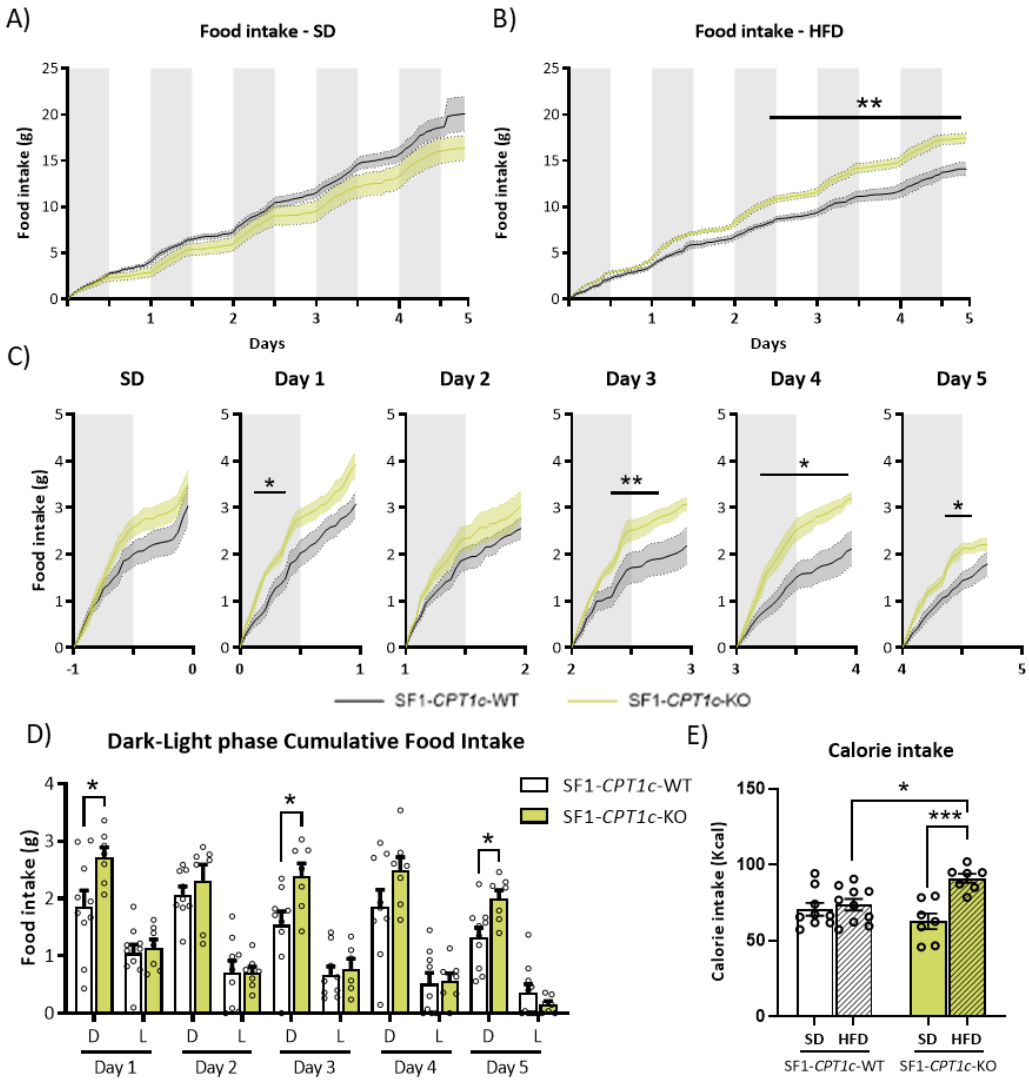

Fig. 37. **Male mice food intake of the first five days exposed to HFD.** A) Food intake of the five previous days to HFD exposition. B) Food intake of the first 5 days exposed to HFD. C) Cumulative daily food intake over time of the previous day of changing diets (SD) and the first 5 days of HFD (Day 1 to 5) D) Cumulative food intake separated by dark(D)/light(L) phase. E) Cumulative calorie intake of five days with SD or HFD. Data were represented as mean ± SEM, male mice, 16-week-old, n= 7-10/ group. *p<0.05, **p<0.01, ***p<0.001 vs SF1-*CPT1c*-WT. Statistical significance was determined by ANOVA test with post-hoc Bonferroni.

After five days of HFD exposition, mass distribution was investigated using the MRI technology at Dr Cota's lab. Both genotypes were analysed at SD (just before starting HFD) and after the five days on HFD. Results showed no differences in lean mass **(Fig. 38A)** but a significant increase in fat mass was observed in SF1-*CPT1c*-KO after five days of HFD feeding compared to WT **(Fig. 38B)**. These results were in line with the assumption that SF1-*CPT1c*-KO mice present an obesogenic phenotype and an impaired adaptation to the new metabolic situation.

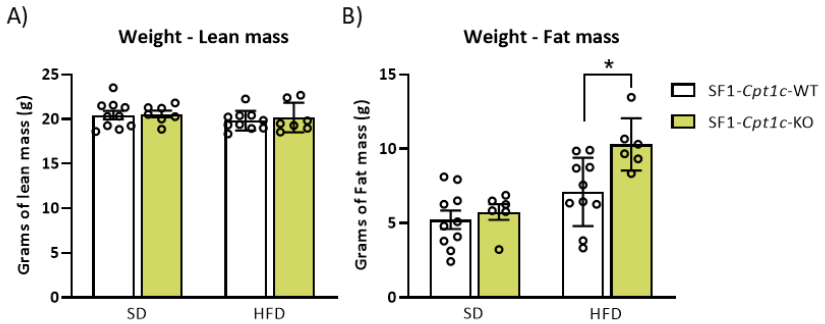

Fig. 38. Lean and fat mass previous and after the five days of HFD exposure. A) Lean mass under SD and HFD conditions. B) Fat mass under SD and HFD conditions. Data were represented as mean ± SEM, male mice, 16-week-old, n= 7-10/ group. *p<0.05 vs SF1-*CPT1c*-WT. Statistical significance was determined by a t-student test between genotypes for each condition.

3.1.2 Energy expenditure and RER parameters

During these 5 days of HFD in the metabolic chambers, different components of energy expenditure and RER were also explored. For assessing total energy expenditure and basal locomotor activity, we used indirect calorimetry and, for checking BAT thermogenesis, mRNA thermogenic markers were analysed in BAT. Regarding energy expenditure and locomotor activity, no differences were observed between the genotypes **(Fig. 39A, B)**. BAT thermogenesis was investigated using two different approaches: 7 days of HFD and central leptin administration. For the first approach, HFD was administered for 7 days because previous results in our groups showed a maximum peak of thermogenesis activation at this time point. Under these conditions, no differences in the expression of BAT thermogenesis markers were found between both genotypes **(Fig. 39C)**, accordingly with the lack of differences observed in the energy expenditure **(Fig 39A)**. Evaluation of icv leptin-induced BAT thermogenesis, revealed that thermogenic activation was blunted in SF1-*CPT1c*-KO mice compared to the response in control littermates **(Fig. 39D)**.

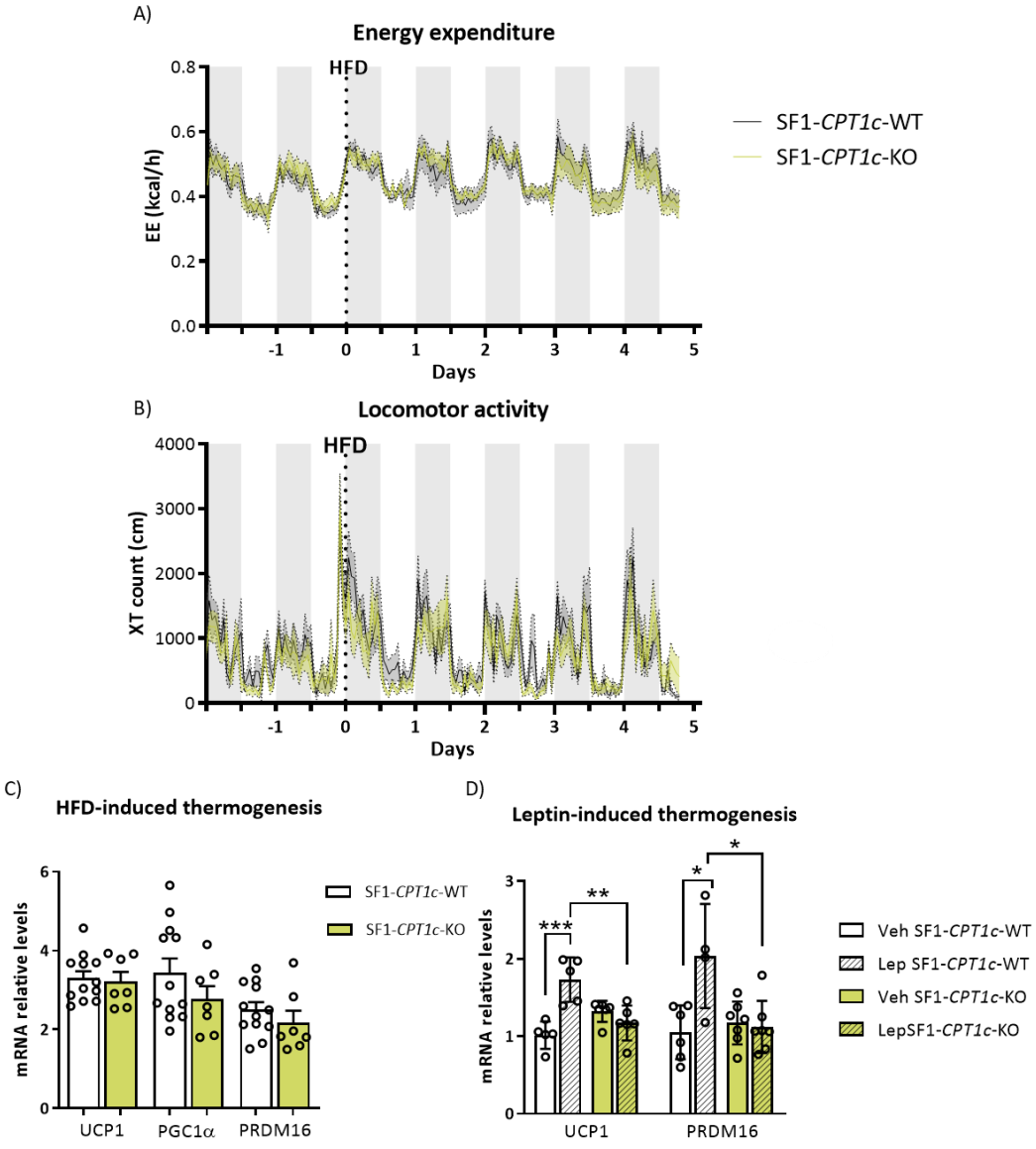

Fig. 39. Energy expenditure (EE), locomotor activity and BAT thermogenesis of male mice. A) EE. B) Locomotor activity on the horizontal axis of the cage (XT). C) Thermogenic markers from BAT after seven days of HFD exposure. D) Thermogenic markers from BAT three hours post icv leptin administration. GAPDH was used as housekeeping gene to normalize mRNA markers. Data were represented as mean ± SEM, male mice, 16-week-old in EE and locomotor activity and 8-week old in BAT thermogenesis, n= 7-10/ group for calorimetry analysis, n=8-11/group for analysis of thermogenic markers and n=5-7/group for leptin approach. *p<0.05; **p<0.01, ***p<0.001 vs SF1-*CPT1c*-WT. Statistical significance was determined by ANOVA test with post-hoc Bonferroni (A-B and D) and by t-student test (C). EE: energy expenditure; PGC1α Peroxisome proliferator-activated receptor γ co-activator 1 α; PRDM16: PR domain containing16; UCP1: uncoupling protein 1.

Looking at RER, mice of both genotypes showed a reduced RER value when exposed to a short-term HFD, as expected since they were using more fat as substrate for energy production. Interestingly, RER did not change equally between the groups, since SF1-*CPT1c*-KO mice presented higher nocturnal RER than SF1-*CPT1c*-WT mice. Differences became significant on the dark phase of the third day of HFD feeding, the same timeframe in which significant differences in cumulative food intake between the genotypes were found **(Fig. 40)**.

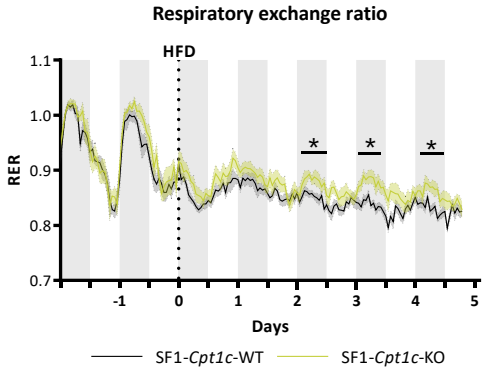

Fig. 40. Respiratory exchange ratio (RER) of male mice monitored from the previous two days and until day five of HFD exposure. Data were represented as mean ± SEM, male mice, 16-week old, n= 7-10/ group. *p<0.05 vs SF1-*CPT1c*-WT. Statistical significance was determined by ANOVA test with post-hoc Bonferroni.

Neither total energy expenditure nor basal locomotor activity were changed and diet-induced thermogenesis was also similar between genotypes, therefore these parameters play a minimal role in the control of body weight of SF1-*CPT1c*-KO mice. Interestingly, RER analysis indicated that the specific KO mice carried on a less pronounced switch to adjust to the new metabolic situation, using less fat as energy substrate than the control littermates, although they were eating more amount of it. This impaired adaptation to the metabolic challenge and the higher food intake values observed in SF1-*CPT1c*-KO mice are probably the main contributors to the higher fat mass accumulation and, therefore, higher body weight under a short-term HFD exposure.

3.2 Long-term exposure to high-fat diet

After the interesting results obtained with a short exposure to HFD, we aimed to analyse the metabolic response after several weeks of HFD feeding when obesity is already established. The first experiments of this study were performed with 8-week-old male and

female mice, whereas 16-week-old male mice were used for the assays in Dr Cota's lab (data from MRI and calorimetric chambers).

3.2.1 Body weight, food intake monitoring and mass distribution

Body weight was weekly monitored over 8 weeks of HFD, always at the same time and same day of the week. SF1-*CPT1c*-KO male mice showed greater body weight compared to their control littermate mice from day 7 of HFD onwards **(Fig. 41A)**. When analysing the cumulative body weight gain evolution, differences were significant after the first month on HFD **(Fig. 41B)**. In parallel, we performed the same experiment using female mice. In this case, significant differences in body weight and body weight change between genotypes appeared after 6 weeks of HFD exposure **(Fig. 41C, D)**. SF1-*CPT1c*-KO mice of both sexes gain more weight during long-term HFD administration, although the obesogenic phenotype in KO females was observed later than in male mice.

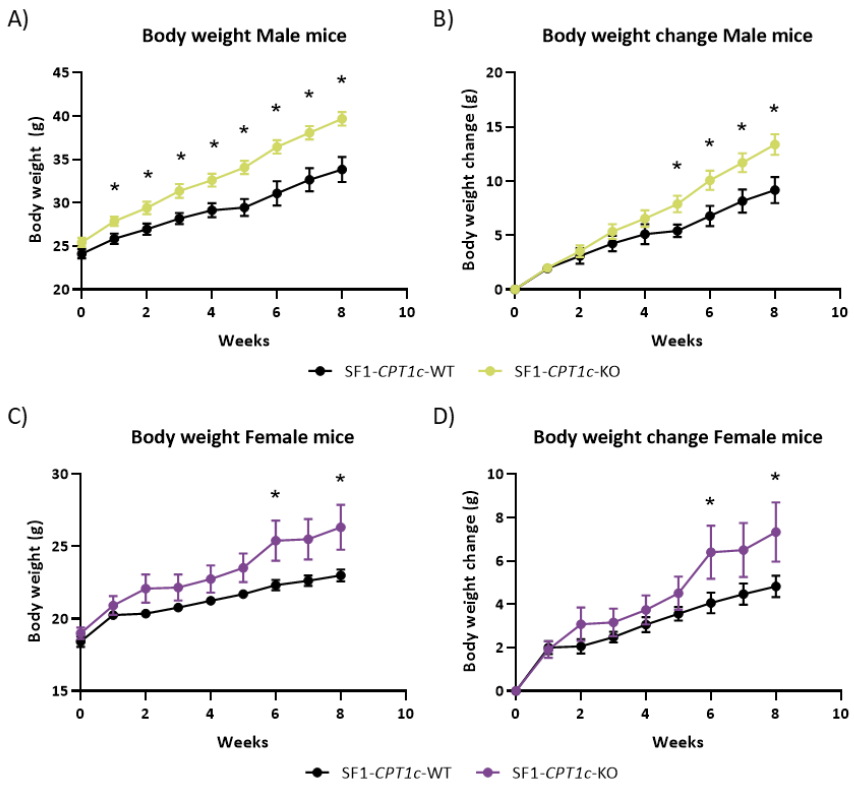

Fig. 41. Male and female mice body weight evolution over eight weeks fed HFD. A) Male body weight. B) Male body weight change. C) Female body weight. D) Female body weight change. Data were represented as mean ± SEM, male and female mice, 8-week-old, n= 8-10/ group. *p<0.05 vs SF1-*CPT1c*-WT. Statistical significance was determined by ANOVA test with post-hoc Bonferroni. Olive green: male mice; purple: female mice.

Food intake analysis in both male and female mice revealed no differences between genotypes during 8 weeks of HFD feeding **(Fig. 42A, B)**. These results indicate that CPT1c in SF1 neurons is involved in body weight control but not in food intake regulation under long-term exposure to a HFD challenge.

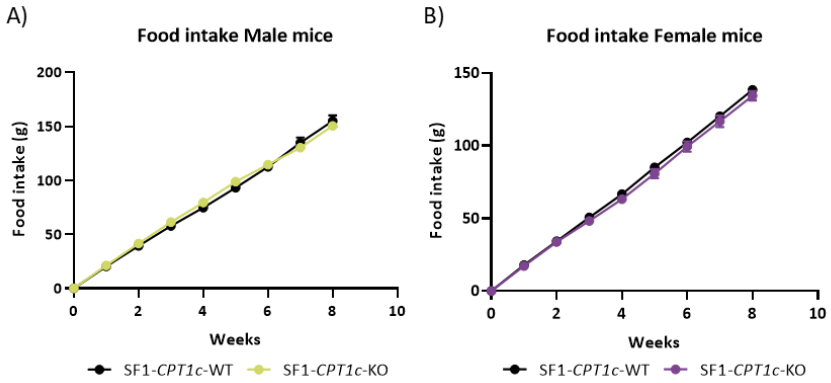

Fig. 42. Male and female mice cumulative food intake over eight weeks fed HFD. A) Male mice cumulative food intake. B) Female mice cumulative food intake. Data were represented as mean ± SEM, male and female mice, 8-week-old, n= 8-10/ group. *p<0.05 vs SF1-*CPT1c*-WT. Statistical significance was determined by ANOVA test with post-hoc Bonferroni.

For the study of mass distribution, mice were sacrificed after 8 weeks of HFD administration and BAT, sWAT and eWAT tissues were collected and weighed. Results with male mice showed that SF1-*CPT1c*-KO mice had heavier fat depots than their control littermates **(Fig. 43A-C)**. These studies were completed at Dr Cota's lab using the MRI technology in male mice. SF1-*CPT1c*-KO mice presented more grams of fat mass in their body composition **(Fig. 43E)** while lean mass was the same for both genotypes **(Fig. 43D)**. Regarding female mice, sWAT depots were bigger in SF1-*CPT1c*-KO mice, but the other two tissues weighed the same between genotypes **(Fig. 43F-H)**. SF1-*CPT1c*-KO mice accumulates more amount of fat than their control littermates, which reinforces the idea of lacking CPT1c in SF1 neurons results into an obesogenic phenotype.

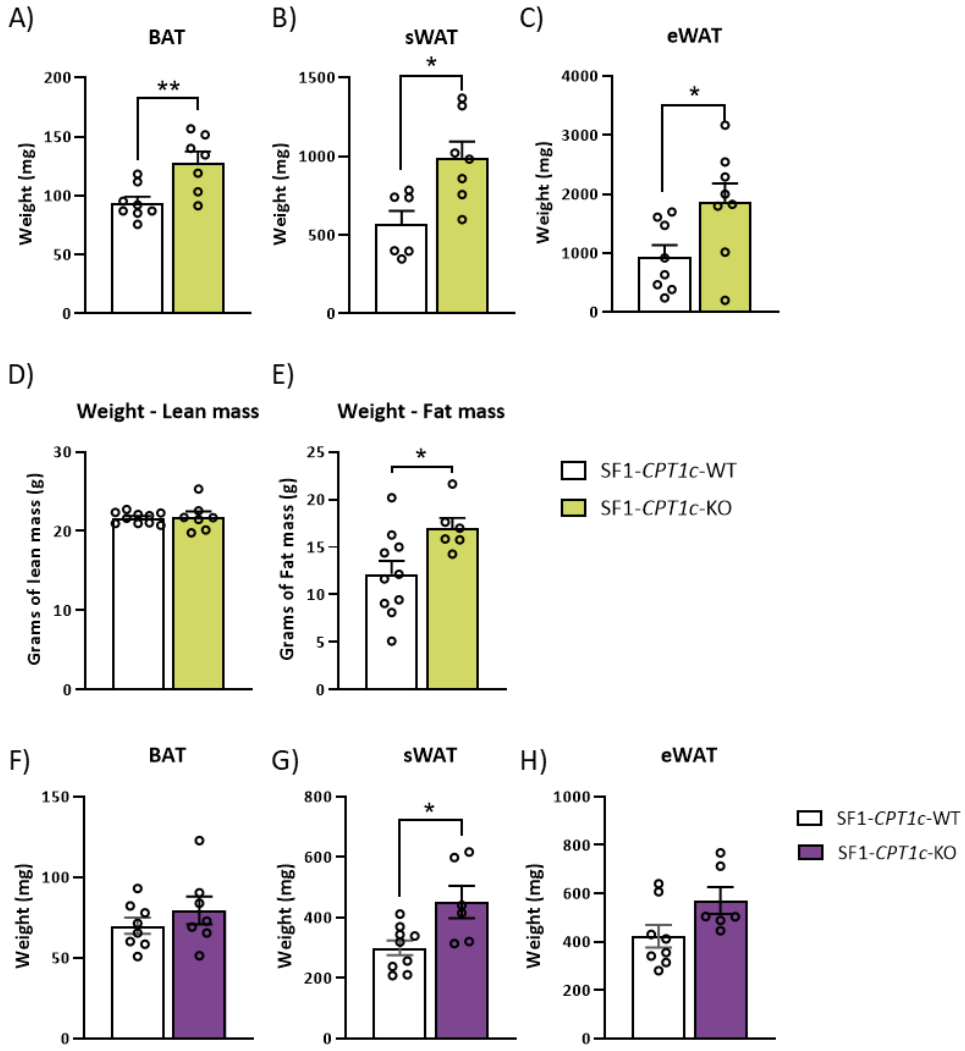

Fig. 43. Body weight composition of male and female mice after long-term exposure to HFD. A-C) Weight of BAT (A), sWAT (B) and eWAT (C) of male mice after sacrifice. D) Lean mass of male mice analyzed by MRI. E) Fat mass of male mice analyzed by MRI. F-H) Weight of BAT (F), sWAT (G) and eWAT (H) of female mice after sacrifice. Data were represented as mean ± SEM, male and female mice, 8-week-old for tissue's weight and 16-week-old for MRI analyses, n= 7-10/ group. *p<0.05, **p<0.01 vs SF1-*CPT1c*-WT. Statistical significance was determined by ANOVA test with post-hoc Bonferroni. Olive green: male mice, purple: female mice.

3.2.2 Energy expenditure and RER parameters

Calorimetric studies were performed in male mice after 6 weeks of HFD in Dr Cota's lab. Concerning energy expenditure, basal locomotor activity, iBAT temperature and total energy expenditure measured through indirect calorimetry were analysed. Total energy expenditure and locomotor activity showed no differences between genotypes **(Fig. 44A-B),** contrary to what was observed in short-term HFD exposure **(Fig. 39A-B)**.

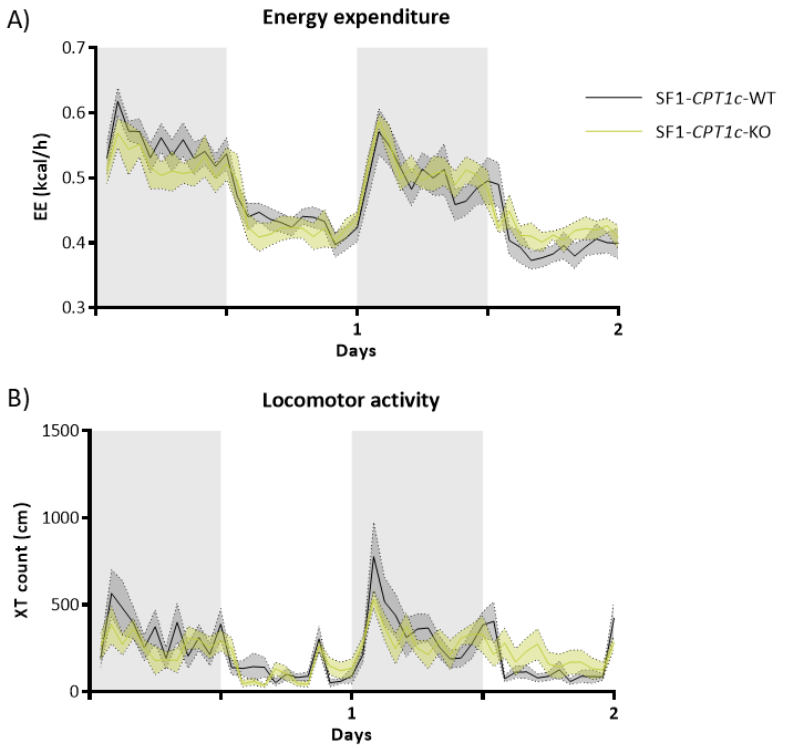

Fig. 44. Energy expenditure (EE) and locomotor activity of male mice monitored after six weeks of HFD. A) Energy expenditure. B) Locomotor activity on the horizontal axis of the cage (XT). Data were represented as mean ± SEM, male and female mice, 16-week-old, n= 7-10/ group. Statistical significance was determined by ANOVA test with post-hoc Bonferroni.

BAT thermogenesis was analysed by iBAT temperature through IR imaging. Although a significant difference in BAT weight were found between genotypes in male mice **(Fig. 43A)**, BAT thermogenesis activity remained unchanged in KO compared to WT mice in both male and female mice **(Fig. 45A-D)**.

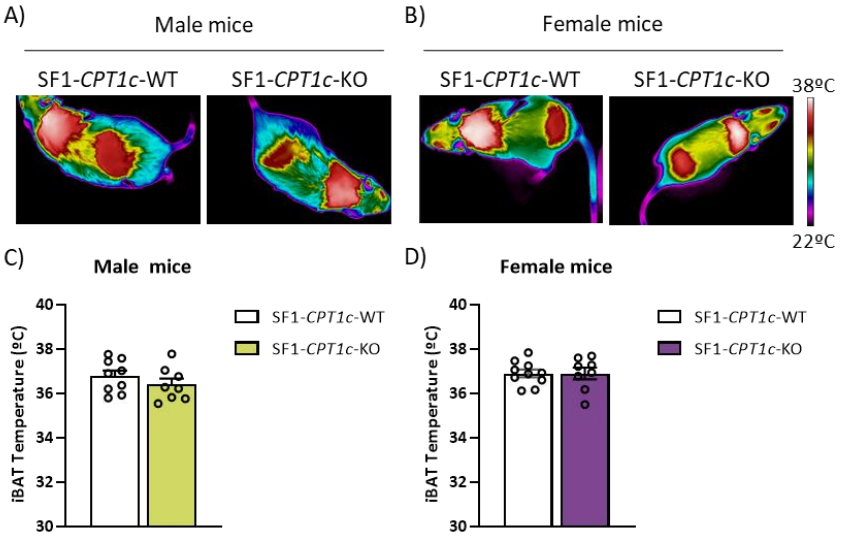

Fig. 45. iBAT temperature of male and female mice after eight weeks on HFD. A-B) Representative IR pictures used for iBAT temperature measurement for male (A) and female (B) mice. C-D) iBAT temperature normalized to the temperature of back's male (C) and female (D) mice. Data were represented as mean ± SEM, male and female mice, 8-week-old, n= 8-10/ group. Statistical significance was determined by ANOVA test with post-hoc Bonferroni. Olive green: male mice, purple: female mice.

Regarding RER analysis, surprisingly and in contrast to that observed in the first 5 days of HFD, RER values were similar in specific KO and WT mice after long-term HFD administration **(Fig. 46)**.

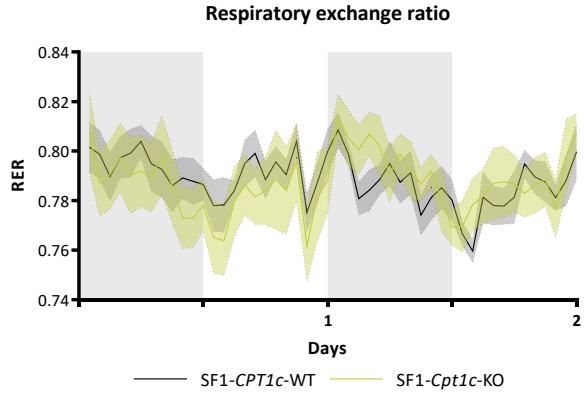

Fig. 46. Respiratory exchange ratio (RER) of male mice monitored after six weeks of HFD. Data were represented as mean ± SEM, male mice, 16-week-old, n= 7-10/ group. Statistical significance was determined by ANOVA test with post-hoc Bonferroni.

Although mice lacking CPT1c in SF1 neurons exposed to long-term HFD administration presented an obesogenic phenotype compared to the control littermate mice, alterations of SF1-*CPT1c*-KO mice were limited to an increased body weight gain and higher adiposity.

The impairment in the metabolic switch to adapt to the new diet found during the first days of HFD administration is lost at longer periods of HFD feeding. These data indicate that CPT1c in SF1 neurons is playing a key role during the onset of diet-induced obesity by adjusting calorie intake and increasing fat oxidation, but once obesity is established, its role is not so crucial. Impairment of CPT1c-mediated signalling in SF1 neurons at those initial phases of HFD consumption enhances fat deposition and accelerates obesity development.

3.2.3 Glucose metabolism

Due to the importance of SF1 neurons in controlling glucose homeostasis, we evaluated glucose and insulin tolerance on mice after 8 weeks of HFD. Regarding male mice, SF1-*CPT1c*-KO mice showed a significant impairment in GTT and ITT compared to WT mice **(Fig. 47A-B)**. Basal glycaemia before the GTT was similar for both genotypes **(Fig. 47C)**, but SF1-*CPT1c*-KO mice failed to sense high blood glucose levels and triggered its uptake by peripheral tissues.

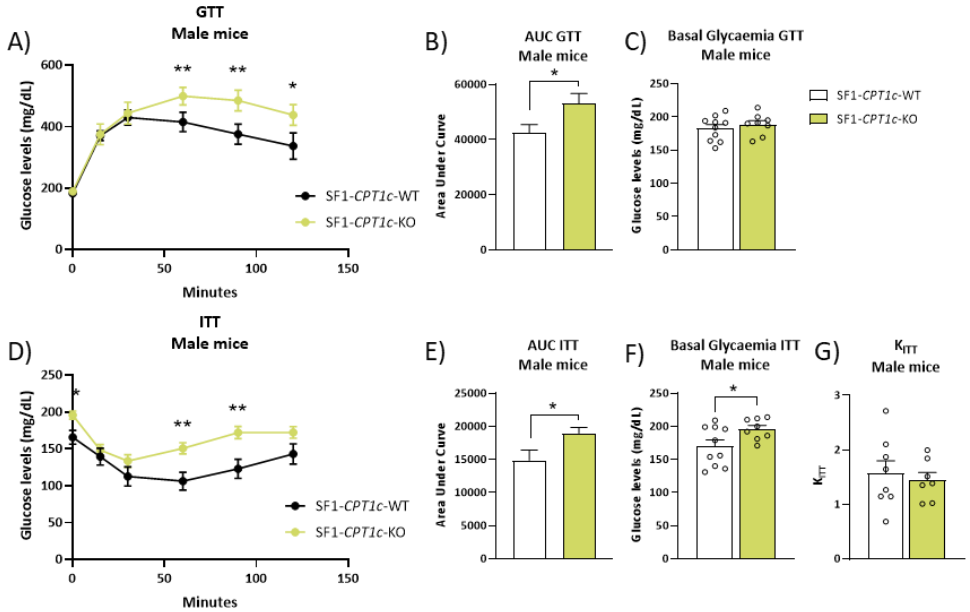

Fig. 47. Glucose and insulin tolerance tests in male mice after eight weeks on HFD. A) GTT. B) Area under curve of GTT. C) Basal glycaemia of GTT. D) ITT. E) Area under curve of ITT. F) Basal glycaemia of ITT. G) K_{ITT} calculated on the first 30 min of ITT. Data were represented as mean ± SEM, male mice, 8-week-old, n= 8-10/ group. *p<0.05, **p<0.01 vs SF1-*CPT1c*-WT. Statistical significance was determined by ANOVA test with post-hoc Bonferroni (A and D) and by t-student test (B-C and E-G). GTT: glucose tolerance test. ITT: insulin tolerance test.

However, ITT results revealed that SF1-*CPT1c*-KO male mice had higher basal blood glucose levels but the glucose clearance rate assessed by the K_{ITT} (the first 30 minutes of the curve) was similar between groups **(Fig. 47D - G)**. Differences in ITT were observed after the 30 minutes' point, which could indicate that the CRR is altered in SF1-*CPT1c*-KO mice.

SF1-*CPT1c*-KO female mice also presented intolerance to glucose **(Fig. 48A-C)** but, in contrast to male mice, normal insulin tolerance was showed **(Fig. 48D-G)**. The lower affectation of the glucose homeostasis in female SF1-*CPT1c*-KO mice is in accordance with their reduced adiposity compared to male mice. CPT1c in SF1 neurons seems to play a role in the control of glucose metabolism when mice are exposed to HFD for a long period of time.

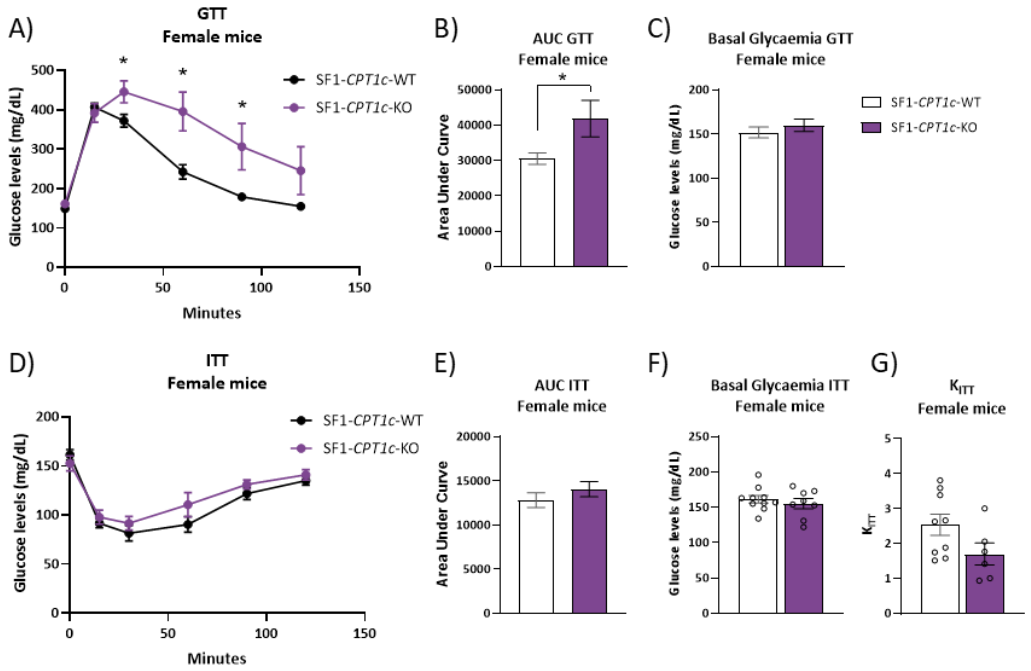

Fig. 48. Glucose and insulin tolerance tests in female mice after eight weeks on HFD. A) GTT. B) Area under curve of GTT. C) Basal glycaemia of GTT. D) ITT. E) Area under curve of ITT. F) Basal glycaemia of ITT. G) K_{ITT} calculated on the first 30 min of ITT. Data were represented as mean ± SEM, male mice, 8-week-old, n= 8-10/ group. *p<0.05 vs SF1-*CPT1c*-WT. Statistical significance was determined by ANOVA test with post-hoc Bonferroni (A and D) and by t-student test (B-C and E-G). GTT: glucose tolerance test. ITT: insulin tolerance test.

4 Metabolic phenotype of SF1-CPT1c-KO mice under fasting

To study the metabolic adaptation of SF1-*CPT1c*-KO mice to fasting and central hypoglycemia, three types of studies were done, all in male mice:

I. Analysis of liver metabolism and glucose homeostasis after 24 hours of fasting. These experiments were performed in our laboratory with 8-week-old mice.
II. Analysis of the CRR in response to central 2-DG-administration. These experiments were performed in our laboratory with 8-week-old mice.
III. Analysis of calorimetric parameters in mice exposed to 24 hours of fasting and then 48 hours of refeeding. These experiments were done in Dr Cota's lab with 13-week-old mice.

4.1 Liver metabolism and glucose homeostasis upon 24 h-fasting

With the aim of characterizing the fasting metabolic response, body weight loss was evaluated and compared between genotypes after 24 h of fasting. Data obtained showed no differences between both groups **(Fig. 49)**.

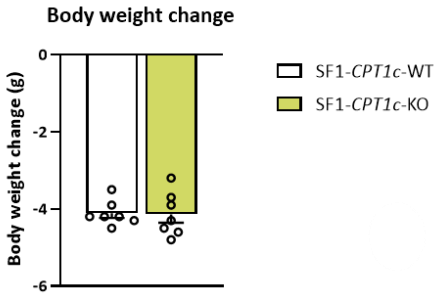

Fig. 49. Body weight change after 24 hours of fasting. Body weight change measured as the difference between initial body weight and final body weight after 24 hours of fasting**.** Data were represented as mean ± SEM, 8-week-old male mice, n= 7/ group. Statistical significance was determined by t-student test.

Collected liver of fasted mice revealed a yellowish colour in SF1-*CPT1c*-KO compared to SF1-*CPT1c*-WT mice **(Fig. 50A)**, that could be associated to a disruption in liver metabolism adaptation to fasting. Therefore, we first measured triglycerides, glycerol and glycogen levels in the livers of both WT and KO mice **(Fig. 50B-D)**. SF1-*CPT1c*-KO mice presented a tendency of having higher levels of triglycerides in liver **(Fig. 50B),** and showed higher hepatic levels of glycerol compared to WT **(Fig. 50C)**. By contrast, no differences were

found in glycogen. **(Fig. 50D)**. The higher content in triglycerides and glycerol might be the cause of the yellowish colour of SF1-*CPT1c*-KO's liver and may indicate that liver fat oxidation is reduced and that glycerol is not being used for gluconeogenesis. Therefore, we checked liver fat oxidation by measuring CPT1a mRNA levels, but we did not find differences between genotypes **(Fig. 50E)**. Apart from fat oxidation, another liver metabolic adaptation during fasting is the inhibition of pyruvate dehydrogenase (PDH), to stop pyruvate conversion into acetyl-CoA, so it can be used as substrate in gluconeogenesis. Since PDK4 is responsible for PDH inhibition in a hypoglycaemic situation such as fasting, PDK4 mRNA levels in liver were analysed, but no differences were observed between genotypes **(Fig. 50F)**.

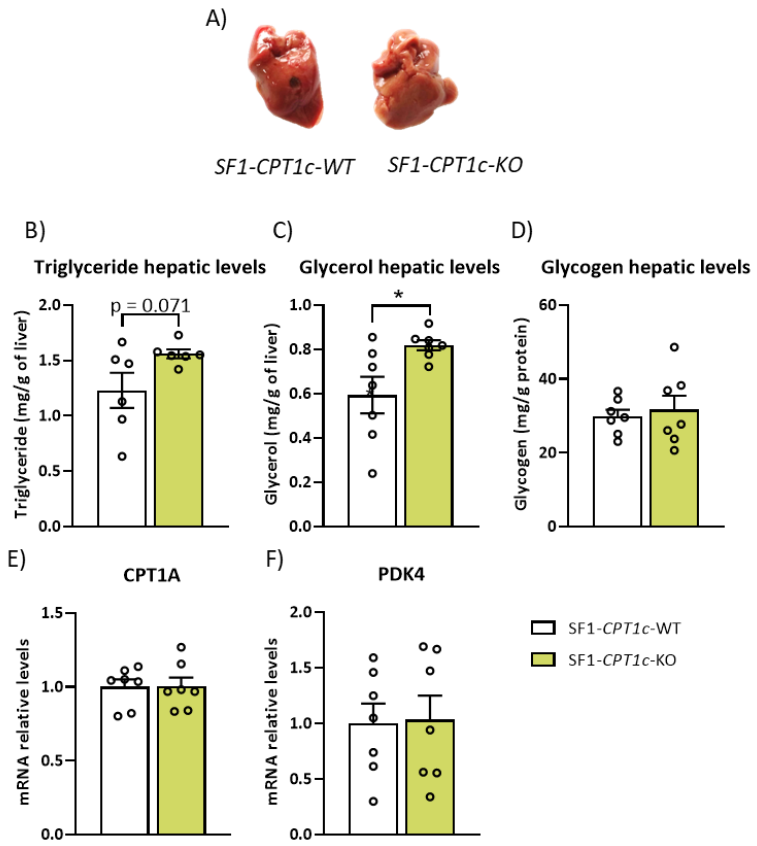

Fig. 50. Liver metabolism after 24 hours of fasting. A) Representative pictures of livers from SF1-*CPT1c*-WT and SF-*CPT1c*-KO mice. B) Triglyceride hepatic levels. C) Glycerol hepatic levels. D) Glycogen hepatic levels. E) CPT1a mRNA hepatic levels. F) PDK4 mRNA hepatic levels. S18 was used as housekeeping gene to normalize levels of mRNA markers. Data were represented as mean ± SEM, 8-week-old male mice, n= 7/ group. * $p<0.05$ vs SF1-*CPT1c*-WT. Statistical significance was determined by t-student test.

As glycerol was being accumulated in SF1-*CPT1c*-KO's liver, we hypothesized that liver was producing less glucose than their control littermates. Then, gluconeogenesis markers G6P and PEPCK mRNA hepatic levels were analysed **(Fig. 51A-B)** and blood glucose levels were explored between genotypes after the 24-hour fasting **(Fig. 51C)**. However, no differences in gluconeogenesis markers or glycaemia were found between genotypes.

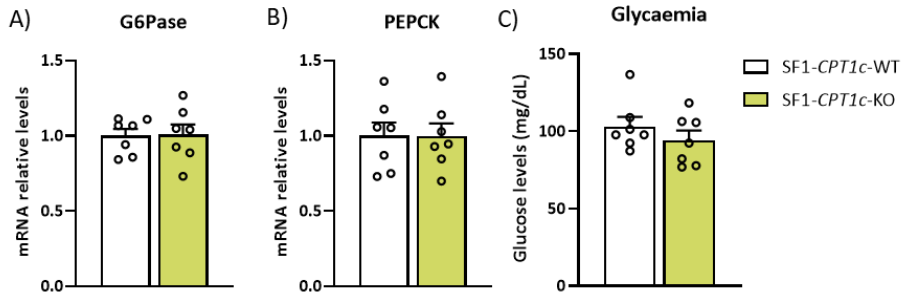

Fig. 51. Gluconeogenesis and glycaemia after 24 hours of fasting. A) mRNA levels of hepatic G6Pase. B) mRNA levels of hepatic PEPCK. C) Blood glucose levels. S18 was used as housekeeping gene to normalize levels of mRNA markers. Data were represented as mean ± SEM, 8-week-old male mice, n= 7/ group. Statistical significance was determined by t-student test.

Overall, results indicate that there is some alteration in liver lipid metabolism but not in glucose metabolism. Future experiments are needed to study liver and WAT lipolysis, as well as the liver AMPK pathway, in order to get deeper insight in lipid metabolism of SF1- *CPT1C*-KO livers.

4.2 Analysis of the CRR to central 2-DG administration

Because of some of the SF1 transgenic mice have been shown an impaired CRR, central hypoglycaemia was induced in SF1-*CPT1c*-KO mice, minimizing the peripheral changes evoked by 24 hours of fasting. Therefore, 2-DG was icv administered to recreate the fasting situation only in the brain. Blood glycaemia after 30 minutes of 2-DG administration were higher in both WT and KO mice compared to their corresponding vehicle-treated groups, which indicated that CRR was similarly activated in both genotypes **(Fig. 52A)**. Liver expression of gluconeogenesis genes revealed a significant increase in SF1-*CPT1c*-KO mice treated with 2-DG compared to the vehicle group, but this change was not found in control mice **(Fig. 52B)**. These data suggest that SF1-*CPT1c*-KO mice show an enhanced liver response to acute central hypoglycaemia even though it is not enough to produce a higher increase in blood glucose levels.

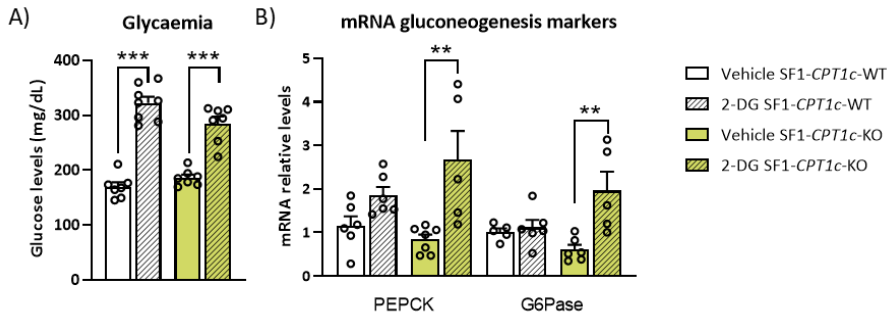

Fig. 52. Glycaemia and gluconeogenesis after icv 2-DG administration. A) Blood glucose levels. B) Liver PEPCK and G6Pase mRNA levels. S18 was used as housekeeping gene to normalize levels of mRNA markers. Data were represented as mean ± SEM, 8-week-old male mice, n= 7/ group. **p<0.01; ***p<0.001. Statistical significance was determined by ANOVA test with post-hoc Bonferroni.

4.3 Calorimetric analysis of fasting-refeeding

In order to analyse the refeeding response after fasting, during Dr Cota's lab internship, we exposed 13-week-old SF1-*CPT1c*-KO male mice to 24-hour fasting followed by refeeding monitoring for 2 days. During the refeeding phase, body weight and food intake were analysed **(Fig. 53A-B)**, and we found that the recovery of body weight and food intake induced by the refeeding was similar in both genotypes.

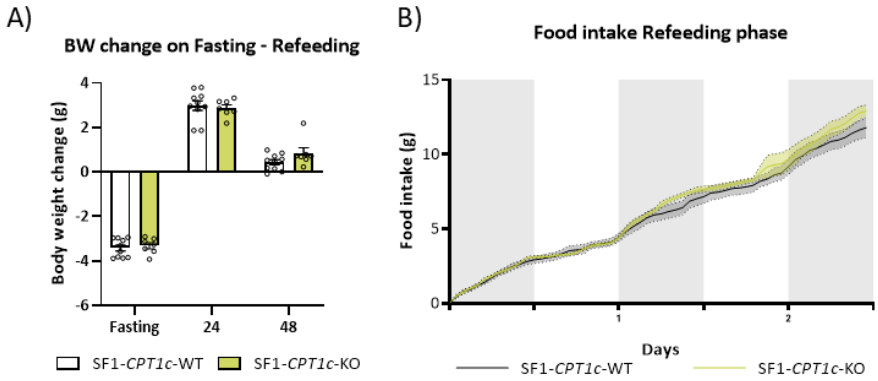

Fig. 53. Body weight and food intake during the 24-hour fasting and 48h-refeeding. A) Daily body weight change during fasting day and the 48 hours of refeeding. B) Cumulative food intake in the refeeding phase. Data were represented as mean ± SEM, 13-week old male mice, n= 7-10/ group. Statistical significance was determined by ANOVA test with post-hoc Bonferroni.

Energy expenditure and RER were also analysed using the calorimetric chamber, but no differences between genotypes were appreciated **(Fig. 54A-B)**. Altogether, these results indicate that CPT1c in SF1 neurons plays a subtle role in metabolic adaptation to fasting without impacting in the refeeding stage. The high liver glycerol levels and increased expression of gluconeogenic genes after central-induced hypoglycaemia found in SF1-*CPT1c*-KO mice may indicate that some of the hepatic processes during fasting response are impaired by CPT1c deletion in these neurons.

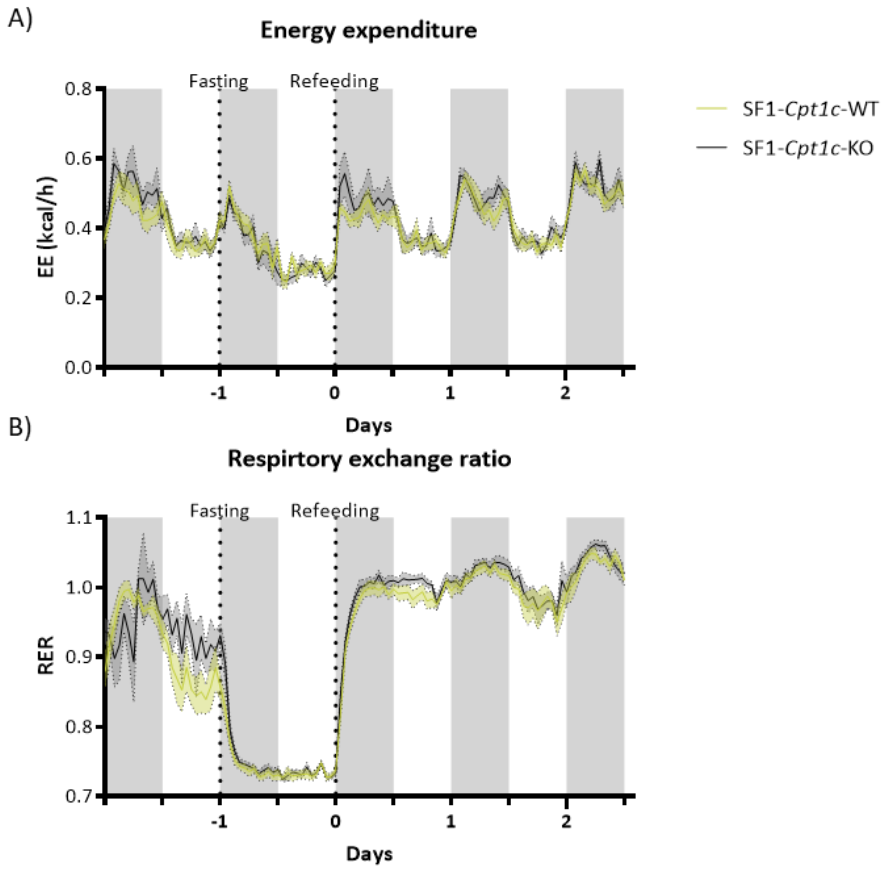

Fig. 54. Energy expenditure (EE) and Respiratory exchange ratio (RER) previous to fasting, during the 24h-fasting and the 48h-refeeding. A) EE. B) RER. Data were represented as mean ± SEM, 13-week old male mice, n= 7-10/ group. Statistical significance was determined by ANOVA test with post-hoc Bonferroni.

5 Metabolic phenotype of SF1-CPT1c-KO mice under thermoneutrality and cold exposure

5.1 Thermoneutrality studies

Thermoneutrality temperature for mice is 33ºC but they are normally housed at 22ºC. Then, we analysed whether metabolic parameters such as body weight, food intake, energy expenditure and RER were different between genotypes at thermoneutrality. Both genotypes were housed at 33 ºC during 48 hours for studying the transition between 22 ºC and 33 ºC. Body weight and food intake did not differ between genotypes **(Fig. 55A-B)**.

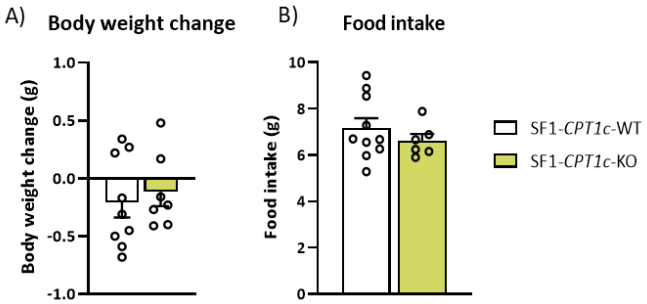

Fig. 55. Body weight and food intake after 48 hours on thermoneutrality. A) Body weight change between initial body weight and final body weight after 48 hours at 33ºC. B) Cumulative food intake during the 48 hours at thermoneutrality. Data were represented as mean ± SEM, 12-week old male mice, n= 7-10/ group. Statistical significance was determined by ANOVA test with post-hoc Bonferroni.

Energy expenditure and RER were also analysed using the calorimetric chambers, and no differences were observed in these parameters between SF1-*CPT1c*-WT and SF1-*CPT1c*-KO mice **(Fig. 56A-B)**. Altogether, both genotypes at thermoneutrality have the same metabolic phenotype under chow diet.

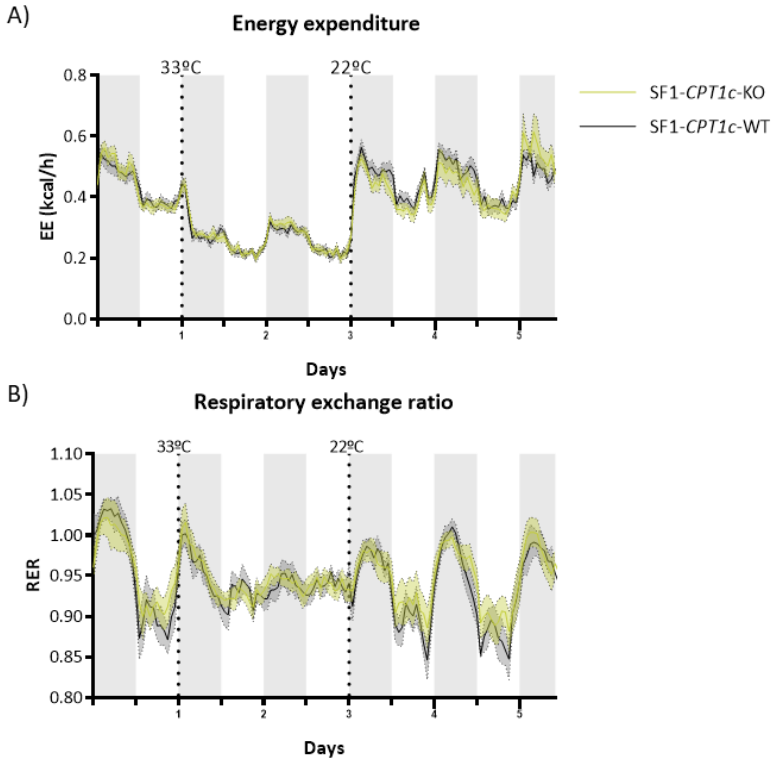

Fig. 56. Energy expenditure (EE) and Respiratory exchange ratio (RER) under thermoneutrality conditions. A) EE. B) RER. Data were represented as mean ± SEM, 12-week old male mice, n= 7-10/ group. Statistical significance was determined by ANOVA test with post-hoc Bonferroni.

5.2 Cold exposure studies under chow diet

For studying cold exposure effects, we did a first approach keeping mice at 4ºC for 6 h and analysing cold-induced BAT thermogenesis activation and glycaemia since unpublished observations from our group had shown that global mice deficient for CPT1c had a different adaptation to cold exposure compared to WT mice in terms of glycaemia and body temperature. SF1-*CPT1c*-KO mice display a tendency to have higher iBAT temperature than WT littermates **(Fig. 57A)**. Regarding glycaemia, null mice presented higher blood glucose levels **(Fig. 57B)**.

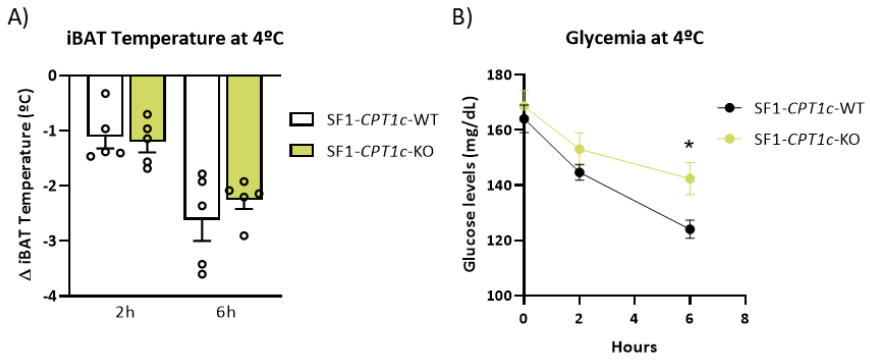

Fig. 57. BAT thermogenesis and glycaemia on cold exposure (4ºC) for six hours. A) Difference of iBAT temperature between the starting point and after 6 h at 4ºC. B) Glycaemia evolution over the 6 h. Data were represented as mean ± SEM, 14-week old male mice, n= 5/group. *p<0.05. Statistical significance was determined by ANOVA test with post-hoc Bonferroni.

The second experimental approach was performed using the calorimetric chambers in Dr Cota's lab. Mice were exposed to 4ºC for 24 h and during this period, similar values of body weight change and food intake were recorded in both WT and specific KO mice **(Fig. 58A-B)**.

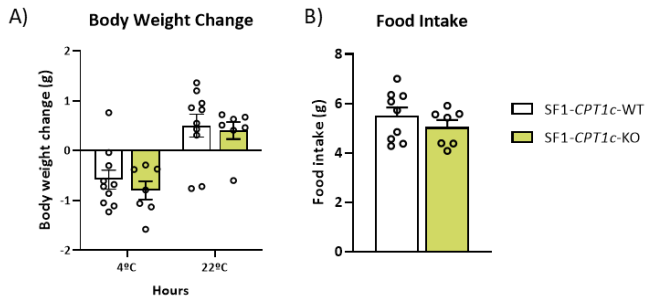

Fig. 58. Body weight change and food intake after 24 h of cold exposure (4ºC). A) Body weight change of the first 24 h exposed to 4ºC and the following 24 h at 22ºC. B) Cumulative 24-hour food intake at 4ºC. Data were represented as mean ± SEM, 14-week old male mice, n= 7-10/ group. Statistical significance was determined by t-student test.

Under these cold conditions, energy expenditure and RER were also analysed for 24 h. No differences in energy expenditure were found between genotypes **(Fig. 59A- B)**. RER analysis showed similar values between WT and KO mice during the dark phase, but a significant difference was appreciated in the light phase, being lower in SF1-*CPT1c*-KO than in control mice **(Fig. 59C-D)**. These results suggest that SF1-*CPT1c*-KO mice are using more fat as a fuel source than WT mice, which would be in line with the previous

observations of SF1-*CPT1c*-KO showing higher glycaemia and a tendency of higher iBAT temperature after 6 h of cold exposure **(Fig. 57A, B)**.

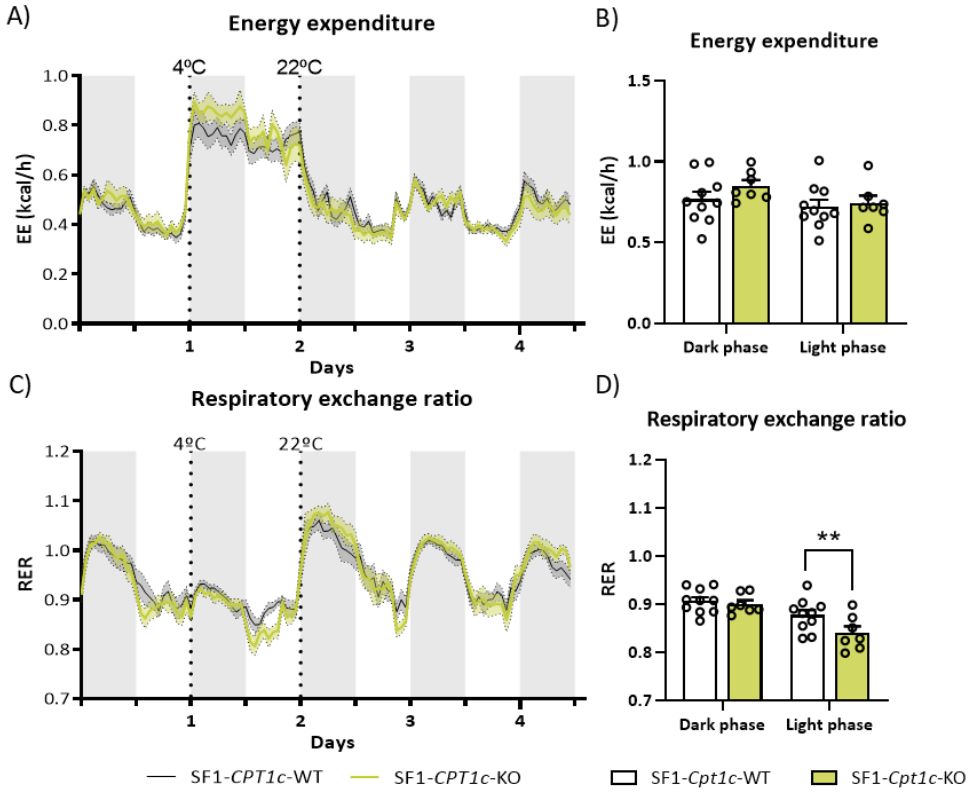

Fig. 59. Energy expenditure (EE) and Respiratory exchange ratio (RER) during cold exposure (4ºC). A) EE. B) EE at 4ºC separated by dark/light phase. C) RER. D) RER at 4ºC separated by dark/light phase. Data were represented as mean ± SEM, 14-week old male mice, n= 7-10/ group. **p<0.01. Statistical significance was determined by ANOVA test with post-hoc Bonferroni.

Thermoneutrality studies were also used for calculating the basal metabolic rate (BMR). Considering all the parameters involved in energy expenditure calculated from the calorimetric chambers, we performed a comparison of the energy expenditure components between the three temperatures (4ºC, 22ºC and 33ºC) at which mice were exposed to. Despite SF1-*CPT1c*-KO mice tended to have higher thermogenesis activity when exposed to 4ºC, no significant differences between the specific KO and the WT mice were found when analysing the physical activity energy expenditure (PAEE), the thermal effect of food (TEF), the basal metabolic rate (BMR) and the cold-induced thermogenesis (CIT) **(Fig. 60)**.

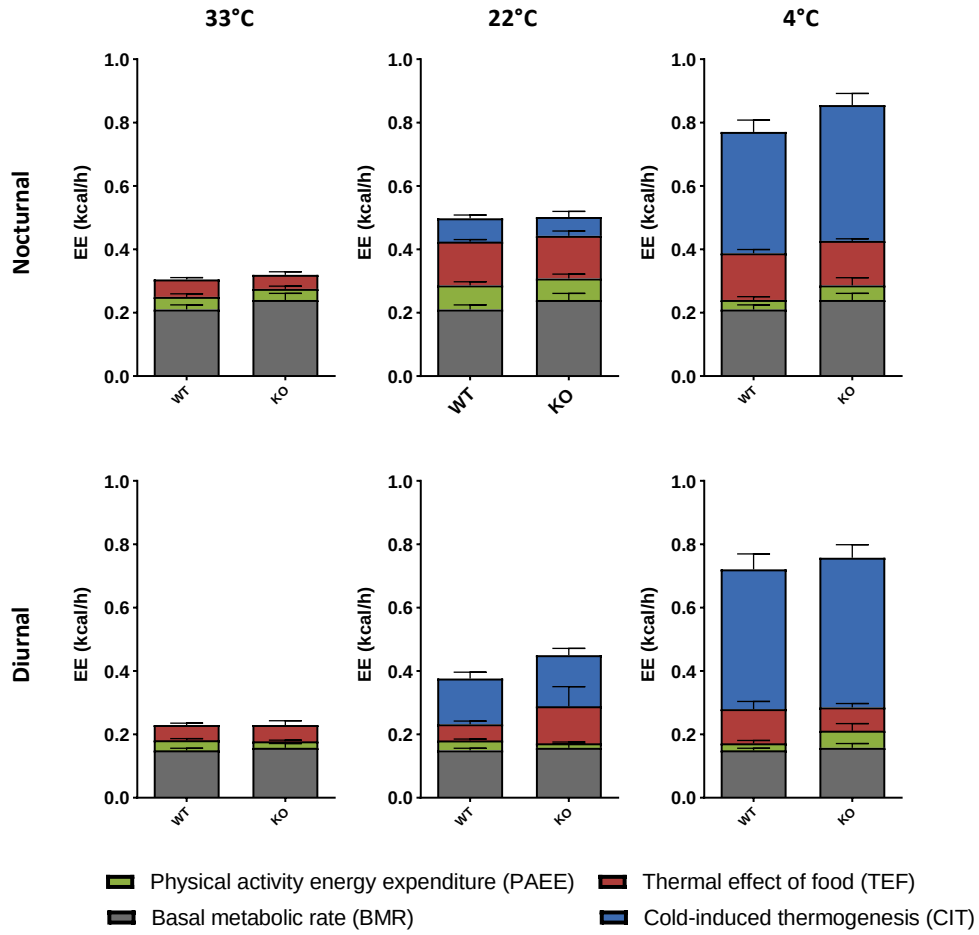

Fig. 60. Energy expenditure (EE) components at 4ºC, 22ºC and 33ºC. Basal metabolic rate, the thermal effect of food, the physical activity and thermogenesis activity were represented as part of the total energy expenditure calculated by indirect calorimetry in WT and SF1-*CPT1c*-KO mice. Data were represented as mean ± SEM, male mice, n= 7-10/ group. Statistical significance was determined by ANOVA test with post-hoc Bonferroni.

5.3 Cold exposure studies in HFD-fed mice

Considering the impaired adaptation of SF1-*CPT1c*-KO mice to a HFD, cold exposure was also evaluated in obese mice fed with HFD for 6 weeks. During the exposure at 4ºC for 24 h, no differences in body weight, food intake, energy expenditure or RER were observed between the genotypes **(Fig. 61A-D)**. Therefore, CPT1c in SF1 neurons could be playing a role in the metabolic adaptation to cold, avoiding excessive fat consumption, but this role is compromised when obesity is established.

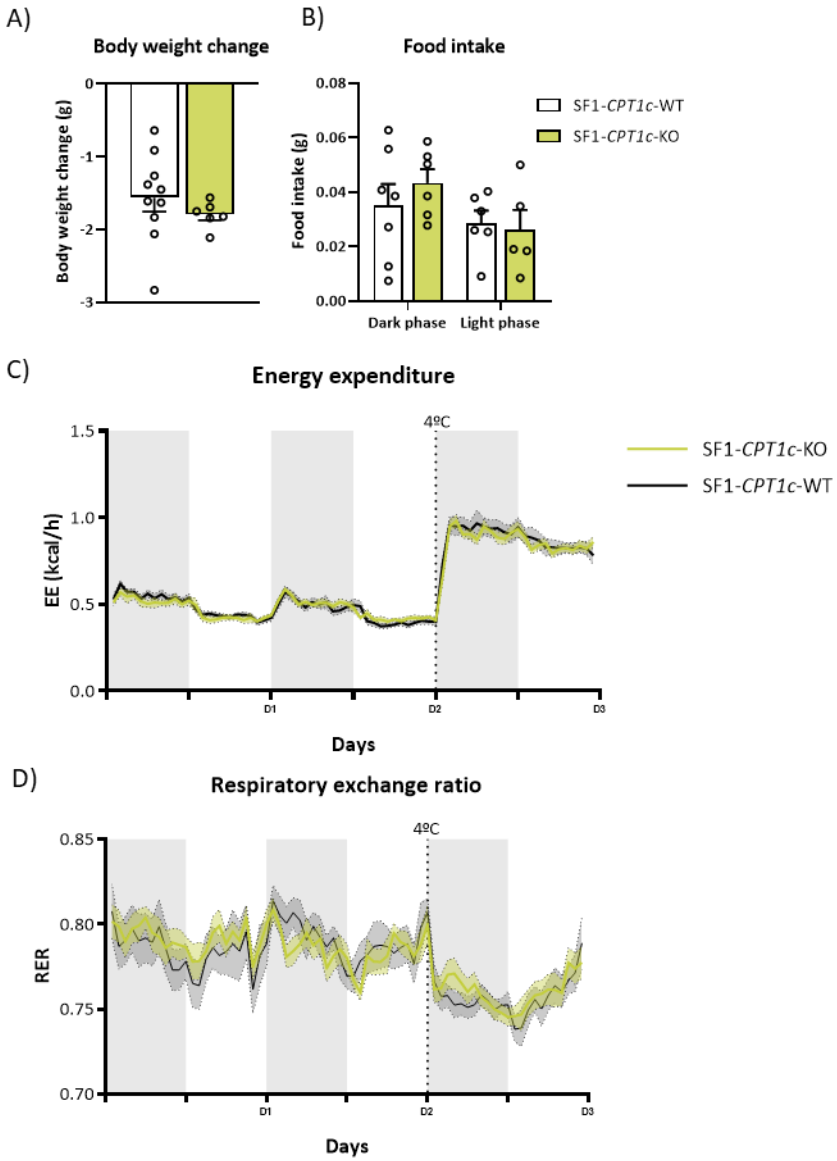

Fig. 61. Body weight, food intake, energy expenditure (EE) and Respiratory exchange ratio (RER) at cold exposure (4ºC) under HFD conditions. A) Body weight change between initial body weight and body weight after 24 hours at 4ºC. B) Cumulative food intake separated by dark/light phase. C) EE D) RER. Data were represented as mean ± SEM, male mice, n= 7-10/ group. Statistical significance was determined by ANOVA test with post-hoc Bonferroni.

6 Results summary of Chapter I

The main results obtained from the study of the metabolic phenotype of SF1-*CPT1c*-KO mice are the following **(Fig. 62)**:

- Under SD conditions, the analysis of various metabolic parameters related to energy homeostasis showed that SF1-*CPT1c*-KO mice did not differ from SF1-*CPT1c*-WT mice. However, SF1-*CPT1c*-KO male mice tended to accumulate more fat versus floxed mice. This trend was observed using two different batches of mice and two different techniques in male mice. Regarding glucose metabolism, there was also observed some sex effect: SF1-*CPT1c*-KO male mice presented higher glucose disappearance rate compared to the WT mice, while these effects were not observed in female mice.

- After a short-term exposure to HFD (5 days), SF1-*CPT1c*-KO mice significantly gained more weight than their control littermates. This finding was supported by higher food intake and higher fat accumulation in the transgenic mice group. In line with these results, RER results indicated that SF1-*CPT1c*-KO mice were using less fat than SF1-*CPT1c*-WT mice for energy production. In response to central leptin administration, SF1-*CPT1c*-KO mice were not able to activate BAT thermogenesis in contrast to that observed in WT mice. Thus, CPT1c in SF1 neurons seems to be necessary to adapt to the metabolic challenge that represents HFD feeding, playing a key role in the metabolic switch to the new situation. These experiments were only done in male mice.

- After long-term exposure to HFD, body weight differences between SF1-*CPT1c*-KO and WT were maintained over time in male mice. Regarding female mice, these body weight differences were appreciated after 6 weeks of HFD. These results were accompanied with a higher accumulation of fat mass in SF1-*CPT1c*-KO mice. Any other parameter of energy metabolism studied was not different between both genotypes. Regarding glucose metabolism, null male mice showed intolerance to glucose and an altered CRR compared to WT mice. Transgenic female mice showed glucose intolerance but a proper insulin response.

- Under fasting conditions, mice deficient for CPT1c in SF1 neurons were able to adapt to the hypoglycaemic situation, but they showed higher glycerol levels and

a tendency of higher triglyceride levels in the liver compared to WT mice. Therefore, it could be said that CPT1c in SF1 neurons is needed for a proper liver lipid metabolism under fasting conditions.

- Under cold exposure, mice lacking CPT1c in SF1 neurons presented a reduced RER and they seemed to have higher BAT thermogenesis, which represents a different adaptation to cold, avoiding a reduction in body temperature, and maintaining higher blood glucose levels. Both results suggest an increased use of fat as energy substrate in KO mice. Once obesity is established in mice, the different response to cold exposure between genotypes is not appreciated.

Altogether evidence that CPT1c in SF1 neurons is playing a key role in the early onset of obesity and in the adaptation of fasting and cold exposure, but not once mice have developed obesity.

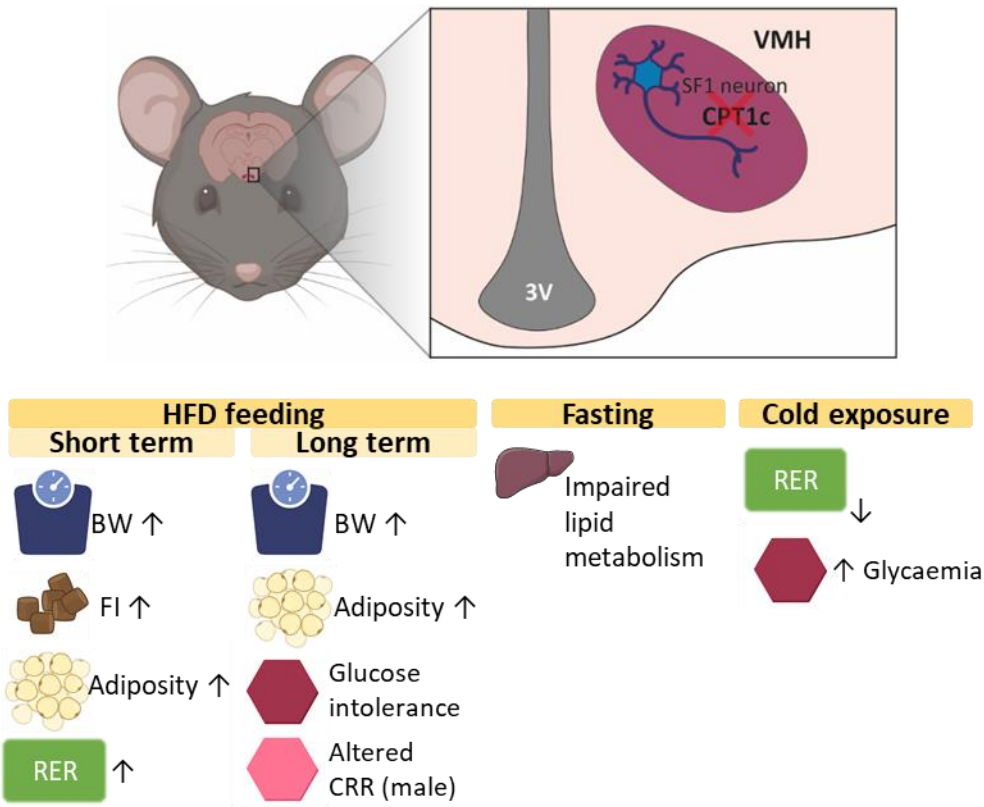

Fig. 62. Graphical Abstract of Chapter I. Main results of the study of the metabolic phenotype of mice deficient of CPT1c in SF1 neurons in response to HFD and other metabolic challenges. BW: body weight; CRR: counterregulatory response; FI: food intake; RER: respiratory exchange ratio; VMH: ventromedial nucleus.

Chapter II

Differential role of long-chain fatty acids in the regulation of energy balance and involvement of CPT1c

In this chapter, we aimed to explore the central effects of LCFA on body weight, food intake and BAT thermogenesis, considering the degree of saturation of the FA chain. We were also interested in elucidating the hypothalamic nuclei involved and the molecular mechanisms mediating LCFA-induced BAT thermogenesis activation. Finally, we analysed whether CPT1c, the main target of this thesis, is crucial for the central role of LCFAs in peripheral metabolism.

To address the different effects that LCFAs have on the metabolic phenotype we used two different approaches: i) administration of diets enriched with LCFAs, which is a more physiological approach, and ii) LCFA icv administration to discriminate the central effects on energy metabolism.

1 Metabolic response of WT mice to diets enriched with different LCFAs on the control of energy homeostasis

To address if LCFAs have different effects on the control of body weight, food intake and energy balance, we exposed WT mice to fat-rich diets with different composition in saturated or unsaturated LCFAs. In particular, mice were fed for seven days with three different types of diets (see composition of diets in **table 4** in methodology section 1.2.5): a high-fat diet enriched only with unsaturated fatty acids (MUFA diet, 49% Kcal from fat), a high-fat diet enriched only with saturated fatty acids (SFA diet, 49% Kcal from fat) and a low-fat diet (SD, 10% Kcal from fat), being the later used as a control diet. During this period, mice were monitored every two days.

The seven-days approach was chosen based on previous results of our group, in which Dr Rodríguez-Rodríguez and colleagues showed the importance of the first seven days to adapt to the new metabolic challenge to counteract obesity development under HFD exposure (Rodríguez-Rodríguez *et al.* 2019). That study also identified a maximum activation peak of BAT thermogenesis at 7 days of HFD feeding. Considering that BAT thermogenic response to FAs is a specific objective of the present thesis, we decided to use the same period of dietary administration.

1.1 Body weight and food intake

As commented in the introduction, previous studies have shown that unsaturated FAs induce body weight loss and reduce food intake while saturated FAs have a negative effect on both parameters. To gain a better insight of the effect that MUFA and SFA diets have on energy balance, we analysed body weight and food intake. After seven days on these diets, a positive trend in body weight in the experimental groups fed with MUFA and SFA diets was observed compared to the SD group, but only the group fed with the SFA diet presented a significant difference compared to the control group **(Fig. 63)**.

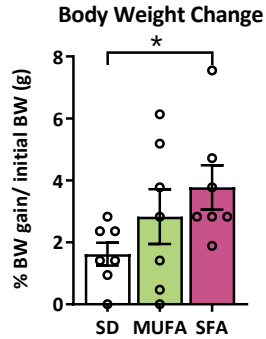

Fig. 63. Body weight change after administration of SD, MUFA and SFA diets to WT mice for seven days. Body weight (BW) change is presented as a percentage normalised to initial body weight. Data were represented as mean ± SEM, male mice, 8-12 weeks of age, n= 7/group. *p<0.05. Statistical significance was determined by ANOVA test with post-hoc Bonferroni. BW: body weight; MUFA: unsaturated fatty acid-enriched diet; SD: standard diet; SFA: saturated fatty acid-enriched diet.

Despite the lack of significant effects of MUFA diet on body weight gain, this type of diet led to a significant increase in food intake and in the amount of calorie intake compared to the other experimental groups **(Fig. 64A-B)**. Contrarily, the SFA group was the one that ate less amount of food at the end of the seven days **(Fig. 64A)**. Taking into account the calorie intake results **(Fig. 64B)**, mice fed with SFA diet adjusted the amount of food eaten to the higher caloric composition of the diet whereas the MUFA diet group did not adapt food intake to the new caloric situation. The results indicate that, although mice fed a MUFA diet showed increased levels of food and calorie intake, it did not imply a significant increase in body weight compared to the SD group. In contrast, SFA diet administration led to a significant increase in body weight gain despite food and calorie intake remained unchanged versus SD-fed mice **(Fig. 64A-B)**. Taking into account that the caloric intake

was higher in the MUFA group but not in the SFA group compared to control mice, results suggest that the energy expenditure might be increased by MUFA diet while reduced by the SFA diet.

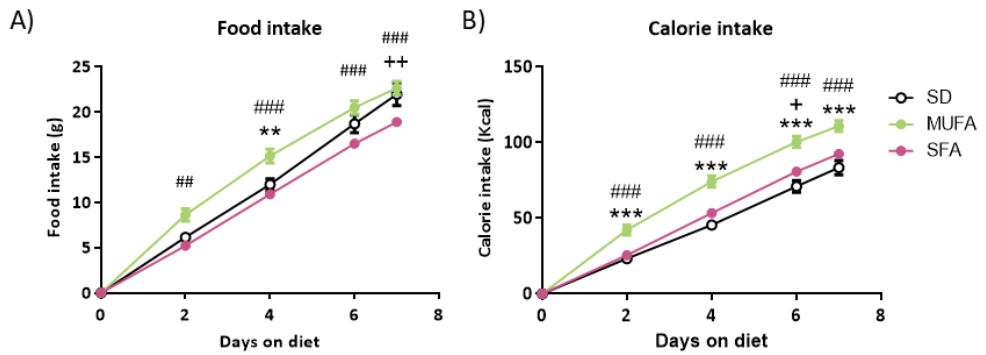

Fig. 64. Food intake and calorie intake monitoring of WT mice after seven days of SD, MUFA and SFA diets feeding. A) Cumulative food intake. B) Cumulative calorie intake. Data were represented as mean ± SEM, male mice, 8-12 weeks of age, n= 7/group. **p<0.01, ***p<0.001 MUFA vs SD; ##p<0.01, ###p<0.001 SFA vs MUFA;. +p<0.05, ++p<0.01 SFA vs SD. Statistical significance was determined by ANOVA test with post-hoc Bonferroni. MUFA: unsaturated fatty acid-enriched diet; SD: standard diet; SFA: saturated fatty acid-enriched diet.

1.2 BAT thermogenic response

We focused on BAT thermogenesis activity analysis because it has a great impact on body weight during the first days of HFD exposure and also because is one of the protective responses against the onset of obesity. To study this activity, we used two different methodologies: measurement of the iBAT temperature and mRNA thermogenic markers.

After 7 days on special diets, IR images revealed a significant increase in iBAT temperature only in those mice fed with MUFA diet, whereas this increase was not appreciated in the SFA diet-fed group **(Fig. 65A, B)**. After these measurements, mice were sacrificed and BAT was collected to check the mRNA thermogenic markers UCP1, PGC1 α and PRDM16. Results showed an increased expression of the three thermogenic markers with both type of HFD, but this increase was more remarkable on mice fed with MUFA diet **(Fig. 65C)**. Altogether, iBAT and thermogenic genes analysis indicate that mice fed with the MUFA diet had the highest thermogenic activity on BAT compared to the other experimental groups.

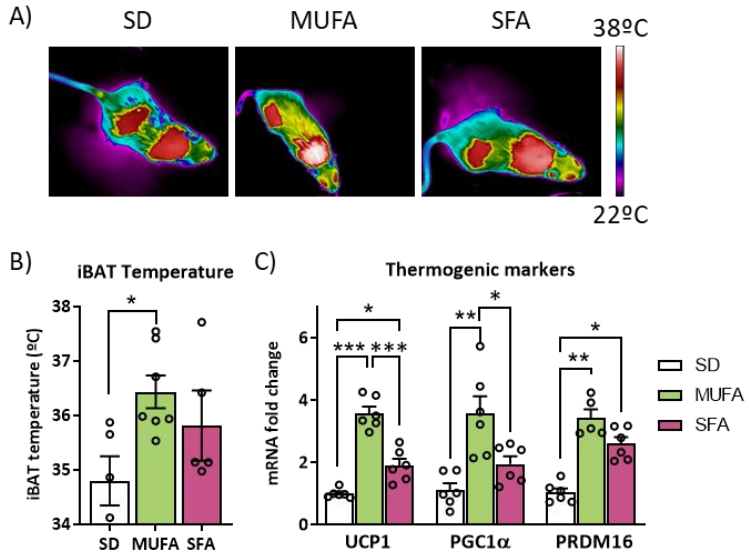

Fig. 65. BAT thermogenesis of WT mice after seven days of SD, MUFA and SFA diet feeding. A) Representative IR pictures for iBAT temperature measurement. B) iBAT temperature after 7 days on diets. C) Thermogenic markers UCP1, PGC1α and PRDM16 from BAT after 7 days on diets. GAPDH was used as housekeeping gene to normalize mRNA markers. Data were represented as mean ± SEM, male mice, 8-12 weeks of age, n= 5/group for iBAT temperature and n=7/ group for thermogenic markers results. *p<0,05, **p<0.01, ***P<0.001. Statistical significance was determined by ANOVA test with post-hoc Bonferroni. iBAT: interscapular BAT; MUFA: unsaturated fatty acid – enriched diet; SD: standard diet; SFA: saturated fatty acid – enriched diet.

Considering the results of body weight, food intake and BAT thermogenesis activity in response to these diets, it could be suggested that mice fed MUFA diet are gaining less weight likely due to an increase in BAT thermogenesis activity even though they were eating more amount of food, in contrast to that observed in SFA-fed mice.

1.3 Hypothalamic c-Fos expression

As stated in the introduction section, it is well known that the hypothalamus is the brain area that detect different stimuli such as nutrients and other signalling molecules sensing the energy status of the organism and, then, it orchestrates the peripheral responses needed. In order to evaluate which hypothalamic nuclei could be responsible for the different metabolic responses to the type of diets under study, an immunohistochemistry for c-Fos was performed after a fast-refeeding approach. C-Fos is a rapidly expressed gen and its expression is an indirect marker of neuronal activity in response to a new stimulus. Mice were fasted for three hours and then refed with the experimental diet for two hours without previous presentation. After that, mice were intracardiacally perfused **(Fig. 66A)**.

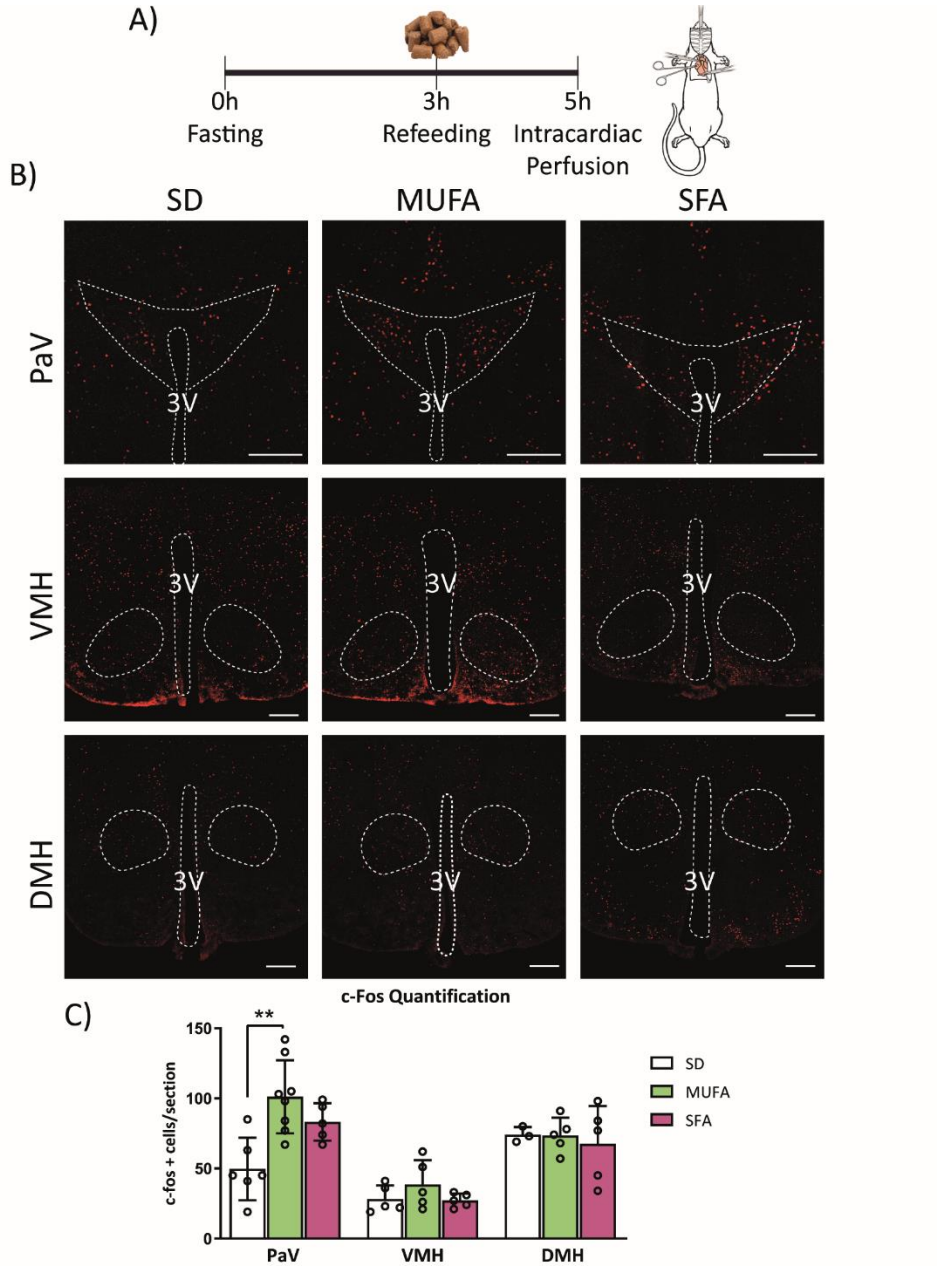

Fig. 66. Assessment of neuronal activity after administration of SD, MUFA and SFA diet to WT mice. A) Experiment's timeline. B) Immunohistochemistry of c-Fos expression in PaV, VMH and DMH 2 h after refeeding with special diets. C) Quantification of c-Fos positive cells per section of each nucleus. Data were represented as mean ± SEM, male mice 8-12 weeks of age, n= 3 /group (2 slices/mice). ** p<0,01 vs SD. Statistical significance was determined by ANOVA test with post-hoc Bonferroni. DMH: dorsomedial hypothalamus; MUFA: unsaturated fatty acid – enriched diet; PaV: paraventricular nucleus; SD: standard diet; SFA: saturated fatty acid – enriched diet; VMH: ventromedial hypothalamus. Scale bar: 250 µm.

We decided to analyse three nuclei of the hypothalamus related to feeding and BAT thermogenesis activation: PaV, VMH and DMH. As illustrated on **figure 66**, the PaV was significantly activated by the MUFA diet, but not by the SFA diet, in comparison to the control low-fat diet group **(Fig. 66B-C)**. The VMH presented a tendency to show the same results as the PaV, although differences between groups were not significant **(Fig. 66B-C)**. Finally, the DMH nucleus was also analysed and the three experimental groups had a very similar number of c-Fos positive cells **(Fig. 66B-C)**. Among the three nuclei analysed, the PaV was the one with the highest neuronal activity in response to a MUFA diet.

2 Metabolic response of WT mice to different central FAs on the control of energy homeostasis

In order to characterize the metabolic response of central LCFA, four different kinds of FAs were icv administrated to mice: oleic acid (C18:1), linoleic acid (C18:2), stearic acid (C18:0) and palmitic acid (C16:0). Each FA was compared to its corresponding vehicle. Since these saturated FAs under study share the same vehicle, they were tested together in the same experiment. Using this central administration strategy, we could omit the peripheral effects that LCFAs have when ingested through a diet and focus the study on the central action.

2.1 Body weight and food intake analyses

To analyse the central effects of LCFA on body weight and food intake, we designed a protocol of administration based on previous publications (Schwinkendorf *et al.* 2011; Cintra *et al.* 2012) and preliminary studies of the group. In particular, we administered a total of 36 nmol of FA into 4 injections over 48 hours: 2 infusions of 9 nmol per day, one hour after the dark phase (9 a.m.) and one hour before the dark phase (7 p.m.). In this thesis, we refer to this protocol as the 48 hours' protocol **(Fig. 67A)**.

Results showed that central administration of the unsaturated FAs, oleic and linoleic acid, reduced body weight change compared to mice treated with vehicle **(Fig. 67B-C)**, whereas the saturated FAs, palmitic and stearic acid, had no significant effects on body weight **(Fig. 67D-E)**.

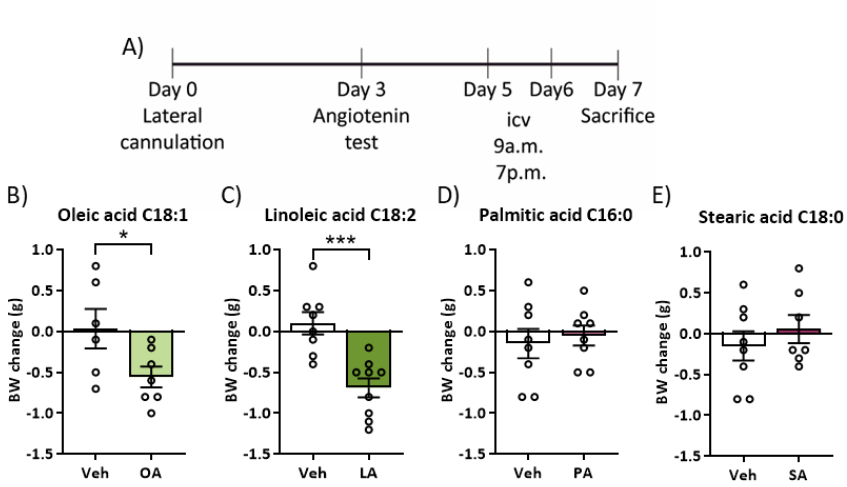

Fig. 67. Effect of central administration of four different fatty acids on body weight of WT mice. A) Timeline of 48-hour's protocol. B-E) Body weight (BW) change between the initial and final body weight after the 48 treatment: oleic acid (B), linoleic acid (C), palmitic acid (D) and stearic acid (E). Data were represented as mean ± SEM, n= 7-9/group. * p<0.05, *** p<0.001 versus vehicle. Statistical significance was determined by t-student. BW: body weight; OA: oleic acid, LA: linoleic acid, PA: palmitic acid, SA: stearic acid; Veh: vehicle.

Food intake analysis revealed a significant reduction after central administration of oleic and linoleic acid **(Fig. 68A-B)**, in agreement with body weight results **(Fig. 67 A-B)**, whereas it remained unchanged after icv administration of stearic or palmitic acid **(Fig. 68C-D)**. As a conclusion of these results, unsaturated FAs have a centrally-mediated effect on metabolism by reducing food intake and body weight, while saturated FAs do not have this effect.

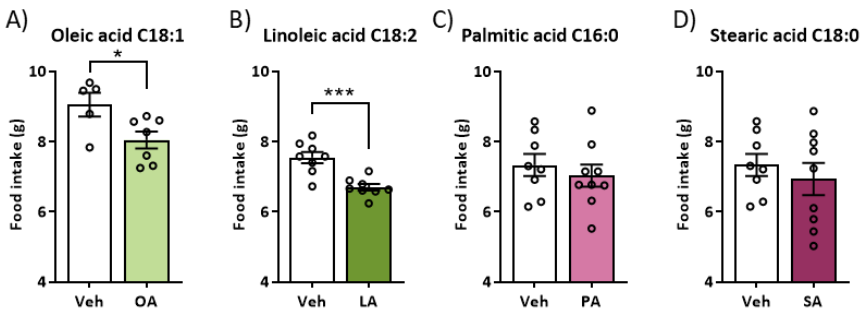

Fig. 68. Effect of central administration of four different LCFAs on food intake of WT mice. A-D) Cumulative food intake during the 48h of treatment with oleic acid (A), linoleic acid (B), palmitic acid (C) and stearic acid (D). Data were represented as mean ± SEM, n= 7-9/ group. * p<0.05, *** p<0.001 versus vehicle. Statistical significance was determined by t-student. OA: oleic acid, LA: linoleic acid, PA: palmitic acid, SA: stearic acid; Veh: vehicle.

2.2 BAT thermogenic response

Considering that icv administration of unsaturated FAs reduces body weight, we decided to analyse the central effect of this kind of LCFAs on energy expenditure. Moreover, MUFA and SFA diet exposure increased BAT thermogenesis activity of mice. Therefore, we evaluated whether BAT thermogenesis activity was modulated by the central administration of the four LFCA under study. As in the diet-based approach, we used two strategies to check the thermogenic response after the 48 hours' protocol. First, the measurement of iBAT temperature by IR imaging revealed that the unsaturated FAs, oleic and linoleic acid, tended to activate thermogenesis in BAT **(Fig. 69A-C)**, resulting in an increment of the interscapular temperature, while saturated FAs reduced this activity as iBAT temperature diminished **(Fig. 69A, D-E)**.

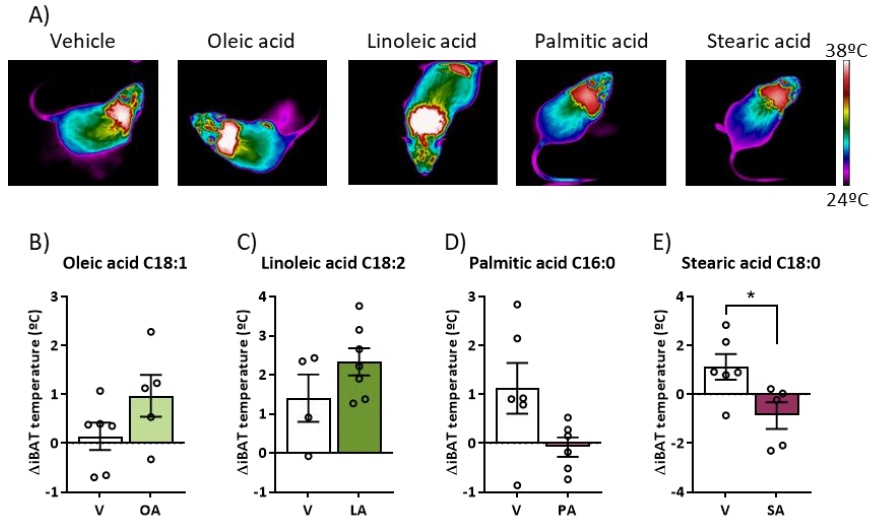

Fig. 69. Interscapular BAT temperature in response to LCFA icv administration in WT mice. A) Representative IR pictures of mice used for iBAT temperature measurement. B-E) Difference of iBAT temperature before and after the 48 hours of icv administration of oleic acid (B), linoleic acid (C), palmitic acid (D) and stearic acid (E). Data were represented as mean ± SEM, male mice, 8-12 weeks of age, n= 6 /group. * $p<0.05$ versus vehicle of the same condition. Statistical significance was determined by t-student. OA: oleic acid; LA: linoleic acid; PA: palmitic acid; SA: stearic acid; V: vehicle.

Although most of the differences found in iBAT temperature results were not statistically significant, there was a tendency in line with the results obtained with mRNA thermogenic markers **(Fig. 70)**. Particularly, icv administration of oleic acid and linoleic acid led to a

higher expression of thermogenic markers in BAT compared to their vehicles, pointing to an increased thermogenic activity **(Fig. 70A-B)**. Looking into saturated fatty acids treatment, icv administration of palmitic acid did not induce a raise in the markers of thermogenesis expression but a significant reduction in UCP1 and PGC1α **(Fig. 70C)**. Those mice administrated with stearic acid had more UCP1 mRNA expression compared to the vehicle group, but the two other thermogenic markers were unchanged **(Fig. 70D)**.

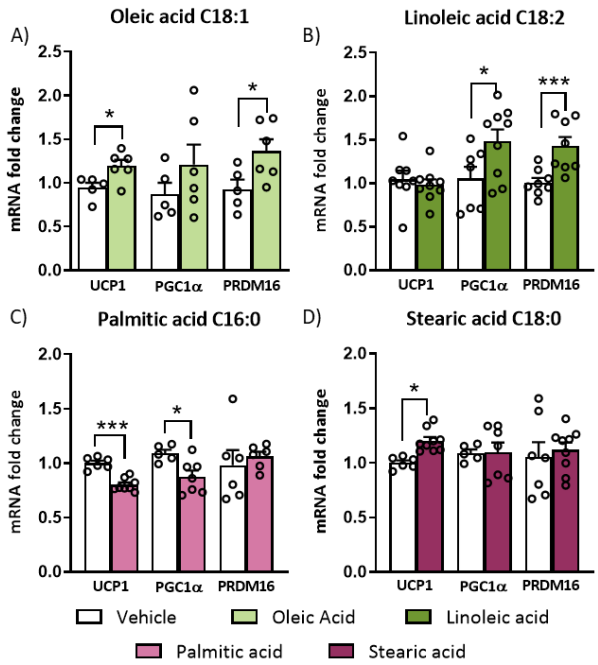

Fig. 70. mRNA thermogenic markers expression after central LCFA administration in WT mice. mRNA thermogenic markers after A) oleic acid treatment, B) linoleic acid treatment, C) palmitic acid treatment, D) and stearic acid treatment. GAPDH was used as housekeeping gene to normalize mRNA markers. Data were represented as mean ± SEM, male mice, 8-12 weeks of age, n= 7-9/group. * p<0.05, *** p<0.001 versus vehicle of the corresponding thermogenic marker. Statistical significance was determined by t-student for each thermogenic marker.

Overall, data suggest that unsaturated FAs have a central positive impact in controlling body weight, reducing food intake and increasing BAT thermogenesis, while saturated FAs do not have this effect.

2.3 Hypothalamic AMPK – ACC and FAS pathway

As explained in the introduction, the hypothalamic fuel sensor AMPK is activated through phosphorylation when there is a deficit of ATP, leading to ACC activity inhibition. ACC is

needed for malonyl-CoA production, which has been defined to regulate CPT1c function (Casals *et al.* 2016). To explore this axis, hypothalamic samples were collected after icv administration of the four LCFAs using the 48 hours' protocol commented above. AMPK and ACC phosphorylation and total protein levels were analysed by immunoblotting **(Fig. 71A)**. Surprisingly, oleic and linoleic acid have different effects on this signal axis. While oleic acid treatment resulted in a reduction of pAMPK levels and of the ratio of pAMPK/ total AMPK levels, the linoleic acid treatment presented a significant increase in pAMPK expression, with no significant changes in the ratio pAMPK/AMPK **(Fig. 71A-D)**.

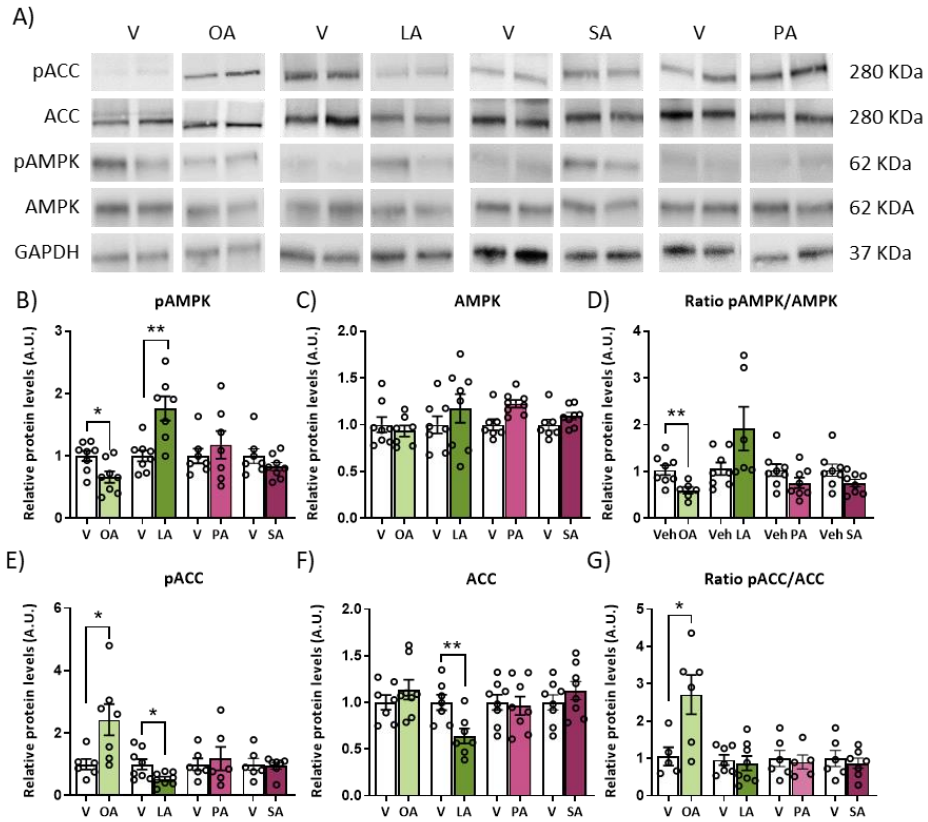

Fig. 71. Hypothalamic expression of AMPK and ACC after central administration of four LCFAs in WT mice. A) Immunoblotting of pACC, ACC, pAMPK, AMPK and GAPDH. B-G) Immunoblot quantification of pAMPK (B), total AMPK (C), ratio of pAMPK/AMPK (D), pACC (E), total ACC (F) and ratio of pACC/ACC levels (G). GAPDH was used as housekeeping protein to protein levels. Data were represented as mean ± SEM, n= 8/group. *p<0.05, **p<0.01 versus corresponding vehicle. Statistical significance was determined by t-student. A.U.: arbitrary units; OA: oleic acid; LA: linoleic acid; PA: palmitic acid; SA: stearic acid; V: vehicle.

Regarding ACC levels, oleic acid presented higher expression of pACC resulting into a higher ratio between phosphorylation and total levels, while linoleic acid diminished both phosphorylation and total levels of ACC, but the ratio did not differ from the vehicle group **(Fig. 71A, E-G)**. Otherwise, saturated FAs seemed to have no influence in the AMPK-ACC signalling, since no changes were observed in the expression of these proteins in the hypothalamus of palmitic or stearic acid-treated mice **(Fig. 71)**.

Another key player in the response of the hypothalamus to the nutritional state is the enzyme FAS. This enzyme catalyses the synthesis of palmitate from malonyl-CoA, so its activation is expected to result in a diminution of malonyl-CoA levels. After central administration of unsaturated fatty acids, FAS expression was significantly reduced after linoleic acid and showed a clear tendency in response to oleic acid **(Fig. 72)**. In contrast, FAS expression was significantly raised in response to the central administration of saturated fatty acids **(Fig. 72)**.

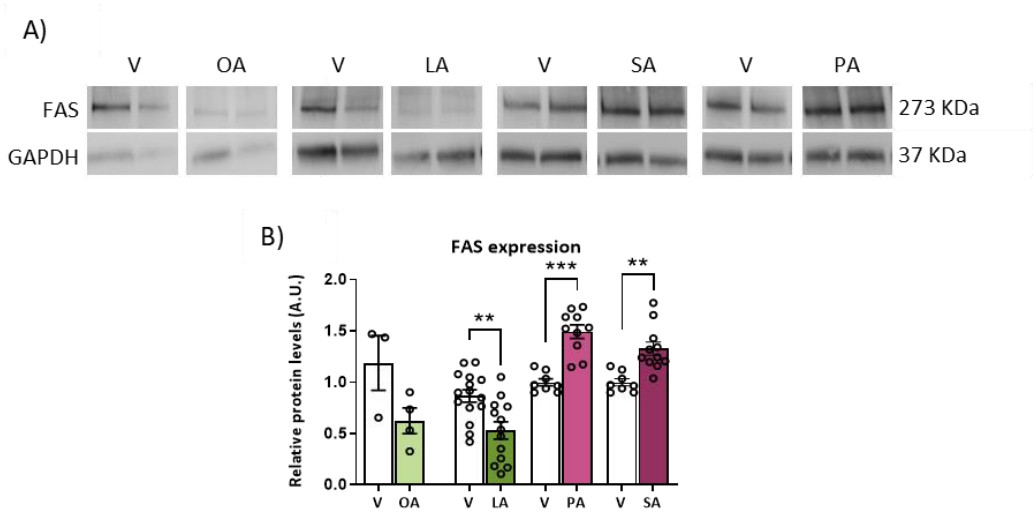

Fig. 72. Hypothalamic expression of FAS after central administration of four LCFAs in WT mice. A) Representative blots of FAS and GAPDH. B) Immunoblot quantification of FAS levels. GAPDH was used as housekeeping protein to protein levels. Data were represented as mean ± SEM, n= 10-12/group, except OA n=3-4/ group. **p<0.01, ***p<0.001 versus vehicle. Statistical significance was determined by t-student. A.U.: arbitrary units; OA: oleic acid; LA: linoleic acid;; PA: palmitic acid; SA: stearic acid; V: vehicle.

Overall, these results indicate that unsaturated FAs are inhibiting the fatty acid synthesis pathway while saturated FAs are activating it. Moreover, results of hypothalamic expression of FAS suggest fluctuations in malonyl-CoA levels after LCFAs administration, which could facilitate to understand the action of CPT1c.

2.4 Hypothalamic c-Fos expression

In order to determine the hypothalamic nuclei involved in the different central responses to LCFAs, c-Fos immunohistochemistry was performed, focusing in PaV, VMH and ARC.

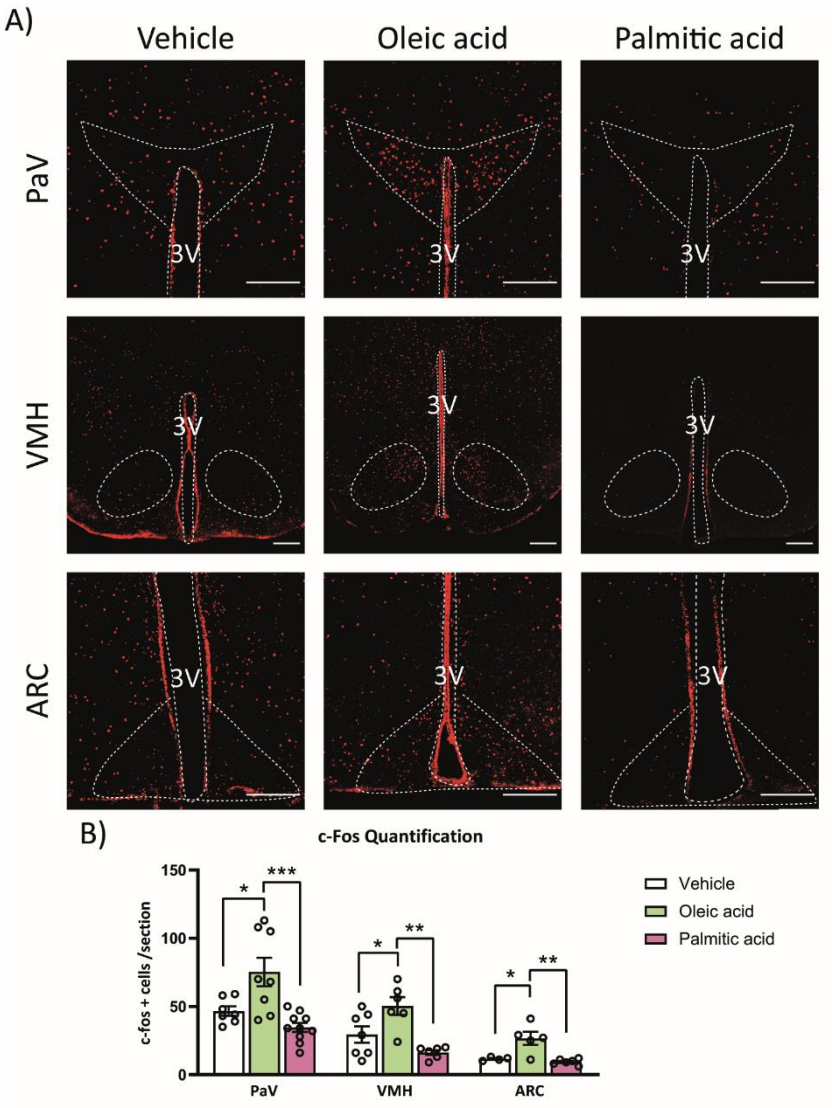

Fig. 73. Effects of central oleic acid and palmitic acid administration on neuronal activation assessed by c-Fos expression in the PaV, VMH and ARC in WT mice. A) Immunohistochemistry of c-Fos expression. B) Quantification of c-Fos positive cells per section. Data were represented as mean ± SEM, n= 3/group (2-3 slices/mice). *p<0.05, **p<0.01, ***p<0.001 versus vehicle. Statistical significance was determined by ANOVA test with post-hoc Bonferroni. 3V: 3rd ventricle; ARC: arcuate nucleus; PaV: paraventricular nucleus; VMH: ventromedial nucleus. Scale bar: 250 µm.

C-Fos expression was tested two hours after the administration of one dose of the unsaturated oleic acid and the saturated palmitic acid, mimicking MUFA and SFA diets, respectively. Results showed a different expression in the PaV, VMH and ARC hypothalamic nuclei after icv administration of oleic acid compared to the control group, but no differences were observed in the palmitic acid-treated mice **(Fig. 73)**. In line with the MUFA diet-based studies, oleic acid promoted c-Fos expression in the three nuclei, particularly in the PaV with the highest amount of c-Fos positive cells.

2.5 Hypothalamic Neuropeptides mRNA expression

Because of the results obtained on food intake and c-Fos expression in ARC and PaV in response to oleic acid, we analysed the expression of the neuropeptides POMC, NPY and AgRP after the oleic acid treatment using the 48 hours' protocol. The mRNA neuropeptide expression could explain food intake results, but also can be an indicative of ACR signalling to PaV (Sohn 2015). In agreement with food intake results, the expression of the anorexigenic neuropeptide POMC was higher after oleic acid treatment compared to vehicle, whereas the orexigenic neuropeptides NPY and AgRP expression did not change **(Fig. 74)**.

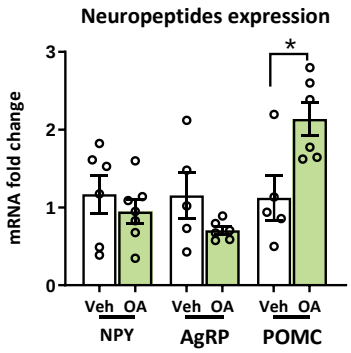

Fig. 74. Hypothalamic expression of neuropeptides after central administration of oleic acid in WT mice. mRNA hypothalamic expression of the neuropeptides NPY, AgRP and POMC after oleic acid treatment. GAPDH was used as housekeeping gene to normalize mRNA markers. Data were represented as mean ± SEM, n= 6/group. *p<0.05 versus vehicle. Statistical significance was determined by t-student. A.U.: arbitrary units. OA: oleic acid; PA: palmitic acid; Veh: vehicle.

This result is in line with the increased c-Fos expression in the ARC and PaV after icv oleic acid treatment. POMC is the precursor of αMSH, being this hormone released by POMC neurons to activate MC4R in the PaV. These findings reinforce the idea that both nuclei play an important role in the central sensing of oleic acid.

2.6 Hypothalamic inflammation

Since central administration of LCFA could promote hypothalamic inflammation, we analysed microglia activation in the PaV after icv administration of unsaturated or saturated FAs. We performed an immunohistochemistry for IBA-1, which is upregulated when microglia are activated. The number of IBA-1 positive cells and total IBA-1 expression were quantified in the PaV. Results showed that after icv oleic acid treatment, inflammation was not increased, whereas palmitic acid induced a significant increase in the number of IBA-1 positive cells, with higher fluorescence intensity compared to either oleic acid or vehicle group **(Fig. 75A-C)**. The increase in inflammation in terms of microglia activation evoked by central palmitic acid might contribute to explain the lack of effects of this type of FAs on satiety promotion and BAT thermogenesis.

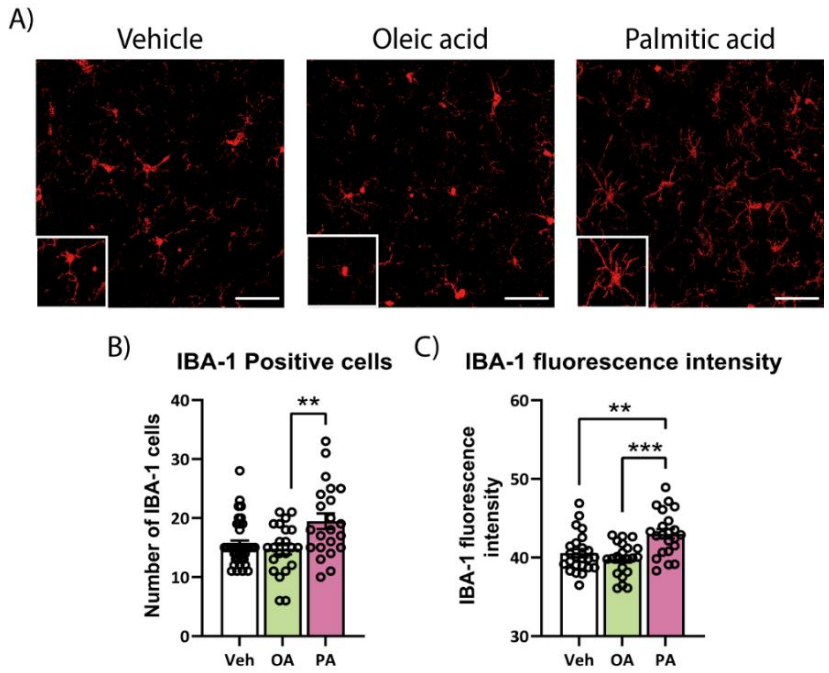

Fig. 75. **Microglia activation in the PaV after central administration of oleic and palmitic acid in WT mice.** A) Immunohistochemistry of IBA-1 expression after oleic acid and palmitic acid icv administration. Left corner contains a zoom picture. B) Quantification of IBA-1 positive cells per section of PaV. C) Quantification of IBA-1 fluorescence intensity. Data were represented as mean ± SEM, n= 4/group (4 slices/group). ** $p<0.01$ versus vehicle, *** $p<0.001$ versus vehicle. Statistical significance was determined by ANOVA.; OA: oleic acid; PA: palmitic acid. Scale bar: 25 µm.

2.7 Effect of the melanocortin receptor inhibition in oleic acid-induced neuronal activation

Taking into account that the PaV nucleus was the one with the higher number of c-Fos positive cells after central oleic acid administration **(Fig. 73)**, we then focused our study on this nucleus. The PaV has different types of neurons, including MC4R expressing neurons, which have been described as key players in the anorexigenic role of oleic acid (Schwinkendorf *et al.* 2011). Moreover, we have demonstrated that POMC neuronal activation is higher after oleic acid central injection **(Fig. 74)**, which could indicate that there is an activation of the melanocortin pathway in the PaV. Then, we investigated if MC4R neurons of PaV were involved in the response to oleic acid treatment **(Fig. 73)**. For this reason, we studied the central effect of oleic acid combined with a MC3R and MC4R inhibitor. An antagonist of these receptors, SHU9119, was icv administered with or without oleic acid to WT mice and two hours later the animals were perfused and brains were collected for c-Fos immunohistochemistry.

In agreement with previous results, icv oleic acid increased the number of c-Fos positive cells in the PaV, but this rise was not observed in the presence of SHU9119 **(Fig. 76A-B)**. These findings indicate that this type of melanocortin neurons could be responsible for the effect that unsaturated LCFAs have on BAT thermogenesis activity. Regarding the VMH, the increased c-Fos expression observed after oleic acid administration was also attenuated after the administration of oleic acid with SHU9119 **(Fig. 76A- B)**. Since this melanocortin receptor antagonist targets neurons from the PaV, results in VMH could indicate that this particular nucleus could be downstream the PaV in the central signalling of oleic acid. However, an effect of the antagonist on MC3R of the VMH, could not be dismissed. Finally, ARC showed an increased number of c-Fos positive cells in those brain slices of the oleic acid-treated in comparison to the vehicle group but, unlike the other two nuclei, this high c-Fos expression remained unchanged in mice treated with oleic acid together with SHU9119 **(Fig. 76A-B)**. The lack of effect of the melanocortin receptor antagonist on oleic acid-induced c-Fos activation in the ARC suggests that this nucleus is upstream of the PaV in the MC4R-mediated signalling of oleic acid.

After the observation of these results, it could be thought that MC4R expressing neurons in the PaV are crucial players for the central effects of oleic acid on food intake and peripheral regulation of energy metabolism and that these neurons could be activated by

POMC neurons of the ARC. Results also suggest that the VMH activation is mediated directly or indirectly by the melanocortin pathway.

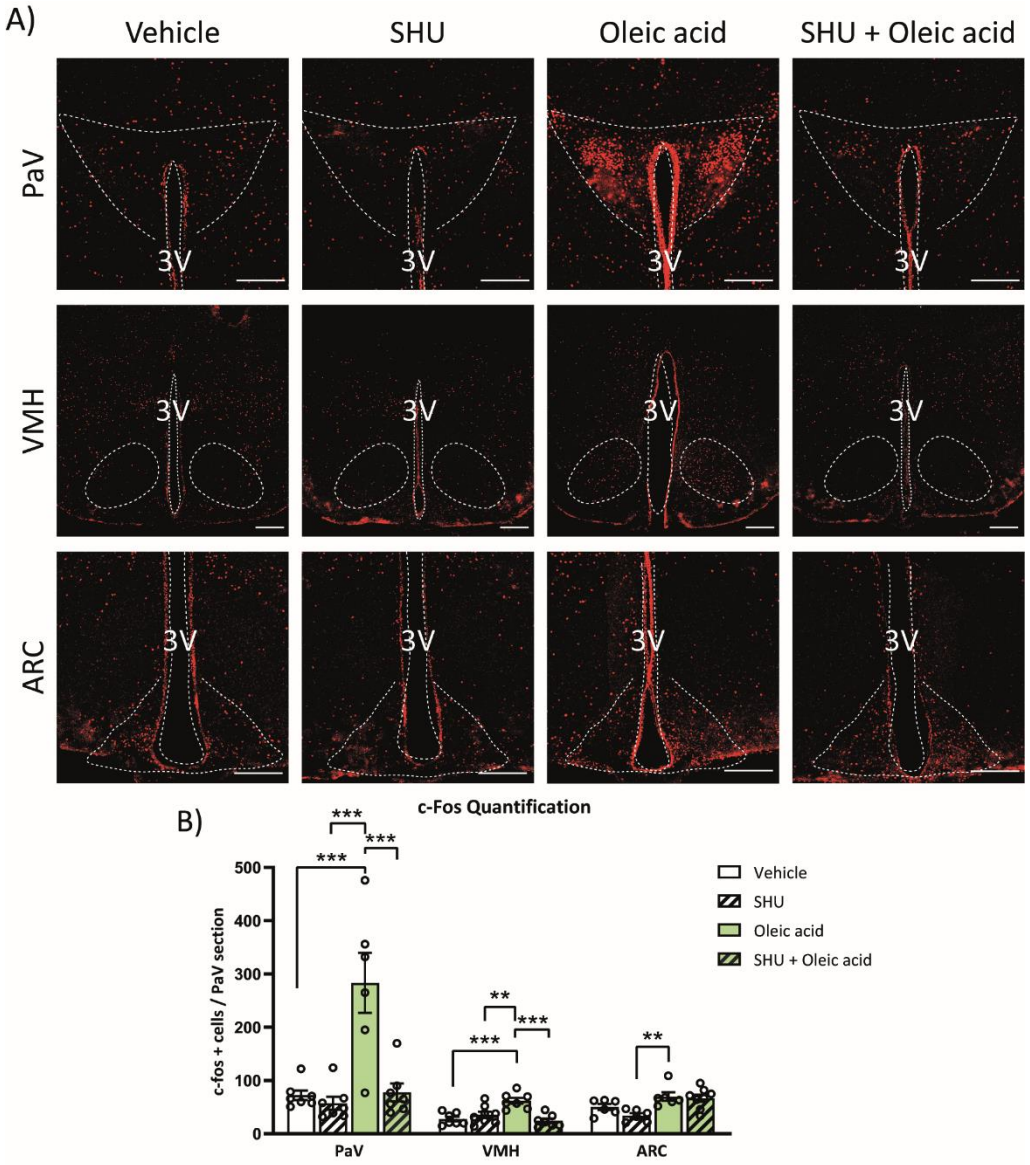

Fig. 76. Effects of the central administration of the MC3R and MC4R antagonist SHU9119 and/or oleic acid on neuronal activation assessed by c-Fos expression in the PaV, VMH and ARC nuclei in WT mice. A) Immunohistochemistry of c-Fos expression after SHU and/or oleic acid icv administration. B) Quantification of c-Fos positive cells per section of each nucleus. Data were represented as mean ± SEM, n= 3/group (2-3 slices/mice). **p<0.01, ***p<0.001. Statistical significance was determined by ANOVA test with post-hoc Bonferroni. 3V: 3rd ventricle; ARC: arcuate nucleus; PaV: paraventricular nucleus; SHU: SHU9119; VMH: ventromedial nucleus. Scale bar: 250µm.

3 Elucidation of the role of CPT1c in unsaturated LCFAs – induced BAT thermogenesis and neuronal activation

Considering that CPT1c has a role in BAT thermogenesis activation when fed a short-term HFD (Rodríguez-Rodríguez *et al.* 2019), the involvement of CPT1c in the central effects induced by unsaturated FAs was also investigated by using CPT1C-KO mice. Since central saturated FAs did not change the metabolic response of WT mice, the studies with CPT1C-KO mice were only based on the use of the unsaturated oleic and linoleic acid.

3.1 Body weight and food intake in CPT1c-KO mice

Body weight and food intake were monitored after the central administration of oleic acid and linoleic acid using the 48 hours' protocol. In contrast to WT mice, body weight and food intake remained unchanged in CPT1c-KO mice treated with oleic acid **(Fig. 77A-C)**. However, CPT1c-KO mice treated with linoleic acid showed a significant reduction in body weight even though food intake remained unchanged compared to WT mice **(Fig. 77B-D)**. Results suggest that CPT1c may play a key role in the central effect of unsaturated fatty acids in the control of food intake, but only in the monounsaturated FA effects on the control of body weight.

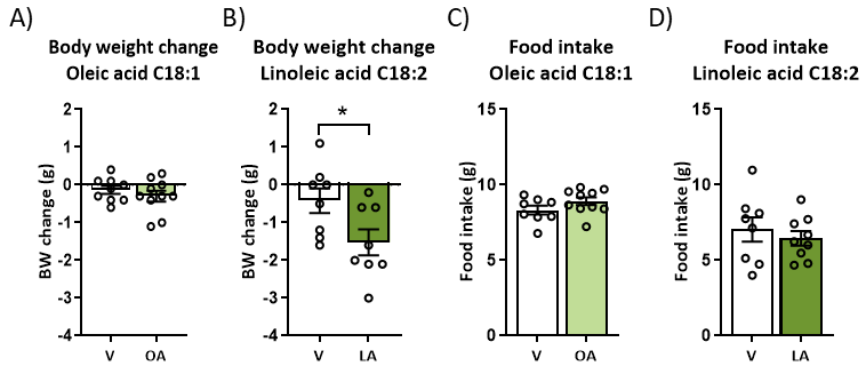

Fig. 77. Effects of unsaturated central fatty acids on body weight and food intake of CPT1C-KO mice. A-B) Body weight change between the initial body weight and the final body weight after the 48h central administration of oleic acid (A) and linoleic acid (B). C-D) Cumulative food intake after the 48h treatment of oleic acid (C) and linoleic acid (D). Data were represented as mean ± SEM, n= 7-9/group. * p<0.05 versus vehicle. Statistical significance was determined by t-student. BW: body weight; OA: Oleic acid. LA: linoleic acid. V: vehicle.

3.2 BAT thermogenic response in CPT1c-KO mice

BAT thermogenesis activity was tested after central icv administration of the unsaturated FAs, using the 48 hours' protocol. In contrast to that observed in WT mice, iBAT temperature was not increase in oleic or linoleic acid-treated CPT1C-KO mice, as the mean difference from initial time and final time was near 0ºC, although vehicles showed a non-significant reduction in both experiments **(Fig. 78A-C)**. In the same line to iBAT temperature results, central administration of oleic acid and linoleic acid to CPT1c-KO mice did not raise the expression of UCP1, PGC1α or PRDM16, so it could be said that CPT1c is necessary for the thermogenesis activity induced by unsaturated FAs **(Fig. 78)**.

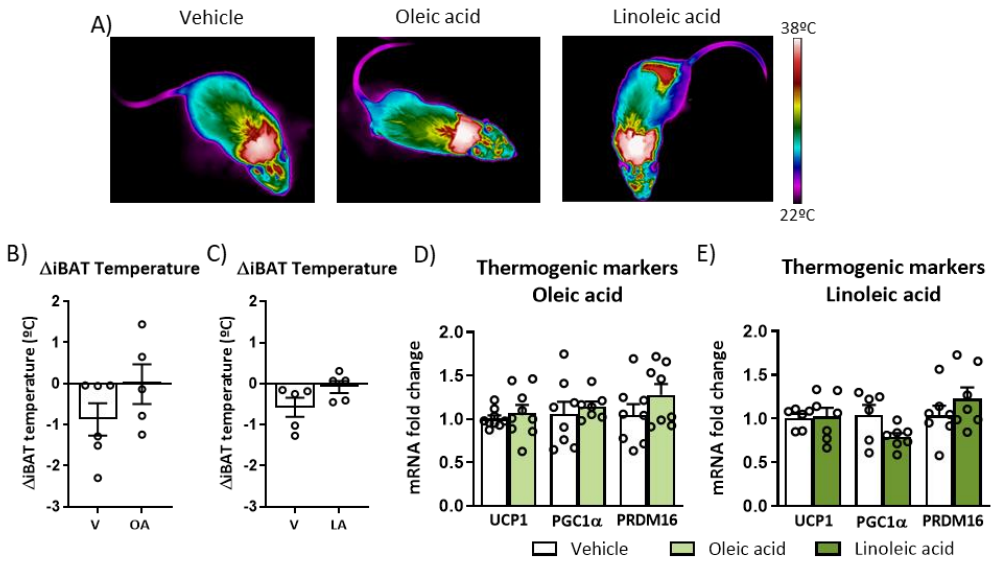

Fig. 78. Effects of unsaturated central fatty acids on BAT thermogenesis in CPT1c-KO mice. A) Representative mice IR pictures used for iBAT temperature measurement at the end of each treatment. B-C) Mice interscapular temperature changes after administration of oleic acid (B) and linoleic acid (C) D-E) mRNA thermogenic markers UCP1, PGC1α and PRDM16 from BAT after administration of oleic acid (D) and linoleic acid (D). GAPDH was used as housekeeping gene to normalize mRNA markers. Data are represented as mean ± SEM, male mice, 8-12 weeks of age. For iBAT temperature measurements n= 5/group, for mRNA thermogenic markers n=7-9/group. Statistical significance was determined by t-student. LA: Linoleic acid; OA: Oleic acid; V: vehicle.

3.3 Hypothalamic AMPK – ACC pathway and FAS expression in CPT1c-KO mice

As demonstrated before, the hypothalamic AMPK – ACC pathway could have a role in the central sensing of LCFAs. Then, we analysed this pathway in CPT1C-KO mice in response

to unsaturated LCFA using the 48 hours' protocol. Oleic acid in CPT1C-KO mice was not able to significantly downregulate pAMPK and pAMPK/AMPK, in contrast to that previously observed in WT mice, whereas this ratio was significantly increased by linoleic acid **(Fig. 79)**.

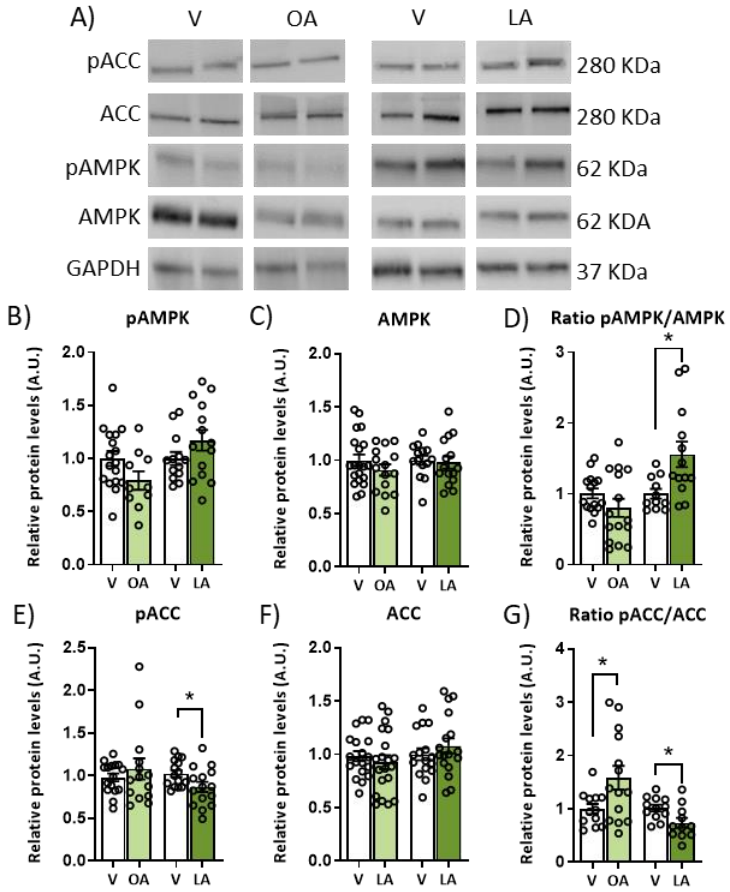

Fig. 79. Effects of central unsaturated fatty acids on the hypothalamic expression of AMPK and ACC in CPT1c-KO mice. A) Immunoblotting of pACC, ACC, pAMPK, AMPK and GAPDH. B-C) Quantification of pAMPK levels (B) and total AMPK levels (C). D) Ratio of pAMPK/total AMPK levels. E-F) Quantification of pACC levels (E) and total ACC levels (F). G) Ratio of pACC/total ACC levels. GAPDH was used as housekeeping protein to protein levels. Data are represented as mean ± SEM, n= 8/group. *p<0.05 versus vehicle. Statistical significance was determined by t-student. A.U.: arbitrary units; LA: linoleic acids; OA: oleic acid.

Regarding ACC expression in the hypothalamus, central oleic acid led to a higher ratio pACC/ACC, while linoleic reduced it **(Fig. 79G)**. Both results are in line with the

observations found in WT mice. Changes in the axis AMPK-ACC after linoleic acid treatment in the null mice are also in agreement with those changes observed in WT mice.

Analysis of FAS expression, in contrast to WT results, showed significantly higher levels after unsaturated FAs administration to CPT1c-KO mice **(Fig. 80)**. It is important to note that the results of FAS expression after oleic and linoleic acid treatment in CPT1c null mice show the same tendency as that reported by saturated FAs in WT mice.

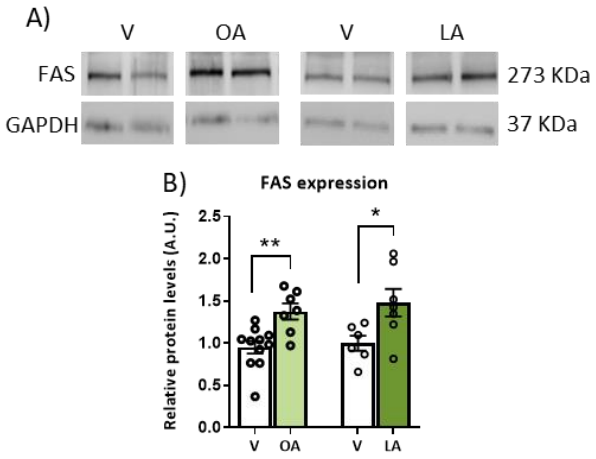

Fig. 80. Effects of central unsaturated fatty acids on hypothalamic FAS expression in CPT1c-KO mice. A) Immunoblotting of FAS and GAPDH. B) Immunoblot quantification of FAS levels. GAPDH was used as housekeeping protein to protein levels. Data are represented as mean ± SEM, n= 6-8/group. Significance: *p<0.05, **p<0.01 versus vehicle. Statistical significance was determined by t-student. A.U.: arbitrary units; LA: linoleic acid; OA: oleic acid.

The fact that the AMPK-ACC axis in CPT1C-KO mice is similar to WT animals, is consistent with the idea that CPT1c would be downstream of AMPK in the signalling pathway to activate BAT thermogenesis through the hypothalamus (Rodríguez-Rodríguez *et al.* 2019). However, we did observe differences in FAS expression, which led us to think that CPT1c could have an impact on its expression, at least during the hypothalamic sensing of unsaturated FAs.

3.4 Hypothalamic c-Fos expression in CPT1c- KO mice

c-Fos immunohistochemistry was performed in brain slices from CPT1c-KO mice perfused two hours after oleic acid treatment. As illustrated on **figure 81**, oleic acid was unable to increase c-Fos expression in hypothalamic nuclei of CPT1c-KO mice in contrast to that

observed in WT mice. Particularly, in mice lacking CPT1C, the hypothalamic nuclei PaV, VMH and ARC were not activated but even were inhibited by the central administration of oleic acid **(Fig. 81A-B)**.

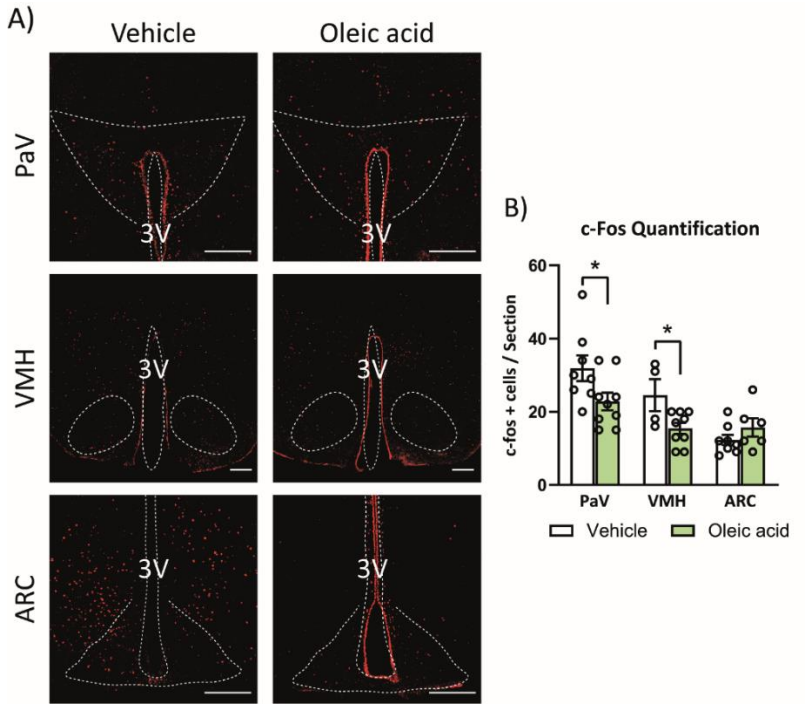

Fig. 81. Effects of oleic acid on neuronal activation assessed by c-Fos expression in the PaV, VMH and ARC in CPT1c-KO mice. A) Immunohistochemistry of c-Fos expression after oleic acid administration. B) Quantification of c-Fos positive cells per section of each nucleus. Data were represented as mean ± SEM, male mice, 8-12 weeks of age, n= 3/group (2-3 slices/mice). * $p<0.05$ versus vehicle. Statistical significance was determined by t-student. 3V: 3rd ventricle; ARC: arcuate nucleus; PaV: paraventricular nucleus; VMH: ventromedial nucleus. Scale bar: 250µm.

Taking into account that VMH is involved in the central response to oleic acid in WT **(Fig. 73)** and this response is lost in mice deficient for CPT1c **(Fig. 81)**, we decided to repeat the experiment presented above using SF1-*CPT1c*-KO mice. In this model, central oleic acid was unable to increase or reduce the number of c-Fos positive cells in the VMH, PaV and ARC **(Fig. 82)**. However, ARC presented a tendency to be activated, which would be in line with the idea of VMH being downstream of that nucleus in the central lipid sensing circuitry **(Fig. 82)**.

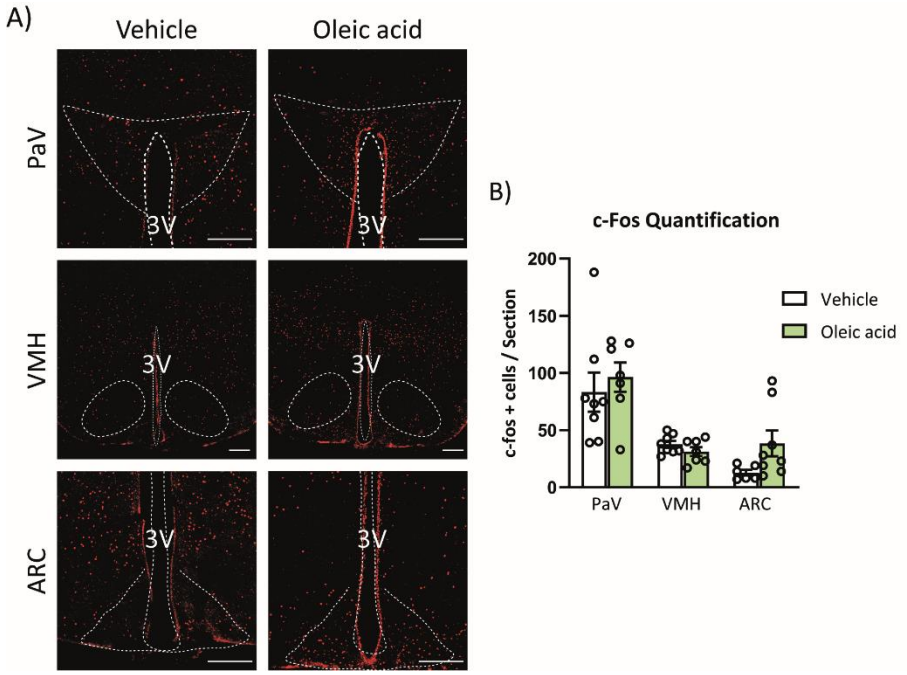

Fig. 82. Effects of oleic acid on neuronal activation assessed by c-Fos expression in the PaV, VMH and ARC in SF1-*CPT1c*-KO mice. A) Immunohistochemistry of c-Fos expression after oleic acid administration. B) Quantification of c-Fos positive cells per section of each nucleus. Data are represented as mean ± SEM, male mice, 8-12 weeks of age, n= 3/group (2-3 slices/mice). Statistical significance was determined by t-student. 3V: 3rd ventricle; ARC: arcuate nucleus; PaV: paraventricular nucleus; VMH: ventromedial nucleus. Scale bar: 250µm.

All these results obtained from experiments using global CPT1c-KO and SF1-CPT1c-KO mice led us to think that CPT1c could be involved in the central response of unsaturated FAs to regulate body weight, food intake and BAT thermogenesis.

4 Results summary of Chapter II

All these findings have been summarized in **Table 12** (diet results), **Table 13** (icv approach results) and **figure 83**.

In this chapter of results, we have elucidated the differential central effect that LCFAs have on body weight, food intake and BAT thermogenesis depending on the level of saturation. The first differences were observed using the diet-based approach: mice treated with a MUFA diet presented higher BAT thermogenesis activity compared to the other experimental diets.

The results obtained after icv administration of the different LCFAs in WT mice revealed that unsaturated FAs had a positive impact in body weight attenuation through a reduction of food intake and an increase in energy expenditure, in particular by increasing BAT thermogenesis activity. In contrast, saturated FA did not change body weight or food intake and did not activate BAT thermogenesis. Exploration of the hypothalamic AMPK-ACC and FAS signalling indicated a potential role of this pathway in the different response induced by central LCFAs depending on the level of saturation in feeding, body weight and thermogenesis. In addition, CPT1c protein was identified as a player in this molecular axis, as CPT1C deficiency resulted in lack of central unsaturated FAs treatment effects in the metabolic parameters analysed.

Regarding the investigation of the hypothalamic nuclei important for the response to LCFA, we found that the ARC, PaV and VMH are important in this process. In the case of the PaV, MC4R expressing neurons seemed to be involved and to signal to VMH. The ARC could be responsible for the activation of this type of neurons by releasing POMC neuropeptide, which is cleavage to α-MSH, a major ligand of MC4R in PaV, and the VMH seems to be downstream of this interaction.

Table 12. Summarized results of the diet-based approach. Symbols are indicating the result of special diet compared to SD.

WT MICE		MUFA DIET	SFA DIET
Body weight		=	↑
Calorie intake		↑	=/↑
BAT Thermogenesis		↑	↑
C-Fos expression	**PaV**	↑	=
	VMH	=	=
	DMH	=	=

= : no changes; ↑: higher; ARC: arcuate nucleus; MUFA: monounsaturated fatty acid; PaV: paraventricular nucleus; SFA: saturated fatty acid; VMH: ventromedial nucleus.

Table 13. Summarized results of the icv-based approach. Symbols are indicating the result of LCFA administration compared to vehicle.

WT MICE		OA	LA	PA	SA
Body weight		↓	↓	=	=
Food intake		↓	↓	=	=
BAT Thermogenesis		↑	↑	=	=
pAMPK/AMPK ratio		↓	=	=	=
pACC/ACC ratio		↑	=	=	=
FAS expression		↓	↓	↑	↑
C-Fos expression	**PaV**	↑	-	=	-
	VMH	↑	-	=	-
	ARC	↑	-	=	-

CPT1C-KO MICE		OA	LA
Body weight		=	↓
Food intake		=	=
BAT Thermogenesis		=	=
pAMPK/AMPK ratio		=	↑
pACC/ACC ratio		↑	↓
FAS expression		↑	↑
C-Fos expression	**PaV**	↓	-
	VMH	↓	-
	DMH	=	-

-: not studied; =: no changes; ↑: higher; ↓: lower; ARC: arcuate nucleus; LA: linoleic acid; OA: oleic acid; Pa: palmitic acid; PaV: paraventricular nucleus; SA: stearic acid; VMH: ventromedial nucleus.

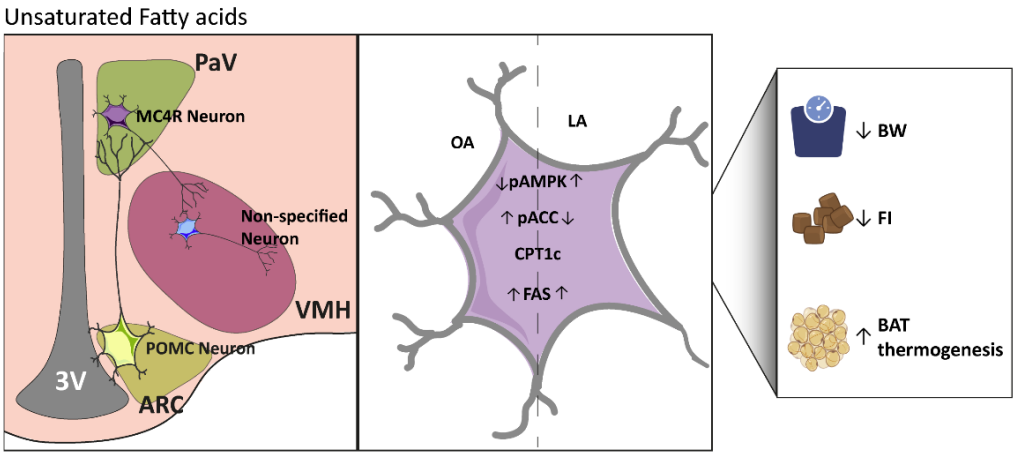

Fig. 83. Graphical Abstract of Chapter II. Main results of the proposed circuit, molecular mechanisms and peripheral effect in response to hypothalamic sensing of unsaturated FA. ARC: arcuate nucleus; BAT: brown adipose tissue; BW: body weight; FI: food intake; OA: oleic acid; PaV: paraventricular nucleus; LA: linoleic acid; VMH: ventromedial nucleus.

DISCUSSION

In the last fifty years, obesity has spread over the world with pandemic proportions. On the one hand, western societies and increasingly non-western societies present easier accessibility to high-caloric food, which at the same time is more palatable and it results in a high increase in energy intake. On the other hand, lifestyle is more sedentary than years ago, contributing to a reduced energy expenditure. Genetic and environmental factors have also to be taken into account. Collectively, it is difficult to maintain a proper energy homeostasis leading to obesity and its comorbidities. It is curious and alarming at the same time that there is still no effective treatment despite all the efforts of the scientific community. Thereby, understanding all the physiological processes involved in the central control of feeding and energy expenditure is an urgent need in order to overcome the limitations of current therapies and also for the prevention of obesity and its complications.

In this thesis, we have studied some of the hypothalamic molecular mechanisms underlying obesity. For the first time, it has been developed a specific KO mouse model of the brain-specific protein CPT1c, which is the most enigmatic isoform of the CPT family. The role of CPT1c in the regulation of energy homeostasis within the VMH-specific neurons has been investigated. We have found that this protein in SF1 neurons is crucial for the metabolic switch needed for the metabolic adaptation to a short-term HFD exposure, in order to delay the onset of obesity and also for the control of adiposity once obesity is stablished. Previous studies reported that CPT1c-KO mice had an obesogenic phenotype (Dai *et al.* 2007; Wolfgang *et al.* 2008) and now we demonstrate that CPT1c in SF1 neurons is, in part, responsible for this phenotype. CPT1c was also described to be important for central leptin response, specifically in the VMH (Rodríguez-Rodríguez *et al.* 2019). Thus, we tested the leptin-induced BAT thermogenic activity in the specific KO mouse model, being this response blunted compared to control mice. We also have identified that CPT1c in the VMH is necessary for the metabolic switch needed under a cold exposure, never explored until now.

SF1 neurons are also important players in the regulation of glucose metabolism, modulating insulin response and CRR (Meek *et al.* 2016; Coutinho *et al.* 2017). In this thesis, we have described that CPT1c in this neuronal population has an impact in the activation of the CRR. Some differences have been shown in the insulin response between male and female mice, indicating the sex-dependent activity of these neurons. These

findings consolidate the idea of hypothalamic CPT1c as a key piece of the puzzle that controls energy homeostasis.

Finally, we found a link between CPT1c and hypothalamic FA sensing. Although FA sensing has been previously studied, it is not known how LCFA of the same length but different level of saturation influence on the regulation of energy balance throughout hypothalamic sensing. Moreover, the relation between LCFA and BAT thermogenesis has not been widely studied: the molecular mechanism and neuronal circuits involved has not been identified. For this reason, we have addressed these issues in WT mice but also in CPT1c-KO mice to describe the role of CPT1c in this nutrient sensing process.

Regarding the hypothesis of this thesis of CPT1c as a sensor of different types of FA and hormone signals within the hypothalamus, especially in the VMH, for the appropriate adaptation to metabolic challenges, we could conclude that it has been proved but with some nuances, as commented below. The discussion is divided in two parts, following the same structure as results section, and a final section containing the main conclusions.

1 CPT1c in SF1 neurons is involved in the metabolic switch to adapt to specific metabolic challenges

CPT1c, through its binding to malonyl-CoA, is a sensor of the nutritional status of the organism and plays a critical role in energy homeostasis. It is also important for metabolic flexibility under challenges such as HFD or fasting (Pozo *et al.* 2017; Rodríguez-Rodríguez *et al.* 2019; Fadó *et al.* 2021; Miralpeix *et al.* 2021b). In an attempt to clarify the contribution of CPT1c in SF1 neurons, in this thesis we have developed two mouse models: the CPT1c floxed mice and the SF1-*CPT1c*-KO mice. The first one represents a new tool for the study of the CPT1c, being a new strategy for the group to study the role of CPT1c in specific neurons. The second mouse model has been part of the focus of this thesis and it has been a further step to better understand the role of CPT1c in the regulation of energy balance, which up to now was only evaluated in the global CPT1c-KO mice. We focused our efforts on SF1 neurons because our group had defined VMH as a relevant nucleus of the hypothalamus to regulate BAT thermogenesis activity in a CPT1c-dependent manner (Rodríguez-Rodríguez *et al.* 2019). The study of SF1-*CPT1c*-KO

phenotype was analysed in collaboration with Dr Daniela Cota (Neurocentre Magendie, France) in her laboratory for the calorimetric study of mice.

Two limitations on the study of SF1-*CPT1c*-KO have to be mentioned. First, the high heterogeneity among SF1 neurons as they can be responsive to leptin, insulin, glucose or be non-sensing neurons (Fosch *et al.* 2021), which means that CPT1c deletion in all SF1 neurons can mask the specific effects on each subpopulation. The second limitation is the possibility of a developmental compensatory mechanism that could hide the role of CPT1c in this neuronal population, as it has been described in other SF1 transgenic mice (Yang *et al.* 2016).

The analysis of SF1-*CPT1c*-KO mice phenotype revealed no differences in body weight, food intake or energy expenditure compared to their control littermates when fed a chow diet, which is in concordance with the phenotype of the majority of the SF1-specific transgenic mice, especially those not related to the leptin signalling pathway (Fosch *et al.* 2021) (Table 1, introduction section). Only male SF1-*CPT1c*-KO mice presented a tendency of accumulating more fat under chow diet. In concordance, CPT1c-KO mice did not show body weight differences compared to WT mice in young-adult ages. However, the global KO was defined to accumulate more fat over age with significant differences at 8-month old (Pozo *et al.* 2017). It is likely to postulate that the tendency of higher fat mass observed in SF1-*CPT1c*-KO mice would become significant over time, following the same direction as the global KO. It is important to highlight that the global lack of CPT1c results in a reduced synaptic transmission of glutamatergic neurons due to a decrease of AMPA-type glutamate receptor (AMPAR) in the postsynaptic membrane (Fadó *et al.* 2015). Therefore, since SF1 neurons are mainly glutamatergic (Tong *et al.* 2007; Fagan *et al.* 2020), we suggest that SF1 neurons in the specific KO mice could be less active in response to the glutamatergic inputs coming from other hypothalamic nuclei, such as PaV and ARC. The trend of having higher fat depots in SF1-*CPT1c*-KO mice agrees with the fact that chemogenetically inhibition of SF1 neurons over 3 weeks resulted in 15-20% increase of adiposity that those that received vehicle (Viskaitis *et al.* 2017). The hypothesis that SF1 neurons lacking CPT1c could be less active requires confirmation by electrophysiological studies.

Although energy expenditure analysed by calorimetric chambers did not differ between SF1-*CPT1c*-KO and SF1-*CPT1c*-WT mice, we evaluated BAT thermogenesis activity because: (i) specific KO mice could be burning less fat as they tend to accumulate a higher

amount of it versus floxed mice and (ii) post-natal deletion of SF1 factor or deletion of other targets related to hormone molecular cascades in SF1 neurons resulted in a reduced thermogenesis (Dhillon *et al.* 2006; Xu *et al.* 2010; Kim *et al.* 2011). As expected by the energy expenditure results, BAT thermogenesis between both genotypes was not different when mice were exposed to HFD, although SF1-*CPT1c*-KO mice failed to activate BAT thermogenesis after the central leptin stimulus.

Hypothalamic changes in response to a HFD during the first days of exposition have been previously described, and these changes precede the subsequent alterations in brain systems that control energy homeostasis. Inflammatory signals in the hypothalamus appeared between days 1 and 3 using a DIO model, before the peripheral inflammation and body weight gain was observed (Thaler *et al.* 2012). This acute hypothalamic inflammation is reversed by compensatory neuroprotective mechanisms, although HFD exposition for longer periods of time leads to a steady inflammation at both central and peripheral levels (Thaler *et al.* 2012). Changes in the expression of feeding-related neuropeptides are also initial hypothalamic mechanisms to compensate calorie surplus. In particular, NPY and AgRP expression are decreased between 30 to 50% the first 2 days of HFD feeding even though food consumption is not reduced, likely for the high palatable diet (Ziotopoulou *et al.* 2000). After one week, NPY and AgRP returned to baseline levels of expression (Ziotopoulou *et al.* 2000), which probably indicates the loss of the compensatory mechanism and the initiation of obesity development. The impairment in the compensatory effects during these early stages will determine an earlier obesogenic phenotype.

In the last years, several investigations have focused on the early dysregulation of neuronal function in energy balance during the onset of obesity. So far, there are no studies available about the role of SF1 neurons in these first days in the DIO model. In the present investigation, we observed that during the first days of HFD, significant differences between SF1-*CPT1c*-KO and SF1-*CPT1c*-WT mice were presented. Transgenic mice were gaining more weight and the tendency of having bigger fat depots on SD resulted a significant difference after five days on HFD. All these changes were related to food intake as the SF1-*CPT1c*-KO mice were eating more amount of food than their control littermates and no significant differences were found on total energy expenditure. SF1-*CPT1c*-WT adapted the amount of food to eat the same calories as they were eating before HFD exposure, while SF1-*CPT1c*-KO mice did not adapt food intake as fast as the

control littermates did, which results into more calories ingested. Although the approach of short-term exposure to HFD has not been studied in other SF1 transgenic mice, optogenetic and chemogenetic stimulation of SF1 neurons reduces food intake and its inhibition increases feeding (Coutinho *et al.* 2017; Viskaitis *et al.* 2017). These results are also in concordance with the hypothesis that the deficiency of CPT1c reduces SF1 neuronal activity. Lacking CPT1c in SF1 neurons hampers the metabolic adaptation of mice to a HFD feeding, which is in line with the described obesogenic phenotype of global CPT1c-KO mice in response to a HFD (Wolfgang *et al.* 2006; Rodríguez-Rodríguez *et al.* 2019). These differences in feeding, body weight and adiposity appeared just at the moment of switching from SD to HFD and were maintained at least for the first five days of the higher caloric diet administration, while in other SF1 transgenic male mice, BW differences appeared later, at least after 3 weeks of HFD feeding (Gonçalves *et al.* 2014), and the first days of HFD were not evaluated. It is important to consider that, since the VMH is a satiety nucleus (Fosch *et al.* 2021), we cannot discard that the fact that SF1-*CPT1c*-KO mice are eating more food may be also related to a disruption in the satiety circuits in which SF1 neurons are involved.

All the changes in food intake were mainly observed during the dark phase, which could be an indication of CPT1c having a circadian activity pattern. It is known that SF1 neurons participate in the control of circadian rhythms by nutritional inputs in a SIRT1-dependent manner (Orozco-Solis *et al.* 2015). Moreover, previous studies have defined that CPT1c regulates SIRT1 expression under the metabolic challenge of fasting (Pozo *et al.* 2017). This link between CPT1c and SIRT1 or other circadian clock regulators remains to be studied.

Another significant finding of this study were the RER analysis during the first 5 days of HFD exposure. At this early stage, both genotypes showed a decrease in RER although the specific KO mice presented higher values of this ratio, indicating that they were using more carbohydrates compared to the WT mice, despite the higher availability of fat. We can assume that if null mice are not selecting the adequate fuel substrates for energy production and they continue using carbohydrates, the storage of ingested fats is promoted. In agreement with this, CPT1c has been previously defined to be necessary in the PaV of hypothalamus for the appropriate dietary selection (Okamoto *et al.* 2018) and for the fuel substrate selection in the MBH (Pozo *et al.* 2017) upon fasting. In this thesis

we have shown that CPT1c in SF1 neurons within the VMH is involved in fuel substrate selection upon HFD feeding.

Neither BAT thermogenesis, basal locomotor activity nor total energy expenditure were differently altered in the specific KO compared to the WT mice in response to short-term HFD. These BAT thermogenesis findings disagree with our previous studies in the global CPT1c-KO, whose activation of BAT thermogenesis activity at 7 days of HFD was lower compared to WT and the re-expression of CPT1c only in the VMH reversed this impairment (Rodríguez-Rodríguez *et al.* 2019). After the results exposed in this thesis, we could assume that CPT1c in SF1 neurons are not responsible for activating thermogenesis in a diet-dependent manner. Other neurons of the VMH or other nuclei interconnected to the VMH could be responsible for it. SF1 neurons are working in conjunction with other type of neurons and it is likely that other redundant neuronal circuits could also be regulating BAT thermogenesis in response to HFD in SF1-*CPT1c*-KO mice. Although diet-induced thermogenesis seems not to be regulated by CPT1c in SF1 neurons, central acute leptin-induced thermogenesis was abolished when CPT1c is missing in this neuronal population, being these results in agreement to those obtained with the global CPT1c-KO mice (Rodríguez-Rodríguez *et al.* 2019).

CPT1c has been defined to be downstream of AMPK in the regulation of BAT thermogenesis within the VMH (Rodríguez-Rodríguez *et al.* 2019). The current hypothesis was that inhibition of AMPK in SF1 neurons would increase malonyl-CoA levels, which will bind to CPT1c to trigger BAT thermogenesis. Accordingly to this, the specific KO mice of $AMPK_{\alpha1}$ in SF1 neurons presented protection to obesity when exposed to long-term HFD (Seoane-Collazo *et al.* 2018) by increasing BAT thermogenesis in in a feeding-independent manner. By contrast, even though SF1-*CPT1c*-KO mice showed an obesogenic phenotype upon HFD (as expected), we did not find alterations in BAT thermogenesis but changes in food intake and RER. This could be explained by the following reasons: it would be possible that the axis AMPK-CPT1c in SF1 neurons is not relevant for RER, food intake or energy expenditure and another possibility would be that AMPK has other effectors whose different activities could be masking CPT1c effects.

Focusing on the studies performed after a long-term exposure to HFD (6-8 weeks), once obesity is stablished, body weight and adiposity differences observed in the first five days of HFD exposure in male mice were increased over time, but the food intake differences were not sustained after 6 weeks of HFD feeding. This obesity-prone phenotype is also

observed in those transgenic male mice in which leptin signalling is inhibited (Dhillon *et al.* 2006; Xu *et al.* 2010; Fujikawa *et al.* 2019), in accordance to the leptin-protective role to DIO. Female mice lacking CPT1c in SF1 neurons also presented an obesogenic phenotype compared to their control littermates, although body weight differences did not appear until week 6 of HFD, and body weight gain was slower than male mice. This different behaviour between male and female mice could be due to the female delayed body weight gain described in WT mice (Miralpeix *et al.* 2019) or to the sex-effect of SF1 neurons observed by different authors (Xu *et al.* 2011; Chiappini *et al.* 2014; Felsted *et al.* 2020).

The impairment in the metabolic switch reported in SF1-*CPT1c*-KO mice to adapt to the new diet is not maintained over time as food intake and RER differences between genotypes disappeared after 6 weeks of HFD administration. Therefore, WT mice try to "fight" against obesity during the first days but it evolves to obesity when HFD feeding extends in time. SF1-*CPT1c*-KO mice are not able to restrain the onset of obesity as the initial metabolic switch is impaired in these mice. Although food intake and RER differences are not maintained in long-term exposure to HFD, body weight and adiposity remain higher than control littermates and it could be due to the impaired onset of obesity.

We have also studied glucose metabolism of SF1-*CPT1c*-KO mice. Male mice showed a higher $K_{ITT,}$ which could mean higher glucose uptake, in line with some studies of other specific SF1 transgenic mice such as those deleting FOXO1 or IR in these neurons (Kim *et al.* 2012), both factors related to insulin signalling. Regarding glucose metabolism in DIO, male mice lacking CPT1c in SF1 neurons presented an over-activated CRR, which is in contrast to the hypothesis of the hypoactivity of SF1 neurons lacking CPT1c because when SF1 neurons are inhibited by optogenetic approach, the CRR is impaired (Meek *et al.* 2016). One hypothesis could be that CPT1c could be acting as a sensor to promote the inactivation of SF1 neurons firing and then reduce CRR to stop the rise of blood glucose levels, therefore, when CPT1c is missing, CRR would be activated although higher levels of glycaemia are achieved. In addition, activity of GI SF1 neurons is dependent of AMPK (Quenneville *et al.* 2020), thus, it would be interesting to explore the axis AMPK-CPT1c in SF1 neurons to explore if this axis is controlling the CRR. Glucose intolerance was also observed in SF1-CPT1c-KO male and female mice under DIO. However, another possible explanation for the impairment observed in glucose homeostasis is because of the higher

adiposity and the obesogenic phenotype instead of a direct consequence of CPT1C deficiency: since SF1-*CPT1c*-KO mice become obese faster, the comorbidities linked to this disease could also appear before. Further studies in hypothalamus, muscle and liver must be carried out to better elucidate the role of CPT1c in SF1 neurons in the central regulation of glucose homeostasis.

Regarding the cold exposure challenge, previous unpublished results of our group using CPT1c-KO mice, suggested that CPT1c could be playing a role in the metabolic adaptation to cold exposure: mice had higher body temperature and higher glycaemia compared to WT during two hours at 4 ºC. In this thesis, the same response has been studied in those mice lacking CPT1c in SF1 neurons. BAT thermogenesis in these mice seemed more activated compared to WT, although differences were not significant, and glycaemia was also increased compared to control mice. Moreover, RER was reduced under cold exposure, reinforcing the idea that more fat is being used as energy substrate. These findings suggest that SF1-*CPT1c*-KO mice are not responding as WT mice to the cold situation because they present higher thermogenesis activity and higher blood glucose levels, they are "wasting" more energy substrate needed for long-term survival in front of this kind of challenge.

CPT1c has also been described to participate in fasting metabolic adaptation. Under a food deprivation, there are higher levels of CPT1c in the mediobasal hypothalamus (Pozo *et al.* 2017). Moreover, global KO of CPT1c mice have been described to present an impaired hepatic and muscle response under fasting conditions compared to WT mice (Pozo *et al.* 2017). In this thesis, we fasted our specific transgenic mice for 24 hours and checked hepatic metabolism. Although SF1-*CPT1c*-KO mice did not present reduced glycogen levels, they had higher levels of glycerol, indicating that these mice were mobilizing fat depots to be used as a substrate but glycerol was not being used for gluconeogenesis. We also induced central fasting trough icv administration of 2-DG to avoid the peripheral signalling. In this case, SF1-*CPT1c*-KO mice presented higher hepatic gluconeogenesis than control animals, in agreement with that observed in fasted CPT1c-KO mice (Pozo *et al.* 2017). These results, together with the fact that blood glucose levels under fasting were the same in both genotypes, suggest that most of the peripheral tissues keep using glucose instead of fatty acids as fuel under fasting conditions, and the liver is increasing the gluconeogenesis rate to supply them, as it happens to the CPT1c-KO mice (Pozo *et al.* 2017). However, we have not observed changes in RER under 24 h of

fasting, therefore, further research is needed to unravel the specific role of CPT1c in SF1 neurons within food deprivation.

In conclusion, the study described in chapter I of results section points that CPT1c in SF1 neurons is involved in the regulation of the metabolic switch needed for adaptation to HFD, fasting and cold exposure. These results also open new questions that need to be addressed, for instance, the temporal evolution from the first days of HFD to the establishment of diet-induced obesity. Unravelling the no-return point during obesity progression, could facilitate the development of new drugs not only to treat but also to prevent obesity.

2 CPT1c plays an important role in lipid sensing within different hypothalamic nuclei

Peripheral metabolism is not only regulated by the direct interaction between tissues and nutrients, but also by the nutrient sensing in the hypothalamus. In this thesis we have shown how central administration of unsaturated fatty acid resulted in a reduction of body weight and food intake and in an enhanced BAT thermogenesis activity. We have studied the route of AMPK-ACC and FAS signalling, observing a different pattern of protein expression depending on the type of LCFA. We have also investigated the role of different hypothalamic nuclei defining that ARC could signal to PaV through the melanocortin system, with the final result of BAT thermogenesis activation in response to central monounsaturared FAs. Finally, we have studied the contribution of CPT1c to all these mentioned processes. CPT1c has been defined to sense malonyl-CoA fluctuations and to participate in complex lipid metabolism such as ceramides and endocannabinoids (Gao *et al.* 2011; Ramírez *et al.* 2013; Miralpeix *et al.* 2021a, b). In this thesis, we demonstrate that CPT1c also plays a role in hypothalamic LCFA sensing and in the mechanisms involved in central FA-induced BAT thermogenesis.

Oleic acid has been widely described to reduce food intake. Obici and colleagues described that only one high dose (30 nmols) of oleic acid was enough to reduce food intake to 50% - 60% of baseline for 48 hours (Obici *et al.* 2002). Another study not only described oleic acid effect but also tested palmitic acid and the polyunsaturated DHA (Schwinkendorf *et al.* 2011). In particular, the unsaturated fatty acids reduced food intake

for 48 hours using the same dosage as Obici and colleagues, whereas palmitic acid did not change feeding (Schwinkendorf *et al.* 2011). In that study, body weight was also reduced in response to unsaturated FAs, in agreement with the food intake result. In the present investigation, using the diet-based approach and the central administration of different type of LCFAs, the findings were in line with the outcomes of unsaturated FAs showing a protective role in front of obesity (reducing body weight and food intake) and saturated FAs inducing the opposite effects in WT mice. The difference between the two previous publications (Obici *et al.* 2002; Schwinkendorf *et al.* 2011) and our study relies at the dosage used, since we have demonstrated that food intake is also reduced with a lower dose of unsaturated FAs maintained over time. However, the administration of this type of FAs through the diet resulted in higher calorie intake compared to the SD group, which we assume is related to a higher palatability of the diet. High levels of unsaturated LCFAs in the hypothalamus have been defined as a satiety signal that reduces the release of orexigenic neuropeptides NPY and AgRP and increases the release of the anorexigenic neuropeptide POMC (Obici *et al.* 2003; Cintra *et al.* 2012). We have observed that central administration of oleic acid resulted into higher hypothalamic expression of POMC, with no differences in NPY and AgRP compared to the vehicle, in agreement with the satiety signal previously described.

Regarding BAT thermogenesis, very few studies have been carried out to compare the role of 18-carbon fatty acids, abundant in dietary nutrients, on the regulation of thermogenic activity. BAT and WAT thermogenesis have been defined to be altered depending on the fat composition of diets. In fact, 12-weeks feeding diets enriched with unsaturated fatty acids, but not diets enriched with stearic acid, activate BAT thermogenesis in mice trough the SNS (Shin & Ajuwon 2018). In line with these outcomes, we have observed that thermogenesis is highly activated after seven days of MUFA diet administration. Using the SFA diet, we also observed a higher BAT thermogenic activity in comparison to the SD fed group, although this response was not as much intense as the one observed with MUFA diet. The SFA-induced thermogenic response could indicate a compensatory mechanism for delaying the onset of obesity when fed a more caloric diet (Miralpeix *et al.* 2019). However, when we centrally administered LCFAs, saturated FAs did not activate thermogenesis or even they seemed to reduce it, while unsaturated FAs induced a substantial activation of BAT thermogenesis. In the same direction, Cintra and colleagues defined that central administration of oleic and linoleic acids have a pro-thermogenic effect increasing UCP1 expression in BAT. They linked this effect to the

improved leptin signalling observed after treatment with these FAs (Cintra *et al.* 2012). Our results in BAT thermogenesis would be also in concordance with the beneficial effects of the Mediterranean diet for combating obesity. The high content of MUFA of this diet has been shown to activate diet-induced thermogenesis in obese patients (Bergouignan *et al.* 2009). Altogether, these findings reinforce the protective role of unsaturated FAs against obesity.

To unravel the role of CPT1c in LCFA sensing, we performed the same studies in mice deficient for this protein (CPT1c-KO). The effects of icv administration of oleic acid on body weight, food intake and BAT thermogenesis were totally blunted in CPT1c-KO mice. Unexpectedly, central linoleic acid administration resulted in a reduction in body weight, although food intake and BAT thermogenesis did not change. These results indicate that CPT1c is participating in the lipid sensing response to regulate energy metabolism, particularly in response to oleic acid.

BAT thermogenesis regulation has been widely linked to hypothalamic AMPK activity (López *et al.* 2016). Lacking $AMPK_{\alpha1}$ or reducing the activity of this protein using a plasmid encoding for a dominant negative mutant in SF1 neurons resulted in a substantial increase of BAT thermogenesis through the overactivity of the SNS and in a feeding-independent manner (Seoane-Collazo *et al.* 2018; Milbank *et al.* 2021). AMPK in the hypothalamus is also crucial to mediate the central action of specific hormones, such as estradiol, thyroid hormones, glucagon or leptin on BAT thermogensis via SNS (Tanida *et al.* 2013; Beiroa *et al.* 2014; Martínez De Morentin *et al.* 2014; Martínez-Sánchez *et al.* 2017). Focusing on the core of this thesis, CPT1c has been reported to participate in the axis AMPK(VMH)-SNS-BAT thermogenesis. Our group has described that CPT1c is downstream of AMPK, since genetic inhibition of $AMPK_{\alpha1}$ in the VMH of the CPT1c-KO mice resulted in the lack of activation of BAT thermogenesis (Rodríguez-Rodríguez *et al.* 2019). Moreover, AMPK regulates ACC activity, which is responsible of the malonyl-CoA levels in conjunction with the enzyme FAS, being CPT1c function dependent on malonyl-CoA (Casals *et al.* 2016).

For these reasons, we studied the hypothalamic AMPK-ACC pathway after central administration of the different types of LCFAs in WT and in CPT1c-KO mice. Taking into account that phosphorylation of AMPK leads to ACC phosphorylation, our results showed some contradictions as oleic acid-treated mice had lower levels of pAMPK but higher levels of pACC, and linoleic acid treatment showed the opposite results. The fact that oleic acid reduces pAMPK expression within the hypothalamus and, therefore, activates BAT

thermogenesis has not been described before, and it remains to be tested if this thermogenic regulation is mediated by the SNS. The polyunsaturated DHA has been described to reduce hypothalamic pAMPK (Gomez-Pinilla & Ying 2010) and its central administration has the same effects in food intake and body weight as oleic acid administration (Schwinkendorf *et al.* 2011). The fact that DHA and linoleic acid show opposite results in AMPK phosphorylation can be due to the position of the double bond, as DHA is an ω3 and linoleic acid is an ω6 FA, and both type of FAs have demonstrated different metabolic effects (Saini & Keum 2018). The different impact of oleic and linoleic acid in the hypothalamic AMPK-ACC axis could be linked to the fact that linoleic acid, but not oleic acid, also reduced body weight in mice deficient of CPT1c. Linoleic acid could be also activating an alternative CPT1c-independent route to regulate body weight.

Concerning ACC expression, it has been published that icv administration of oleic or linoleic acid increases its phosphorylated levels (Cintra *et al.* 2012), which would be in line with our observation with central oleic acid treatment. In that study, hypothalamic FAS expression was reduced after the unsaturated fatty acid administration. In accordance, we have observed that unsaturated fatty acids reduce FAS hypothalamic expression while saturated fatty acids increase it. These results are also in line with the inhibition of FAS resulting into food intake and body weight reduction (Loftus *et al.* 2000), the same metabolic effects that we have found. Obici and colleagues described that inhibition of CPT1a, which resulted in higher levels of LCFA-CoA, also had the outcome of food intake reduction (Obici *et al.* 2003), therefore it was proposed that LCFA-CoAs act as signal of energy surfeit (Lam *et al.* 2005a). Levels of malonyl-CoA are also a signal of energy overload in response to central unsaturated LCFAs (Fadó *et al.* 2021). The fact that in WT mice FAS levels are attenuated in response to unsaturated fatty acids and ACC phosphorylation is also reduced after oleic acid treatment indicate that malonyl-CoA levels are higher in those mice, and high levels of malonyl-CoA in the hypothalamus have been defined to activate BAT thermogenesis in a CPT1c-dependent manner (Rodríguez-Rodríguez *et al.* 2019) and to inhibit CPT1a activity, which also would be in concordance with the study of Obici and colleagues (Obici *et al.* 2003). In addition, administration of saturated LCFAs increased FAS expression, which means malonyl-CoA levels are reduced and, therefore, there is no reduction in food intake, as we have observed. We hypothesize that CPT1c is mediating the sensing of LCFAs throughout the regulation of the activity of other proteins likely in a malonyl-CoA-dependent manner; one possibility, that remains to be tested, is that CPT1c is regulating the trafficking of AMPA receptors (Casas *et al.*

2020) to consequently impact into the excitability of the hypothalamic neurons that sense fatty acids. Another possibility is that CPT1c is also regulating ABHD6 activity, which in turn maintains 2-AG levels and the excitability of the neurons involved (Miralpeix *et al.* 2021a).

We reported that central administration of unsaturated FAs to mice deficient in CPT1c evoked similar results of hypothalamic phosphorylation of AMPK/ACC as shown in WT mice. This agrees with the idea that CPT1c is acting downstream of this axis in the hypothalamus (Okamoto *et al.* 2018; Rodríguez-Rodríguez *et al.* 2019). We also observed that oleic and linoleic acid icv administration resulted into increased FAS expression in CPT1c-KO mice, as it happened with the administration of saturated FAs in WT mice, which would explain the blunted effects that unsaturated FAs have on energy metabolism in CPT1c-KO mice. Altogether, the axis of AMPK – ACC – malonyl-CoA – CPT1c is important for sensing LCFAs within the hypothalamus and for regulating the food intake and BAT thermogenesis response.

In this thesis, we not only investigated the possible molecular mechanisms of the LCFA hypothalamic response but also the hypothalamic nuclei implicated. Published studies had defined that intracarotid lipid infusion increases c-Fos positive cells in ARC, PaV and VMH, but this intralipid infusion was mainly composed of polyunsaturated FAs and it had low doses of monounsaturated and saturated fatty acids (Moullé *et al.* 2013). We have also demonstrated the involvement of ARC, PaV and VMH in this response. We have showed for the first time that the three nuclei presented higher number of c-Fos positive cells after central administration of oleic acid, but not after the central administration of palmitic acid, and the same output was observed only in the PaV in response to MUFA or SFA diets. In agreement with our observations, the PaV has been described to be the responsible for oleic acid effects on food intake through the POMC/MC4R signalling (Schwinkendorf *et al.* 2011). A more recent study reported that trioctanoic acid (triglyceride with three molecules of octanoic acid, a MCFA) reduced food intake because of the enhancement of α-MSH signalling and neuronal activity in the PaV (Haynes *et al.* 2020). They defined this higher activity as a result of the activation of POMC neurons by the octanoic acid, however, in the same study they also tested trioleic acid (triglyceride with three molecules of oleic acid) with the outcome of not having any of the effects described (Haynes *et al.* 2020). Considering our results of PaV, the nucleus that showed the highest number of c-Fos positive cells in response to unsaturated FA, and also the fact

that hypothalamic POMC expression increases after central oleic acid treatment, we assumed that central oleic acid is increasing POMC neurons activity and this leads into α-MSH release in the PaV. We used an antagonist of the melanocortin receptors MC4R/MC3R, SHU9119, for testing this hypothesis. Administrating oleic acid together with SHU9119 resulted in the loss of neuronal activation in PaV and VMH but not in the ARC, which would be in line with our hypothesis. It has to be mentioned that MC3R, also inhibited by SHU9119, are expressed in VMH neurons and they have been linked to BAT thermogenesis activation (Gavini *et al.* 2016), however no investigations have been performed to study the role of icv LCFAs administration in this receptor. The antagonist SHU9119 has only been tested in neuronal activation, but it would be necessary to demonstrate that the effects of central oleic acid on BAT thermogenesis are also blunted after the antagonism of the melanocortin receptor. This particular study has not been presented in this thesis for several reasons: (i) we were unable to reproduce the 24h- and 48h-food intake results after SHU9119 administration previously published (Schwinkendorf *et al.* 2011), (ii) SHU9119 have been described to stimulate ARC nucleus by itself (Li *et al.* 2019), (iii) SHU9119 is the antagonist of MC3R and MC4R receptors which are not exclusively expressed in the PaV and (iv) SHU9119 has been characterized to highly stimulate food intake over 48 h (Schwinkendorf *et al.* 2011), therefore it impacts directly to peripheral metabolism being difficult to know if BAT thermogenesis regulation is affected because of oleic acid effects or because of higher food intake. Therefore, it would be interesting to use alternative approaches to investigate the role of MC4R neurons of the PaV in the BAT thermogenesis response after central oleic acid administration. Pharmacological approaches using specific agonists for each type of MCR receptor or genetic approaches using siRNA or shRNA to inhibit MC4R in PaV would be feasible options. It would be also necessary to pair-fed all groups of the experiment.

We also studied the role of CPT1c in the neuronal activation of these three nuclei by oleic acid. CPT1c-KO mice did not show neuronal activation after oleic acid administration, which would be in line with the blunted responses in food intake and BAT thermogenesis observed in this mouse model. To also test the role of VMH in LCFA sensing, in a CPT1c-dependent manner, we used the SF1-*CPT1c*-KO mice developed for this thesis to test oleic acids effects on neuronal activaty as CPT1c has been defined as a key player in the regulation of BAT thermogenesis in this nucleus (Rodríguez-Rodríguez *et al.* 2019). We found no differences between SF1-*CPT1c*-KO mice treated with the oleic acid or the vehicle, although we observed a trend of ARC having more c-Fos positive cells after oleic

acid treatment. Taken together, we proposed that icv oleic acid stimulates POMC neurons and they signal to PaV and VMH with the final outcome of increasing BAT thermogenesis in a CPT1c-dependent manner. However, it is also possible that each nucleus directly response to oleic acid.

Hypothalamic inflammation by dietary FA precedes the first signs of obesity (Thaler *et al.* 2012). It has been described that palmitic acid, but not oleic acid, also produces hypothalamic inflammation (Milanski *et al.* 2009; Cintra *et al.* 2012). In our case, we checked hypothalamic inflammation, in terms of microglia activation, just two hours after oleic and palmitic acid administration, and found activated microglia in palmitic acid but not in oleic acid-treated mice, being these data in agreement with the previous studies. Hypothalamic inflammation has been related to a reduction of the thermogenic markers UCP1 and PGCα1 in BAT (Arruda *et al.* 2011b), which would be in concordance with our observation of palmitic acid reducing this activity. Saturated fatty acids also activate ER stress (Milanski *et al.* 2009), and the ER has been defined to be a ‘‘nutrient sensing’’ apparatus, establishing specific functional links with metabolic signalling (Hotamisligil 2010). Hypothalamic ER stress caused by lipotoxicity is associated with a blunted BAT thermogenesis (Contreras *et al.* 2017b). Moreover, CPT1c-KO mice have been defined to present higher ER stress than WT mice under short-term HFD exposure (Rodríguez-Rodríguez *et al.* 2019). Taking into account that palmitic acid did not activate BAT thermogenesis in WT mice as it happens with oleic acid in CPT1c-KO mice, it would be possible that these responses are also related to increased levels of ER stress in the KO model. This assumption needs further experiments to check if ER stress is a determinant factor for the effects of central administration of oleic and palmitic acid in WT and CPT1c-KO mice.

In conclusion, unsaturated fatty acids reduce food intake and stimulate BAT thermogenesis through the hypothalamus with a final result of body weight reduction. Saturated fatty acids do not impact in these metabolic parameters. The molecular mechanisms defined for the unsaturated FA effects relies, at least in part, to AMPK-ACC-CPT1c axis and FAS expression, and we have identified that CPT1c is necessary for LCFA sensing and oleic acid-induced BAT thermogenesis. Regarding the hypothalamic nuclei involved, we propose that POMC neurons from ARC activate MC4R neurons at PaV, which could activate VMH, this nucleus could also be directly activated by ARC. This circuit is needed for the control of food intake and BAT thermogenesis in response to central FAs.

3 Concluding remarks

Overall, this thesis has focused on the role of hypothalamic CPT1c in lipid sensing and in the control of energy and glucose homeostasis under different metabolic challenges **(Fig. 83)**. We have demonstrated that CPT1c in SF1 neurons acts as a sensor of energy status for the regulation of body weight, food intake and adiposity during the first days of HFD feeding. CPT1c in SF1 neurons is also regulating RER under different metabolic challenges such as short-term HFD exposure and cold exposure, which means CPT1c plays a role in the energy substrate selection. In addition, CPT1c in this neuronal population also plays a role in regulating hepatic lipid metabolism under fasting conditions as well as the CRR under a central fasting and DIO (**Fig. 62 and 83)**. On the other hand, CPT1c is involved in hypothalamic lipid sensing not only in SF1 neurons but also in other types of hypothalamic neurons. We have defined that unsaturated LCFAs through the AMPK-ACC axis and FAS expression modify signals of energy surfeit to regulate energy homeostasis and that CPT1c is downstream of the AMPK-ACC axis in the regulation of food intake and BAT thermogenesis in response to central administration of unsaturated LCFAs. ARC, PaV and VMH are stimulated by unsaturated FAs but not by saturated fats (**Fig. 82 and 83)**.

Altogether and, from the health point of view, targeting CPT1c specifically in SF1 neurons may be useful to delay the onset of obesity. Moreover, targeting of this protein in paraventricular and ventromedial nucleus of the hypothalamus in combination of a diet enriched with unsaturated LCFAs may also be a possible treatment for reducing obesity.

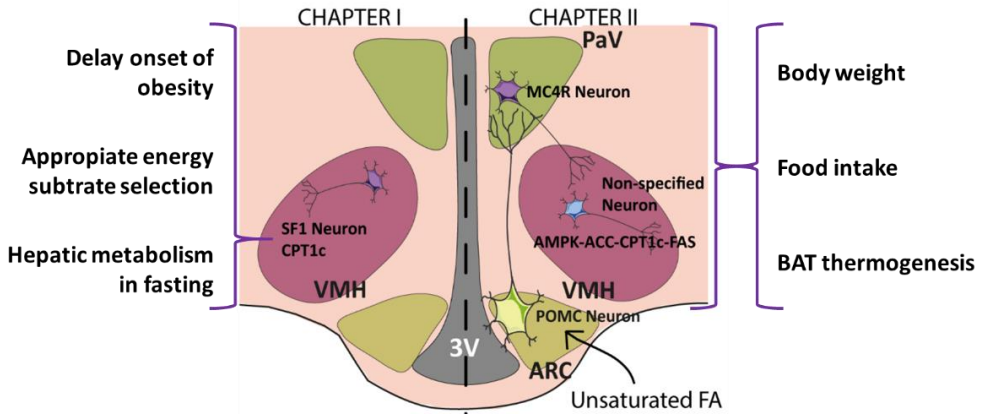

Fig. 83. Graphical abstract of Thesis concluding remarks. Schematic summary of main conclusions of chapter I of Results in on the left of the image and of chapter II of Results in on the right of the image. ARC: arcuate nucleus; BAT: brown adipose tissue; BW: body weight; FA: fatty acid; PaV: paraventricular nucleus; VMH: ventromedial nucleus.

CONCLUSIONS

1. Under short-term HFD exposure, CPT1c deficiency in SF1 neurons leads to an increase in food intake and adiposity, accompanied by an altered selection of energy substrate, as shown by an insufficient decrease of RER in these mice. This indicates that CPT1c in SF1 neurons is important for the metabolic adaptation during the first days of HFD feeding to delay the onset of obesity.

2. Once diet-induced obesity is established, male and female mice lacking CPT1c in SF1 neurons present higher body weight and adiposity and glucose intolerance, although food intake, energy expenditure and respiratory exchange ratio are not altered compared to WT mice.

3. Male mice deficient for CPT1c in SF1 neurons presented an overactivation of CRR under insulin-induced hypoglycaemia in diet-induced obesity.

4. SF1-*CPT1c*-KO mice also presented an impaired metabolic adaptation under fasting conditions observed by higher hepatic levels of glycerol after 24 hours of fasting and increased CRR after 2 hours of central-induced hypoglycaemia.

5. Deficiency of CPT1c in SF1 neurons alters the adaptation to cold exposition, since SF1-*CPT1c*-KO mice show a lower reduction of glycaemia probably due to a decreased use of glucose as fuel substrate, in contrast to that observed in WT mice under this condition.

6. Unsaturated LCFA, but not saturated fatty acids, have a centrally-mediated CPT1c-dependent effect on energy homeostasis reducing food intake and body weight and increasing BAT thermogenesis.

7. Hypothalamic AMPK-ACC axis and FAS expression are differently activated depending on the level of saturation of LCFA, which can be related to the LCFA-hypothalamic signalling.

8. Unsaturated LCFAs, but not the saturated ones, activate neurons on arcuate, paraventricular and ventromedial hypothalamic nuclei and this neuronal activation is blunted when CPT1c is missing.

REFERENCES

Agostoni C & Bruzzese MG 1992 Fatty acids: their biochemical and functional classification. *La Pediatria medica e chirurgica : Medical and surgical pediatrics* **14** 473–479. (doi:PMID:1488301)

Arruda AP, Milanski M & Velloso LA 2011a Hypothalamic inflammation and thermogenesis: The brown adipose tissue connection. *Journal of Bioenergetics and Biomembranes* **43** 53–58. (doi:10.1007/s10863-011-9325-z)

Arruda AP, Milanski M, Coope A, Torsoni AS, Ropelle E, Carvalho DP, Carvalheira JB & Velloso LA 2011b Low-grade hypothalamic inflammation leads to defective thermogenesis, insulin resistance, and impaired insulin secretion. *Endocrinology* **152** 1314–1326. (doi:10.1210/en.2010-0659)

Beiroa D, Imbernon M, Gallego R, Senra A, Herranz D, Villarroya F, Serrano M, Fernø J, Salvador J, Escalada J *et al.* 2014 GLP-1 agonism stimulates brown adipose tissue thermogenesis and browning through hypothalamic AMPK. *Diabetes* **63** 3346–3358. (doi:10.2337/db14-0302)

Bélanger M, Allaman I & Magistretti PJ 2011 Brain energy metabolism: Focus on Astrocyte-neuron metabolic cooperation. *Cell Metabolism* **14** 724–738. (doi:10.1016/j.cmet.2011.08.016)

Bence KK, Delibegovic M, Xue B, Gorgun CZ, Hotamisligil GS, Neel BG & Kahn BB 2006 Neuronal PTP1B regulates body weight, adiposity and leptin action. *Nature Medicine* **12** 917–924. (doi:10.1038/nm1435)

Berger A, Kablan A, Yao C, Ho T, Podyma B, Weinstein LS & Chen M 2016 Gsα deficiency in the ventromedial hypothalamus enhances leptin sensitivity and improves glucose homeostasis in mice on a high-fat diet. *Endocrinology* **157** 600–610. (doi:10.1210/en.2015-1700)

Bergouignan A, Momken I, Schoeller DA, Simon C & Blanc S 2009 Metabolic fate of saturated and monounsaturated dietary fats: The Mediterranean diet revisited from epidemiological evidence to cellular mechanisms. *Progress in Lipid Research* **48** 128–147. (doi:10.1016/j.plipres.2009.02.004)

Bi S, Kim YJ & Zheng F 2012 Dorsomedial hypothalamic NPY and energy balance control. *Neuropeptides* **46** 309–314. (doi:10.1016/j.npep.2012.09.002)

Bingham NC, Verma-Kurvari S, Parada LF & Parker KL 2006 Development of a steroidogenic factor 1/Cre transgenic mouse line. *Genesis* **44** 419–424. (doi:10.1002/dvg.20231)

Blouet C & Schwartz GJ 2010 Hypothalamic nutrient sensing in the control of energy homeostasis. *Behavioural Brain Research* **209** 1–12. (doi:10.1016/j.bbr.2009.12.024)

Borg WP, During MJ, Sherwin RS, Borg MA, Brines ML & Shulman GI 1994 Ventromedial hypothalamic lesions in rats suppress counterregulatory responses to hypoglycemia.

Journal of Clinical Investigation **93** 1677–1682. (doi:10.1172/JCI117150)

Brechet A, Buchert R, Schwenk J, Boudkkazi S, Zolles G, Siquier-Pernet K, Schaber I, Bildl W, Saadi A, Bole-Feysot C *et al.* 2017 AMPA-receptor specific biogenesis complexes control synaptic transmission and intellectual ability. *Nature Communications* **8** 1–14. (doi:10.1038/ncomms15910)

Brewis A, SturtzSreetharan C & Wutich A 2018 Obesity stigma as a globalizing health challenge. *Globalization and Health* **14** 1–6. (doi:10.1186/s12992-018-0337-x)

Bruce KD, Zsombok A & Eckel RH 2017 Lipid processing in the brain: A key regulator of systemic metabolism. *Frontiers in Endocrinology* **8** 1–11. (doi:10.3389/fendo.2017.00060)

Cao J & Patisaul HB 2011 Sexually dimorphic expression of hypothalamic estrogen receptors α and β and Kiss1 in neonatal male and female rats. *Journal of Comparative Neurology* **519** 2954–2977. (doi:10.1002/cne.22648)

Cao JK, Kaplan J & Stella N 2019 ABHD6: Its Place in Endocannabinoid Signaling and Beyond. *Trends in Pharmacological Sciences* **40** 267–277.

Cardinal P, André C, Quarta C, Bellocchio L, Clark S, Elie M, Leste-Lasserre T, Maitre M, Gonzales D, Cannich A *et al.* 2014 CB1 cannabinoid receptor in SF1-expressing neurons of the ventromedial hypothalamus determines metabolic responses to diet and leptin. *Molecular Metabolism* **3** 705–716. (doi:10.1016/j.molmet.2014.07.004)

Carrasco P, Sahún I, McDonald J, Ramírez S, Jacas J, Gratacós E, Sierra AY, Serra D, Herrero L, Acker-Palmer A *et al.* 2012 Ceramide levels regulated by carnitine palmitoyltransferase 1C control dendritic spine maturation and cognition. *Journal of Biological Chemistry* **287** 21224–21232. (doi:10.1074/jbc.M111.337493)

Carrasco P, Jacas J, Sahún I, Muley H, Ramírez S, Puisac B, Mezquita P, Pié J, Dierssen M & Casals N 2013 Carnitine palmitoyltransferase 1C deficiency causes motor impairment and hypoactivity. *Behavioural Brain Research* **256** 291–297. (doi:10.1016/j.bbr.2013.08.004)

Casals N, Zammit V, Herrero L, Fadó R, Rodríguez-Rodríguez R & Serra D 2016 Carnitine palmitoyltransferase 1C: From cognition to cancer. *Progress in Lipid Research* **61** 134–148. (doi:10.1016/j.plipres.2015.11.004)

Casas M, Fadó R, Domínguez JL, Roig A, Kaku M, Chohnan S, Solé M, Unzeta M, Miñano-Molina AJ, Rodríguez-Álvarez J *et al.* 2020 Sensing of nutrients by CPT1C controls SAC1 activity to regulate AMPA receptor trafficking. *Journal of Cell Biology* **219**. (doi:10.1083/JCB.201912045)

Cheung CC, Kurrasch DM, Liang JK & Ingraham HA 2013 Genetic labeling of steroidogenic factor-1 (SF-1) neurons in mice reveals ventromedial nucleus of the hypothalamus (VMH) circuitry beginning at neurogenesis and development of a separate non-SF-1

neuronal cluster in the ventrolateral VMH. *Journal of Comparative Neurology* **521** 1268–1288. (doi:10.1002/CNE.23226)

Chiappini F, Catalano KJ, Lee J, Peroni OD, Lynch J, Dhaneshwar AS, Wellenstein K, Sontheimer A, Neel BG & Kahn BB 2014 Ventromedial hypothalamus-specific Ptpn1 deletion exacerbates diet-induced obesity in female mice. *Journal of Clinical Investigation* **124** 3781–3792. (doi:10.1172/JCI68585)

Cintra DE, Ropelle ER, Moraes JC, Pauli JR, Morari J, de Souza CT, Grimaldi R, Stahl M, Carvalheira JB, Saad MJ *et al.* 2012 Unsaturated fatty acids revert diet-induced hypothalamic inflammation in obesity. *PLoS ONE* **7** e30571. (doi:10.1371/journal.pone.0030571)

Contreras C, González-García I, Martínez-Sánchez N, Seoane-Collazo P, Jacas J, Morgan DA, Serra D, Gallego R, Gonzalez F, Casals N *et al.* 2014 Central ceramide-induced hypothalamic lipotoxicity and ER stress regulate energy balance. *Cell Reports* **9** 366–377. (doi:10.1016/j.celrep.2014.08.057)

Contreras C, Nogueiras R, Diéguez C, Rahmouni K & López M 2017a Traveling from the hypothalamus to the adipose tissue: The thermogenic pathway. *Redox Biology* **12** 854–863. (doi:10.1016/j.redox.2017.04.019)

Contreras C, González-García I, Seoane-Collazo P, Martínez-Sánchez N, Liñares-Pose L, Rial-Pensado E, Fernø J, Tena-Sempere M, Casals N, Diéguez C *et al.* 2017b Reduction of hypothalamic endoplasmic reticulum stress activates browning of white fat and ameliorates obesity. *Diabetes* **66** 87–99. (doi:10.2337/db15-1547)

Correa R V., Domenice S, Bingham NC, Billerbeck AEC, Rainey WE, Parker KL & Mendonca BB 2004 A microdeletion in the ligand binding domain of human steroidogenic factor 1 causes XY sex reversal without adrenal insufficiency. *Journal of Clinical Endocrinology and Metabolism* **89** 1767–1772. (doi:10.1210/jc.2003-031240)

Coutinho EA, Okamoto S, Ishikawa AW, Yokota S, Wada N, Hirabayashi T, Saito K, Sato T, Takagi K, Wang CC *et al.* 2017 Activation of SF1 neurons in the ventromedial hypothalamus by DREADD technology increases insulin sensitivity in peripheral tissues. *Diabetes* **66** 2372–2386. (doi:10.2337/db16-1344)

Cypess AM, Lehman S, Williams G, Tal I, Rodman D, Goldfine AB, Kuo FC, Palmer EL, Tseng YH, Doria A *et al.* 2009 Identification and importance of brown adipose tissue in adult humans. *Obstetrical and Gynecological Survey* **64** 519–520. (doi:10.1097/OGX.0b013e3181ac8aa2)

Dai Y, Wolfgang MJ, Cha SH & Lane MD 2007 Localization and effect of ectopic expression of CPT1c in CNS feeding centers. *Biochemical and Biophysical Research Communications* **359** 469–474. (doi:10.1016/j.bbrc.2007.05.161)

Davis AM, Seney ML, Stallings NR, Zhao L, Parker KL & Tobet SA 2004 Loss of steroidogenic factor 1 alters cellular topography in the mouse ventromedial nucleus of the

hypothalamus. *Journal of Neurobiology* **60** 424–436. (doi:10.1002/neu.20030)

Demaugre F, Bonnefont JP, Cepanec C, Scholte J, Saudubray JM & Leroux JP 1990 Immunoquantitative analysis of human carnitine palmitoyltransferase I and II defects. *Pediatric Research* **27** 497–500. (doi:10.1203/00006450-199005000-00016)

Dhillon H, Zigman JM, Ye C, Lee CE, McGovern RA, Tang V, Kenny CD, Christiansen LM, White RD, Edelstein EA *et al.* 2006 Leptin directly activates SF1 neurons in the VMH, and this action by leptin is required for normal body-weight homeostasis. *Neuron* **49** 191–203. (doi:10.1016/j.neuron.2005.12.021)

Dietrich MO & Horvath TL 2012 Limitations in anti-obesity drug development: The critical role of hunger-promoting neurons. *Nature Reviews Drug Discovery* **11** 675–691. (doi:10.1038/nrd3739)

DiMicco JA & Zaretsky D V. 2007 The dorsomedial hypothalamus: A new player in thermoregulation. *American Journal of Physiology - Regulatory Integrative and Comparative Physiology* **292** R47–R63. (doi:10.1152/ajpregu.00498.2006)

Dragano NRV, Solon C, Ramalho AF, de Moura RF, Razolli DS, Christiansen E, Azevedo C, Ulven T & Velloso LA 2017 Polyunsaturated fatty acid receptors, GPR40 and GPR120, are expressed in the hypothalamus and control energy homeostasis and inflammation. *Journal of Neuroinflammation* **14** 1–16. (doi:10.1186/s12974-017-0869-7)

Dragano NR, Monfort-Pires M & Velloso LA 2020 Mechanisms Mediating the Actions of Fatty Acids in the Hypothalamus. *Neuroscience* **447** 15–27. (doi:10.1016/j.neuroscience.2019.10.012)

Fabbrini E, Sullivan S & Klein S 2010 Obesity and Nonalcoholic Fatty Liver Disease: Biochemical, Metabolic and Clinical Implications. *Hepatology* **51** 679–689. (doi:10.1002/hep.23280)

Fabelo C, Hernandez J, Chang R, Seng S, Alicea N, Tian S, Conde K & Wagner EJ 2018 Endocannabinoid signaling at hypothalamic steroidogenic factor-1/proopiomelanocortin synapses is sex-and diet-sensitive. *Frontiers in Molecular Neuroscience* **11** 1–23. (doi:10.3389/fnmol.2018.00214)

Fadó R, Soto D, Miñano-Molina AJ, Pozo M, Carrasco P, Yefimenko N, Rodríguez-Álvarez J & Casals N 2015 Novel regulation of the synthesis of α-Amino-3-hydroxy-5-methyl-4-isoxazolepropionic Acid (ampa) receptor subunit glua1 by carnitine palmitoyltransferase 1C (CPT1C) in the Hippocampus. *Journal of Biological Chemistry* **290** 25548–25560. (doi:10.1074/jbc.M115.681064)

Fadó R, Rodríguez-Rodríguez R & Casals N 2021 The return of malonyl-CoA to the brain: Cognition and other stories. *Progress in Lipid Research* **81** 101071. (doi:10.1016/j.plipres.2020.101071)

Fagan MP, Ameroso D, Meng A, Rock A, Maguire J & Rios M 2020 Essential and sex-specific effects of mGluR5 in ventromedial hypothalamus regulating estrogen signaling and glucose balance. *Proceedings of the National Academy of Sciences of the United States of America* **117** 19566–19577. (doi:10.1073/pnas.2011228117)

Felsted JA, Chien CH, Wang D, Panessiti M, Ameroso D, Greenberg A, Feng G, Kong D & Rios M 2017 Alpha2delta-1 in SF1+ Neurons of the Ventromedial Hypothalamus Is an Essential Regulator of Glucose and Lipid Homeostasis. *Cell Reports* **21** 2737–2747. (doi:10.1016/j.celrep.2017.11.048)

Felsted JA, Meng A, Ameroso D & Rios M 2020 Sex-specific Effects of a2d-1 in the Ventromedial Hypothalamus of Female Mice Controlling Glucose and Lipid Balance. *Endocrinology (United States)* **161** 1–13. (doi:10.1210/endocr/bqaa068)

Fisette A, Tobin S, Décarie-Spain L, Bouyakdan K, Peyot M-LL, Madiraju SRMM, Prentki M, Fulton S & Alquier T 2016 α/β-Hydrolase Domain 6 in the Ventromedial Hypothalamus Controls Energy Metabolism Flexibility. *Cell Reports* **17** 1217–1226. (doi:10.1016/j.celrep.2016.10.004)

Flak JN, Goforth PB, Dell'Orco J, Sabatini P V., Li C, Bozadjieva N, Sorensen M, Valenta A, Rupp A, Affinati AH *et al.* 2020 Ventromedial hypothalamic nucleus neuronal subset regulates blood glucose independently of insulin. *Journal of Clinical Investigation* **130** 2943–2952. (doi:10.1172/JCI134135)

Le Foll C, Irani BG, Magnan C, Dunn-Meynell AA & Levin BE 2009 Characteristics and mechanisms of hypothalamic neuronal fatty acid sensing. *AJP: Regulatory, Integrative and Comparative Physiology* **297** R655–R664. (doi:10.1152/ajpregu.00223.2009)

Le Foll C, Dunn-Meynell A, Musatov S, Magnan C & Levin BE 2013 FAT/CD36: A major regulator of neuronal fatty acid sensing and energy homeostasis in rats and mice. *Diabetes* **62** 2709–2716. (doi:10.2337/db12-1689)

Fosch A, Zagmutt S, Casals N & Rodríguez-Rodríguez R 2021 New insights of sf1 neurons in hypothalamic regulation of obesity and diabetes. *International Journal of Molecular Sciences* **22** 1–22. (doi:10.3390/ijms22126186)

Fresno M, Alvarez R & Cuesta N 2011 Toll-like receptors, inflammation, metabolism and obesity. *Http://Dx.Doi.Org/10.3109/13813455.2011.562514* **117** 151–164. (doi:10.3109/13813455.2011.562514)

Fujikawa T, Castorena CM, Pearson M, Kusminski CM, Ahmed N, Battiprolu PK, Kim KW, Lee S, Hill JA, Scherer PE *et al.* 2016 SF-1 expression in the hypothalamus is required for beneficial metabolic effects of exercise. *ELife* **5** 1–17. (doi:10.7554/eLife.18206)

Fujikawa T, Choi YH, Yang DJ, Shin DM, Donato J, Kohno D, Lee CE, Elias CF, Lee S & Kim KW 2019 P110β in the ventromedial hypothalamus regulates glucose and energy metabolism. *Experimental and Molecular Medicine* **51** 1–9. (doi:10.1038/s12276-

019-0249-8)

Gao XF, Chen W, Kong XP, Xu AM, Wang ZG, Sweeney G & Wu D 2009 Enhanced susceptibility of Cpt1c knockout mice to glucose intolerance induced by a high-fat diet involves elevated hepatic gluconeogenesis and decreased skeletal muscle glucose uptake. *Diabetologia* **52** 912–920. (doi:10.1007/s00125-009-1284-0)

Gao S, Zhu G, Gao X, Wu D, Carrasco P, Casals N, Hegardt FG, Moran TH & Lopaschuk GD 2011 Important roles of brain-specific carnitine palmitoyltransferase and ceramide metabolism in leptin hypothalamic control of feeding. *Proceedings of the National Academy of Sciences of the United States of America* **108** 9691–9696. (doi:10.1073/pnas.1103267108)

Gavini CK, Jones WC & Novak CM 2016 Ventromedial hypothalamic melanocortin receptor activation: regulation of activity energy expenditure and skeletal muscle thermogenesis. *Journal of Physiology* **594** 5285–5301. (doi:10.1113/JP272352)

de Git KCG & Adan RAH 2015 Leptin resistance in diet-induced obesity: The role of hypothalamic inflammation. *Obesity Reviews* **16** 207–224. (doi:10.1111/obr.12243)

'Global Obesity Observatory'. (doi:https://data.worldobesity.org/economic-impact/countries/#ES)

Gomez-Pinilla F & Ying Z 2010 Differential effects of exercise and dietary docosahexaenoic acid (DHA) on molecular systems associated with control of allostasis in the hypothalamus and hippocampus. *Neuroscience* **168** 130–137. (doi:10.1016/j.neuroscience.2010.02.070)

Gonçalves GHM, Li W, Garcia AVCG, Figueiredo MS & Bjørbæk C 2014 Hypothalamic agouti-related peptide neurons and the central melanocortin system are crucial mediators of leptin's antidiabetic actions. *Cell Reports* **7** 1093–1103. (doi:10.1016/j.celrep.2014.04.010)

Gratacòs-Batlle E, Yefimenko N, Cascos-García H & Soto D 2015 AMPAR interacting protein CPT1C enhances surface expression of GLuA1-containing receptors. *Frontiers in Cellular Neuroscience* **8** 469. (doi:10.3389/fncel.2014.00469)

Hardie DG 2015 AMPK: Positive and negative regulation, and its role in whole-body energy homeostasis. *Current Opinion in Cell Biology* **33** 1–7. (doi:10.1016/j.ceb.2014.09.004)

Hasegawa T, Fukami M, Sato N, Katsumata N, Sasaki G, Fukutani K, Morohashi KI & Ogata T 2004 Testicular dysgenesis without adrenal insufficiency in a 46,XY patient with a heterozygous inactive mutation of steroidogenic factor-1. *Journal of Clinical Endocrinology and Metabolism* **89** 5930–5935. (doi:10.1210/jc.2004-0935)

Haynes VR, Michael NJ, van den Top M, Zhao FY, Brown RD, De Souza D, Dodd GT, Spanswick D & Watt MJ 2020 A Neural basis for Octanoic acid regulation of energy

balance. *Molecular Metabolism* **34** 54–71. (doi:10.1016/j.molmet.2020.01.002)

Hetherington AW & Ranson SW 1942 The relation of various hypothalamic lesions to adiposity in the rat. *Journal of Comparative Neurology* **76** 475–499. (doi:10.1002/cne.900760308)

Hoivik EA, Lewis AE, Aumo L & Bakke M 2010 Molecular aspects of steroidogenic factor 1 (SF-1). *Molecular and Cellular Endocrinology* **315** 27–39. (doi:10.1016/j.mce.2009.07.003)

Hotamisligil GS 2010 Endoplasmic Reticulum Stress and the Inflammatory Basis of Metabolic Disease. *Cell* **140** 900–917. (doi:10.1016/j.cell.2010.02.034)

Ikeda Y, Takeda Y, Shikayama T, Mukai T, Hisano S & Morohashi KI 2001 Comparative localization of Dax-1 and Ad4BP/SF-1 during development of the hypothalamic-pituitary-gonadal axis suggests their closely related and distinct functions. *Developmental Dynamics* **220** 363–376. (doi:10.1002/dvdy.1116)

Innes JK & Calder PC 2018 Omega-6 fatty acids and inflammation. *Prostaglandins Leukotrienes and Essential Fatty Acids* **132** 41–48. (doi:10.1016/j.plefa.2018.03.004)

Jais A & Brüning JC 2022 Arcuate Nucleus-Dependent Regulation of Metabolism—Pathways to Obesity and Diabetes Mellitus. *Endocrine Reviews* **43** 314–328. (doi:10.1210/endrev/bnab025)

Jeremic N, Chaturvedi P & Tyagi SC 2017 Browning of White Fat: Novel Insight Into Factors, Mechanisms, and Therapeutics. *Journal of Cellular Physiology* **232** 61–68. (doi:10.1002/jcp.25450)

Jo Y-H, Su Y, Gutierrez-Juarez R, Chua S, Y-h J & Jr Oleic CS 2009 Oleic Acid Directly Regulates POMC Neuron Excitability in the Hypothalamus. *J Neurophysiol* **101** 2305–2316. (doi:10.1152/jn.91294.2008)

Karmi A, Iozzo P, Viljanen A, Hirvonen J, Fielding BA, Virtanen K, Oikonen V, Kemppainen J, Viljanen T, Guiducci L *et al.* 2010 Increased brain fatty acid uptake in metabolic syndrome. *Diabetes* **59** 2171–2177. (doi:10.2337/db09-0138)

Kim KW, Zhao L, Donato J, Kohno D, Xu Y, Eliasa CF, Lee C, Parker KL & Elmquist JK 2011 Steroidogenic factor 1 directs programs regulating diet-induced thermogenesis and leptin action in the ventral medial hypothalamic nucleus. *Proc Natl Acad Sci U S A* **108** 10673–10678. (doi:10.1073/pnas.1102364108)

Kim KW, Donato J, Berglund ED, Choi YH, Kohno D, Elias CF, DePinho RA & Elmquist JK 2012 FOXO1 in the ventromedial hypothalamus regulates energy balance. *Journal of Clinical Investigation* **122** 2578–2589. (doi:10.1172/JCI62848)

Klöckener T, Hess S, Belgardt BF, Paeger L, Verhagen LAW, Husch A, Sohn JW, Hampel B, Dhillon H, Zigman JM *et al.* 2011 High-fat feeding promotes obesity via insulin receptor/PI3K-dependent inhibition of SF-1 VMH neurons. *Nature Neuroscience* **14**

911–918. (doi:10.1038/nn.2847)

Kreuz S, Schoelch C, Thomas L, Rist W, Rippmann JF & Neubauer H 2009 Acetyl-CoA carboxylases 1 and 2 show distinct expression patterns in rats and humans and alterations in obesity and diabetes. *Diabetes/Metabolism Research and Reviews* **25** 577–586. (doi:10.1002/dmrr.997)

Lam TK, Schwartz GJ & Rossetti L 2005a Hypothalamic sensing of fatty acids. *Nature Neuroscience* **8** 579–584. (doi:10.1038/nn1456)

Lam TK, Pocai A, Gutierrez-Juarez R, Obici S, Bryan J, Aguilar-Bryan L, Schwartz GJ & Rossetti L 2005b Hypothalamic sensing of circulating fatty acids is required for glucose homeostasis. *Nature Medicine* **11** 320–327. (doi:10.1038/nm1201)

Lane MD, Wolfgang M, Cha SH & Dai Y 2008 Regulation of food intake and energy expenditure by hypothalamic malonyl-CoA. *International Journal of Obesity* **32** S49-54. (doi:10.1038/ijo.2008.123)

Li X, Fan K, Li Q, Pan D, Hai R & Du C 2019 Melanocortin 4 receptor–mediated effects of amylin on thermogenesis and regulation of food intake. *Diabetes/Metabolism Research and Reviews* **35** 1–10. (doi:10.1002/dmrr.3149)

Loftus TM, Jaworsky DE, Frehywot CL, Townsend CA, Ronnett G V., Daniel Lane M & Kuhajda FP 2000 Reduced food intake and body weight in mice treated with fatty acid synthase inhibitors. *Science* **288** 2379–2381. (doi:10.1126/science.288.5475.2379)

Lohse I, Reilly P & Zaugg K 2011 The CPT1C 5'UTR contains a repressing upstream open reading frame that is regulated by cellular energy availability and AMPK. *PLoS ONE* **6** 23–27. (doi:10.1371/journal.pone.0021486)

Longo M, Zatterale F, Naderi J, Parrillo L, Formisano P, Raciti GA, Beguinot F & Miele C 2019 Adipose tissue dysfunction as determinant of obesity-associated metabolic complications. *International Journal of Molecular Sciences* **20** 2358. (doi:10.3390/ijms20092358)

López M, Nogueiras R, Tena-Sempere M & Diéguez C 2016 Hypothalamic AMPK: a canonical regulator of whole-body energy balance. *Nature Reviews Endocrinology* **12** 421–432. (doi:10.1038/nrendo.2016.67)

Majdic G, Young M, Gomez-Sanchez E, Anderson P, Szczepaniak LS, Dobbins RL, McGarry JD & Parker KL 2002 Knockout mice lacking steroidogenic factor 1 are a novel genetic model of hypothalamic obesity. *Endocrinology* **143** 607–614. (doi:10.1210/endo.143.2.8652)

Martínez-Sánchez N, Seoane-Collazo P, Contreras C, Varela L, Villarroya J, Rial-Pensado E, Buqué X, Aurrekoetxea I, Delgado TC, Vázquez-Martínez R *et al.* 2017 Hypothalamic AMPK-ER Stress-JNK1 Axis Mediates the Central Actions of Thyroid Hormones on

Energy Balance. *Cell Metabolism* **26** 212–229. (doi:10.1016/j.cmet.2017.06.014)

Martínez De Morentin PB, González-García I, Martins L, Lage R, Fernández-Mallo D, Martínez-Sánchez N, Ruíz-Pino F, Liu J, Morgan DA, Pinilla L *et al.* 2014 Estradiol regulates brown adipose tissue thermogenesis via hypothalamic AMPK. *Cell Metabolism* **20** 41–53. (doi:10.1016/j.cmet.2014.03.031)

McGarry JD & Brown NF 1997 The mitochondrial carnitine palmitoyltransferase system. From concept to molecular analysis. *European Journal of Biochemistry* **244** 1–14. (doi:10.1111/j.1432-1033.1997.00001.x)

McLellan MA, Rosenthal NA & Pinto AR 2017 Cre-loxP-Mediated Recombination: General Principles and Experimental Considerations. *Current Protocols in Mouse Biology* **7** 1–12. (doi:10.1002/CPMO.22)

Meek TH, Matsen ME, Dorfman MD, Guyenet SJ, Damian V, Nguyen HT, Taborsky GJ & Morton GJ 2013 Leptin action in the ventromedial hypothalamic nucleus is sufficient, but not necessary, to normalize diabetic hyperglycemia. *Endocrinology* **154** 3067–3076. (doi:10.1210/en.2013-1328)

Meek TH, Nelson JT, Matsen ME, Dorfman MD, Guyenet SJ, Damian V, Allison MB, Scarlett JM, Nguyen HT, Thaler JP *et al.* 2016 Functional identification of a neurocircuit regulating blood glucose. *Proc Natl Acad Sci U S A* **113** E2073-2082. (doi:10.1073/pnas.1521160113)

Michael NJ & Watt MJ 2020 Long Chain Fatty Acids Differentially Regulate Sub-populations of Arcuate POMC and NPY Neurons. *Neuroscience* **451** 164–173. (doi:10.1016/j.neuroscience.2020.09.045)

Milanski M, Degasperi G, Coope A, Morari J, Denis R, Cintra DE, Tsukumo DML, Anhe G, Amaral ME, Takahashi HK *et al.* 2009 Saturated fatty acids produce an inflammatory response predominantly through the activation of TLR4 signaling in hypothalamus: Implications for the pathogenesis of obesity. *Journal of Neuroscience* **29** 359–370. (doi:10.1523/JNEUROSCI.2760-08.2009)

Milanski M, Arruda AP, Coope A, Ignacio-Souza LM, Nunez CE, Roman EA, Romanatto T, Pascoal LB, Caricilli AM, Torsoni MA *et al.* 2012 Inhibition of hypothalamic inflammation reverses diet-induced insulin resistance in the liver. *Diabetes* **61** 1455–1462. (doi:10.2337/db11-0390)

Milbank E, Dragano NRV, González-García I, Garcia MR, Rivas-Limeres V, Perdomo L, Hilairet G, Ruiz-Pino F, Mallegol P, Morgan DA *et al.* 2021 Small extracellular vesicle-mediated targeting of hypothalamic AMPKα1 corrects obesity through BAT activation. *Nature Metabolism* **3** 1415–1431. (doi:10.1038/s42255-021-00467-8)

Minokoshi Y, Haque MS & Shimazu T 1999 Microinjection of leptin into the ventromedial hypothalamus increases glucose uptake in peripheral tissues in rats. *Diabetes* **48** 287–291. (doi:10.2337/diabetes.48.2.287)

Miralpeix C, Fosch A, Casas J, Baena M, Herrero L, Serra D, Rodríguez-Rodríguez R & Casals N 2019 Hypothalamic endocannabinoids inversely correlate with the development of diet-induced obesity in male and female mice. *Journal of Lipid Research* **60** 1260–1269. (doi:10.1194/jlr.M092742)

Miralpeix C, Reguera AC, Fosch A, Casas M, Lillo J, Navarro G, Franco R, Casas J, Alexander SPHP, Casals NN *et al.* 2021a Carnitine palmitoyltransferase 1C negatively regulates the endocannabinoid hydrolase ABHD6 in mice, depending on nutritional status. *British Journal of Pharmacology* **178** 1507–1523. (doi:10.1111/bph.15377)

Miralpeix C, Reguera AC, Fosch A, Zagmutt S, Casals N, Cota D & Rodríguez-Rodríguez R 2021b Hypothalamic endocannabinoids in obesity: an old story with new challenges. *Cellular and Molecular Life Sciences* **78** 7469–7490. (doi:10.1007/s00018-021-04002-6)

Mitchell RW, On NH, Del Bigio MR, Miller DW & Hatch GM 2011 Fatty acid transport protein expression in human brain and potential role in fatty acid transport across human brain microvessel endothelial cells. *Journal of Neurochemistry* **117** 735–746. (doi:10.1111/j.1471-4159.2011.07245.x)

Monda M, Sullo A, De Luca V, Viggiano A & Pellicano MP 1997a Acute lesions of the ventromedial hypothalamus reduce sympathetic activation and thermogenic changes induced by PGE1. *Journal of Physiology Paris* **91** 285–290. (doi:10.1016/S0928-4257(97)82408-4)

Monda M, Sullo A & De Luca B 1997b Lesions of the ventromedial hypothalamus reduce postingestional thermogenesis. *Physiology and Behavior* **61** 687–691. (doi:10.1016/S0031-9384(96)00520-3)

Morgan K, Obici S & Rossetti L 2004 Hypothalamic responses to long-chain fatty acids are nutritionally regulated. *Journal of Biological Chemistry* **279** 31139–31148. (doi:10.1074/jbc.M400458200)

Moullé VS, Le Foll C, Philippe E, Kassis N, Rouch C, Marsollier N, Bui LC, Guissard C, Dairou J, Lorsignol A *et al.* 2013 Fatty Acid Transporter CD36 Mediates Hypothalamic Effect of Fatty Acids on Food Intake in Rats. *PLoS ONE* **8** 1–8. (doi:10.1371/journal.pone.0074021)

Moullé VS, Picard A, Le Foll C, Levin BE & Magnan C 2014 Lipid sensing in the brain and regulation of energy balance. *Diabetes and Metabolism* **40** 29–33. (doi:10.1016/j.diabet.2013.10.001)

Nilsson C, Raun K, Yan FF, Larsen MO & Tang-Christensen M 2012 Laboratory animals as surrogate models of human obesity. *Acta Pharmacologica Sinica* **33** 173–181. (doi:10.1038/aps.2011.203)

'Obesity - Our world in data'. (doi:https://ourworldindata.org/obesity#what-share-of-adults-are-obese)

Obici S, Feng Z, Morgan K, Stein D, Karkanias G & Rossetti L 2002 Central administration of oleic acid inhibits glucose production and food intake. *Diabetes* **51** 271–275. (doi:10.2337/diabetes.51.2.271)

Obici S, Feng Z, Arduini A, Conti R & Rossetti L 2003 Inhibition of hypothalamic carnitine palmitoyltransferase-1 decreases food intake and glucose production. *Nature Medicine* **9** 756–761. (doi:10.1038/nm873)

Okamoto S, Sato T, Tateyama M, Kageyama H, Maejima Y, Nakata M, Hirako S, Matsuo T, Kyaw S, Shiuchi T *et al.* 2018 Activation of AMPK-Regulated CRH Neurons in the PVH is Sufficient and Necessary to Induce Dietary Preference for Carbohydrate over Fat. *Cell Reports* **22** 706–721. (doi:10.1016/j.celrep.2017.11.102)

Oldfield BJ, Allen AM, Davern P, Giles ME & Owens NC 2007 Lateral hypothalamic 'command neurons' with axonal projections to regions involved in both feeding and thermogenesis. *European Journal of Neuroscience* **25** 2404–2412. (doi:10.1111/j.1460-9568.2007.05429.x)

Orozco-Solis R, Ramadori G, Coppari R & Sassone-Corsi P 2015 SIRT1 relays nutritional inputs to the circadian clock through the Sf1 neurons of the ventromedial hypothalamus. *Endocrinology* **156** 2174–2184. (doi:10.1210/en.2014-1805)

Palomo-Guerrero M, Fadó R, Casas M, Pérez-Montero M, Baena M, Helmer PO, Domínguez JL, Roig A, Serra D, Hayen H *et al.* 2019 Sensing of nutrients by CPT1C regulates late endosome/lysosome anterograde transport and axon growth. *ELife* **8** 1–26. (doi:10.7554/eLife.51063)

Parker KL, Rice DA, Lala DS, Ikeda Y, Luo X, Wong M, Bakke M, Zhao L, Frigeri C, Hanley NA *et al.* 2002 Steroidogenic factor 1: An essential mediator of endocrine development. *Recent Progress in Hormone Research* **57** 19–36. (doi:10.1210/rp.57.1.19)

Pozo M, Rodriguez-Rodriguez R, Ramirez S, Seoane-Collazo P, Lopez M, Serra D, Herrero L & Casals N 2017 Hypothalamic regulation of liver and muscle nutrient partitioning by brain-specific carnitine palmitoyltransferase 1C (CPT1C) in male mice. *Endocrinology* **158** 2226–2238. (doi:10.1210/en.2017-00151)

Price NT, Van Der Leij FR, Jackson VN, Corstorphine CG, Thomson R, Sorensen A & Zammit VA 2002 A novel brain-expressed protein related to carnitine palmitoyltransferase I. *Genomics* **80** 433–442. (doi:10.1006/geno.2002.6845)

Quarta C, Claret M, Zeltser LM, Williams KW, Yeo GSH, Tschöp MH, Diano S, Brüning JC & Cota D 2021 POMC neuronal heterogeneity in energy balance and beyond: an integrated view. *Nature Metabolism* **3** 299–308. (doi:10.1038/s42255-021-00345-3)

Quenneville S, Labouèbe G, Basco D, Metref S, Viollet B, Foretz M & Thorens B 2020 Hypoglycemia-sensing neurons of the ventromedial hypothalamus require AMPK-induced TXN2 expression but are dispensable for physiological counterregulation. *Diabetes* **69** 2253–2266. (doi:10.2337/db20-0577)

Ramadori G, Lee CE, Bookout AL, Lee S, Williams KW, Anderson J, Elmquist JK & Coppari R 2008 Brain SIRT1: Anatomical distribution and regulation by energy availability. *Journal of Neuroscience* **28** 9989–9996. (doi:10.1523/JNEUROSCI.3257-08.2008)

Ramadori G, Fujikawa T, Anderson J, Berglund ED, Frazao R, Michán S, Vianna CR, Sinclair DA, Elias CF & Coppari R 2011 SIRT1 deacetylase in SF1 neurons protects against metabolic imbalance. *Cell Metabolism* **14** 301–312. (doi:10.1016/j.cmet.2011.06.014)

Ramírez S, Martins L, Jacas J, Carrasco P, Pozo M, Clotet J, Serra D, Hegardt FG, Diéguez C, López M *et al.* 2013 Hypothalamic ceramide levels regulated by cpt1c mediate the orexigenic effect of ghrelin. *Diabetes* **62** 2329–2337. (doi:10.2337/db12-1451)

Rapoport SI 1996 In vivo labeling of brain phospholipids by long-chain fatty acids: Relation to turnover and function. *Lipids* **31** S97-101. (doi:10.1007/bf02637059)

Rein ML & Deussing JM 2012 The optogenetic (r)evolution. *Molecular Genetics and Genomics* **287** 95–109. (doi:10.1007/s00438-011-0663-7)

Rinaldi C, Schmidt T, Situ AJ, Johnson JO, Lee PR, Chen K, Bott LC, Fadó R, Harmison GH, Parodi S *et al.* 2015 Mutation in CPT1C Associated With Pure Autosomal Dominant Spastic Paraplegia. *JAMA Neurology* **72** 561–570. (doi:10.1001/jamaneurol.2014.4769)

Roa-Mansergas X, Fadó R, Atari M, Mir JF, Muley H, Serra D & Casals N 2018 CPT1C promotes human mesenchymal stem cells survival under glucose deprivation through the modulation of autophagy. *Scientific Reports* **8** 1–13. (doi:10.1038/s41598-018-25485-7)

Rodríguez-Rodríguez R, Miralpeix C, Fosch A, Pozo M, Calderón-Domínguez M, Perpinyà X, Vellvehí M, López M, Herrero L, Serra D *et al.* 2019 CPT1C in the ventromedial nucleus of the hypothalamus is necessary for brown fat thermogenesis activation in obesity. *Molecular Metabolism* **19** 75–85. (doi:10.1016/j.molmet.2018.10.010)

Romano A, Koczwara JB, Gallelli CA, Vergara D, Micioni Di Bonaventura MV, Gaetani S & Giudetti AM 2017 Fats for thoughts: An update on brain fatty acid metabolism. *International Journal of Biochemistry and Cell Biology* **84** 40–45. (doi:10.1016/j.biocel.2016.12.015)

Sadovsky Y, Crawford PA, Woodson KG, Polish JA, Clements MA, Tourtellotte LM, Simburger K & Milbrandt J 1995 Mice deficient in the orphan receptor steroidogenic factor 1 lack adrenal glands and gonads but express P450 side-chain-cleavage enzyme in the placenta and have normal embryonic serum levels of corticosteroids. *Proceedings of the National Academy of Sciences of the United States of America* **92** 10939–10943. (doi:10.1073/pnas.92.24.10939)

Saini RK & Keum YS 2018 Omega-3 and omega-6 polyunsaturated fatty acids: Dietary sources, metabolism, and significance — A review. *Life Sciences* **203** 255–267.

(doi:10.1016/j.lfs.2018.04.049)

Samanta S, Situ AJ & Ulmer TS 2014 Structural Characterization of the Regulatory Domain of Brain Carnitine Palmitoyltransferase 1. *Biopolymers* **101** 398–405. (doi:10.1002/bip.22396)

Sanchez-Macedo N, Feng J, Faubert B, Chang N, Elia A, Rushing EJ, Tsuchihara K, Bungard D, Berger SL, Jones RG *et al.* 2013 Depletion of the novel p53-target gene carnitine palmitoyltransferase 1C delays tumor growth in the neurofibromatosis type i tumor model. *Cell Death and Differentiation* **20** 659–668. (doi:10.1038/cdd.2012.168)

Sarma S, Sockalingam S & Dash S 2021 Obesity as a multisystem disease: Trends in obesity rates and obesity-related complications. *Diabetes, Obesity and Metabolism* **23** 3–16. (doi:10.1111/dom.14290)

Sawadogo W, Tsegaye M, Gizaw A & Adera T 2022 Overweight and obesity as risk factors for COVID-19-associated hospitalisations and death: systematic review and meta-analysis. *BMJ Nutrition, Prevention & Health*. (doi:10.1136/bmjnph-2021-000375)

Scherer T, Sakamoto K & Buettner C 2021 Brain insulin signalling in metabolic homeostasis and disease. *Nature Reviews Endocrinology* **17** 468–483. (doi:10.1038/s41574-021-00498-x)

Schwinkendorf DR, Tsatsos NG, Gosnell BA & Mashek DG 2011 Effects of central administration of distinct fatty acids on hypothalamic neuropeptide expression and energy metabolism. *International Journal of Obesity* **35** 336–344. (doi:10.1038/ijo.2010.159)

Seeley RJ, Drazen DL & Clegg DJ 2004 The critical role of the melanocortin system in the control of energy balance. *Annual Review of Nutrition* **24** 133–149. (doi:10.1146/annurev.nutr.24.012003.132428)

Senn SS, Le Foll C, Whiting L, Tarasco E, Duffy S, Lutz TA & Boyle CN 2019 Unsilencing of native LepRs in hypothalamic SF1 neurons does not rescue obese phenotype in LepR-deficient mice. *American Journal of Physiology. Regulatory, Integrative and Comparative Physiology* **317** R451–R460. (doi:10.1152/ajpregu.00111.2019)

Seoane-Collazo P, Roa J, Rial-Pensado E, Liñares-Pose L, Beiroa D, Ruíz-Pino F, López-González T, Morgan DA, Pardavila JÁ, Sánchez-Tapia MJ *et al.* 2018 SF1-specific AMPKa1 deletion protects against diet-induced obesity. *Diabetes* **67** 2213–2226. (doi:10.2337/db17-1538)

Shin S & Ajuwon KM 2018 Effects of diets differing in composition of 18-C fatty acids on adipose tissue thermogenic gene expression in mice fed high-fat diets. *Nutrients* **10** 256. (doi:10.3390/nu10020256)

Sierra AY, Gratacós E, Carrasco P, Clotet J, Ureña J, Serra D, Asins G, Hegardt FG & Casals N 2008 CPT1c is localized in endoplasmic reticulum of neurons and has carnitine

palmitoyltransferase activity. *Journal of Biological Chemistry* **283** 6878–6885. (doi:10.1074/jbc.M707965200)

Sohn JW 2015 Network of hypothalamic neurons that control appetite. *BMB Reports* **48** 229–233. (doi:10.5483/BMBRep.2015.48.4.272)

Sohn JW, Oh Y, Kim KW, Lee S, Williams KW & Elmquist JK 2016 Leptin and insulin engage specific PI3K subunits in hypothalamic SF1 neurons. *Molecular Metabolism* **5** 669–679. (doi:10.1016/j.molmet.2016.06.004)

Soler-Vázquez MC, Mera P, Zagmutt S, Serra D & Herrero L 2018 New approaches targeting brown adipose tissue transplantation as a therapy in obesity. *Biochemical Pharmacology* **155** 346–355. (doi:10.1016/j.bcp.2018.07.022)

Sternson SM & Roth BL 2014 Chemogenetic tools to interrogate brain functions. *Annual Review of Neuroscience* **37** 387–407. (doi:10.1146/annurev-neuro-071013-014048)

Stuber GD & Wise RA 2016 Lateral hypothalamic circuits for feeding and reward. *Nature Neuroscience* **19** 198–205. (doi:10.1038/nn.4220)

Sutton AK, Myers MG & Olson DP 2016 The Role of PVH Circuits in Leptin Action and Energy Balance. *Annual Review of Physiology* **78** 207–221. (doi:10.1146/annurev-physiol-021115-105347)

Tanida M, Yamamoto N, Shibamoto T & Rahmouni K 2013 Involvement of Hypothalamic AMP-Activated Protein Kinase in Leptin-Induced Sympathetic Nerve Activation. *PLoS ONE* **8** e56660. (doi:10.1371/journal.pone.0056660)

Tchang BG, Aras M, Kumar RB & Aronne LJ 2000 Pharmacologic Treatment of Overweight and Obesity in Adults. In *NCBI Bookshelf- Endotext*. Endotext. (doi:www.ncbi.nlm.nih.gov/books/NBK279038/)

Thaler JP, Yi CX, Schur EA, Guyenet SJ, Hwang BH, Dietrich MO, Zhao X, Sarruf DA, Izgur V, Maravilla KR *et al.* 2012 Obesity is associated with hypothalamic injury in rodents and humans. *Journal of Clinical Investigation* **122** 153–162. (doi:10.1172/JCI59660)

Thon M, Hosoi T & Ozawa K 2016 Possible integrative actions of leptin and insulin signaling in the hypothalamus targeting energy homeostasis. *Frontiers in Endocrinology* **7** 1–7. (doi:10.3389/fendo.2016.00138)

Tokutake Y, Onizawa N, Katoh H, Toyoda A & Chohnan S 2010 Coenzyme A and its thioester pools in fasted and fed rat tissues. *Biochemical and Biophysical Research Communications* **402** 158–162. (doi:10.1016/j.bbrc.2010.10.009)

Tong Q, Ye CP, McCrimmon RJ, Dhillon H, Choi B, Kramer MD, Yu J, Yang Z, Christiansen LM, Lee CE *et al.* 2007 Synaptic Glutamate Release by Ventromedial Hypothalamic Neurons Is Part of the Neurocircuitry that Prevents Hypoglycemia. *Cell Metabolism* **5** 383–393. (doi:10.1016/j.cmet.2007.04.001)

Tracey TJ, Steyn FJ, Wolvetang EJ & Ngo ST 2018 Neuronal lipid metabolism: Multiple pathways driving functional outcomes in health and disease. *Frontiers in Molecular Neuroscience* **11** 10. (doi:10.3389/fnmol.2018.00010)

Trayhurn P 2017 Origins and early development of the concept that brown adipose tissue thermogenesis is linked to energy balance and obesity. *Biochimie* **134** 62–70. (doi:10.1016/j.biochi.2016.09.007)

Velloso LA & Schwartz MW 2011 Altered hypothalamic function in diet-induced obesity. *International Journal of Obesity* **35** 1455–1465. (doi:10.1038/ijo.2011.56)

Verma S & Hussain ME 2017 Obesity and diabetes: An update. *Diabetes and Metabolic Syndrome: Clinical Research and Reviews* **11** 73–79. (doi:10.1016/j.dsx.2016.06.017)

Viskaitis P, Irvine EE, Smith MA, Choudhury AI, Alvarez-Curto E, Glegola JA, Hardy DG, Pedroni SMA, Paiva Pessoa MR, Fernando ABP *et al.* 2017 Modulation of SF1 Neuron Activity Coordinately Regulates Both Feeding Behavior and Associated Emotional States. *Cell Reports* **21** 3559–3572. (doi:10.1016/j.celrep.2017.11.089)

Wang HH, Lee DK, Liu M, Portincasa P & Wang DQH 2020 Novel insights into the pathogenesis and management of the metabolic syndrome. *Pediatric Gastroenterology, Hepatology and Nutrition* **23** 189–230. (doi:10.5223/PGHN.2020.23.3.189)

Whittle A, Relat-Pardo J & Vidal-Puig A 2013 Pharmacological strategies for targeting BAT thermogenesis. *Trends in Pharmacological Sciences* **34** 347–355. (doi:10.1016/j.tips.2013.04.004)

WHO Obesity and overweight. (doi:https://www.who.int/news-room/fact-sheets/detail/obesity-and-overweight)

Wolfgang MJ & Lane MD 2006 The role of hypothalamic malonyl-CoA in energy homeostasis. *Journal of Biological Chemistry* **281** 37265–37269. (doi:10.1074/jbc.R600016200)

Wolfgang MJ, Kurama T, Dai Y, Suwa A, Asaumi M, Matsumoto S -i., Cha SH, Shimokawa T & Lane MD 2006 The brain-specific carnitine palmitoyltransferase-1c regulates energy homeostasis. *Proceedings of the National Academy of Sciences* **103** 7282–7287. (doi:10.1073/pnas.0602205103)

Wolfgang MJ, Cha SH, Millington DS, Cline G, Shulman GI, Suwa A, Asaumi M, Kurama T, Shimokawa T & Lane MD 2008 Brain-specific carnitine palmitoyl-transferase-1c: Role in CNS fatty acid metabolism, food intake, and body weight. *Journal of Neurochemistry* **105** 1550–1559. (doi:10.1111/j.1471-4159.2008.05255.x)

Woods SC, Stein LJ, McKay LD & Porte D 1984 Suppression of food intake by intravenous nutrients and insulin in the baboon. *American Journal of Physiology - Regulatory Integrative and Comparative Physiology* **247** R393–R401.

(doi:10.1152/ajpregu.1984.247.2.r393)

Xu AW, Kaelin CB, Takeda K, Akira S, Schwartz MW & Barsh GS 2005 PI3K integrates the action of insulin and leptin on hypothalamic neurons. *Journal of Clinical Investigation* **115** 951–958. (doi:10.1172/JCI200524301)

Xu Y, Hill JW, Fukuda M, Gautron L, Sohn JW, Kim KW, Lee CE, Choi MJ, Lauzon DA, Dhillon H *et al.* 2010 PI3K signaling in the ventromedial hypothalamic nucleus is required for normal energy homeostasis. *Cell Metabolism* **12** 88–95. (doi:10.1016/j.cmet.2010.05.002)

Xu Y, Nedungadi TP, Zhu L, Sobhani N, Irani BG, Davis KE, Zhang X, Zou F, Gent LM, Hahner LD *et al.* 2011 Distinct hypothalamic neurons mediate estrogenic effects on energy homeostasis and reproduction. *Cell Metabolism* **14** 453–465. (doi:10.1016/j.cmet.2011.08.009)

Xu Y, O'Malley BW & Elmquist JK 2017 Brain nuclear receptors and body weight regulation. *Journal of Clinical Investigation* **127** 1172–1180. (doi:10.1172/JCI88891)

Yang H, An JJ, Sun C & Xu B 2016 Regulation of energy balance via BDNF expressed in nonparaventricular hypothalamic neurons. *Molecular Endocrinology* **30** 494–503. (doi:10.1210/me.2015-1329)

Zaugg K, Yao Y, Reilly PT, Kannan K, Kiarash R, Mason J, Huang P, Sawyer SK, Fuerth B, Faubert B *et al.* 2011 Carnitine palmitoyltransferase 1C promotes cell survival and tumor growth under conditions of metabolic stress. *Genes and Development* **25** 1041–1051. (doi:10.1101/gad.1987211)

Zhang R, Dhillon H, Yin H, Yoshimura A, Lowell BB, Maratos-Flier E & Flier JS 2008 Selective inactivation of Socs3 in SF1 neurons improves glucose homeostasis without affecting body weight. *Endocrinology* **149** 5654–5661. (doi:10.1210/en.2008-0805)

Zhang Y, Xu Q, Liu YH, Zhang XS, Wang J, Yu XM, Zhang RX, Xue C, Yang XY & Xue CY 2015 Medium-Chain Triglyceride Activated Brown Adipose Tissue and Induced Reduction of Fat Mass in C57BL/6J Mice Fed High-fat Diet. *Biomedical and Environmental Sciences : BES* **28** 97–104. (doi:10.3967/BES2015.012)

Zhang F, Hao G, Shao M, Nham K, An Y, Wang Q, Zhu Y, Kusminski CM, Hassan G, Gupta RK *et al.* 2018 An Adipose Tissue Atlas: An Image-Guided Identification of Human-like BAT and Beige Depots in Rodents. *Cell Metabolism* **27** 252-262.e3. (doi:10.1016/j.cmet.2017.12.004)

Zhang J, Chen D, Sweeney P & Yang Y 2020 An excitatory ventromedial hypothalamus to paraventricular thalamus circuit that suppresses food intake. *Nature Communications* **11**. (doi:10.1038/s41467-020-20093-4)

Zhao L, Ki WK, Ikeda Y, Anderson KK, Beck L, Chase S, Tobet SA & Parker KL 2008 Central nervous system-specific knockout of steroidogenic factor 1 results in increased

anxiety-like behavior. *Molecular Endocrinology* **22** 1403–1415. (doi:10.1210/me.2008-0034)

Ziotopoulou M, Mantzoros CS, Hileman SM & Flier JS 2000 Differential expression of hypothalamic neuropeptides in the early phase of diet-induced obesity in mice. *American Journal of Physiology - Endocrinology and Metabolism* **279** 838–845. (doi:10.1152/ajpendo.2000.279.4.e838)

ABBREVIATIONS

2-AG	2 - Arachidonoylglycerol
2-DG	2 - Deoxy-D-Glucose
3V	3rd ventricle
4-AP	4-Aminophenazone
AAV	Adeno-associated viruses
ABHD6	α/β-Hydrolase domain containing 6
aBNST	Anterior bed nucleus of the stria terminalis
ACC	Acetyl-CoA carboxylase
ACS	Acetyl-CoA synthetase
aCSF	Articifial cerebrospinal fluid
AgRP	Agouti-related protein
AMPAR	α-amino-3-hydroxy-5-methyl-4-isoxazolepropionic acid receptor
AMPK	AMP-activated protein kinase
ARC	Arcuate nucleus of hypotahalamus
ATP	Adenosine triphosphate
AUC	Area under curve
BAT	Brown adipose tissue
BBB	Blood brain barrier
BCA	Bicinchoninic acid assay
BDNF	Brain-derived neurotrophic factor
BMI	Body mass index
BMP	Bis(monoacylglycerol)phosphate
BMR	Basal metabolic rate
BSA	Bovine serum albumin
BW	Body weight
CB1	Cannabinoid receptor type 1
ChR	Channelrhodopsin
CIT	Cold-induced thermogenesis
CNO	Clozapine-N-oxide
CNS	Central nervous system
CPT1	Carnitine palmitoyltransferase 1
CRR	Counterregulatory response
CTX	Cortex
D	Dark phase
DAP	Dihydroxyacetone phosophate
DHA	Docosahexaenoic acid
DIO	Diet-induced obesity
DMH	Dorsomedial nucleus of hypothalamus
DREADD	Designer Receptors Exclusively Activated by Designer Drugs

EE	Energy expenditure
ER	Endoplasmic reticulum
ERα	Estrogen receptor alpha
ESPA	Sodium N-ethyl-N-(3-sulfopropyl) m-anisidine
EST	Expressed sequence tag
eWAT	Epididymal WAT
F	Forward
FA	Fatty acid
FAO	Fatty acid oxidation
FAS	Fatty acis synthase
FFA	Free-fatty acids
FI	Food intake
FISH	Fluorescence in-situ hybridization
FlP	Flippase
FOXO1	Forkhead-box-O1
FRT	Flippase recognition target
G-1-P	Glycerol-1-phosphate
G6P	Glucose 6-phosphatase
GAPDH	Glyceraldehyde-3-phosphate dehydrogenase
GE	Glucose excited
GI	Glucose inhibited
GK	Glycerol kinase
GNP	Gross national product
GOD	Glucose oxidase enzyme
GPO	Glycerol phosphate oxidase
GPR40	G-protein coupled receptor 40
GTT	Glucose tolerance test
HC	Hippocampus
Het	Heterozygous
HFD	High-fat diet
Hom	Homozygous
HPB	2-hyrdroxypropyl-β-cyclodextrin
HSP	Hereditary Spastic Paraplegia
iBAT	Interscapular BAT
icv	Intracerebroventricular
IL	Interleukine
ip	Intraperitoneal
IR	Insulin receptor
ITT	Insulin tolerance test

IVF	In vitro fecundation
K_{ITT}	Glucose dissapearance rate
KO	Knock-out
L	Light phase
LA	Linoleic acid
LCFA	Long-chain fatty acids
LD	Lipid droplets
LE/Lys	Late endosomes/lysosomes
Lep	Leptin
LEPR	Leptin receptor
LHA	Lateral hypothalamic area
MC4R	Melanocortin 4 receptor
MCFA	Medium-chain fatty acids
mGluR5	Metabotropic glutamate receptor 5
MRI	Magnetic resonance imaging
MUFA	Monounsaturated fatty acids
NPY	Neuropeptide Y
OA	Oleic acid
PA	Palmitic acid
PAEE	Physical activity energy expenditure
PaV	Paraventricular nucleus f hypothalamus
PCR	Polymerase chain reaction
PDK4	Pyruvate deshydrigenase kinase 4
PEPCK	Phosphoenolpyruvate carboxykinase
$PGC_{\alpha}1$	Peroxisome proliferator-activated receptor γ co-activator 1 α
PI3K	Phosphoinositide 3-kinase
POD	Peroxidase
POMC	Pro-opiomelanocortin
PRDM16	PR domain containing 16
PTP1B	Protein-tyrosine phosphatase 1B
PUFA	Polyunsaturated fatty acids
PVDF	Polyvinylidene fluoride
R	Reverse
Ref	Reference
RER	Respiratory exchange ratio
RIPA	Radioimmunoprecipitation assay
ROS	Reactive oxygen species
SA	Stearic acid
SCFA	Short-chain fatty acids

SD	Standard diet
SDS-PAGE	Sodium dodecyl sulfate polyacrylamide gel electrophoresis
SEM	Standard error of the mean
SF1	Sterodogenic factor 1
SFA	Saturated fatty acids
SIM 1	single-minded 1
SIRT1	Sirtuin 1
SNS	Sympathetic nervous sytem
SOCS3	Suppressor of cytokine signaling 3
sWAT	Subcutaneous WAT
TEF	Thermal effect of food
TG	Triglycerides
TLR4	Toll-like receptor 4
TNFα	Tumour Necrosis Factor alpha
UCP1	Uncoupling protein 1
V/Veh	Vehicle
VGLUT2	Vesicular glutamate transporter 2
VLCFA	Very long-chain fatty acids
VMH	Ventromedial nucleus of hypothalamus
WAT	White adipose tissue
WHO	World health organization
WT	Wyld-type
αMSH	α-Melanocyte-stimulating hormone

LISTS OF FIGURES AND TABLES

Figures

Tables

APPENDIX

Publications related to this Thesis

Miralpeix C, Reguera AC, **Fosch A**, Zagmutt S, Casals N, Cota D, Rodríguez-Rodríguez R. **2021** Hypothalamic endocannabinoids in obesity: an old story with new challenges. **Cell Mol Life Sci.** Dec;78(23):7469-7490. doi: 10.1007/s00018-021-04002-6. Q1; IF=9.261

Fosch A, Zagmutt S, Casals N, Rodríguez-Rodríguez R. **2021** New Insights of SF1 Neurons in Hypothalamic Regulation of Obesity and Diabetes. **Int J Mol Sci.** Jun 8;22(12):6186. doi: 10.3390/ijms22126186. Q1; IF=5.924

Miralpeix C, Reguera AC, **Fosch A**, Casas M, Lillo J, Navarro G, Franco R, Casas J, Alexander SPH, Casals N, Rodríguez-Rodríguez R. **2021** Carnitine palmitoyltransferase 1C negatively regulates the endocannabinoid hydrolase ABHD6 in mice, depending on nutritional status. **Br J Pharmacol.** Apr;178(7):1507-1523. doi: 10.1111/bph.15377. Q1; IF=8.740

Miralpeix C, **Fosch A**, Casas J, Baena M, Herrero L, Serra D, Rodríguez-Rodríguez R, Casals N. **2019** Hypothalamic endocannabinoids inversely correlate with the development of diet-induced obesity in male and female mice. **J Lipid Res.** Jul;60(7):1260-1269. doi: 10.1194/jlr.M092742. Q1; IF=5.922

Rodríguez-Rodríguez R, Miralpeix C, **Fosch A**, Pozo M, Calderón-Domínguez M, Perpinyà X, Vellvehí M, López M, Herrero L, Serra D, Casals N. **2019** CPT1C in the ventromedial nucleus of the hypothalamus is necessary for brown fat thermogenesis activation in obesity. **Mol Metab.** Jan;19:75-85. doi: 10.1016/j.molmet.2018.10.010. Q1; IF=7.422